Hadronic productions of a Higgs boson in association with two jets at next-to-leading order

WILLIAMS, CIARAN

Hadronic production of a Higgs boson in association with two jets at next-to-leading order

Ciaran Williams

A Thesis presented for the degree of
Doctor of Philosophy

Institute for Particle Physics Phenomenology
Department of Physics
University of Durham
England

August 2010

Dedicated to

My Parents

Hadronic production of a Higgs boson in association with two jets at next-to-leading order

Ciaran Williams

Submitted for the degree of Doctor of Philosophy
August 2010

Abstract

We present the calculation of hadronic production of a Higgs boson in association with two jets at next-to-leading order in perturbation theory. We consider amplitudes in an effective theory in which the Higgs couples to gluons in the limit of a large top quark mass. We treat the Higgs as the real part of the complex field ϕ that couples to the self-dual field strengths. We use modern on-shell inspired methods to calculate helicity amplitudes and we give a detailed review of unitarity based and on-shell methods. Using these unitarity methods we derive the cut-constructible pieces of the general ϕ-MHV amplitudes in which the positions of the two negative gluons are arbitrary. We then generate the cut-constructible pieces of the ϕ-NMHV four parton amplitudes $A_4^{(1)}(\phi, 1^+, 2^-, 3^-, 4^-)$ and $A_4^{(1)}(\phi, 1_q^-, 2_{\overline{q}}^+, 3^-, 4^-)$. We generate the rational pieces of these amplitudes and the four-gluon ϕ-MHV amplitude $A_4^{(1)}(\phi, 1^-, 2^+, 3^-, 4^+)$, using Feynman diagrams. For the ϕ-MHV amplitude we also use the unitarity-boostrap method to calculate the rational pieces. We then implement these, and analytic results from previous calculations, into MCFM. Using this program we are able to perform some phenomenological studies at the Tevatron and LHC.

Declaration

The work in this thesis is based on research carried out at the Institute for Particle Physics Phenomenology, University of Durham, England. No part of this thesis has been submitted elsewhere for any other degree or qualification.
The research described in this thesis was carried out in collaboration with, Simon D. Badger, John M. Campbell, R. Keith Ellis, E. W. Nigel Glover and Pierpaolo Mastrolia. Aspects of chapters 2, 3, 4, 5 and 6 are based on the following published works:

- J. M. Campbell, R. K. Ellis and C. Williams, *Hadronic production of a Higgs boson and two jets at next-to-leading-order*, *Phys. Rev.* D **81**, 074023 (2010).
- S. D. Badger, J. M. Campbell, R. K. Ellis and C. Williams, *Analytic results for the one-loop NMHV $Hq\bar{q}gg$ amplitude*, *JHEP* **12** (2009) 035.
- S. D. Badger, E. W. N. Glover, P. Mastrolia and C. Williams, *One-Loop Higgs plus four gluon Amplitudes: Full analytic results*, *JHEP* **01** (2010) 036
- E. W. N. Glover and C. Williams, *One-Loop Gluonic Amplitudes from Single Unitarity Cuts*, *JHEP* **12** (2008) 067
- E. W. N. Glover, P. Mastrolia and C. Williams, *One-loop phi-MHV amplitudes using the unitarity bootstrap: the general helicity case*, *JHEP* **08** (2008) 017

Acknowledgements

First and foremost I would like to thank my supervisor Nigel Glover, whose help and guidance has been amazing. Your advice and support has been invaluable.

I would like to thank my collaborators from whom I have learnt a great deal, Simon Badger, John Campbell, Keith Ellis, Valya Khoze and Pierpaolo Mastrolia.

I would like to thank all at the IPPP who have made my four years here extremely enjoyable, I would like to thank Linda Wilkinson and Trudy Forster, who have helped me countless times with various problems (usually of my own making). I would like to thank Daniel Maitre for hours of free Mathematica tutorials, and David Ambrose-Griffith and Peter Richardson for helping me get started on the GRID. I would also like to thank my office mates Nehir Ikizlerli, Joao Pires and newbie James Currie who have provided great banter, together we made one great Nigel tracking team. Special mention should also go to Jamie "Tatts" Tattersall possibly the second greatest TuxKart racer that ever lived. Thanks to all the other postdocs, PhD students and staff that made the IPPP so fun, there's too many to list explicitly here but you know who you are!

I would like to thank my friends and family for their love and support, especially Mum, Dad, Ryan, Steve, Dave, Tim, Phil and Chelle.

Finally I would like to thank Heather, for more than can ever be written down, but especially for the abstract reading!

This work was funded by an STFC studentship.

Contents

List of Figures

List of Tables

Chapter 1

Introduction

The outstanding problem in theoretical particle physics over the past forty or so years, is to adequately describe the mechanism by which electroweak symmetry is broken. This ultimately results in the generation of the observed masses for the W and Z vector bosons. By far the most widely accepted solution to this problem is the Higgs mechanism which introduces a new massive scalar into the standard model. The verification of the electroweak symmetry breaking mechanism, together with the discovery of the Higgs boson is one of the major physics goals of the world's current leading particle accelerators, Fermilab's Tevatron and CERN's Large Hadron Collider (LHC). These are hadronic colliders and therefore an intimate knowledge of Quantum Chromodynamics (QCD) is required in order to make predictions of cross sections and other physical observables. In this thesis, the one-loop Higgs plus four parton one-loop amplitudes are calculated analytically. These amplitudes have now been implemented into the public program MCFM [1–5] which is designed to calculate cross sections at Next-to-Leading Order (NLO). In the final chapter MCFM is used to perform some phenomenological studies of Higgs plus jet physics at hadron colliders.

This chapter consists of a brief introduction to the Standard Model (SM) of particle physics, focussing primarily on the need to break electroweak symmetry spontaneously and the resulting addition of the Higgs boson to the particle spectrum. The second half of this chapter will describe Higgs phenomenology, with particular

emphasis on Higgs production in hadronic environments and in the heavy-top limit.

1.1 The Standard Model of Particle Physics

The Standard Model is arguably the great scientific achievement of the 20$^{\text{th}}$ Century. Consistently its predictions have been met with experimental confirmation at ever increasing levels of precision. Nevertheless, there are several theoretical problems at the heart of the SM, which leads one to ultimately go beyond it. The enduring problem of recent times has been to describe how electroweak symmetry is broken, and, as result, how the acquisition of masses for the W and Z vector bosons occurs. In this section we introduce the SM and describe its main features.

1.1.1 Standard Model: Yang-Mills theories and gauge invariance.

QED and $U(1)$ gauge invariance

At the heart of the SM is the notion of gauge invariance. We will show how the notion of the invariance under local phase rotations can be used to construct the Lagrangian of QED [1]. QED (Quantum Electrodynamics) was the first quantum field theory to be studied [8–13] and is the simplest of those that make up the SM. We begin by showing that if one starts with the Dirac Lagrangian

$$\mathcal{L}_{Dirac} = \overline{\psi}(i\partial\!\!\!/ - m)\psi \tag{1.1}$$

and enforces invariance under transformations of the form,

$$\psi(x) \rightarrow e^{i\alpha(x)}\psi(x) \tag{1.2}$$

then one naturally arrives at the QED Lagrangian. Firstly, it is trivial to see that the mass term in the Lagrangian $m\overline{\psi}\psi$ is invariant under these transformations (since

[1] Gauge invariance and the standard model are the topics of several good textbooks (e.g. see [6,7] and others), in the following derivations we use the definitions of [6]

the conjugation ensures that the α dependence drops out). However, the derivative term is not invariant. This is because the derivative operation naturally acts on fields by deforming x by small amounts $x \to x + \epsilon$. However the points x and $x + \epsilon$ transform with different rotations under eq. (1.2), so no cancellation occurs. We wish to define an object which transforms in the following way

$$D(x, y) \to e^{i\alpha(y)} D(x, y) e^{-i\alpha(x)} \tag{1.3}$$

This then ensures that $D(x, y)\psi(y)$ has the same transformation as $\psi(x)$. Using this we can construct a covariant derivative which has the correct transformation properties,

$$n^\mu D_\mu \psi = \lim_{\epsilon \to 0} \frac{1}{\epsilon} (\psi(x + \epsilon n) - D(x + \epsilon n, x)\psi(x)) \tag{1.4}$$

where we have defined an arbitrary direction n^μ in which the derivative acts. We can perform a Taylor expansion on $D(x + \epsilon n, x)$

$$D(x + \epsilon n, x) = 1 - ig\epsilon n^\mu A_\mu(x) + \mathcal{O}(\epsilon^2). \tag{1.5}$$

The coefficient of the displacement ϵn^μ is a new vector field A_μ, which we use to build the covariant derivative,

$$D_\mu \psi(x) = \partial_\mu \psi(x) + igA_\mu \psi(x). \tag{1.6}$$

Inserting the Taylor series expansion into the transformation equation eq. (1.3) we observe that the vector field A_μ must transform in the following way

$$A_\mu(x) \to A_\mu(x) - \frac{1}{g} \partial_\mu \alpha(x). \tag{1.7}$$

We can verify that $D_\mu \psi(x)$ now behaves as we would wish,

$$\begin{aligned} D_\mu \psi(x) &\to \left[\partial_\mu + ig \left(A_\mu - \frac{1}{g} \partial_\mu \alpha \right) \right] e^{i\alpha(x)} \psi(x) \\ &= e^{i\alpha(x)} (\partial_\mu + igA_\mu) \psi(x) \end{aligned} \tag{1.8}$$

such that $\gamma^\mu \overline{\psi} D_\mu \psi$ is now gauge invariant as required. We observe that the new term in the Lagrangian is none other than the interaction term in the QED Lagrangian. We now check that the kinetic term for the photon is also gauge invariant. This is

easy to show since upon inserting eq. (1.7) into the definition of the field strength tensor,

$$F_{\mu\nu} = \partial_\mu A_\nu - \partial_\nu A_\mu \rightarrow \partial_\mu(A_\nu - \frac{1}{g}\partial_\nu\alpha) - \partial_\nu(A_\mu - \frac{1}{g}\partial_\mu\alpha)$$
$$= F_{\mu\nu} - \frac{1}{g}(\partial_\mu\partial_\nu + \partial_\nu\partial_\mu)\alpha = F_{\mu\nu} \tag{1.9}$$

we observe that $F_{\mu\nu}$ is invariant under gauge transformations. Since $\mathcal{L}_{Maxwell} = -\frac{1}{4}F^{\mu\nu}F_{\mu\nu}$ the QED Lagrangian is clearly gauge invariant.

It is also simple to see that a photon mass term, $m^2A^\mu A_\mu$ is manifestly not gauge invariant, thus gauge invariance requires that $m_\gamma = 0$. We shall see that problems associated with generating a mass term for a vector field motivates the introduction of the Higgs shortly.

In summary, we observed that if we wish to create a field theory for Dirac fermions which is manifestly invariant under local phase rotations, we needed to introduce an additional vector field A_μ which through its coupling to the fermions allows the derivative to possess the correct transformation properties. Remarkably this new term in the Lagrangian is exactly that which in QED is associated with the photon - fermion - fermion vertex. Eq. (1.2) is actually an example of a mathematical group known as $U(1)$. A natural extension to the above example is to generalise the principle of constructing gauge invariant Lagrangians to include other mathematical groups. We will show that the invariance under $SU(N)$ transformations can be used to construct the Lagrangians of QCD and indeed the entire SM Lagrangian.

$SU(N)$ gauge invariance

In the previous discussion we constructed a Lagrangian based upon the principle of invariance under local phase rotations, here we wish to generalise the approach to include transformations of the form,

$$\psi(x) \rightarrow V(x)\psi(x) \tag{1.10}$$

and now we allow $V(x)$ to become an $n \times n$ unitarity matrix, implying that fields $\psi(x)$ form an n-plet. In general one can expand an infinitesimal transformation as

follows,

$$V(x) = 1 + i\alpha^a t^a + \mathcal{O}(\alpha^2). \tag{1.11}$$

Here t^a is a matrix and the set of t's are the basic generators of the symmetry group. Indeed since $V(x)$ is unitarity we find that

$$V(x)V^\dagger(x) = 1 \implies t^a - (t^\dagger)^a = 0 \tag{1.12}$$

so t^a are Hermitian. A continuous group with Hermitian operators of this kind is known as a Lie group and the vector space spanned by the generators defined with the following commutation relation,

$$[t^a, t^b] = if^{abc}t^c \tag{1.13}$$

defines a Lie algebra. Here f^{abc} are called the structure constants of the group. Lie groups can be quite diverse but in this discussion we restrict ourselves to the group of $N \times N$ unitary matrices with determinants equal to 1 ($SU(N)$). These theories were first studied by Yang and Mills [14], hence the resulting gauge invariant $SU(N)$ Lagrangian is referred to as the Yang-Mills Lagrangian. The traceless Hermitian matrices t^a define the fundamental representation of the group, and it is this representation which will govern how fermions will transform given an infinitesimal transformation. The structure constants f^{abc} define the adjoint representation of the group and it is this representation that determines how vector bosons transform. We also note that if the structure constants all vanish (an example of which is the $U(1)$ gauge group) then the group is called Abelian. If however, there are non-zero commutation relations between group generators the group is non-Abelian. We shall see presently that this has a huge effect on the physics of a gauge theory.

Now that we have defined the properties of the groups with which we want physics to be invariant under, we must define the infinitesimal field transformations and gauge invariant combinations of fields that can be used to construct Lagrangians.

The generalisation of the covariant derivative eq. (1.6) is straightforward,

$$D_\mu = \partial_\mu - igA^a_\mu t^a. \tag{1.14}$$

The covariant derivative simply contains a vector field for each generator of the representation. The infinitesimal field transformations have the following form,

$$\psi \rightarrow (1 + i\alpha^a t^a)\psi, \tag{1.15}$$

$$A^a_\mu \rightarrow A^a_\mu + \frac{1}{g}\partial_\mu \alpha^a + f^{abc} A^b_\mu \alpha^c, \tag{1.16}$$

and the finite transformation of A^a_μ ensures the correct transformation of the covariant derivative,

$$A^a_\mu(x)t^a \rightarrow V(x)\left(A^a_\mu(x)t^a + \frac{i}{g}\partial_\mu\right)V^\dagger(x) \tag{1.17}$$

The field strength for a non-Abelian theory extends that of QED,

$$F^a_{\mu\nu} = \partial_\mu A^a_\nu - \partial_\nu A^a_\mu + g f^{abc} A^b_\mu A^c_\mu. \tag{1.18}$$

Using the transformation of the vector field eq. (1.17) we find that under a gauge transformation,

$$F^a_{\mu\nu} t^a \rightarrow V(x) F^a_{\mu\nu} t^a V^\dagger(x). \tag{1.19}$$

In contrast to the abelian case the field strength tensor is no longer separately gauge invariant, however traces of $F^a_{\mu\nu}t^a$ will always be gauge invariant (because of the cyclic nature of traces). Hence we can construct gauge invariant terms by considering traces of $F^a_{\mu\nu}t^a$'s. The Yang-Mills Lagrangian then has the following form,

$$\mathcal{L}_{SU(N)} = \overline{\psi}(i\not{D})\psi - \frac{1}{2}(F^i_{\mu\nu})^2 - m\overline{\psi}\psi \tag{1.20}$$

In the above we have used the normalised the colour matrices using $\mathrm{tr}(t^a t^b) = \delta^{ab}$, which differs from Peskin and Schroeder [6] by a factor of 1/2. The major difference between the QED Lagrangian and the Yang-Mills Lagragian above is the presence of three- and four-point vertices which couple vector bosons to themselves. In QED there are no such vertices and the resulting changes in physics are remarkable. Asymptotic freedom, (meaning that the colour charge grows weaker with increasing energy) is a result of these vertices and is responsible for confinement of coloured particles.

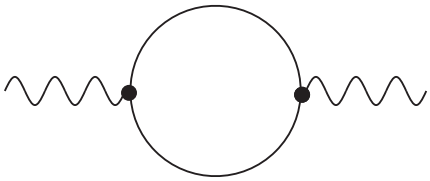

Figure 1.1: A simple one-loop Feynman diagram

We have now described all the pieces needed to construct guage-invariant Lagrangians and hence build the SM. All that remains to do is to define the particular gauge group in which represents the various theories of nature. As we have shown, QED arises naturally from a $U(1)$ gauge group where g, the coupling of matter to photons, is given by the electric charge of the fermions. The strong force described by Quantum Chromodynamics (QCD) was over time shown to be described by an $SU(3)$ non-Abelian gauge theory[2]. The weak force is more subtle. Over time it was established that the weak force was chiral in nature (i.e. it coupled to particles depending on their spin orientation relative to the direction of motion) and that the desired gauge group to describe the theory was $SU(2)$. The problem of assigning a mass to the W and Z vector bosons in a gauge-invariant way resulted in the concept of electroweak symmetry breaking, which we will discuss in section 1.2. First we review a couple of other topics which are relevant to the work performed in this thesis, the regularisation of loop amplitudes and the kinematics of a hadronic collision.

1.1.2 Regularisation of UV and IR divergences

In this section we briefly describe the concepts regarding the regularisation of loop amplitudes in quantum field theories. The need arises for regularisation when one moves beyond the calculation of tree-level (0-loop) amplitudes. When one considers loop diagrams it is simple to see that one can assign any momentum to a loop particle in the diagram. This results in the need to integrate over all allowed momenta when one considers a loop diagram. One of the simplest non-trivial loop diagrams is the

[2]For a nice historical overview of QCD see [15].

bubble diagram shown in Fig 1.1. Application of the Feynman rules and reduction of intermediate tensor integrals [16] would ultimately lead to the following sort of term,

$$I_2^{4D} = \int \frac{d^4\ell}{(2\pi)^4} \frac{1}{(\ell^2)(\ell - P)^2} \tag{1.21}$$

This diagram diverges as $\ell \to \infty$ (known as UV divergence) and to expose the singularity structure of the integral we wish to regularise the integral at intermediate stages. By far the most popular method of regularisation is that of dimensional regularisation, first proposed by 't Hooft and Veltman [17]. In this approach one alters the number of spacetime dimensions to $4 - 2\epsilon$. Singularities then reveal themselves as inverse powers of ϵ. This method has numerous advantages, including maintaining gauge-invariance and regularising both UV ($\ell \to \infty$) and IR ($\ell \to 0$) singularities at the same time. This point needs some clarification since these singularities arise from different sources, a UV singularity occurs when the powers of ℓ in the numerator dominate as $\ell \to \infty$. To regularise these divergences we would wish to define $\epsilon > 0$. Clearly the situation is reversed for IR singularities, where the denominator dominates and we would wish that $\epsilon < 0$. However, in practical calculations one can define $\epsilon > 0$, reguarlise and renormalise (which will be explained shortly) the UV singularities and then analytically continue to $\epsilon < 0$, which regulates the remaining IR singularities.

How one treats external particles is up to the discretion of the calculator, and several schemes exist and are related to each other by predictable quantities. In this thesis unless stated we will work in the four-dimensional helicity scheme (FDH). This allows us to keep external particles strictly in four-dimensions, whilst only the loop momenta (and the metric) are D-dimensional. The t'Hooft-Veltman scheme [17] defines γ^μ in d dimensions with $\gamma^5 = i\gamma^0\gamma^1\gamma^2\gamma^3$ defined such that it anticommutes with γ^μ for $\mu \in \{0, 1, 2, 3\}$ and commutes with γ^μ for all other μ.

Of course one does not expect to predict infinite cross sections, and this certainly is not what is observed at colliders! Ultimately we wish to remove the singularities in ϵ and there are systematic ways of doing this. Ultraviolet divergences can be removed by a process known as renormalisation. Basically the physical quantities written in

the Lagrangian such as charges and masses are not the true physical quantities observed in nature. At each loop order one must calculate counterterms which are absorbed into the masses and charges. When combined with divergent integrals these counter terms lead to (UV) finite amplitudes at each order in perturbation theory. Infra-red divergences arise from two sources, when $\ell^2 \to 0$ in a loop amplitude and when an external (spin-1) particle becomes soft ($E_0 \to 0$) or collinear to another external particle[3]. In the second case, an $(n+1)$ parton amplitude is observationally equivalent to an n parton amplitude. In the first case the loop particle does not affect the momentum flow of the diagram and the n parton m loop amplitude tends towards an n parton $(m-1)$ loop amplitude. Therefore we see that in an IR region one can combine $(n+1)$ parton $(m-1)$-loop amplitudes with n-parton m loop amplitudes, resulting in IR pole cancellation. This procedure works systematically at all loop orders [18–20] and in our case we will need to combine $(n+1)$ parton tree level amplitudes with n-parton one-loop amplitudes.

1.1.3 An overview of a hadronic collision

In this section we provide an extremely brief overview of a particle collision in an hadronic environment. We discuss factorisation of QCD amplitudes, jets and hadronisation.

Factorisation and cross sections

A hadronic collider such as the Tevatron or the LHC collides composite objects rather than fundamental particles (such as electrons and positrons at LEP). In general a cross-section for a physical observable can be obtained from the following formula [7, 21],

$$\sigma(S) = \sum_{i,j} \int dx_1 dx_2 f_i(x_1, \mu^2) f_j(x_2, \mu^2) \hat{\sigma}_{ij}(\hat{s} = x_1 x_2 S, \alpha_S(\mu^2), \frac{Q^2}{\mu^2}) \qquad (1.22)$$

[3]Quark pairs can also produce collinear singularities through $q\overline{q} \to g$.

and explaining the various terms in this formula is the goal of this section. Calculating quantities in QCD is considerably more difficult than those in QED, primarily because we do not observe isolated coloured particles, but instead we observe colourless bound states (hadrons). At a certain scale ($\approx \Lambda_{QCD} \sim 1$ GeV) hadronisation occurs resulting in the varied spectrum of baryons and mesons observed in detectors. The problem is exacerbated by the fact that we initially collide hadrons! How can we make predictions using perturbation theory when we are colliding bound states?

Fortunately, the situation is not as bad as may be first thought. Factorisation allows us to split up the various problems associated with the different physical scales in the problem. This factorisation is apparent in eq. (1.22). The scattering which occurs at high energies (hard scale) is calculated using perturbation theory ($\hat{\sigma}$), the scale μ represents the factorisation scale below which interactions are absorbed into f_i, the parton-distribution functions (PDFs). The PDFs incorporate both perturbative and non-perturbative physics and can be thought of as the probability of extracting a parton of type i with a momentum fraction x_1 of the total proton momentum. PDF's are calculated from both experimental data and theoretical predictions [22–26] and as result are quoted in terms of the order of perturbation theory with which they are matched to. Currently Next-to-Next-to Leading Order (NNLO) PDF's are available, in this thesis we use the (LO or NLO) MSTW08 PDF sets [22].

The strategy to generate a partonic cross section is now clear. One firsts calculates the partonic cross section for the hard process of interest. Then to produce a cross section which can be compared with experiment one must convolve the partonic cross section with the PDFs and integrate over x_i, the partonic momenta fraction. This deals with the issue of colliding bound states. However the final states produced in a hadronic collision are predominately coloured objects. The issues associated with hadronisation are considered in the next section.

Showers and jets

Immediately upon looking at an image of a high-energy collision one can spot a collection of hadrons which are grouped into a roughly cone sized area. These hadrons, which have travelled roughly collinear to each other, are known as jets. Therefore, to compare theory to experiment one needs a suitable jet algorithm to define exactly what is meant by a jet and the properties it has. Several jet algorithms exist [27–31], the one we will use in this thesis is known as the k_T algorithm and works in the following way [32]:

- The algorithm begins with a set of preclusters, which for our theoretical calculations with MCFM means partons. Each precluster is expressed in the following form

$$(E, \mathbf{p}) = E(1, \cos\phi \sin\theta, \sin\phi \sin\theta, \cos\theta) \tag{1.23}$$

  where E is the precluster energy and ϕ and θ are the azimuthal and polar angles respectively.

- For each precluster define the square of the transverse momenta and rapidity,

$$d_i^2 = p_{T,i}^2, \quad p_T^2 = p_x^2 + p_y^2 \quad \text{and} \quad y = \frac{1}{2}\ln\frac{E + p_z}{E - p_z}, \tag{1.24}$$

- For each pair (i, j) $(i \neq j)$ of preclusters define,

$$\begin{aligned} d_{ij} &= \min(p_{T,i}^2, p_{T,j}^2)\frac{\Delta R_{ij}^2}{D^2} \\ &= \min(p_{T,i}^2, p_{T,j}^2)\frac{(y_i - y_j)^2 + (\phi_i - \phi_j)^2}{D^2} \end{aligned} \tag{1.25}$$

  where $D \approx 1$ is a parameter of the jet algorithm.

- Find the minimum of all the d_i and d_{ij} and call it d_{min}.

- If d_{min} is a d_{ij} remove preclusters i and j from the list and replace them with a new merged precluster (E_{ij}, p_{ij}), given by

$$\begin{aligned} E_{ij} &= E_i + E_j \\ \mathbf{p_{ij}} &= \mathbf{p_i} + \mathbf{p_j} \end{aligned} \tag{1.26}$$

- If d_{min} is a d_i then the precluster is not mergeable, remove precluster from the list and define it as a jet.
- Continue until no preclusters remain.

We observe that the algorithm produces a list of jets which are separated by $\Delta R > D$ and that this algorithm can be applied equally well to theoretical calculations or experimental data.

Perturbation theory naturally produces amplitudes containing a fixed number of partons, however the naive approximation that a jet is represented by a single hard parton (at higher orders in perturbation theory this is somewhat improved) is not reproduced in nature. The multiple emissions of partons in the soft and collinear regions (which then hadronise to form jets) are modeled theoretically by a parton shower [4]. Parton showers are a key element in Monte Carlo event generators, which for the most part merge [33] leading order matrix elements with parton showers and hadronisation to form a realistic prediction of particle physics collision. Some modern examples are HERWIG [34–36], SHERPA [37, 38] and PYTHIA [39, 40].

1.2 Electroweak Symmetry Breaking

The study of electroweak symmetry by spontaneously broken symmetries originally started in the 1960's [41–45]. Yet the search for the Higgs is only now, nearly fifty years later, reaching its climax. In this section we introduce the main features of the Higgs mechanism and briefly review some Higgs phenomenology.

1.2.1 Spontaneous breaking of $O(N)$ symmetries, Goldstone bosons

In this section we introduce the main aspects of a gauge theory which is spontaneously broken showing how within these theories gauge bosons naturally acquire a

[4] for an overview of parton showers see Chapter 5 of [7]

mass. We follow [6] and begin by describing spontaneous symmetry of a continuous symmetry first before moving onto discuss the breaking of gauge symmetries. We consider the following Lagrangian consisting of a set of N real scalar fields $\phi^i(x)$,

$$\mathcal{L}_{LS} = \frac{1}{2}(\partial_\mu \phi^i)^2 + \frac{1}{2}\mu^2(\phi^i)^2 - \frac{\lambda}{4}[(\phi^i)^2]^2 \tag{1.27}$$

which is known as the linear sigma model. Here we choose $\lambda, \mu^2 > 0$. The above Lagrangian is invariant under the group of orthogonal rotations $O(N)$,

$$\phi^i \to R^{ij}\phi^j \tag{1.28}$$

The lowest-energy classical configuration is a constant field ϕ_0^i whose value minimises the potential,

$$V(\phi^i) = -\frac{1}{2}\mu^2(\phi^i)^2 + \frac{\lambda}{4}[(\phi^i)^2]^2 \tag{1.29}$$

ϕ_0^i satisfies,

$$(\phi_0^i)^2 = \frac{\mu^2}{\lambda} \tag{1.30}$$

We observe that this constraint merely fixes the length of the vector ϕ_0^i, its direction is arbitrary. We choose coordinates such that ϕ_0^i points in the N-th direction,

$$\phi_0^i = (0, 0, \ldots, 0, v), \tag{1.31}$$

where $v = \mu/\sqrt{\lambda}$. We now choose to expand the fields around the lowest energy solution,

$$\phi^i(x) = (\pi^k(x), v + \sigma(x)), \quad k = 1, \ldots N-1 \tag{1.32}$$

Written in terms of these fields the Lagrangian takes the following form,

$$\begin{aligned}\mathcal{L}_{LS} = \frac{1}{2}(\partial_\mu \pi^k)^2 + \frac{1}{2}(\partial_\mu \sigma)^2 - \frac{1}{2}(2\mu^2)\sigma^2 - \sqrt{\lambda}\mu\sigma^3 - \sqrt{\lambda}\mu(\pi^k)^2 \\ -\frac{\lambda}{4}\sigma^4 - \frac{\lambda}{2}(\pi^k)^2\sigma^2 - \frac{\lambda}{4}[(\pi^k)^2]^2.\end{aligned} \tag{1.33}$$

We note the appearance of one massive field σ and $N-1$ massless fields π^k. The original symmetry group of the Lagrangian $O(N)$ is no longer apparent, there is only an $O(N-1)$ symmetry which rotates π^k fields amongst themselves. In this

example we have spontaneously broken the $O(N)$ continuous symmetry by choosing to express the ground state in terms of a particular direction in ϕ space. The remaining symmetry is $O(N-1)$ so we would describe this breaking as $O(N) \rightarrow O(N-1)$.

The appearance of massless fields as a result of spontaneous symmetry breaking is a general result of theorem proven by Goldstone [46, 47]. Goldstone's theorem states that for every spontaneously broken continuous symmetry the theory must contain a massless particle. In the above example the original symmetry $O(N)$ had $(N(N-1))/2$ symmetries, when it was broken to $O(N-1)$ this changed to $(N-2)(N-1)/2$. This resulted in a loss of $N-1$ symmetries, hence we observed $N-1$ Goldstone bosons.

1.2.2 Spontaneous breaking of scalar QED

Next we consider the following Lagrangian which couples a complex scalar to itself and to an electromagnetic field,

$$\mathcal{L} = -\frac{1}{4}(F_{\mu\nu})^2 + |D_\mu \phi|^2 - V(\phi) \tag{1.34}$$

where $D_\mu = \partial_\mu + ieA_\mu$. As can be seen from the discussion of section 1.1.1 the Lagrangian is invariant under the following $U(1)$ transformations (provided $V(\phi)$ is a function of $\phi^*\phi$),

$$\phi(x) \rightarrow e^{i\alpha(x)}\phi(x), \quad A_\mu(x) \rightarrow A_\mu(x) - \frac{1}{e}\partial_\mu \alpha(x). \tag{1.35}$$

An interesting, and relevant choice of potential is the following

$$V(\phi) = -\mu^2 \phi^*\phi + \frac{\lambda}{2}(\phi^*\phi)^2. \tag{1.36}$$

In exactly the same manner as the previous section when $\mu^2 > 0$ there is a non-zero vacuum expectation value (vev),

$$\langle \phi \rangle = \phi_0 = \left(\frac{\mu^2}{\lambda}\right)^{1/2}. \tag{1.37}$$

When we expand $\phi(x)$ areound the vacuum state,

$$\phi(x) = \phi_0 + \frac{1}{\sqrt{2}}(\phi_1(x) + \phi_2(x)) \tag{1.38}$$

the potential takes the following form,

$$V(\phi) = -\frac{1}{2\lambda}\mu^4 + \frac{1}{2}(2\mu^2)\phi_1^2 + \mathcal{O}(\phi_i^3). \tag{1.39}$$

We note that ϕ_1 gains the mass $\sqrt{2}\mu$ and ϕ_2 is the massless Goldstone boson. Until now the discussions of this section and that preceding it have been identical. However, this Lagrangian contains a covariant derivative linking ϕ to the electromagnetic field A_μ, and we must also inspect what happens to this term in the Lagrangian as a result of the symmetry breaking.

$$|D_\mu\phi|^2 = \sum_{i=1}^{2}\frac{1}{2}(\partial_\mu\phi_i)^2 + \sqrt{2}e\phi_0 A_\mu\partial^\mu\phi_2 + e^2\phi_0^2 A^\mu A_\mu + \dots \tag{1.40}$$

where $\dots$ represent cubic and quartic interactions of the fields. The piece we are most interested in is

$$\mathcal{L}_{m_A} = \frac{1}{2}m_A^2 A^\mu A_\mu = e^2\phi_0^2 A^\mu A_\mu \tag{1.41}$$

i.e. the photon has acquired a mass which is proportional to the vacuum expectation value ϕ_0. This illustrates how the mechanism of spontaneous symmetry breaking can be responsible for the W and Z vector boson masses. The question remains as to the specific gauge group to break to correctly generate the observed spectrum of vector boson masses.

1.2.3 The Higgs mechanism

Merely breaking the group $SU(2)$ does not generate the correct spectrum of masses observed in nature, one can generate either three identical mass vector bosons or two identical and one massless vector boson depending on the representation of the scalar field. However when we couple the scalar to both $SU(2)$ and $U(1)$ fields we can correctly generate massive bosons with different masses. A beautiful feature of breaking $SU(2)\times U(1)$ is that there is also one residual massless boson with a $U(1)$ gauge symmetry. This naturally becomes electrodynamics, and as result the weak and electrodynamic forces can be unified into the larger gauge group.

In terms of $SU(2)\times U(1)$ gauge theory the covariant derivative for ϕ is

$$D_\mu\phi = (\partial_\mu - igA_\mu^a - i\frac{1}{2}g'B_\mu)\phi \tag{1.42}$$

We note that the since the $SU(2)$ and $U(1)$ gauge factors commute with each other, they can have different coupling constants. We also note that we have assigned a charge of $1/2$ to the scalar under the $U(1)$ symmetry and this is to eventually ensure that the scalar remains electrically neutral. Assuming that the field acquires a vev of the form

$$\langle\phi\rangle = \frac{1}{\sqrt{2}}\begin{pmatrix} 0 \\ v \end{pmatrix}, \tag{1.43}$$

then gauge transformations of the form

$$\phi \rightarrow e^{i\alpha^a\tau^a}e^{i\beta/2}\phi \tag{1.44}$$

with $\alpha^1 = \alpha^2 = 0$, $\alpha^3 = \beta$ leaves the vev invariant. It is this invariance to a particular combination of generators which leaves one of the vector bosons massless. When we expand the quadratic terms in the Lagrangian we find,

$$\mathcal{L}_{mass} = \frac{1}{2}\frac{v^2}{4}[g^2(A^1_\mu)^2 + g^2(A^2_\mu)^2 + (-gA^3_\mu + g'B_\mu)^2], \tag{1.45}$$

resulting in three massive vector bosons,

$$W^\pm_\mu = \frac{1}{\sqrt{2}}(A^1_\mu \pm iA^2_\mu), \qquad m_W = g\frac{v}{2}, \tag{1.46}$$

and

$$Z^0_\mu = \frac{1}{\sqrt{g^2+g'^2}}(gA^3_\mu - g'B_\mu), \quad m_Z = \sqrt{g^2+g'^2}\frac{v}{2}. \tag{1.47}$$

The remaining combination of vector fields is the massless photon,

$$A_\mu = \frac{1}{\sqrt{g^2+g'^2}}(gA^3_\mu + g'B_\mu) \quad m_A = 0 \tag{1.48}$$

We have seen how spontaneously breaking symmetries can result in the spectrum of masses observed in nature. The unified theory of electroweak interactions makes predictions about the relationship between the W and Z boson, masses, in particular it produces a larger Z mass naturally. To successfully break the symmetry one needed to introduce a new scalar field into the Standard Model. This field transforming in the $SU(2)\times U(1)$ gauge group has a potential with the correct parameters to introduce a non-zero vev to the theory. The physical manifestation of this new scalar is the Higgs boson. In the remainder of this chapter we will discuss Higgs phenomenology at colliders and introduce the gluon-Higgs effective coupling.

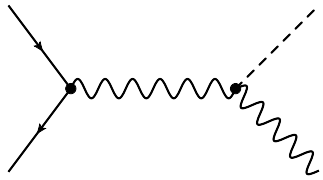

Figure 1.2: A sample Higgsstrahlung diagram in which the Higgs boson is radiated from a massive Z vector boson. Since the Higgs-electron coupling is small this was the dominant Higgs production mechanism at LEP.

1.3 Higgs searches at colliders

In this section we describe the results of various searches for the Higgs boson at different colliders. We discuss the current lowest bound on the Higgs mass, which comes from LEP. We also discuss the exclusion region around $2m_W$ observed by the Tevatron, and discuss search strategies and potentials at the LHC.

1.3.1 Higgs searches at LEP

The Large Electron-Positron (LEP) collider operated at CERN between 1989 and 2000, colliding electrons and positrons with a centre of mass energy between 90 and 209 GeV. Its Higgs searches focused primarily on direct production whilst precision measurements of the W and Z mass allowed constraints to be placed on m_H through quantum effects. These indirect searches constrained $m_H < 193\,\mathrm{GeV/c^2}$ at the 95% confidence level and favoured a mass in the range $81^{+51}_{-33}\,\mathrm{GeV/c^2}$ [48].

Direct production of a Higgs boson at a lepton collider is made more difficult since the colliding particles have very small couplings to the Higgs (since the coupling is proportional to the mass of the particle). This means that the dominant production mechanism of a Higgs boson at a lepton collider is through the Higgsstrahlung process, (in which a Higgs is radiated from a Z boson) for which a sample diagram is shown in Fig. 1.2 [49,50]. For the range of Higgs boson masses which were relevant for the LEP studies the Higgs predominately decayed to $b\overline{b}$ pairs (with a branching

ratio of 74%). The branching ratios for the decays to $\tau^+\tau^-$, WW^* and gg are around 7% with the remaining $\approx 4\%$ decay to $c\overline{c}$.

The final states which were included in the final combined analyses [51–55] were the four-jet final state $(H \to b\overline{b})(Z \to q\overline{q})$, the missing energy final state $(H \to b\overline{b})(Z \to \nu\overline{\nu})$, the leptonic final state $(H \to b\overline{b})(Z \to \ell^+\ell^-)$ $\ell \in \{e, \mu\}$ and the tau lepton final states, $(H \to b\overline{b})(Z \to \tau^+\tau^-)$ and $(H \to \tau^+\tau^-)(Z \to q\overline{q})$. The result of the combined direct searches, [51] was a limit on the lightest a SM Higgs boson could be. They found a lower bound of $114.4\,\mathrm{GeV/c^2}$ at the 95% confidence level. Fig. 1.3 summarises these results.

1.3.2 Higgs searches at the Tevatron and the LHC

The two colliders currently searching for the Higgs boson, Fermilab's Tevatron and CERN's LHC are both hadronic colliders (the Tevatron collides protons and antiprotons, the LHC collides protons). As such the main Higgs production mechanisms are completely different from those at LEP and are shown in Figs. 1.4-1.5, the larger energy associated with these colliders also introduces new Higgs decay modes, which are shown in Fig. 1.6.

The dominant production mechanism at both colliders occurs through the gluon fusion process, which is the main topic of the next section. It is interesting to note the differences between the subdominant production mechanisms between the colliders. At the Tevatron the second largest source of Higgs bosons occurs through W and Z Higgsstrahlung, the quark equivalent of the main process at LEP. However, at the LHC it is Vector-boson fusion (VBF or sometimes referred to as WBF) which is the sub-dominant process. This is not merely due to the difference in centre of mass energies between the colliders, but due to the fact that in an anti-proton there are more valence anti-quarks than in a proton and as result processes in which quark annihilation occur are favoured at the Tevatron.

We note that in Fig. 1.6 there is a clear change in Higgs branching ratio around $m_H \approx 130$ GeV below these values the Higgs decays mostly into $b\overline{b}$ pairs, whilst

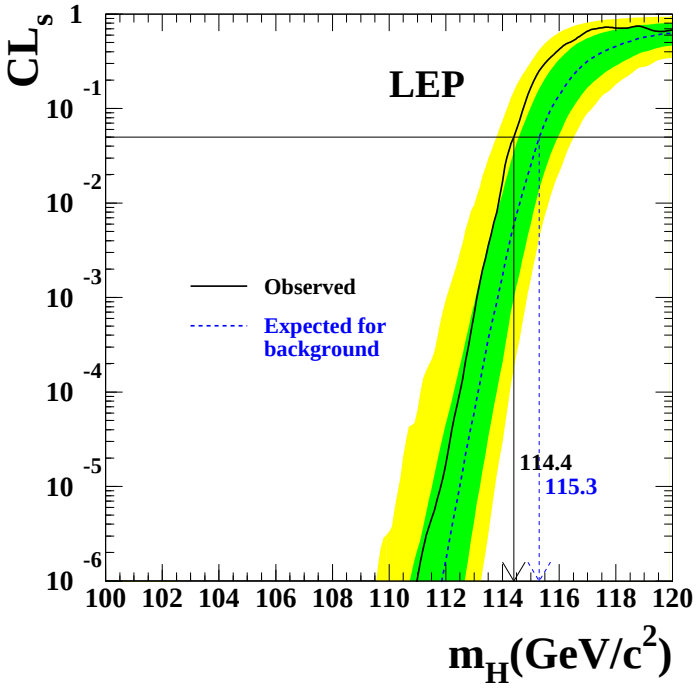

Figure 1.3: Search results from the LEP collaboration [51], the solid line indicates observation, the dashed line indicating the median expectation for the background. The dark shaded bands indicate the 68% and 95% probability bands. The intersection of the horizontal line for $CL_s = 0.05$ with the observed curve is used to define the 95% confidence lower bound on m_H.

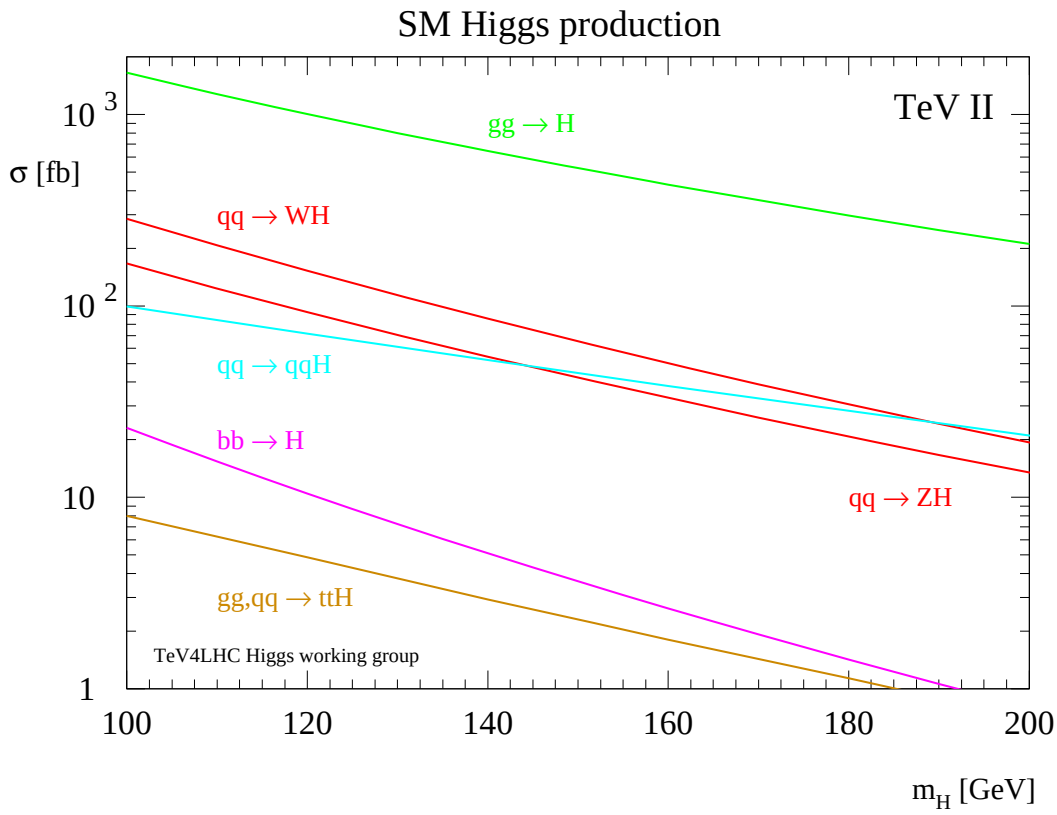

Figure 1.4: Higgs production at the Tevatron (taken from [56]), Run II of the Tevatron collides protons and anti-protons at a centre of mass energy of 1.96 TeV. The dominant production mechanism is gluon fusion. The second most dominant mechanism is W Higgsstrahlung, followed by Vector-boson-fusion (VBF).

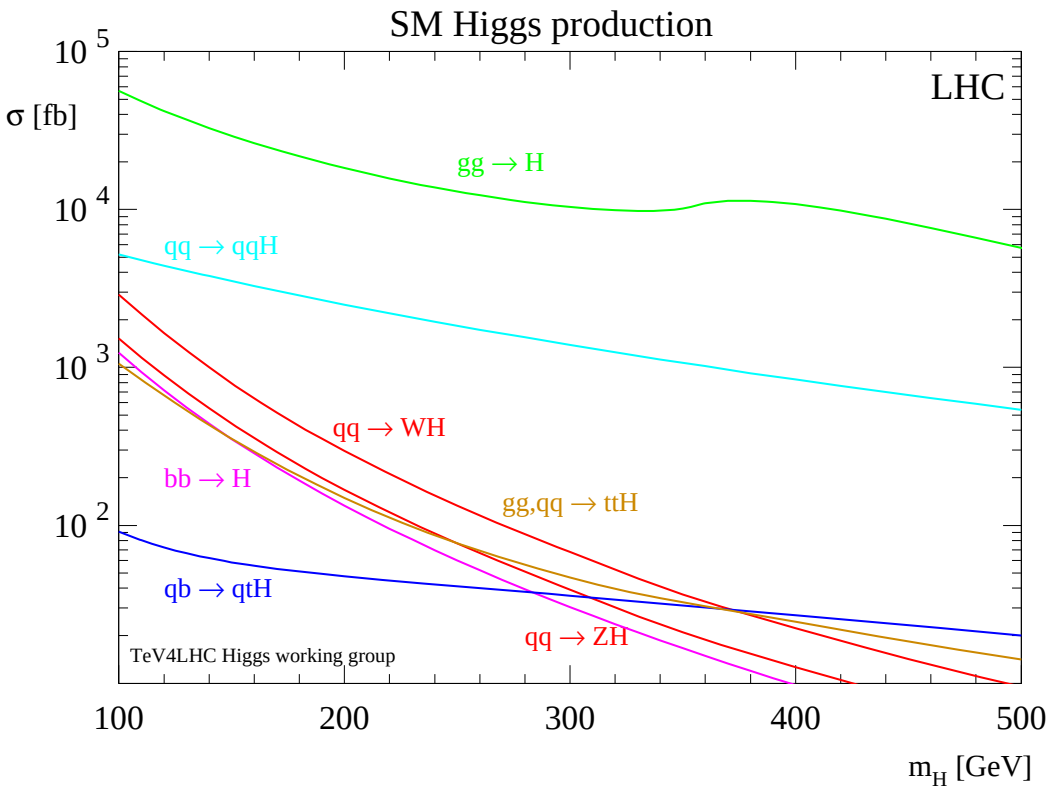

Figure 1.5: Higgs production at the LHC (taken from [56]) for a design centre of mass energy of 14 TeV. In a similar fashion to the Tevatron gluon fusion dominates over all other channels, however, for the LHC VBF is now the subdominant channel and Higgsstrahlung is suppressed.

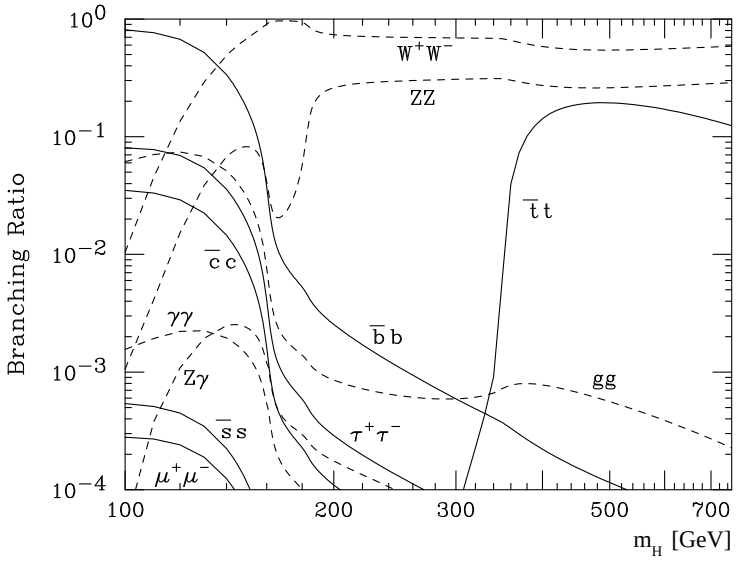

Figure 1.6: Higgs decay modes for an interesting range of Higgs masses [56, 57]. For light Higgs bosons ($m_H \lessapprox 130$ GeV) $b\bar{b}$ is the dominant decay mode. For all other masses W^+W^- dominates, for large masses $t\bar{t}$ becomes an important cannel.

above these masses the Higgs decays preferentially into W^+W^-. This latter channel with leptonic W decay is much cleaner at hadron colliders since in an hadronic environment picking out QCD decays of the Higgs is extremely difficult due to the large irreducible backgrounds.

The peak in the $H \to W^+W^-$ spectrum around $m_H \approx 2m_W$ gives a particular sensitivity to a Higgs boson in this mass range. Indeed the Tevatron has recently produced results [58] which exclude a Higgs boson in the mass range 162-166 GeV at the 95% CL. This is based on the combined analysis [58] of 4.8 [59] (CDF) and 5.4 [60] (D0) fb^{-1} data sets. The experiments investigated events with large missing transverse energy and two oppositely charged leptons, targeting the $H \to W^+W^-$ signal, in which both Ws decay leptonically. The results are shown in Fig. 1.7. It should be noted that in this analysis theoretical predictions for the Higgs cross section play a crucial role, which we will talk more about in Chapter 6. Very recently, [61] the combined CDF (5.9) fb^{-1} and D0 (6.7) fb^{-1} results have been published, increasing the exclusion limits to $158 < m_H < 175$ GeV/c^2, the results are summarised in Fig 1.8.

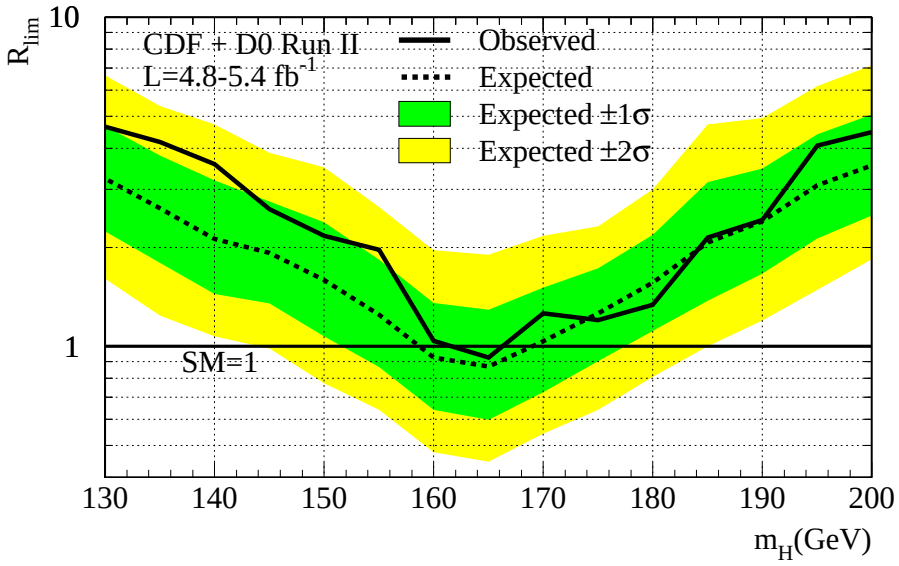

Figure 1.7: Combined CDF and D0 Higgs search results [58]. The sensitivity around $2m_W$ allows an exclusion region to develop around these masses. The exclusion occurs where the observed line falls below the theoretical prediction.

Over the next decade, as the LHC gathers a large enough data set, the Higgs boson will either be observed or excluded in the theoretically acceptable region. Like the Tevatron, the LHC will be more sensitive to a heavy Higgs [62], however it should gather a enough data to allow even very rare decays (but experimentally favourable) of light Higgs bosons such as $H \to \gamma\gamma$ to be investigated.

1.4 Effective coupling between gluons and a Higgs in the limit of a heavy top quark

1.4.1 Effective Lagrangian

In this section we introduce the effective Lagrangian which couples gluons to the Higgs boson [63–65]. Since the Higgs boson only couples to massive particles the interaction proceeds predominantly through a top quark loop. The dependence on the top mass quickly makes calculations extremely difficult, since at LO in the full

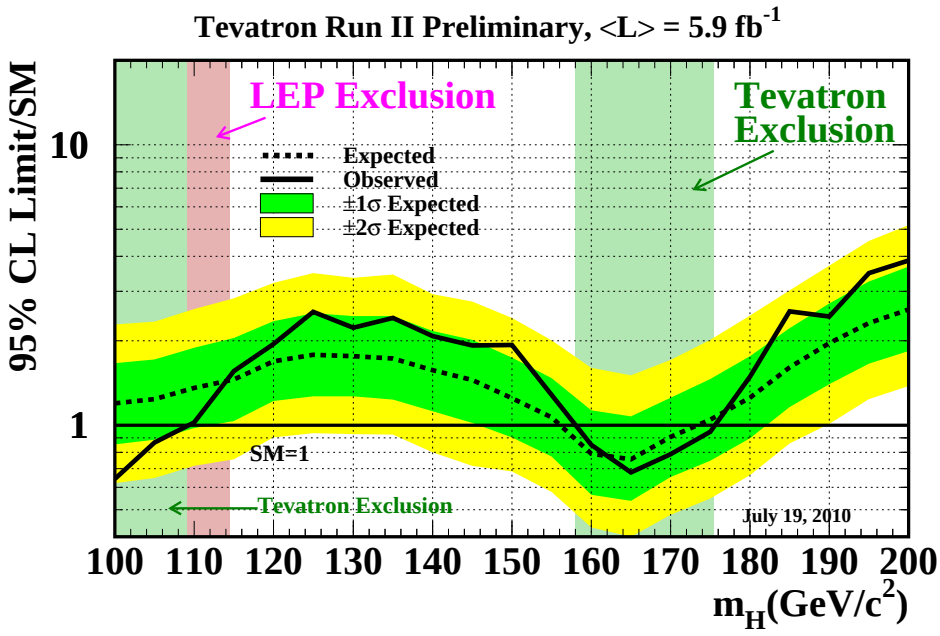

Figure 1.8: Combined CDF and D0 results [61], the increased data set (relative to [58]) has increased the exclusion limit around $2m_W$. The results are also beginning to approach the LEP lower limit on the Higgs mass.

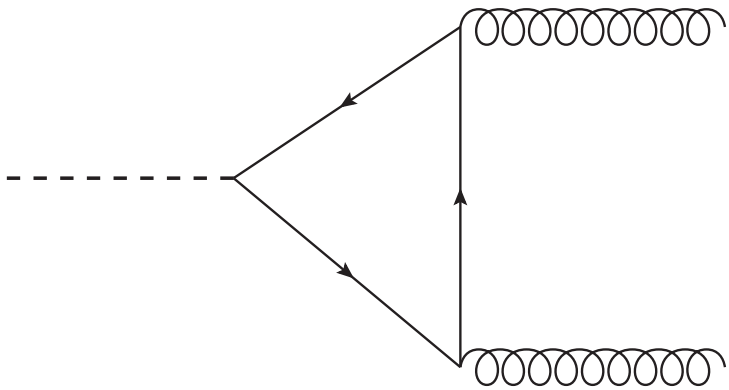

Figure 1.9: The Higgs-gluon coupling in the Standard Model proceeds through a top quark loop, at LO order in the full theory this is the only contributing diagram.

theory one must deal with massive loops and massive external particles. Amplitudes with a Higgs boson and up to four gluons have been calculated at LO in the full theory [66–68]. Processes which allow large amounts of colour annihilation typically have large K factors, and as such we expect NLO contributions to gluon fusion to be large. Since NLO calculations in the full theory involve two loop diagrams with a massive loop, these calculations are formidable. To simplify the problem we can work in an effective theory in which the top mass is sent to infinity [63–65]. This approximation will work well provided that $m_H < 2m_t$. In this effective theory the top loops are integrated out to produce vertices. These vertices arise from higher-dimensional terms in the Lagrangian which directly couple Higgs bosons and gluon field strengths. The first of these terms is five dimensional, successive terms, which are higher dimensional, contain higher powers of gluon field strengths,

$$\mathcal{L}_{eff}^{int} = \frac{1}{2} C H \,\mathrm{tr}\, G^{\mu\nu} G_{\mu\nu} + C' H \,\mathrm{tr}\, G^{\mu}_{\nu} G^{\nu}_{\rho} G^{\rho}_{\mu} + \ldots . \tag{1.49}$$

Since each term in the Lagrangian is ultimately four dimensional we observe that $C' \sim C/m_t^2$, i.e. each of the higher dimensional Lagrangian pieces are suppressed by powers of m_t. Therefore in the $m_t \to \infty$ limit only the first term contributes to Higgs plus gluon amplitudes. $\mathcal{O}(m_H^2/m_t^2)$ corrections can be included by calculating amplitudes using the higher-dimensional pieces of the Lagrangian. One can use these higher-dimensional effective operators to calculate $\mathcal{O}(1/m_t^2)$ corrections to Higgs plus jet amplitudes in the effective theory [69].

To make predictions using the effective theory Lagrangian we must obtain the Wilson coefficient C, this can be done by matching to fixed order calculations in the full theory. In this way one obtains C as a perturbation series in α_S, for example at leading order the (colour stripped) matrix element for $H \to gg$ in the effective theory is,

$$\mathcal{M}^{Eff}(H \to gg) = -iC g_{\mu\nu} p_1 \cdot p_2 \epsilon_1^{*\mu} \epsilon_2^{*\nu} \tag{1.50}$$

where p_i and ϵ_i^* represent the momentum and polarisation vector of gluon i. We can also calculate the $H \to gg$ amplitude in the full theory,where there is only one diagram, the triangle diagram shown in Fig 1.9. In the $m_t \to \infty$ limit the matrix

element takes the following form,

$$\mathcal{M}^{FT}_{m_t\to\infty}(H\to gg) = -i\frac{\alpha_s}{6\pi v}g_{\mu\nu}p_1\cdot p_2\epsilon_1^{*\mu}\epsilon_2^{*\nu}+\dots \tag{1.51}$$

where ... represent pieces which are suppressed in the large top limit. We can determine the coefficient C by matching eq. (1.50) and eq. (1.51).

$$C^{\alpha_S} = \frac{\alpha_S}{6\pi v} \tag{1.52}$$

To compute C to higher orders in α_S one must calculate $\mathcal{M}^{FT}_{m_t\to\infty}(H\to gg)$ at higher loops, The effective coupling C has been calculated up to order $\mathcal{O}(\alpha_s^3)$ in [70]. However, for our purposes we need it only up to order $\mathcal{O}(\alpha_s^2)$ [71],

$$C^{\alpha_S^2} = \frac{\alpha_s}{6\pi v}\left(1+\frac{11}{4\pi}\alpha_s\right)+\mathcal{O}(\alpha_s^3) \tag{1.53}$$

One can also define the following quantity R which is given by the ratio

$$R = \frac{\sigma(H\to gg)}{\sigma_{m_t\to\infty}(H\to gg)}, \tag{1.54}$$

where $\sigma(gg\to H)$ is the total cross section. Setting $x = 4m_t^2/m_H^2$ the correction for the finite mass of the top quark in the region $x > 1$ is [72],

$$R = \left[\frac{3x}{2}\Big(1-(x-1)\Big[\sin^{-1}\frac{1}{\sqrt{x}}\Big]^2\Big)\right]^2. \tag{1.55}$$

This quantity when used to normalise an effective theory cross section provides a good approximation of the cross section from the full theory, see Ref. [66] and references therein.

It has been known for a long time that the radiative corrections to Higgs production through gluon fusion are large [72–74]. These NLO studies showed that going beyond NLO was essential and impressively fully differential cross-sections at NNLO have now been calculated [75–82]. Recent calculations have studied the effect of finite top masses on the NNLO calculations [83–88]. They found them to be reasonably small, indicating that for Higgs production through gluon fusion the effective theory works well. The NNLO results can also be improved by including next-to-next-to-leading logarithmic (NNLL) soft gluon resummation [89] [5].

[5] At the Tevatron this results in an increase in cross section of around 13%.

These calculations have been confirmed by calculation of soft terms to N^{3}LO accuracy [90, 91].

When more partons are considered in the final state top mass effects become more pronounced. It has been shown that top and bottom quark mass effects can play an important role [92] in deviations from the effective theory results [93, 94] for Higgs plus jet calculations at NLO. We discuss the role of additional jets further (with an emphasis on two jets) in section 1.5.

1.4.2 $\phi, \phi^\dagger$ splitting of the Effective Lagrangian

When we look at a simple Higgs plus gluon helicity amplitude at tree-level a hint of structure jumps out at us,

$$A_4^{(0)}(\phi, 1^-, 2^+, 3^-, 4^+) = \frac{\langle 13\rangle^4}{\langle 12\rangle\langle 23\rangle\langle 34\rangle\langle 41\rangle} + \frac{[24]^4}{[12][23][34][41]}. \tag{1.56}$$

Here we have used the spinor helicity formalism, which is described in Appendix A. Eq. (1.56) has a clear structure, if momentum were conserved amongst the gluons ($p_H \to 0$) then the two terms would be conjugates of each other. With this in mind we make the following definitions, [95],

$$\phi = \frac{(H + iA)}{2}, \qquad \phi^\dagger = \frac{(H - iA)}{2}. \tag{1.57}$$

Here A is a massive pseudo-scalar. We also wish to divide the gluon field strength tensor $G^{\mu\nu}$ into self-dual (SD) and anti-self dual (ASD) pieces,

$$G^{\mu\nu}_{SD} = \frac{1}{2}(G^{\mu\nu} + {}^*G^{\mu\nu}) \quad G^{\mu\nu}_{ASD} = \frac{1}{2}(G^{\mu\nu} - {}^*G^{\mu\nu}), \tag{1.58}$$

with

$${}^*G^{\mu\nu} = \frac{i}{2}\epsilon^{\mu\nu\rho\sigma}G_{\rho\sigma}. \tag{1.59}$$

In terms of these definitions the Lagrangian takes the following form,

$$\begin{aligned} \mathcal{L}^{int}_{H,A} &= \frac{C}{2}\left[H\mathrm{tr}G^{\mu\nu}G_{\mu\nu} + iA\mathrm{tr}G^*_{\mu\nu}G^{\mu\nu}\right] \\ &= C\left[\phi\mathrm{tr}G_{SD\,\mu\nu}G^{\mu,\nu}_{SD} + \phi^\dagger\mathrm{tr}G_{ASD\,\mu\nu}G^{\mu,\nu}_{ASD}\right]. \end{aligned} \tag{1.60}$$

The effective interaction linking gluons and scalar fields splits into a piece containing ϕ and the self-dual gluon field strengths and another part linking $\phi^\dagger$ to the anti-self-dual gluon field strengths. The last step conveniently embeds the Higgs interaction within the MHV structure of the QCD amplitudes. The self-duality of ϕ amplitudes also results in them having a simpler structure than Higgs amplitudes. The full Higgs amplitudes are then written as a sum of the ϕ (self-dual) and $\phi^\dagger$ (anti-self-dual) components,

$$A_n^{(l)}(H;\{p_k\}) = A_n^{(l)}(\phi,\{p_k\}) + A_n^{(l)}(\phi^\dagger,\{p_k\}). \tag{1.61}$$

We can also generate pseudo-scalar amplitudes from the difference of ϕ and $\phi^\dagger$ components,

$$A_n^{(l)}(A;\{p_k\}) = \frac{1}{i}\left(A_n^{(l)}(\phi,\{p_k\}) - A_n^{(l)}(\phi^\dagger,\{p_k\})\right). \tag{1.62}$$

Furthermore parity relates ϕ and $\phi^\dagger$ amplitudes,

$$A_n^{(m)}(\phi^\dagger, g_1^{\lambda_1},\ldots,g_n^{\lambda_n}) = \left(A_n^{(m)}(\phi, g_1^{-\lambda_1},\ldots,g_n^{-\lambda_n})\right)^*. \tag{1.63}$$

From now on, we will only consider ϕ-amplitudes, knowing that all others can be obtained using eqs. (1.61)–(1.63). We will discuss tree amplitudes containing a ϕ and partons in Appendix A.

1.5 Higgs plus two jets: Its phenomenological role and an overview of this thesis

As has been mentioned earlier in the chapter, an important search channel for the Higgs boson, in the mass range $115 < m_H < 160$ GeV, is production via weak boson fusion [96]. A Higgs boson produced in this channel is expected to be produced relatively centrally, in association with two hard forward jets. These striking kinematic features are expected to enable a search for such events despite the otherwise overwhelming QCD backgrounds. Confidence in the theoretical prediction for the Higgs signal process is based upon knowledge of next-to-leading order corrections in both QCD [97–99] and in the electroweak sector [100, 101].

However, in addition to the weak process, a significant number of such events may also be produced via the strong interaction. In order to accurately predict the signal and, in particular, to simulate faithfully the expected significance in a given Higgs model, a fully differential NLO calculation of QCD production of a Higgs and two hard jets is also required. The interference between the weak boson fusion process and gluon fusion have been calculated and shown to be experimentally negligible [102].

In the Standard Model the Higgs couples to two gluons via a top-quark loop. Calculations which involve the full dependence on m_t are difficult and a drastic simplification can be achieved if one works in an effective theory in which the mass of the top quark is large [65, 72, 73]. For inclusive Higgs production this approximation is valid over a wide range of Higgs masses and, for processes with additional jets, the approximation is justified provided that the transverse momentum of each jet is smaller than m_t [67]. Tree-level calculations have been performed in both the large-m_t limit [64, 103] and with the exact-m_t [67] dependence.

Results for the one-loop corrections to all of the Higgs + 4 parton processes have been published in 2005 [104]. Although analytic results were provided for the Higgs $\bar{q}q\bar{q}q$ processes, the bulk of this calculation was performed using a semi-numerical method. In this approach the loop integrals were calculated analytically whereas the coefficients with which they appear in the loop amplitudes were computed numerically using a recursive method. Although some phenomenology was performed using this calculation [105], the implementation of fully analytic formulae will lead to a faster code and permit more extensive phenomenological investigations, which is the main goal of this thesis.

Since then there has been a drive to produce analytic results for the process, with the aim of improving the speed of the calculation. This thesis contains calculations for the most complicated helicity configurations; the ϕ-NMHV helicity configurations (both the pure gluon and $q\overline{q}gg$ cases), and the non-adjacent MHV helicity gluon configuration. The remaining calculations have been performed elsewhere; the rational amplitudes $(\phi + + + +)$, $(\phi, - + ++)$ and $(\phi, q\overline{q} + +)$ have

been performed in [106] the all minus and adjacent minus MHV case can be found in [107,108], whilst the $\phi q\overline{q}$-MHV amplitudes (as well as $\phi q\overline{q}Q\overline{Q}$ helicity amplitudes) can be found in [109].

This thesis proceeds as follows, in chapter 2 we present an overview of the on-shell techniques which we will use throughout the thesis. Chapter 3 contains the calculation of the ϕ MHV amplitude with general helicites, we present the cut-constructible pieces for all multiplicities, whilst for the rational pieces we focus on the four-gluon amplitude we are ultimately interested in. Chapter 4 describes the calculation of the ϕ-NMHV and summarises the results for the four gluon amplitudes. The last chapter dealing with analytic calculations is chapter 5, which presents the remaining helicity amplitude, the $\phi q\overline{q}$-NMHV amplitude. Chapter 6 then moves from analytic calculations into describing some phenomenology which can be performed with the new results. In chapter 7 we draw our conclusions. Appendix A contains a review of both the spinor helicity formalism and colour ordering of tree and one-loop amplitudes as well as a list of useful tree amplitudes. Appendix B contains explicit formulae for the basis integrals we use in this work.

Chapter 2

Unitarity and on-shell methods

2.1 Unitarity

Inspired by the optical theorem, unitarity techniques have recently become widely used in the calculation of one-loop multi-particle amplitudes. These techniques, originally pioneered by Bern, Dixon, Dunbar and Kosower in the mid-90's [110,111], have been revolutionised over the last few years by the introduction of complex momenta and generalised unitarity.

In this section we will outline the main principles of generalised unitarity. In a broad sense these methods can be classified as either four or D-dimensional techniques, both of which are introduced in the following sections. We will also discuss on-shell techniques for the generation of tree-level amplitudes, the MHV rules and BCFW recursion relations. The unitarity-boostrap, a fully four-dimensional method for generating one-loop amplitudes, is also introduced. Finally we review the recent progress towards one-loop automisation.

2.1.1 Unitarity: An Introduction

At the heart of unitarity methods lies the optical theorem, which relates the discontinuity of a matrix element to its imaginary part. When expanded in a perturbation series in the relevant coupling constant the first non-trivial result relates the product

of two tree level amplitudes to the discontinuity of a one-loop integral function. The discontinuity of a one-loop integral associated with a kinematic scale $s = P^2$ can be determined by replacing (or cutting) the following propagators,

$$\frac{1}{\ell^2 + i\epsilon} \to -2\pi i \delta(\ell^2), \quad \frac{1}{(\ell + P)^2 + i\epsilon} \to -2\pi i \delta((\ell + P)^2). \tag{2.1}$$

In the mid-90's Bern, Dixon, Dunbar and Kosower used these relations to calculate a series of one-loop amplitudes [110, 111]. The method involves taking a cut in a certain kinematic scale and then using the simplifying kinematics of the cut (e.g. a four dimensional on-shell loop momenta) to reduce the complexity of the coefficients of the cut loop functions. The cut propagators are then reinstated so that the integrand returns to being a one-loop integral. This approach successfully determines the coefficients of all basis integrals which contain a cut in the kinematic scale. Integrals which do not contain a cut propagator, but can arise in the reduction process, must be dropped and recovered in the appropriate cuts.

A major simplification occurs when four-dimensional tree amplitudes are used in the cuts. This is because one can use the spinor helicity formalism (which is described in Appendix A) to produce compact helicity amplitudes. However, the price of using four-dimensional cuts is the inability to determine pieces of the amplitude which do not contain discontinuities in the kinematic invariants. These pieces, lacking such discontinuities, are referred to as the rational pieces [110, 111]. Their origin, and elusiveness in four-dimensions can be thought of as follows, a general term in a one-loop amplitude has the following structure,

$$C_i \cdot I_i = (c_0 + c_1\epsilon + c_2\epsilon^2 + \dots) \cdot \left(\frac{I_{-2}}{\epsilon^2} + \frac{I_{-1}}{\epsilon} + I_0 \cdot \log(\{s, t, \dots\}) + \dots \right). \tag{2.2}$$

Here $C_i \cdot I_i$ represents a basis integral I_i with a coefficient C_i. In general I_i can contain poles of up to second order in the dimensionally regulating parameter ϵ. The term $\log(\{s, t, \dots\})$ represents a generic piece of the integral which contains logarithms (these could also be di-logarithms or $\ln^2$). It is these pieces which contain a discontinuity in a kinematic invariant and hence enter the optical theorem. However when one uses four-dimensional trees, one loses all sensitivity to the higher order pieces in ϵ which enter the coefficient multiplying the discontinuity. Hence,

four dimensional cuts are only sensitive to terms of the form $c_0 I_0$. The missing pieces, which are of higher order in ϵ in the coefficient contribute finite pieces when multiplying the pole pieces of the integral. This is why they can be thought of as having no discontinuities in the kinematic invariants (but can still be detected by D-dimensional cuts).

The separation into rational and cut-constructible pieces leads to divide and conquer strategies for methods which rely on four-dimensional cuts. Unitarity techniques can be used to calculate the cut-constructible pieces leaving the rational pieces to be determined by some other method. For amplitudes in $\mathcal{N} = 4$ and $\mathcal{N} = 1$ supersymmetric Yang-Mills (SYM) theories, no additional methods are needed, since these amplitudes are completely determined by their four-dimensional cuts [110, 111]. This realisation has led to many calculations of amplitudes in these theories [110–116]. In addition to being interesting in their own right, these amplitudes can be used to construct gluonic amplitudes. If one combines one $\mathcal{N} = 4$ multiplet (which contains one gluon four fermions and three complex scalars), with four $\mathcal{N} = 1$ chiral multiplets (each one containing one fermion and one complex scalar) one finds that

$$A_n^{gluon} = A_n^{\mathcal{N}=4} - 4A_n^{\mathcal{N}=1} + A_n^{\mathcal{N}=0,scalar} \tag{2.3}$$

Here the gluon loop is represented in terms of two pieces which are cut-constructible and one piece which contains a complex scalar. This last piece, although not cut-constructible in four-dimensions, is simpler than the initial gluon loop. Importantly, the rational pieces can be thought of arising from diagrams which contain scalars, rather than gluons, circulating around the loop. The piece of gluon amplitudes which arises from a fermion loop (and is proportional to the number of light flavours N_F) has a similar breakdown.

$$A_n^{gluon,N_F} = A_n^{\mathcal{N}=1} - A_n^{\mathcal{N}=0,scalar} \tag{2.4}$$

So that the rational parts of pure gluonic amplitudes are always proportional to $(1 - N_F/N_C)$ (which will be useful in later chapters).

The unitarity method as described above (with various techniques to determine

the rational part) was used to calculate several phenomenologically important processes [117–119]. The main drawback of the method being that for a given cut one would find multiple basis integrals (for example a cut could contain box, triangle and bubble contributions and all can enter simultaneously) and the appearance of terms in the reduction of tensors which do not contain the appropriate cut propagators.

In 2004 unitarity methods were reinvigorated by several developments in on-shell techniques. New methods for generating compact helicity expressions were discovered, the BCFW recursion relations, and the MHV rules. At the same time the idea of using multiple cuts was established as a useful technique, known as generalised unitarity.

2.2 Quadruple cuts

2.2.1 The quadruple cut method

As discussed previously, massless one-loop amplitudes can be written in the following basis,

$$A_n^{(1)} = \sum_i (c_{4;i} I_{4,i} + c_{3;i} I_{3;i} + c_{2;i} I_{2;i}) + R_n, \tag{2.5}$$

where $I_{i;j}$ is a basis integral with i propagators with a topology denoted by j (in the above equation the summation is over the various allowed topologies given the external momenta). Since the basis is process independent, the calculation of one-loop amplitudes is essentially reduced to extracting the coefficients of each basis integral as efficiently as possible. With this in mind it was proposed [120] that one could isolate a given box coefficient by applying four (rather than two) cuts. Since only the box terms in eq. (2.5) contain four propagators each four-cut should isolate an individual box,

$$\int d^4\ell \prod_{i=1}^{4} \delta(\ell_i^2) A_1^{(0)}(\ell_1,\ell_2) A_2^{(0)}(\ell_2,\ell_3) A_3^{(0)}(\ell_3,\ell_4) A_4^{(0)}(\ell_4,\ell_1)$$
$$= c_{4,\{P\}} \int d^4\ell \prod_{i=1}^{4} \delta(\ell_i^2) \tag{2.6}$$

Here the LHS of eq. (2.6) represents the application of the four on-shell constraints $\delta(\ell_i^2)$ to the LHS of eq. (2.5), shown schematically in Fig. 2.1, whilst the RHS represents the application of the four cuts to the basis integral. In four-dimensions the loop momenta has the same number of components as there are cut propagators and as such is frozen by the cuts. Since the integral over the cut phase space merely contributes a Jacobian, which is identical on both sides of the equation, we can relate the coefficient of a box (with a given topology P) to the solution of the four products of trees

$$A_1^{(0)}(\ell_1, \ell_2)A_2^{(0)}(\ell_2, \ell_3)A_3^{(0)}(\ell_3, \ell_4)A_4^{(0)}(\ell_4, \ell_1) = c_{4,\{P\}}, \tag{2.7}$$

where the loop momenta are solved via the on-shell constraints.

There is a subtlety, however, regarding the application of four cuts to a one-loop amplitude. There are six classes of box integral which can be classified in terms of the number of legs bunched at each corner. Two or more legs at a specific corner results in a "mass" since the squared sum of corner momenta is no longer zero. For four external (massless) particles it is thus possible to have a zero-mass box. As the number of external particles increase so can the number of masses, one can draw a one-mass box, two two-mass boxes [1], a three-mass and a four-mass box. For all but the the four-mass box, after the application of the four-cut, one finds a corner containing a three-point vertex $A_3^{(0)}(1^{\lambda_1}, 2^{\lambda_2}, 3^{\lambda_3})$. Since this amplitude is Lorentz invariant it must depend only on squares of the individual momenta p_i^2, or invariant products between them $p_i \cdot p_j$. For massless momenta $p_i^2 = 0$ so the amplitude can only depend on invariant products between momenta. However, conservation of momenta forces each product to be zero,

$$(p_i + p_j)^2 = p_k^2 = 0 \quad \Longrightarrow \quad p_i \cdot p_j = 0, \tag{2.8}$$

which implies $A_3^{(0)}(1^{\lambda_1}, 2^{\lambda_2}, 3^{\lambda_3}) = 0$. For real momenta this appears to be a major flaw in the quadruple cut approach. The crucial observation in [120] is that if one switches to complex momenta this obstacle can be overcome. Specifically, in

[1] The integral in which the massive corners are opposite is called the easy configuration. The other configuration in which the masses are adjacent is referred to as the hard configuration

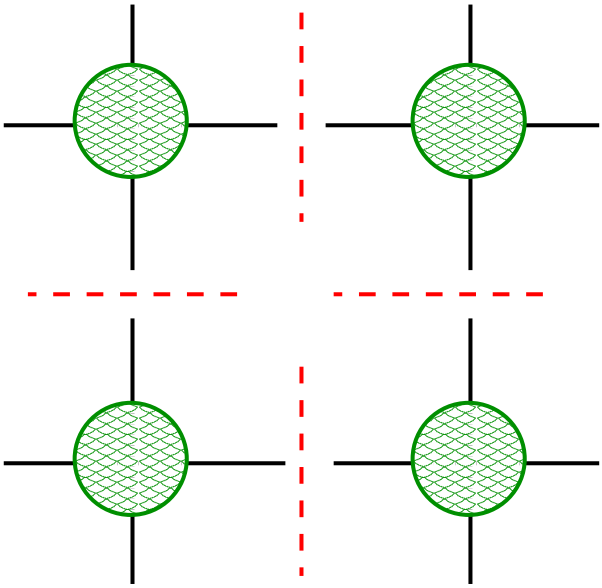

Figure 2.1: The application of four cuts to a one-loop amplitude results in the factorisation onto the product of four tree amplitudes. Since boxes are the only one-loop basis function to contain four propagators each four cut selects a unique box function from the basis. In addition for four-dimensional cuts the loop momenta is frozen by the cutting procedure.

Minkowskii space $(+---)$ a bispinor (light-like four vector) has the form $p_{a\dot{a}} = \lambda_a \tilde{\lambda}_{\dot{a}}$. For real momenta λ and $\tilde{\lambda}$ are complex but are related to each other, $\tilde{\lambda} = \pm\overline{\lambda}$. This means that when an invariant $p_i \cdot p_j = 0$ both $\langle ij \rangle$ and $[ij]$ equal zero (since they are conjugates of each other). If however, one drops the reality condition, such that λ and $\tilde{\lambda}$ are independent, one can still satisfy momenta conservation by having either $[ij] = 0$ and $\langle ij \rangle \neq 0$ or $[ij] \neq 0$ and $\langle ij \rangle = 0$.

Choosing which spinor product should be set equal to zero is made simple by inspecting the structure of the three gluon amplitude. There are two non-zero helicity configurations,

$$A_3^{(0)}(1^+, 2^+, 3^-) = \frac{[12]^3}{[23][31]} \quad \text{and} \quad A_3^{(0)}(1^+, 2^-, 3^-) = \frac{\langle 23 \rangle^3}{\langle 12 \rangle \langle 31 \rangle}. \tag{2.9}$$

For the $(++-)$ configuration one should set $\langle 12 \rangle = \langle 23 \rangle = \langle 31 \rangle = 0$ since the amplitude is independent of these variables and vice versa for $(+--)$. This technique was shown in [120] to correctly reproduce one-loop amplitudes in $\mathcal{N} = 4$ SYM (which contain only box terms to $\mathcal{O}(\epsilon)$).

2.2.2 A quadruple cut example

As an example of the method we calculate the coefficient of a two-mass easy box which appears in the amplitude $A_4^{(1)}(\phi, 1^-, 2^+, 3^-, 4^+)$ $c_{4;\phi|1|23|4}$, the products of four trees are as follows,

$$\begin{aligned} c_{4;\phi|1|23|4} &= A_3^{(0)}(\ell_1^-, \phi, \ell_2^-) A_3^{(0)}(\ell_2^+, 1^-, \ell_3^+) A_4^{(0)}(\ell_3^-, 2^+, 3^-, \ell_4^+) A_3^{(0)}(\ell_4^-, 4^+, \ell_1^+) \\ &= -\langle \ell_1 \ell_2 \rangle^2 \frac{[\ell_2 \ell_3]^3}{[\ell_2 1][1 \ell_3]} \frac{\langle \ell_3 3 \rangle^4}{\langle \ell_3 2 \rangle \langle 23 \rangle \langle 3 \ell_4 \rangle \langle \ell_4 \ell_3 \rangle} \frac{[4 \ell_1]^3}{[\ell_4 4][\ell_4 \ell_1]} \end{aligned} \tag{2.10}$$

Momentum conservation requires that

$$\ell_2 = \ell, \tag{2.11}$$

$$\ell_3 = \ell - p_1, \tag{2.12}$$

$$\ell_4 = \ell - P_{123}, \tag{2.13}$$

$$\ell_1 = \ell - P_{1234}. \tag{2.14}$$

We choose to expand ℓ in terms of a basis made out of the two massless legs,

$$\ell^\mu = \alpha p_1^\mu + \beta p_4^\mu + \frac{1}{2}(\delta \langle 1|\gamma^\mu|4] + \rho \langle 4|\gamma^\mu|1]). \tag{2.15}$$

We now must solve for $\{\alpha, \beta, \delta, \gamma\}$ using the on-shell constraints $\ell_i^2 = 0$. Firstly $p_1 \cdot \ell = 0$ implies that $\beta = 0$, while putting ℓ on-shell $\ell_2^2 = 0$ implies that,

$$0 = s_{14}(\delta\rho) \tag{2.16}$$

so that one of δ or ρ is zero. We choose $\rho = 0$, such that

$$\ell^\mu = \alpha p_1^\mu + \frac{1}{2}\delta\langle 1|\gamma^\mu|4]. \tag{2.17}$$

The next two equations are slightly more complicated,

$$0 = -2\alpha(p_1 \cdot P_{123}) - \delta\langle 1|P_{23}|4] + s_{123} \tag{2.18}$$

$$0 = -2\alpha(p_1 \cdot P_{1234}) - \delta\langle 1|P_{23}|4] + s_{1234} \tag{2.19}$$

The difference of these equations determines α

$$0 = \alpha s_{14} - \langle 4|P_{123}|4] \quad \Longrightarrow \quad \alpha = \frac{\langle 4|P_{123}|4]}{s_{14}} \tag{2.20}$$

We can now solve for δ,

$$\begin{aligned} 0 &= -\frac{\langle 1|P_{123}|1]\langle 4|P_{123}|4]}{s_{14}} - \delta\langle 1|P_{123}|4] + s_{123} \\ &= \frac{\langle 1|P_{123}|4]\langle 4|P_{123}|1]}{s_{14}} - \delta\langle 1|P_{123}|4] \\ \delta &= \frac{\langle 4|P_{123}|1]}{s_{14}} \end{aligned} \tag{2.21}$$

We now have solved for the loop momenta in terms of the external kinematics,

$$\ell^\mu = \frac{\langle 4|P_{123}|4]}{s_{14}} p_1^\mu + \frac{1}{2}\frac{\langle 4|P_{123}|1]}{s_{14}}\langle 1|\gamma^\mu|4]. \tag{2.22}$$

We can simplify this further,

$$\begin{aligned} \ell^\mu &= \frac{1}{2s_{14}}\Big(\langle 4|P_{123}|4]\langle 1|\gamma^\mu|1] + \langle 4|P_{123}|1]\langle 1|\gamma^\mu|4]\Big) \\ &= \frac{\langle 4|P_{123}\gamma^\mu|1\rangle}{2\langle 14\rangle}. \end{aligned} \tag{2.23}$$

The above can be proven by converting the second term into a trace and commuting p_1 with γ^μ. In terms of spinors,

$$|\ell\rangle = |1\rangle \quad |\ell] = \frac{|P_{123}|4\rangle}{\langle 14\rangle} \tag{2.24}$$

We also note that this solution only required knowledge of the two-mass easy box momentum structure. It is, therefore, applicable to any two-mass easy topology with arbitrary helicity structure. However, here we see a problem with our solution, a priori we do not know whether p_1 will be in a MHV or $\overline{\text{MHV}}$ configuration. If it forms part of a MHV three point vertex we see that $\langle \ell_2 1\rangle = 0$, which is not what we wanted. What should be noted is that earlier we explicitly chose $\rho = 0$, if however, we chose $\delta = 0$ we would have found that,

$$\ell^\mu = \alpha p_1^\mu + \frac{1}{2}\rho\langle 1|\gamma^\mu|4] \tag{2.25}$$

Clearly the solution for α is unchanged the equation to determine ρ is given by

$$\begin{aligned} 0 &= \frac{\langle 1|P_{123}|4]\langle 4|P_{123}|1]}{s_{14}} - \rho\langle 4|P_{123}|1] \\ \rho &= \frac{\langle 1|P_{123}|4]}{s_{14}}, \end{aligned} \tag{2.26}$$

such that the second solution for ℓ is given by

$$|\ell] = |1] \quad |\ell\rangle = \frac{|P_{123}|4]}{[41]} \tag{2.27}$$

One should include the contributions from both solutions to the loop momenta when calculating a box coefficient (although in this case one solution is always killed by the MHV or $\overline{\text{MHV}}$ three point amplitude). For our coefficient of interest we first re-write the integrand such that it solely depends on ℓ_2 using momentum conservation then substitute in our calculated result.

$$\begin{aligned} c_{4;\phi|1|23|4} &= \langle \ell_1\ell_2\rangle^2 \frac{[\ell_2\ell_3]^3}{[\ell_2 1][1\ell_3]} \frac{\langle \ell_3 3\rangle^4}{\langle \ell_3 2\rangle\langle 23\rangle\langle 3\ell_4\rangle\langle \ell_4\ell_3\rangle} \frac{[4\ell_1]^3}{[\ell_4 4][\ell_4\ell_1]} \\ &= \frac{[4|\ell_1|\ell_2\rangle^2[\ell_2|\ell_3|3\rangle^3\langle \ell_3 3\rangle[4\ell_1]}{[\ell_2 1][1|\ell_3|2\rangle\langle 23\rangle\langle 3|\ell_4|\ell_1]\langle \ell_3|\ell_4|4]} \\ &= \frac{[4|P_{123}|\ell_2\rangle^2[\ell_2 1]\langle 13\rangle^4}{\langle \ell_2 2\rangle\langle 23\rangle\langle 34\rangle\langle 1|P_{23}|4]} \\ &= A_4^{(0)}(\phi, 1^-, 2^+, 3^-, 4^+)[4|P_{23}1P_{23}|4\rangle \\ &= A_4^{(0)}(\phi, 1^-, 2^+, 3^-, 4^+)(s_{234}s_{123} - s_{1234}s_{23}) \end{aligned} \tag{2.28}$$

Here the coefficient is given by the tree-level amplitude multiplied by a kinematic function associated with the two mass box [121].

The quadruple cut method reduces the extraction of the box coefficients in the one-loop basis expansion (eq. (2.5)) to an algebraic operation. For QCD amplitudes the remaining cut-constructible pieces are the coefficients of the triangle and bubble integral functions. Inspired by the multiple cut techniques, new methods were developed to isolate the coefficients of these integral functions. Two of these are described below, Forde's Laurent expansion method [122] and spinor integration [123].

2.3 Forde's Laurent expansion method

2.3.1 The triple cut method

The Laurent expansion method [122] allows each coefficient in eq. (2.5) to be isolated and determined individually. Once the coefficients of the box terms have been determined from quadruple cuts, one applies a triple cut to the amplitude (as depicted in Fig. 2.2). For four-dimensional loop momenta, three of the components are fixed by the constraints. This means that the loop momenta can be expressed in terms of one free parameter t,

$$\ell^\mu = a_0^\mu t + \frac{1}{t} a_1^\mu + a_2^\mu. \tag{2.29}$$

Here a_i are orthogonal null four-vectors to ensure $\ell^2 = 0$, the a_i are completely fixed by the kinematics of the cut however for now we are interested in the t-dependence of the cut. The denominator of the product of three trees can contain propagators of the general form $(\ell - P)^2$, which we associate with box terms. These propagators go on-shell when the following equation is satisfied,

$$(\ell - P)^2 = 0 \quad \Longrightarrow \quad 2(a_0 \cdot P)t + \frac{2(a_1 \cdot P)}{t} + 2(a_2 \cdot P) - P^2 = 0. \tag{2.30}$$

The use of partial fractioning allows us to separate the pieces arising from poles in t from the remaining terms,

$$\int d^4\ell \prod_{i=0}^{2} \delta(\ell_i^2) A_1 A_2 A_3$$

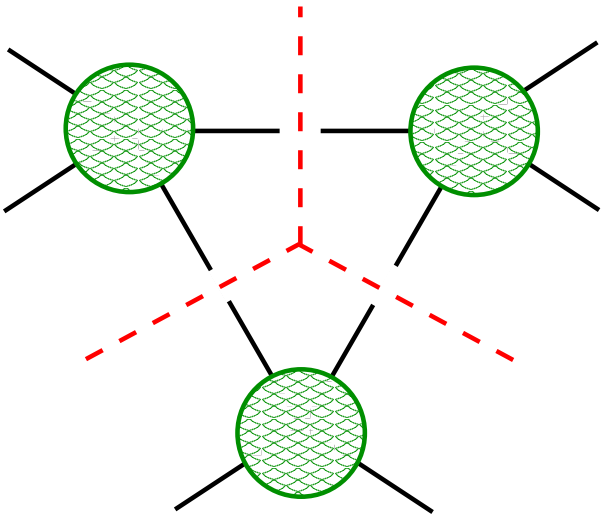

Figure 2.2: The application of three cuts to a one-loop amplitude results in the factorisation onto the product of three tree amplitudes. Both boxes and triangle integral functions appear in a triple cut, since multiple boxes can share a specific set of three propagators more than one box can enter. Each cut selects a specific triangle integral function. For four-dimensional cuts the loop momenta has one free parameter.

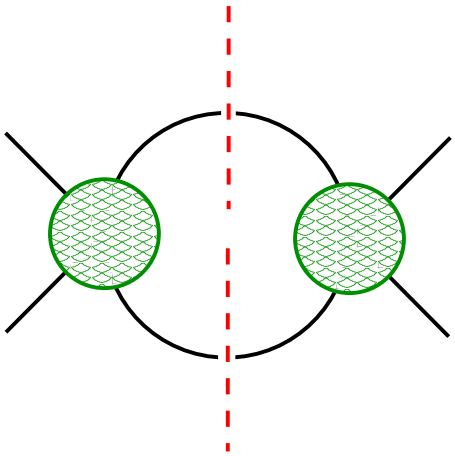

Figure 2.3: The application of two cuts to a one-loop amplitude results in the factorisation onto the product of two tree amplitudes. Boxes, triangle and bubble integral functions appear in a double cut, again with multiple triangle and box contributions with an individual bubble term. For four-dimensional cuts the loop momenta has two free parameters.

$$= \int d^4\ell \prod_{i=0}^{2} \delta(\ell_i^2) \Bigg([\mathrm{Inf}_t A_1 A_2 A_3](t) + \sum_{\text{poles } j} \frac{\mathrm{Res}_{t=t_j} A_1 A_2 A_3}{t - t_j} \Bigg). \tag{2.31}$$

In the above equation $\ell_i = \ell - K_i$ where K_i is one of the two kinematic invariants which appear in the triple cut, $\ell_0 = \ell$. $\mathrm{Inf}_t A_1 A_2 A_3$ contains all the pieces of the integrand which contain no poles[2] in t, i.e.

$$\lim_{t\to\infty} \Bigg([\mathrm{Inf}_t A_1 A_2 A_3](t) - A_1(t) A_2(t) A_3(t)) \Bigg) = 0. \tag{2.32}$$

We can decompose the Inf piece as follows

$$[\mathrm{Inf}_t A_1 A_2 A_3](t) = \sum_{i=0}^{m} f_i t^i. \tag{2.33}$$

The residue contributions in eq. (2.31) arise from propagators of the form $(\ell - P)^2$ going on-shell. Since this equation is quadratic we expect two solutions (labelled $t = t_\pm$) and this is indeed what we observed when calculating solutions to the four on-shell constraints in the previous section.

$$\int d^4\ell \prod_{i=0}^{2} \delta(\ell_i^2) \frac{1}{(\ell - P)^2} \sim \frac{1}{t_+ - t_-} \Bigg(\int d^4\ell \prod_{i=0}^{2} \delta(\ell_i^2) \frac{1}{t - t_+} - \int d^4\ell \prod_{i=0}^{2} \delta(\ell_i^2) \frac{1}{t - t_-} \Bigg) \tag{2.34}$$

Therefore, after suitable partial fractioning we can write the triple cut integrand as follows,

$$\int d^4\ell \prod_{i=0}^{2} \delta(\ell_i^2) A_1 A_2 A_3 = \int dt J_t \Bigg(\sum_{i=0}^{m} f_i t^i \Bigg) + \sum_{\text{boxes}\{l\}} d_l D_0^{cut}. \tag{2.35}$$

Here we sum over the various triple cut boxes in which the t dependence has been eliminated by evaluating the loop momenta at the specific residue values. The remaining piece of the equation is a sum over the positive powers of t. J_t represents a Jacobian factor obtained by the transformation of the integration variable from ℓ to t. Since there is a freedom in how we define the loop expansion (i.e. a freedom in how we choose a_i), we can choose a specific basis in which integrals over non-zero

[2] This operation will also be useful when calculating the rational terms [124]

powers of t vanish,

$$\int d^4\ell \prod_{i=0}^{2} \delta(\ell_i^2) A_1 A_2 A_3 = f_0 \int dt J_t + \sum_{\text{boxes}\{l\}} d_l D_0^{cut}. \tag{2.36}$$

If this parameterisation is possible then one has successfully isolated the coefficient of the scalar triangle (which is represented by $\int dt J_t$) from the previously known box coefficients (although if unknown these can be extracted also). In general the coefficient is given by,

$$c_{3;P} = -[\text{Inf}_t A_1 A_2 A_3](t)\Big|_{t=0}. \tag{2.37}$$

All that remains to be done is to define the correct momentum parameterisation such that integrals over non-zero powers of t vanish. The basis is inspired by one proposed in [125] and relies on the following massless projections of the (potentially) massive vectors K_1 and K_2 (the two momenta which appear as legs of the triangle),

$$K_1^{\flat,\mu} = \frac{K_1^\mu - (S_1/\gamma)K_2^\mu}{1-(S_1S_2/\gamma^2)}, \quad K_2^{\flat,\mu} = \frac{K_2^\mu - (S_2/\gamma)K_1^\mu}{1-(S_1S_2/\gamma^2)}. \tag{2.38}$$

Here $\gamma_\pm = (K_1 \cdot K_2) \pm \sqrt{\Delta}$ and $\Delta = (K_1 \cdot K_2)^2$. When determining the triangle coefficient we must average over the γ solutions. In terms of these basis vectors the loop momenta has the following form,

$$\ell_\mu = \alpha_{02} K_1^{\flat,\mu} + \alpha_{01} K_2^{\flat,\mu} + \frac{t}{2}\langle K_1^{\flat,-}|\gamma^\mu|K_2^{\flat,-}\rangle + \frac{\alpha_{01}\alpha_{02}}{2t}\langle K_2^{\flat,-}|\gamma^\mu|K_1^{\flat,-}\rangle, \tag{2.39}$$

with

$$\alpha_{01} = \frac{S_1(\gamma - S_2)}{(\gamma^2 - S_1S_2)}, \quad \alpha_{02} = \frac{S_2(\gamma - S_1)}{(\gamma^2 - S_1S_2)}. \tag{2.40}$$

The other two on-shell loop momenta $\ell_i = \ell - K_i$ have a similar basis expansion and the coefficients α_{i1} and α_{i2} are given explicitly in [122]. Importantly it has been shown [122, 125] that using this basis

$$\int dt J_t \frac{1}{t^n} = 0, \quad \int dt J_t t^n = 0, \quad \text{for} \quad n \geq 1, \tag{2.41}$$

which ensures the validity of eq.(2.37). Thus to extract a triangle coefficient one merely has to parameterise the loop momenta in the above basis, and extract the coefficient of t^0 in an expansion around $t = \infty$.

2.3.2 A triple cut example

As an example of the triple cut method we describe the calculation of $C_{3;\phi|12|34}$, the coefficient of a three-mass triangle which appears in the ϕ-NMV amplitude $A_4^{(1)}(\phi, 1^+, 2^-, 3^-, 4^-)$. The product of the three amplitudes has the following form,

$$\begin{aligned} C_{3;\phi|12|34} &= A_2^{(0)}(\phi, \ell_0^-, \ell_2^-) A_4^{(0)}(\ell_2^+, 4^-, 3^-, \ell_1^+) A_4^{(0)}(\ell_1^-, 2^-, 1^+, \ell_0^+) \quad (2.42) \\ &= -\langle \ell_0 \ell_2 \rangle^2 \frac{\langle 34 \rangle^3}{\langle \ell_2 4 \rangle \langle 3 \ell_1 \rangle \langle \ell_1 \ell_2 \rangle} \frac{\langle \ell_1 2 \rangle^3}{\langle 12 \rangle \langle 1 \ell_0 \rangle \langle \ell_0 \ell_1 \rangle} \quad (2.43) \end{aligned}$$

We now insert the definitions for ℓ_i in terms of $K_1^{\flat\mu}$ and $K_2^{\flat\mu}$, generating the following t dependent function,

$$C_{3;\phi|12|34} = -\frac{\Delta \langle 34 \rangle^3 (t\langle K_1^\flat 2 \rangle + \langle K_2^\flat 2 \rangle \alpha_{11})^3}{\langle 12 \rangle (t\langle K_1^\flat 1 \rangle + \langle K_2^\flat 1 \rangle \alpha_{01})(t\langle K_1^\flat 3 \rangle + \langle K_2^\flat 3 \rangle \alpha_{11})(t\langle K_1^\flat 4 \rangle + \langle K_2^\flat 4 \rangle \alpha_{21})} \quad (2.44)$$

where

$$\Delta = \frac{(\alpha_{01} - \alpha_{21})^2}{(\alpha_{11} - \alpha_{21})(\alpha_{01} - \alpha_{11})} \quad (2.45)$$

and the definitions for α_{ij} can be found in [122]. The triangle coefficient is found by taking the t^0 coefficient in a series expansion of eq. (2.44) around $t = \infty$.

$$C_{3;\phi|12|34}(\phi, 1^+, 2^-, 3^-, 4^-) = \sum_{\gamma = \gamma_\pm(p_\phi, p_1 + p_2)} -\frac{m_\phi^4 \langle K_1^\flat 2 \rangle^3 \langle 34 \rangle^3}{2\gamma(\gamma + m_\phi^2)\langle K_1^\flat 1 \rangle \langle K_1^\flat 3 \rangle \langle K_1^\flat 4 \rangle \langle 12 \rangle}, \quad (2.46)$$

2.3.3 The double cut method

The Laurent expansion method also includes double cuts [122]. Two cut propagators implies that two parameters are needed to encapsulate the remaining degrees of freedom of the loop momenta,

$$\ell^\mu = \frac{y^2}{t} a_0^\mu + \frac{y}{t} a_1^\mu + y a_2^\mu + t a_3^\mu + a_4^\mu. \quad (2.47)$$

The general approach is the same as the triple cut. One wishes to find a parameterisation of the loop momenta which cleanly separates triangle box and bubble contributions such that we can extract the bubble contribution. Although more

complicated than the triple cut procedure this has been achieved [122]. The analytic results which arise from Forde's double cut method tend to be more complicated than those which arise from spinor integration (which will be described in section 2.4). Since in this thesis we are interested in obtaining compact analytic results for one-loop Higgs plus parton amplitudes this double cut method will not be described in any more detail. The main advantage of the Laurent expansion method is its algorithmic nature and as such it has been successfully implemented in the program Blackhat [126] (which will also be described in section 2.8).

2.4 Spinor integration

The technique known as spinor integration was first proposed in 2005 by Britto, Buchbinder, Cachazo and Feng [123]. Spinor integration naturally separates the integrand into pieces which integrate to logarithmic functions in the kinematic invariants and those which integrate to rational functions. Further, each type of triangle or box has a specific logarithm which can be used to identify it in the cut. This technique was used to calculate the missing three mass triangle and bubble contributions to the six gluon amplitudes in $\mathcal{N} = 1$ [123] and $\mathcal{N}^{scalar} = 0$ [127] theories. In addition a triple cut method based on spinor integration [128] has been used to calculate analytic forms for the six photon amplitude [129].

2.4.1 Spinor integration via the holomorphic anomaly

The starting point, in a similar fashion to all unitarity methods, is the product of two tree amplitudes integrated over a cut phase space,

$$c_{2;P} = \int d^4\ell\delta(\ell^2)\delta((\ell - P)^2)A_1^{(0)}(\ell, \ldots, \ell - P)A_2^{(0)}(-(\ell - P), \ldots, -\ell) \quad (2.48)$$

shown schematically in Fig. 2.3. The name spinor integration arises from the redefinition of the phase space in terms of spinors λ and $\tilde{\lambda} = \overline{\lambda}$ [130, 131],

$$\int d^4\ell\delta(\ell^2) = \int_0^\infty dt\, t \int \langle\lambda, d\lambda\rangle[\tilde{\lambda}, d\tilde{\lambda}]. \quad (2.49)$$

Here we have used $\ell_{\alpha,\dot{\alpha}} = t\lambda_\alpha\tilde{\lambda}_{\dot{\alpha}}$. The integration over t is actually frozen by the second delta function,

$$\delta((\ell - P)^2) = \delta(P^2 - t\langle\lambda|P|\lambda]) \implies t = \frac{P^2}{\langle\lambda|P|\lambda]}. \tag{2.50}$$

A generic double cut integrand has the following form,

$$c_{2;P} = \int \langle\lambda, d\lambda\rangle[\tilde{\lambda}, d\tilde{\lambda}]\frac{P^2}{\langle\lambda|P|\lambda]^2}g(\lambda, \tilde{\lambda}), \tag{2.51}$$

where $g(\lambda, \tilde{\lambda})$ arises from the product of the tree amplitudes. The main crux of the idea behind spinor integration is that in the above equation one can systematically perform one of the integrations (either in λ or $\tilde{\lambda}$), whilst the remaining contour integration can be done via the Residue Theorem. Two different methods have been proposed in order to perform this first integration. In the following section we will discuss performing the integration by the application of Stokes' Theorem [132]. Firstly we describe the method proposed in the original paper [123] via the holomorphic anomaly.

We begin by considering the integration of a simpler function $g(\lambda)$ which depends on λ only, i.e. it has the general form,

$$g(\lambda) = \frac{\prod_{i=1}^{k}\langle\lambda, A_i\rangle}{\prod_{j=1}^{k}\langle\lambda, B_j\rangle}. \tag{2.52}$$

The following identity follows from the Schouten identity,

$$\frac{[\lambda\, d\lambda]}{\langle\lambda|P|\tilde{\lambda}]^2} = -d\tilde{\lambda}^{\dot{c}}\frac{\partial}{\partial\tilde{\lambda}^{\dot{c}}}\left(\frac{[\tilde{\lambda}\eta]}{\langle\lambda|P|\tilde{\lambda}]\langle\lambda|P|\eta]}\right), \tag{2.53}$$

and holds for all values of λ, apart from those where the denominator vanishes along the integration contour (where $\tilde{\lambda} = \overline{\lambda}$) at this point,

$$-d\tilde{\lambda}^{\dot{c}}\frac{\partial}{\partial\tilde{\lambda}^{\dot{c}}}\frac{1}{\langle\lambda\chi\rangle} = 2\pi\overline{\delta}(\langle\lambda, \chi\rangle) \tag{2.54}$$

the definition of $\overline{\delta}$ is such that it freezes the integration in λ,

$$\int\langle\lambda d\lambda\rangle\overline{\delta}(\langle\lambda, \chi\rangle)B(\lambda) = -iB(\chi). \tag{2.55}$$

With the knowledge of the holomorphic anomaly (2.54) in hand, we can re-write eq. (2.53) for use with our function $g(\lambda)$,

$$\frac{[\lambda\, d\lambda]}{\langle\lambda|P|\tilde{\lambda}]^2}g(\lambda) = -d\tilde{\lambda}^{\dot{c}}\frac{\partial}{\partial\tilde{\lambda}^{\dot{c}}}\left(\frac{[\tilde{\lambda}\eta]g(\lambda)}{\langle\lambda|P|\lambda]\langle\lambda|P|\eta]}\right)$$

$$+\frac{2\pi[\tilde{\lambda}\eta]}{\langle\lambda|P|\tilde{\lambda}]}\Big(-\overline{\delta}(\langle\lambda|P|\eta])g(\lambda)+\frac{1}{\langle\lambda|P|\eta]}\sum_{j=1}^{k}\overline{\delta}(\langle\lambda B_j\rangle)g(\lambda)\langle\lambda B_j\rangle\Big). \quad (2.56)$$

That is we sum over the poles coming from $g(\lambda)$ and the denominator $\langle\lambda|P|\lambda]\langle\lambda|P|\eta]$. At first glance one might expect to see a piece proportional to $\overline{\delta}(\langle\lambda|P|\lambda])$, however one cannot satisfy the vanishing of the $\langle\lambda|$ and the conjugation relation simultaneously, so there is no pole here. Upon integration over λ the first term vanishes such that the integral is localised by the remaining $\overline{\delta}$ functions. This allows to write the spinor integral of our function $g(\lambda)$ as,

$$\begin{aligned}\mathcal{I} &= \int\langle\lambda,d\lambda\rangle[\tilde{\lambda},d\tilde{\lambda}]\frac{P^2}{\langle\lambda|P|\lambda]^2}g(\lambda)\\ &= -\frac{1}{P^2}g(\lambda_P)+\sum_{j=1}^{k}\frac{[B_j\eta]}{\langle B_j|P|B_j]\langle B_j|P|\eta]}\frac{\prod_{i=1}^{k}\langle B_jA_i\rangle}{\prod_{l\neq j}\langle B_jB_l\rangle}\end{aligned} \quad (2.57)$$

where $|\lambda_P\rangle = |P|\eta]$. Knowledge of the integral of the function $g(\lambda)$ allows us to trivially determine the double cut of a bubble integral, $g(\lambda)=1$,

$$\Delta\mathcal{I}_2 = -1. \quad (2.58)$$

We can also investigate the cut of a three mass triangle,

$$\begin{aligned}\Delta\mathcal{I}_3 &= \int d^4\ell\,\delta(\ell^2)\delta(\ell-K_1)^2\frac{1}{(\ell+K_3)^2}\\ &= \int_0^\infty t\,dt\int\langle\lambda,d\lambda\rangle[\tilde{\lambda},d\tilde{\lambda}]\frac{\delta(K_1^2-t\langle\lambda|K_1|\tilde{\lambda}])}{K_3^2+t\langle\lambda|K_3|\tilde{\lambda}]}\\ &= \int\langle\lambda,d\lambda\rangle[\tilde{\lambda},d\tilde{\lambda}]\frac{K_1^2}{\langle\lambda|K_1|\tilde{\lambda}]^2}\frac{\langle\lambda|K_1|\lambda]}{K_3^2\langle\lambda|K_1|\tilde{\lambda}]+K_1^2\langle\lambda|K_3|\tilde{\lambda}]}\\ &= \int\langle\lambda,d\lambda\rangle[\tilde{\lambda},d\tilde{\lambda}]\frac{1}{\langle\lambda|K_1|\tilde{\lambda}]\langle\lambda|Q|\tilde{\lambda}]},\end{aligned} \quad (2.59)$$

where $Q^\mu = \frac{K_3^2}{K_1^2}K_1^\mu + K_3^\mu$. We can further simplify this by introducing a Feynman parameter x which combines the two denominators at the cost of one extra integration,

$$\frac{1}{\langle\lambda|K_1|\tilde{\lambda}]\langle\lambda|Q|\tilde{\lambda}]} = \int_0^1 dx\frac{1}{\langle\lambda|R|\tilde{\lambda}]^2} \quad (2.60)$$

with $R=(1-x)K+xQ$. As a result of this transformation the integral over λ is equal to that of the scalar bubble which leaves only the x integration,

$$\Delta\mathcal{I}_3 = -\int_0^1 dx\frac{1}{R^2}. \quad (2.61)$$

The explicit value of this integral is not of interest here (it being dependent on whether the external momenta K_i^2 are positive or negative), the point of interest is that it integrates to a logarithmic function. In fact, all basis integrals other than the scalar bubble integrate in the double cut regime to a logarithmic function of the kinematics. This is a very useful observation, since if one can separate the integral into pieces which integrate to logarithmic funcitons, and those that do not, then the task of extracting the coefficient of the scalar bubble becomes simpler. It was shown in [123] that one can always separate these contributions and determine the coefficient of the scalar bubble using the holomorphic anomaly eq. (2.56). Since the original paper, this approach has been extended to D dimensions [133–135], and closed forms for all basis integrals appear in the double cuts have been provided [136, 137].

In this thesis we used a more recent variant of spinor integration [132], which uses Stokes' Theorem rather than the holomorphic anomaly to perform the integrations in λ. This is described in the following section.

2.4.2 Spinor integration via Stokes' Theorem

In this section we describe the application of spinor integration via Stokes' Theorem [132]. Firstly of course, we start with the double cut measure,

$$\int d^4\ell_1 \delta(\ell_1^2)\delta((\ell_1 - P)^2) = \int_0^\infty t\, dt\, \delta\left(t - \frac{P^2}{\langle \ell | P | \ell]}\right) \int \frac{\langle \ell\, d\ell \rangle [\ell d\ell]}{\langle \ell | P | \ell]} \tag{2.62}$$

Here as in eq. (2.49) we have rescaled ℓ_1 (the loop momenta appearing in the tree products) as $\ell_1^\mu = t\langle \ell | \gamma^\mu | \ell]/2$, which is equivalent to the following spinor shifts,

$$|\ell_1\rangle = \sqrt{t}|\ell\rangle \quad \text{and} \quad |\ell_1] = \sqrt{t}|\ell]. \tag{2.63}$$

At first glance there appears in eq. (2.62) an inverse factor of $\langle \ell | P | \ell]$ relative to eq. (2.49). This however is expected, since in eq. (2.49) the second δ function (which is of the form $\delta(f(t))$ has not been applied, whereas in the above equation the δ function is of the form $\delta(t - a)$.

To proceed one notices that with two free parameters one can write the loop momentum in terms of two vectors p^μ and η^μ, such that the sum of p and η is equal

to the cut momentum P, i.e.

$$\ell^\mu = p_\mu + z\overline{z}\,\eta^\mu + \frac{z}{2}\langle\eta|\gamma^\mu|p] + \frac{\overline{z}}{2}\langle p|\gamma^\mu|\eta]. \tag{2.64}$$

This is identical to making the following spinor shifts,

$$|\ell\rangle = |p\rangle + z|\eta\rangle \quad \text{and} \quad |\ell] = |p] + \overline{z}|\eta]. \tag{2.65}$$

In terms of the new variables the measure becomes,

$$\int d^4\ell_1 \delta(\ell_1^2)\delta((\ell_1 - P)^2) = \oint dz \int d\overline{z} \frac{1}{(1+z\overline{z})^2}. \tag{2.66}$$

Here the notation deserves some justification. We have written the integral over z as a contour integration, with the remaining integration in $\overline{z}$ as an indefinite integral. This is because we intend to perform the explicit integration in $\overline{z}$ thereby producing rational and logarithmic terms (of course we could have swapped the role of z and $\overline{z}$ if we desired). The remaining contour integral is performed by summing over the residues in z, using Cauchy's residue theorem. The details of the proof use Stokes' theorem and are described in [132]. Here we sketch the technique and in the next section we give a detailed example.

In general the product of the two trees will have the following form,

$$A_L^{(0)}(\ell_1, \ell_1 - P)A_R^{(0)}(-\ell_1, -\ell_1 + P) = \frac{A_L^{(0)}(z,\overline{z})A_R^{(0)}(z,\overline{z})}{(1+z\overline{z})^{\alpha_L+\alpha_R}}, \tag{2.67}$$

where $\alpha_{L,R}$ represent the powers of t which arise from the tree amplitudes and are integrated out via the second delta function. This means that one can write the double cut integrand in the following form,

$$\Delta^{2-cut} = \oint dz \int d\overline{z}\, f(z,\overline{z}), \quad \text{with} \quad f(z,\overline{z}) = \frac{P(z,\overline{z})}{Q(z,\overline{z})}. \tag{2.68}$$

Now one introduces a primitive of f with respect to $\overline{z}$, that is

$$F(z,\overline{z}) = \int d\overline{z} f(z,\overline{z}), \tag{2.69}$$

so that the double cut becomes,

$$\Delta^{2-cut} = \oint dz \int d\overline{z}\, F_{\overline{z}}(z,\overline{z}) \tag{2.70}$$

with $F_{\overline{z}} = \partial F/\partial z$. This integral is evaluated by summing the residues in z of the primitive function F, which is proven using the Cauchy-Pompeius formula,

$$f(\chi) = \frac{1}{2\pi i}\int\int_D \frac{f_{\overline{z}}(z)}{\chi - z} d\overline{z} \wedge dz. \tag{2.71}$$

This formula is valid when f vanishes on the boundary of D (which is ensured in our case by the structure of Q). A nice overview of this formula and differential forms can be found online, [138]. In our problem we know that the primitive must differentiate to a rational function, therefore in general it can contain only rational and logarithmic terms,

$$F(z,\overline{z}) = F^{rat}(z,\overline{z}) + F^{log}(z,\overline{z}) \tag{2.72}$$

From our physics understanding we regard the logarithmic pieces as the cuts of triangle and box terms, the rational piece represents the double cut of the scalar bubble function I_2. In fact we can always associate the pure scalar bubble with the $z = 0$ residue,

$$\begin{aligned} \Delta\mathcal{I}_2 &= \oint dz \int d\overline{z} \frac{1}{(1+z\overline{z})^2} \\ &= -\oint dz \frac{1}{(1+|z|^2)z} \\ &= -1. \end{aligned} \tag{2.73}$$

We are content to see that the two spinor integration methods yield the same result for the double cut of a scalar bubble eq.'s (2.58) and (2.73) [3] . We also observe that the $(1+|z|^2)$ will never produce a residue in z (which arises from $\langle\ell|P|\ell]$ and which also didn't contribute when the holomorphic anomaly was used).

The remaining residues ($z \neq 0$) in the rational part of the primitive F contribute to the bubble coefficient but can be traced back to scalar bubbles which have arisen from reduction of tensor triangle and box diagrams.

[3]Here we have been slightly cavalier with our factors of $2\pi i$ although in practical applications these will drop out since we equate the LHS (which is the double cut of the tree amplitudes) with the double cut of the scalar bubble multiplied by the coefficient of interest.

2.4.3 A double cut example

As a more concrete example of the above method, we describe the calculation of a bubble coefficient in the s_{12} channel for the one-loop amplitude $A_4^{(1)}(\phi, 1^-, 2^+, 3^-, 4^+)$. The tree products have the following form,

$$\sum_{i=\pm} A_L^{(0)}(\ell_1^i, \phi, 3^-, 4^+, \ell_2^{-i}) A_R^{(0)}(\ell_2^i, 1^-, 2^+, \ell_1^{-i}) = \frac{-\langle \ell_1 3\rangle^4 \langle \ell_2 1\rangle^4 - \langle \ell_1 1\rangle^4 \langle \ell_2 3\rangle^4}{\langle \ell_1 3\rangle\langle 34\rangle\langle 4\ell_2\rangle\langle \ell_2 1\rangle\langle 12\rangle\langle 2\ell_1\rangle\langle \ell_1\ell_2\rangle^2}. \tag{2.74}$$

Using the Schouten identity we can re-write the numerator in terms of three functions (which will be defined in chapter 3), for now, we concentrate on one of these three functions,

$$\mathcal{F}_{s_{12}} = -\frac{\langle 13\rangle^2 \langle \ell_1 1\rangle \langle \ell_2 3\rangle}{\langle 34\rangle\langle \ell_2 4\rangle\langle 12\rangle\langle \ell_1 2\rangle}. \tag{2.75}$$

Next we use momentum conservation to remove ℓ_1 in favour of ℓ_2,

$$\begin{aligned} \mathcal{F}_{s_{12}} &= -\frac{\langle 13\rangle^2 [\ell_2|\ell_1|1\rangle \langle \ell_2 3\rangle}{\langle 34\rangle\langle \ell_2 4\rangle\langle 12\rangle [\ell_2|\ell_1|2\rangle} \\ &= -\frac{\langle 13\rangle^2 [\ell_2|P_{12}|1\rangle \langle \ell_2 3\rangle}{\langle 34\rangle\langle \ell_2 4\rangle\langle 12\rangle [\ell_2|P_{12}|2\rangle} \end{aligned} \tag{2.76}$$

We rescale $\ell_2 = t\ell$ and perform the trivial t integration,

$$\begin{aligned} \mathcal{F}_{s_{12}} &= \frac{\langle 13\rangle^2 [\ell_2 2]\langle \ell_2 3\rangle}{\langle 34\rangle\langle \ell_2 4\rangle\langle 12\rangle [\ell_2 1]} \\ \Delta\mathcal{F}_{s_{12}} &= \int \frac{t}{\langle \ell|P_{12}|\ell]} \frac{\langle 13\rangle^2 [\ell 2]\langle \ell 3\rangle}{\langle 34\rangle\langle \ell 4\rangle\langle 12\rangle [\ell 1]} \\ &= \int \frac{s_{12}}{\langle \ell|P_{12}|\ell]^2} \frac{\langle 13\rangle^2 [\ell 2]\langle \ell 3\rangle}{\langle 34\rangle\langle \ell 4\rangle\langle 12\rangle [\ell 1]} \end{aligned} \tag{2.77}$$

Here we use $\Delta\mathcal{F}_{s_{12}}$ to represent the double cut integral (for simplicity and to highlight the operations on the integrand we have suppressed the details of the measure). Next we wish to rewrite ℓ in terms of p and η, recall that $p + \eta = P$, here $P = P_{12}$ so an obvious choice for p and η is $p = p_1$ and $\eta = p_2$, so we write that $|\ell] = |1] + \overline{z}|2]$ and integrate in $\overline{z}$ dropping log terms.

$$\Delta\mathcal{F}_{s_{12}} = \int \frac{\langle 13\rangle^2 \langle 3\ell\rangle}{\langle 34\rangle\langle 4\ell\rangle\langle 12\rangle\langle 2\ell\rangle(\langle 2\ell\rangle - \overline{z}\langle 1\ell\rangle)} \tag{2.78}$$

Finally we replace $|\ell\rangle$ and take residues in z,

$$\Delta\mathcal{F}_{s_{12}} = \int \frac{\langle 13\rangle^2(\langle 13\rangle + z\langle 23\rangle)}{\langle 34\rangle(\langle 14\rangle - z\langle 24\rangle)\langle 12\rangle(1 - \overline{z}z)}$$

$$\Delta\mathcal{F}_{s_{12}} = \frac{\langle 13\rangle^2[42]}{\langle 24\rangle\langle 4|P_{12}|4]}. \tag{2.79}$$

We observe that there was no residue at $z = 0$, meaning that the coefficient of the two point function for this integrand came solely from the reduction of tensor triangles, in fact $\langle 4|P_{12}|4]$, which appears in the denominator is a signature of a first rank tensor triangle.

In this thesis we will use the above method to construct the coefficients of scalar bubbles for the various Higgs plus four parton one-loop amplitudes that we study.

2.5 MHV rules and BCFW recursion relations

In this section we discuss two important on-shell techniques for the generation of tree-level amplitudes, the MHV rules [130, 131, 139] and BCFW recursion relations [140, 141]. These techniques have had many important applications, some of which will be described in the following sections.

2.5.1 The MHV/CSW rules

The MHV (or Parke-Taylor) amplitudes have long been known to possess a remarkably simple structure for all gluon multiplicities [142],

$$A_n^{(0)}(1^+,\ldots,i^-,\ldots,j^-,\ldots,n^+) = \frac{\langle ij\rangle^4}{\prod_{\alpha=1}^{n-1}\langle\alpha(\alpha+1)\rangle\langle n1\rangle}. \tag{2.80}$$

MHV stands for Maximally-Helicity-Violating because if one classes amplitudes in terms of the number of negative helicity gluons present these are the first which are non-zero, i.e:

$$A_n^{(0)}(1^+,\ldots,i^+,\ldots,j^+,\ldots,n^+) = A_n^{(0)}(1^+,\ldots,i^+,\ldots,j^-,\ldots,n^+) = 0. \tag{2.81}$$

$\overline{\text{MHV}}$ amplitudes are the conjugates of eq. (2.80),

$$A_n^{(0)}(1^-,\ldots,i^+,\ldots,j^+,\ldots,n^-) = \frac{[ij]^4}{\prod_{\alpha=1}^{n-1}[\alpha(\alpha+1)][n1]}. \tag{2.82}$$

All relevant tree amplitudes (with definitions of spinor products) for this thesis are collected together in Appendix A.

In 2003 Witten interpreted the MHV amplitudes as vertices in a twistor string theory, [131]. That is to say that he proposed that one could build amplitudes with an increasing number of negative helicity gluons from MHV amplitudes. However, one immediately observes an apparent contradiction, the MHV amplitudes eq. (2.80), are defined for on-shell gluons. How then can one promote these to vertices? Vertices are connected together by off-shell propagators, and as such (up to) two of the gluons in the MHV amplitude should be off-shell. The prescription for taking a gluon λ off-shell proceeds as follows [130]. One chooses an arbitrary reference vector η and then wherever one encounters λ inside an MHV vertex one replaces,

$$\lambda_a = p_{a\dot{a}}\eta^{\dot{a}}, \tag{2.83}$$

where $p_{a\dot{a}}$ is the momenta which flows through the vertex. The amplitude should be independent of η, and η should be chosen to be the same for all off-shell gluons in the calculation.

Since the MHV amplitudes can be interpreted as vertices in a Yang-Mills theory, one would expect to find a Lagrangian to derive them from. Such a Lagrangian has been derived from the Yang-Mills Lagrangian using a light-cone expansion [143,144].

In a series of remarkable papers [115, 116, 145] the MHV rules were extended to loop level. A four-dimensional application of the MHV rules was found to directly make contact with unitarity cuts and as such was able to calculate the cut-constructible pieces of the all n gluon MHV one-loop amplitudes in $\mathcal{N} = 4, 1$ and 0 theories. As we have seen, this combination of SYM amplitudes can be used to construct the cut-constructible pieces of the gluonic QCD amplitude.

Another interesting application of the MHV rules relevant for this thesis has been in the construction of the ϕ and $\phi^\dagger$ plus parton amplitudes at tree-level [95, 146]. The Lagrangian which is associated with this splitting of the Higgs field into dual and anti-self dual pieces has been discussed in section 1.4.2. Here we comment on the MHV structure of the theory. It was proven in [95] that the following amplitudes vanish,

$$A_n^{(0)}(\phi, 1^\pm, 2^+, \ldots, n^+) = 0 \tag{2.84}$$

as well as the relevant parity conjugates. This similarity to the pure QCD amplitudes holds at the MHV level, where

$$A_n^{(0)}(\phi, 1^+, \ldots, i^-, \ldots, j^-, \ldots, n^+) = \frac{\langle ij\rangle^4}{\prod_{\alpha=1}^{n-1}\langle\alpha(\alpha+1)\rangle\langle n1\rangle}. \tag{2.85}$$

The only difference being that in the pure QCD case $\sum_{i=1}^n p_i^\mu = 0$, here $\sum_{i=1}^n p_i^\mu = -p_\phi^\mu$. A major difference between QCD and the ϕ plus gluon amplitudes are the all-minus amplitudes (which are zero in QCD). The ϕ all-minus amplitudes have the following form,

$$A_n^{(0)}(\phi, 1^-, \ldots, i^-, \ldots, j^-, \ldots, n^-) = \frac{(-1)^n m_H^4}{\prod_{\alpha=1}^{n-1}[\alpha(\alpha+1)][n1]}. \tag{2.86}$$

ϕ plus parton amplitudes have also been derived [146] and are listed in Appendix A.

MHV rules have also been derived for amplitudes coupling gluons to massive (coloured) scalars [147, 148]. These are relevant since eq. (2.4) shows that the only part of gluon loop amplitudes which are not cut-constructible are the $\mathcal{N}^{scalar} = 0$ pieces. One way of implementing D dimensional unitarity is to consider the -2ϵ pieces of the loop momenta as a mass μ. It has been shown [149], that one can use unitarity cuts to construct one-loop amplitudes from the MHV rules of [147, 148].

2.5.2 The BCFW recursion relations

The BCFW recursion relations [140, 141] represent a remarkably simple yet deep approach to the calculation of tree amplitudes in gauge theories. Essentially they show that the entire spectrum of tree amplitudes can be calculated in a theory from knowledge of the three point vertices alone. The proof is remarkably simple and relies only on complex analysis and the universal factorisation of tree amplitudes. There has been a huge range of applications of the recursion relations, including (but not limited to) QCD [150–154], QED [155, 156] and more exotic theories [157–160]. Here we sketch the details of the proof for a pure gluonic amplitude [141].

One begins by taking an on-shell amplitude $A_n^{(0)}$ and selecting two of the gluons p_i and p_j for special treatment. We wish to shift these momenta such that overall

momentum conservation is retained,

$$p_i^\mu \to p_i^\mu + \frac{z}{2}\langle j|\gamma^\mu|i] \quad \text{and} \quad p_j^\mu \to p_j^\mu - \frac{z}{2}\langle j|\gamma^\mu|i] \tag{2.87}$$

We note that $p_i(z) + p_j(z) = p_i + p_j$ such that local momentum conservation is also preserved. Furthermore

$$p_i^2(z) = (p_i^\mu + \frac{z}{2}\langle j|\gamma^\mu|i])(p_{i,\mu} + \frac{z}{2}\langle j|\gamma_\mu|i]) = 0 \tag{2.88}$$

which implies that $p_i(z)$ is also on-shell. The shifts we have made are equivalent to the following spinor shifts,

$$|i\rangle \to |i\rangle + z|j\rangle \quad \text{and} \quad |j] \to |j] - z|i], \tag{2.89}$$

whilst leaving $|i]$ and $|j\rangle$ unaltered. Immediately we see that we are no longer dealing with real momenta in Minkowski space (where $\overline{\lambda} = \pm\tilde{\lambda}$), and just as in the quadruple cuts of section 2.2 we work with complex momenta.

The shifted amplitude $A_n^{(0)}(z)$ is thus also an on-shell tree amplitude and in particular will share properties associated with physical on-shell tree amplitudes. Firstly we note that $A_n^{(0)}(z)$ is a rational function in z. Indeed $A_n^{(0)}(z)$ only has simple poles in z. This can be seen by considering how poles of tree-level amplitudes occur. Tree-level amplitudes can only develop a pole when an internal propagator goes on-shell i.e. $P_{abc}^2 \to 0$, where P_{abc} is some generic combination of external momenta. Since propagators are quadratic one may expect that double poles in z could arise, however if the propagator $P_{\alpha\ldots\beta}$ goes on-shell and $i \in \{\alpha, \ldots, \beta\}$, $j \notin \{\alpha, \ldots, \beta\}$ then we have,

$$P(z)^2_{\alpha\ldots\beta} = (p_\alpha + \cdots + p_i + z|j\rangle[i| + \cdots + p_\beta)^2 = P^2_{\alpha\ldots\beta} + z\langle j|P_{\alpha\ldots\beta}|i] \tag{2.90}$$

If both $i \in \{\alpha, \ldots, \beta\}$ and $j \in \{\alpha, \ldots, \beta\}$ then the z dependence drops out,

$$P(z)^2_{\alpha\ldots\beta} = (p_\alpha + \cdots + p_i + z|j\rangle[i| + \ldots p_j - z|j\rangle[i] + \cdots + p_\beta)^2 = P^2_{\alpha\ldots\beta}. \tag{2.91}$$

So only simple poles can occur and a residue occurs when z is of the form $z = P^2_{\alpha\ldots\beta}/\langle j|P_{\alpha\ldots\beta}|i]$.

Next we assume that $A(z) \to 0$ as $z \to \infty$, this means that one can write $A(z)$ in the following form

$$A(z) = \sum_{ij} \frac{c_{ij}}{z - z_{ij}}. \tag{2.92}$$

Ultimately we wish to know the physical amplitude $A(0)$,

$$A(0) = \sum_{ij} \frac{c_{ij}}{z_{ij}} \tag{2.93}$$

All that needs to be determined are the coefficients of the residues at z_{ij}, this is a simple task however, since the only source of poles in a tree amplitude occurs when an internal propagator goes on-shell. When this happens the amplitude factors on to two lower point amplitudes (the so-called left and right amplitudes). This means that we can write $A(z)$ as

$$A(z) = \sum_{h=\pm} \sum_{ij} \frac{A^{L,-h}(z_{ij}) A^{R,h}(z_{ij})}{P_{ij}^2(z)}, \tag{2.94}$$

the sum over h represents the two helicity orientations of the propagator. We require $A(0)$ where,

$$A(0) = \sum_{h=\pm} \sum_{ij} \frac{A^{L,-h}(z_{ij}) A^{R,h}(z_{ij})}{P_{ij}^2}. \tag{2.95}$$

Eq. (2.95) is the BCFW recursion relation.

2.6 The unitarity-bootstrap

So far in this chapter we have described methods for calculating the cut-constructible pieces of one-loop amplitudes for massless theories. Eq. (2.5) shows that by working in four dimensions we lose information associated with higher order pieces in ϵ of the coefficient of the basis integrals. These missing pieces are referred to as the rational pieces. In this section we describe a method which obtains these rational pieces and is still four-dimensional, the unitarity-bootstrap [124, 161–165].

2.6.1 BCFW at one-loop

Since the rational pieces of one-loop amplitudes contain no discontinuities they have the same kinematic structure as tree-level amplitudes. This lead to the realisation that they could be calculated, in principle, using BCFW recursion relations [161]. In the previous section the proof of BCFW recursion relations was sketched, here we consider the integral over the shifted amplitude $A(z)$,

$$\mathcal{I} = \frac{1}{2\pi i}\oint_C \frac{A(z)}{z}. \tag{2.96}$$

The contour C is taken around the circle at infinity, if, as was required in the proof, $A(z) \to 0$ as $z \to \infty$, we find the following result,

$$0 = A(0) + \sum_{\text{poles }\alpha} \text{Res}_{z=z_\alpha} \frac{A(z)}{z}. \tag{2.97}$$

If, on the other hand there is a contribution from $A(z)$ as $z \to \infty$ (equal to C_∞), the relation would be

$$A(0) = C_\infty - \sum_{\text{poles }\alpha} \text{Res}_{z=z_\alpha} \frac{A(z)}{z}. \tag{2.98}$$

For one-loop amplitudes many of the properties of the shifted amplitude $A(z)$ change from those at tree-level. For example the proof in the previous section required that the amplitude contained only simple poles which arose from internal propagators going on-shell. At one-loop the situation changes and logarithms appear which possess discontinuities and are defined on the complex plane with a branch cut. The differences between the complex planes for tree-level and one-loop amplitudes are shown schematically in Fig. 2.4 and Fig. 2.5. The BCFW recursion relations must be altered to work at one-loop [161–163]. We begin by assuming once again that for a specific shift $A(z) \to 0$ as $z \to \infty$. We then consider the following vanishing integral which is taken along the circle at ∞ and deformed such that it moves around the branch cuts.

$$0 = \frac{1}{2\pi i}\oint_C \frac{A(z)}{z}. \tag{2.99}$$

The integral, although it still vanishes, is no longer equal to the sum of residues of the simple poles. We must also include the contribution from the line integrals

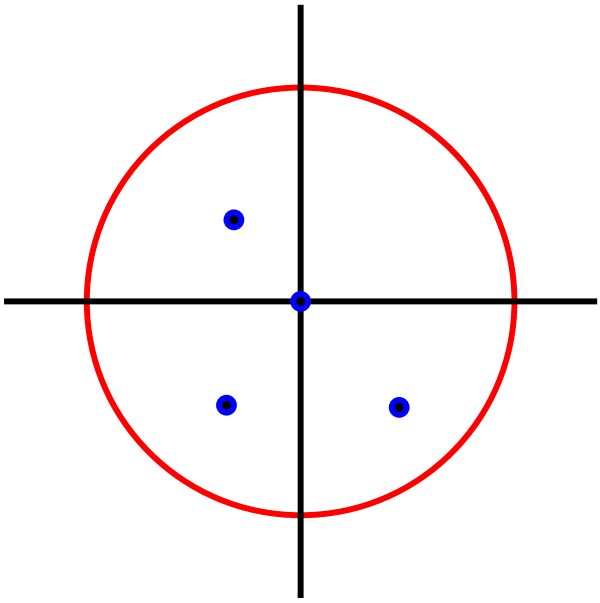

Figure 2.4: Tree-level amplitudes contain only simple poles in the shift parameter z, these are each associated with an internal propagator going on-shell

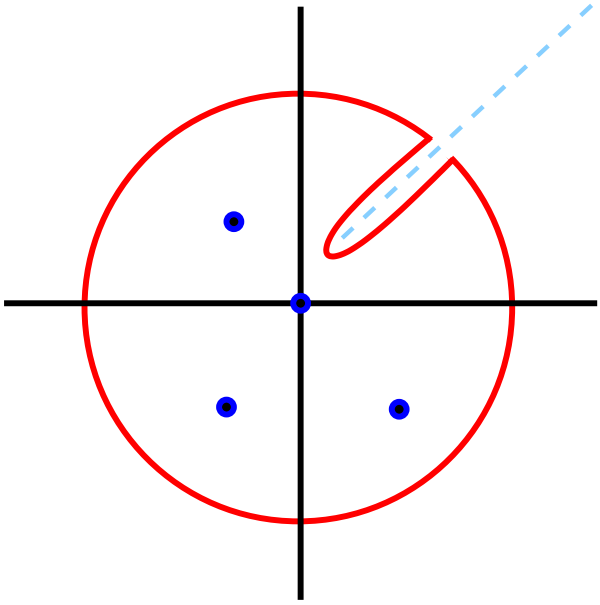

Figure 2.5: One-loop amplitudes contain both simple poles and discontinuous functions (illustrated by the branch cut) in the shift parameter z.

deformed around the discontinuity (here referred to as B),

$$\frac{1}{2\pi i}\oint_{B^{\uparrow}+i\epsilon}\frac{A(z)}{z}+\frac{1}{2\pi i}\oint_{B^{\downarrow}-i\epsilon}\frac{A(z)}{z}. \tag{2.100}$$

Since $A(z)$ has a non-vanishing discontinuity along B,

$$2\pi i\,\mathrm{Disc}_B\,A(z)=A(z+i\epsilon)-A(z-i\epsilon) \tag{2.101}$$

one may write

$$0=A(0)+\sum_{\text{poles}\,\alpha}\mathrm{Res}_{z=z_\alpha}\frac{A(z)}{z}+\sum_{\mathrm{Disc}_B}\int_B\frac{dz}{z}\mathrm{Disc}_B A(z), \tag{2.102}$$

this is the structure of a one-loop amplitude under a BCFW shift. Of course, one must take special care if a pole is located along a branch cut, here must one move the pole away from the branch cut by a small amount δ calculate the branch cut terms separately and take the limit δ goes to zero at the end of the calculation.

2.6.2 Cut-constructible, cut-completion, rational and overlap terms

Eq. (2.102) describes the properties of one-loop amplitudes under a generic BCFW shift (which vanishes at ∞). However, as been described in detail in this chapter, we have simple and generic methods to extract the cut-constructible pieces of one-loop amplitudes. Ideally we would wish to only extract the rational pieces from a recursion relation, which are missed by our four-dimensional methods. Since these pieces contain no discontinuities they should have simpler recursive properties than the whole one-loop amplitude.

There is one complication however since rational and cut-constructible pieces need to communicate with each other to ensure correct factorisation. Specifically we will use the following basis functions which arise from the reduction of tensor triangles,

$$L_i(s,t)=\frac{1}{(s-t)^i}\log(s/t). \tag{2.103}$$

These terms become singular for $i>1$ as $s\to t$, since this is a non-physical singularity it must be cancelled by some part of the rational piece. To aid in the stability

of our results we shift (or complete) the basis such that no basis functions develop unphysical singularities. The completed basis has the following form,

$$\begin{aligned} L_3(s,t) \to \hat{L}_3(s,t) &= L_3(s,t) - \frac{1}{2(s-t)^2}\left(\frac{1}{s}+\frac{1}{t}\right), \\ L_2(s,t) \to \hat{L}_2(s,t) &= L_2(s,t) - \frac{1}{2(s-t)}\left(\frac{1}{s}+\frac{1}{t}\right), \\ L_1(s,t) \to \hat{L}_1(s,t) &= L_1(s,t), \\ L_0(s,t) \to \hat{L}_0(s,t) &= L_0(s,t). \end{aligned} \tag{2.104}$$

The rational pieces associated with the above functions are called the cut-completion terms, we will use the following notation to describe the various pieces of the amplitude. The rational pieces are those left when all of the logs, dilogs and π^2 terms vanish,

$$R_n(z) = \frac{1}{c_\Gamma} A_n \Big|_{\log,\mathrm{Li},\pi^2 \to 0}, \tag{2.105}$$

so that the total (z dependent) amplitude is defined as

$$A_n(z) = c_\Gamma (C_n(z) + R_n(z)). \tag{2.106}$$

As described above the cut-constructible pieces can be completed by including some rational terms,

$$\widehat{C}_n(z) = C_n(z) + \widehat{CR}_n(z) \tag{2.107}$$

where

$$\widehat{CR}_n(z) = \widehat{C}_n(z)\Big|_{rat}. \tag{2.108}$$

Of course the total rational piece R_n is the sum of completion terms CR_n and the remaining rational pieces

$$R_n(z) = \widehat{CR}_n(z) + \widehat{R}_n(z). \tag{2.109}$$

We now wish to consider the following integral

$$\int_B \frac{dz}{z} \mathrm{Disc}_B \widehat{C}_n(z) \tag{2.110}$$

which, since the rational pieces contain no discontinuities, corresponds to the discontinuities of the shifted amplitude $A(z)$. If $\widehat{C}_n(z)$ vanishes as $z \to \infty$, then the same logic which was applied to the total amplitude $A(z)$ can be applied to $\widehat{C}_n(z)$

$$\widehat{C}_n(0) = -\sum_{\text{poles}\,\alpha} \text{Res}_{z=z_\alpha} \frac{\widehat{C}_n(z)}{z} - \sum_{\text{Disc}_B} \int_B \frac{dz}{z} \widehat{C}_n(z) \tag{2.111}$$

Now when we use this information in eq. (2.102) we find

$$\begin{aligned} A_n(0) &= -c_\Gamma \Bigg[\sum_{\text{poles}\,\alpha} \text{Res}_{z=z_\alpha} \frac{\widehat{R}_n(z)}{z} + \sum_{\text{poles}\,\alpha} \text{Res}_{z=z_\alpha} \frac{\widehat{C}_n(z)}{z} + \sum_{\text{Disc}_B} \int_B \frac{dz}{z} \widehat{C}_n(z) \Bigg] \\ &= c_\Gamma \Bigg[\widehat{C}_n(0) - \sum_{\text{poles}\,\alpha} \text{Res}_{z=z_\alpha} \frac{\widehat{R}_n(z)}{z} \Bigg]. \end{aligned} \tag{2.112}$$

This is exactly the form we require and the cut-constructible pieces which we calculate with the unitarity method C_n are cleanly separated from the unknown rational pieces, which only require summing over residues in z to determine. The task is now to determine the exact recursive behaviour of $\widehat{R}_n$.

It was shown in [163] that due to the separate factorisation of rational and cut containing pieces one can devise a one-loop recursion relation for the pure rational pieces,

$$\begin{aligned} -\sum_{\text{poles}\,\alpha} \text{Res}_{z=z_\alpha} \frac{R_n(z)}{z} &= R_n^D \\ &= \sum_{h=\pm} \sum_{ij} \frac{R^{L,-h}(z_{ij}) A^{R,h}(z_{ij})}{P_{ij}^2} + \frac{A^{L,-h}(z_{ij}) R^{R,h}(z_{ij})}{P_{ij}^2} \\ &\quad + A^{L,-h}(z_{ij}) R(P_{ij}^2) A^{R,h}(z_{ij}). \end{aligned} \tag{2.113}$$

Here $R^{L,R}$ represents a lower point rational part of a one-loop amplitude on the left (or right) hand side of the partition which results in the internal (massless) propagator P_{ij}^2 going on-shell. The piece $A^{(0)} R A^{(0)}$ is a new contribution at one-loop and represents one-loop corrections to the propagator[4]. With this recursion relation in place we are nearly finished. Eq. (2.113) does not discriminate between

[4]In MHV helicity configurations this term does not contribute since one of the trees always vanishes.

rational pieces which arise recursively and those which are defined as completion terms. Therefore to avoid double counting we must remove the overlapping residues

$$R_n^D = -\sum_{\text{poles }\alpha} \text{Res}_{z=z_\alpha} \frac{\widehat{CR}_n(z)}{z} - \sum_{\text{poles }\alpha} \text{Res}_{z=z_\alpha} \frac{\widehat{R}_n(z)}{z}. \tag{2.114}$$

So that the final amplitude is given by

$$A_n(0) = c_\Gamma \left[\widehat{C}_n(0) + R_n^D + \sum_{\text{poles }\alpha} \text{Res}_{z=z_\alpha} \frac{\widehat{CR}_n(z)}{z} \right] \tag{2.115}$$

This is the unitarity-bootstrap method. One first calculates C_n using unitarity methods, then after completing the L_i functions one calculates the residues of $\widehat{CR}$ associated with the shift parameter z. Finally from the knowledge of lower point amplitudes one calculates the rational piece R^D.

2.6.3 Techniques for general helicity amplitudes

In the previous section we described the unitarity-bootstrap technique in the optimum case (where $A(z) \to 0$ as $z \to \infty$ and the recursive pieces contained only simple poles). In this section we discuss the general approach when these conditions fail [124, 165].

We begin the discussion with the more serious problem associated with the appearance of double poles. We consider a three vertex $A^\mu(\varepsilon_a, \varepsilon_b)$ for which a and b are external on-shell gluons and μ is the Lorentz index for the intermediate gluon which is going on-shell in a particular way (either $\langle ab \rangle$ or $[ab]$ is zero). The general tensor structure can be written as [124, 166–169],

$$\begin{aligned} A_3^\mu(\varepsilon_a, \varepsilon_b) = g_1 \left(s_{ab}, \frac{k_a \cdot \eta}{(k_a + k_b) \cdot \eta} \right) \frac{1}{s_{ab}} \left(\varepsilon^\mu \varepsilon_b \cdot k_a - \varepsilon_b^\mu \varepsilon_a \cdot k_b + k_b^\mu \varepsilon_a \cdot \varepsilon_b \right) \\ + g_2 \left(s_{ab}, \frac{k_a \cdot \eta}{(k_a + k_b) \cdot \eta} \right) \frac{k_a^\mu}{s_{ab}} \left(\varepsilon_a \cdot \varepsilon_b - \frac{\varepsilon_a \cdot k_b \, \varepsilon_b \cdot k_a}{k_a \cdot k_b} \right). \end{aligned} \tag{2.116}$$

Here the dependence on the reference vector η describes how the form factors depend on the way in which a and b go on-shell. The first tensor structure is that which appears at tree-level,

$$A_3^{tree,\mu}(\varepsilon_a, \varepsilon_b) = \frac{1}{s_{ab}} \left(\varepsilon^\mu \varepsilon_b \cdot k_a - \varepsilon_b^\mu \varepsilon_a \cdot k_b + k_b^\mu \varepsilon_a \cdot \varepsilon_b \right). \tag{2.117}$$

The second tensor structure vanishes when a and b have opposite helicities,

$$\left(\varepsilon_a^+ \cdot \varepsilon_b^- - \frac{\varepsilon_a^+ \cdot k_b \, \varepsilon_b^- \cdot k_a}{k_a \cdot k_b}\right) = -\frac{[aq_b]\langle bq_a\rangle}{\langle aq_a\rangle[bq_b]} + \frac{[ab]\langle bq_a\rangle\langle ba\rangle[aq_b]}{\langle aq_a\rangle[bq_b]\langle ab\rangle[ba]} = 0. \tag{2.118}$$

The definitions of the polarisation vectors in terms of their reference vectors q_i are given in Appendix A. Since the tensor structure vanishes at tree-level it should also vanish for all loops (because the loops only change the form factor g_2). Therefore when the two gluons a and b have opposite helicity only the tree-like tensor structure enters the game and we understand the factorisation for complex momenta. However, when the two momenta have the same helicity the tensor structure no longer vanishes,

$$\begin{aligned}\left(\varepsilon_a^+ \cdot \varepsilon_b^+ - \frac{\varepsilon_a^+ \cdot k_b \, \varepsilon_b^+ \cdot k_a}{k_a \cdot k_b}\right) &= \frac{[ab]\langle q_b q_a\rangle}{\langle aq_a\rangle\langle bq_b\rangle} - \frac{[ab]\langle bq_a\rangle[ba]\rangle\langle aq_b\rangle}{\langle aq_a\rangle\langle bq_b\rangle\langle ab\rangle[ba]} \\ &= -\frac{[ab]}{\langle ab\rangle\langle aq_a\rangle\langle bq_b\rangle}\Big(\langle ab\rangle\langle q_a q_b\rangle + \langle bq_a\rangle\langle aq_b\rangle\Big) \\ &= -\frac{[ab]}{\langle ab\rangle}.\end{aligned} \tag{2.119}$$

This tensor structure still vanishes if we approach the on-shell limit such that $[ab] \to 0$ (or $\langle ab\rangle \to 0$ for the two negative case). In these cases the tree-level also piece also vanishes. If this tensor structure survives in the on-shell limit then it can produce double poles in $\langle ab\rangle$ (when multiplied by the $1/s_{ab}$). These double poles produce subleading single poles whose complex momenta behaviour is not fully understood, and, at the moment, there is no systematic way to include them into the recursion relations.

Therefore when using the recursion relations at one-loop we have to ensure that there are no shifts which contain a three point vertex with two external gluons of the same helicity. However, as mentioned above if the tree-level amplitude for a particular shift vanishes these diagrams do not contribute, e.g. if we shift $|i\rangle \to |i\rangle + z|k\rangle$ and i is a negative gluon found in a tree amplitude with j and $\widehat{P}_{ij}$ then we find,

$$\widehat{P}_{ij}^2 = 0 \implies 0 = P_{ij}^2 + z\langle kj\rangle[ji] \implies z = -\frac{\langle ij\rangle}{\langle kj\rangle}. \tag{2.120}$$

After using the Schouten identity we find that with this z solution

$$|i\rangle = \frac{\langle ik\rangle}{\langle kj\rangle}|j\rangle \implies \langle ij\rangle = 0. \tag{2.121}$$

Thus if we choose our shift such that $|i\rangle$ (and not $|i]$) is shifted and k (the other shifted vector) does not have a non-zero three point tree amplitude with an external gluon of the same helicity, then the unitarity bootstrap will still yield the correct answer.

Clearly unphysical double poles can spoil the BCFW recursion relations at one-loop and shifts which result in this behaviour should be avoided. The other assumption made in deriving eq. (2.115) is that there is no large-z behaviour for the amplitude A_n. If this were not the case then one would have to modify eq. (2.115) as follows,

$$A_n = \mathrm{Inf}A_n + c_\Gamma\left[\widehat{C}_n(0) + R_n^D + O_n\right]. \tag{2.122}$$

Here we have used O_n to denote the overlap terms which appear in eq. (2.115). The appearance of boundary terms is a less serious issue since in general one can determine these contributions. It was shown in [124] that by performing additional shifts one could determine these pieces. For example, suppose a shift $[i,j\rangle$ on A_n had some non-zero $z \to \infty$ terms. Then one could perform an auxiliary shift $[k,l\rangle$ and calculate the rational terms associated with these pieces. Then by applying the original shift to these new rational contributions one would get a polynomial in z. By taking the z^0 term in an expansion around $z = \infty$ we find a piece of $\mathrm{Inf}A_n$. We are only interested in z^0 since higher order pieces do not contribute to the physical ($z = 0$) amplitude we are ultimately interested in. If we choose the auxiliary shift carefully we can determine the $\mathrm{Inf}A_n$ in its entirety[5].

[5]In general one would have to take multiple shifts to determine whether the auxiliary shift had determined $\mathrm{Inf}A_n$ fully. Collinear limits also provide a check. In this thesis we are able to check the rational pieces against a Feynman diagram calculation.

2.7 D-dimensional techniques

This chapter has focused on four-dimensional on-shell techniques for the generation of one-loop amplitudes. As has been described, using four-dimensional trees in the optical theorem results in only a partial reconstruction of the entire amplitude. To obtain the full amplitude from unitarity cuts one should use D-dimensional trees. At first glance this is somewhat unappealing, since when using four-dimensional trees, we have a vast utility of tools and techniques associated with the spinor helicity formalism at our disposal. Indeed the number of polarisations of a gluon in D dimensions is $2-\epsilon$, which spoils the compact helicity amplitudes used previously. To avoid this one can work in the four dimensional helicity scheme (FDH), in which external states are kept in four dimensions and only the loop momenta are continued to D-dimensions. Then one can consider the -2ϵ components of the loop momenta to be a mass μ since the only place these will enter in the FDH scheme are from ℓ^2, and some of the advantages of unitarity can still be used [170].

The scalar n-point function in massless theories is given in D dimensions by,

$$I_n^D[1] = i(-1)^{n+1}(4\pi)^{D/2}\int \frac{d^D L}{(2\pi)^D}\frac{1}{L^2(L-p_1)^2\dots(L-\sum_{i=1}^{n-1}p_i)^2}. \tag{2.123}$$

Here L exists fully in $D=4-2\epsilon$ dimensions, whist in the FDH the external sums of momenta are four dimensional. This allows us to make the separation

$$L = \ell + \mu, \tag{2.124}$$

where ℓ is 4 dimensional and μ are the -2ϵ components of L. This transforms the measure as,

$$\int d^D L = \int d^{-2\epsilon}\mu \int d^4\ell. \tag{2.125}$$

The transformation re-writes (2.123) as,

$$I_n^D[1] = \int \frac{d^{-2\epsilon}\mu}{(2\pi)^{-2\epsilon}}\int \frac{d^4\ell}{(2\pi)^4}\frac{i(-1)^{n+1}(4\pi)^{2-\epsilon}}{(\ell^2-\mu^2)((\ell-p_1)^2-\mu^2)\dots((\ell-\sum_{i=1}^{n-1}p_i)^2-\mu^2)}, \tag{2.126}$$

thus transforming a massless integral in D dimensions into a massive four dimensional integral. An arbitrary numerator now acquires a dependence on μ^2, and a

generic integral becomes a polynomial in this parameter. We can use the results of [170] to relate these integrals with factors of μ^2 in the numerator to higher-dimensional scalar integrals.

$$\begin{aligned} I_n^D[(\mu^2)^r] &= \int \frac{d^{-2\epsilon}\mu}{(2\pi)^{-2\epsilon}} \int \frac{d^4\ell}{(2\pi)^4} \frac{i(-1)^{n+1}(4\pi)^{2-\epsilon}(\mu^{2r})}{(\ell^2-\mu^2)((\ell-p_1)^2-\mu^2)\dots((\ell-\sum_{i=1}^{n-1}p_i)^2-\mu^2)} \\ &= -\epsilon(1-\epsilon)\dots(r-1-\epsilon)I_n^{D+2r}[1]. \end{aligned} \tag{2.127}$$

Over the past few years many authors have investigated D-dimensional unitarity setting varying numbers of denominators on-shell with delta functions. These include D-dimensional generalised unitarity, [171,172] where 4-3 and 2-cuts were used to determine amplitudes. A D-dimensional version of the triple cut was derived in [128]. Double cuts using spinor integration in D-dimensions have been studied extensively in [133–137, 173]. An implementation of the Laurent expansion in D dimensions has also been developed [172].

2.8 Recent progress: One-loop automatisation

Before closing this chapter the culmination of recent years work on automatisation should be reviewed. For a long time the bottleneck in multi-leg processes was the calculation of virtual corrections to $2 \to 4$ processes. The number of Feynman diagrams associated with $2 \to n$ processes grows factorially and as n increases new tensor integrals arise which must be reduced to the known set of basis integrals [16]. Until recently no $2 \to 4$ processes had been completed at one-loop using Feynman diagram techniques, however over the last couple of years great strides in this direction have been made, including the complete calculation of $pp \to t\bar{t} + b\bar{b}$ [174–176] and $q\bar{q} \to b\bar{b}b\bar{b}$ [177]. Despite the recent progress each new parton in the final state brings with it many complications for the older approach. The unitarity methods described in this chapter are well suited to multi-leg processes since the growth in complexity is only linked to the growth in complexity of the (on-shell) tree amplitudes from which the loops are made. Over the last couple of years several groups have implemented these methods into programs which can automatically generate one-loop amplitudes.

Blackhat [126, 178–181] is a program which implements the four-dimensional methods described in this chapter. The Laurent expansion method [122] is applied in four dimensions to determine the coefficients of the cut-constructible pieces. The rational pieces are then calculated using the unitarity-bootstrap approach with multiple shifts [124, 161–165]. The program also includes the D-dimensional application of the Laurent expansion [172] for an alternate method of generating the rational terms. This program has been successfully integrated with the Monte Carlo event generator Sherpa [33, 37, 38], which provides an efficient mechanism for generating the real matrix elements and performing the integration over phase space. Blackhat has been successfully applied to the calculation of $V + 3$ jets (at NLO) [126, 178–181] where V is massive vector boson.

The program Rocket also uses unitarity techniques to numerically generate one-loop amplitudes [182]. Rocket uses a numerical implementation of D-dimensional unitarity [183–185], which can be applied to massive and massless particles. This program also uses the QCDLoop package [186] which calculates the scalar basis integrals. Rocket has also calculated $W + 3$ jets [187, 188] and the results between the two groups are in agreement. Very recently, Rocket has been used with MCFM to compute $pp \to W^+W^+ + 2j$ [189].

In addition to the unitarity based programs described above the Helac-Phegas collaboration [190] have calculated $t\bar{t}b\bar{b}$ production and $t\bar{t} + 2j$ [191] using the OPP reduction technique [125, 192–195]. This reduction algorithm is similar to unitarity techniques in that it is four-dimensional and solves for coefficients of basis integrals using on-shell constraints, however the OPP method can be applied equally to products of amplitudes (as in the unitarity case) or to individual Feynman diagrams. The rational pieces are generated differently however, with a separation into pieces which can be generated recursively and those which can be deduced from the reduction. The OPP method has also been applied to the calculation of tri-boson production [196, 197].

Efforts have also been made to automate $2 \to 4$ Feynman diagram calculations and the GOLEM collaboration [198, 199] has made progress in this direction, in-

cluding the recent calculation of $q\overline{q} \to b\overline{b}b\overline{b}$ [177]. This program uses improved Feynman diagram reduction techniques [200–202] and has been used to calculate the six photon amplitude [129].

2.9 Summary

In this chapter on-shell methods for calculating one-loop amplitudes have been described in detail. Several unitarity methods which will be used in later chapters have been discussed. Inspired by the use of complex momenta generalised unitarity and the BCFW recursion relations have been detailed with examples given of the techniques we will apply in the following chapters. Other on-shell techniques, the MHV rules and D-dimensional unitarity have also been included for completeness, although they will play a limited role in the remainder of this thesis. A short overview of the recent progress towards automisation has been given.

In the next chapter we will use the techniques described in the previous sections to calculate the ϕ-MHV amplitude. We will calculate the cut-constructible pieces for all multiplicities, the rational pieces for the amplitude $A_4^{(1)}(\phi, 1^-, 2^+, 3^-, 4^+)$ will also be calculated using the BCFW recursion relations.

Chapter 3

One-loop ϕ-MHV amplitudes: the general helicity case

3.1 Introduction

In this chapter we present the calculation of the ϕ-MHV amplitudes where the two negative helicity gluons are positioned arbitrarily. This builds on previous work [108] in which the two negative helicity gluons were constrained to be colour adjacent. We will use the methods of generalised unitarity to determine the cut-constructible pieces of the amplitude. Coefficients associated with box integrals will be calculated using the four-cut method of Britto, Cachazo and Feng [120], which has been discussed in section 2.2. It will be shown that for the ϕ-MHV amplitudes only one- and two-mass easy boxes appear. The triangle coefficients will be determined using Forde's Laurent expansion method [122] described in section 2.3 (we will also show that one can use IR conditions to fix the triangles once the box coefficients are known). Finally, the bubble (or 2-point) coefficients will be determined using Mastrolia's Stokes' Theorem method [132], which was introduced in section 2.4. Due to the simplicity of these methods it is easy to generalise the cut-constructible pieces to include n gluon multiplicities.

The rational pieces will be calculated using the unitarity bootstrap approach

[124, 165] (see section 2.6), and checked using Feynman diagrams. For simplicity, we focus our efforts on the four point amplitude $A_4^{(1)}(\phi, 1^-, 2^+, 3^-, 4^+)$ which we are ultimately interested in.

The tree-level ϕ-MHV amplitude has the following form [95],

$$A_n^{(0)}(\phi, 1^-, 2^+, \ldots, m^-, (m+1)^+, \ldots, n^+) = \frac{\langle 1m\rangle^4}{\prod_{\alpha=1}^{n-1}\langle\alpha(\alpha+1)\rangle\langle n1\rangle}. \tag{3.1}$$

Here we refer to the colour stripped primitive amplitude. The details of how to obtain colour dressed ϕ plus parton amplitudes are given in Appendix A. We will decompose the loop amplitude into cut-constructible and rational pieces C_n and R_n respectively, which are defined as follows,

$$\begin{aligned} A_n^{(1)}(\phi, 1^-, 2^+, \ldots, m^-, \ldots, n^+) = c_\Gamma\Big(& C_n(\phi, 1^-, 2^+, \ldots, m^-, \ldots, n^+) \\ & + R_n(\phi, 1^-, 2^+, \ldots, m^-, \ldots, n^+)\Big), \end{aligned} \tag{3.2}$$

where

$$c_\Gamma = \frac{\Gamma^2(1-\epsilon)\Gamma(1+\epsilon)}{(4\pi)^{2-\epsilon}\Gamma(1-2\epsilon)}. \tag{3.3}$$

We will also use the following notation to define the cut-completed cut-constructible pieces $\widehat{C}_n$ and the remaining rational terms $\widehat{R}_n$ (with the completion terms removed).

$$\begin{aligned} A_n^{(1)}(\phi, 1^-, 2^+, \ldots, m^-, \ldots, n^+) = c_\Gamma\Big(& \widehat{C}_n(\phi, 1^-, 2^+, \ldots, m^-, \ldots, n^+) \\ & + \widehat{R}_n(\phi, 1^-, 2^+, \ldots, m^-, \ldots, n^+)\Big). \end{aligned} \tag{3.4}$$

In the following section we calculate the cut-constructible part $\widehat{C}_n$ for all n, then in section 4.3 we use the BCFW recursion relations to calculate the rational contribution $\widehat{R}_n$, which we check against a Feynman diagram calculation. Finally in section 3.4 we justify the calculations by performing extensive collinear and soft checks on the amplitude.

3.2 The cut-constructible parts

In this section we will use generalised unitarity methods to calculate C_n which appears in eq. (3.2). In general the cut-constructible pieces have the following basis

decomposition,

$$C_n(\phi, 1^-, 2^+, \ldots, m^-, \ldots, n^+) = \sum_i C_{4;i} I_{4;i} + \sum_i C_{3;i} I_{3;i} + \sum_i C_{2;i} I_{2;i}. \quad (3.5)$$

Here $C_{j;i}$ represents the coefficient of a j-point scalar basis integral ($I_{j;i}$) with a distribution of momenta $\{i\}$. Using the methods described in Chapter 2 we will isolate each coefficient separately using a dedicated cut for that integral. We work with a top down approach and calculate the box integral coefficients first [120], then the triangle coefficients [122] finally using a double cut to determine the coefficient associated with the two-point functions [132].

3.2.1 Box coefficients from four-cuts

We begin by discussing the boxes which do not contribute to the ϕ-MHV amplitude. Specifically these are the four-, three- and two-mass hard boxes, which are shown in Figs. 3.1-3.3. The three- and four-mass box configurations vanish trivially, since however one assigns the helicities to the loop momenta one always finds at least one zero-tree amplitude at one of the corners. Many of the two-mass hard topologies vanish for a more subtle reason. When two MHV or $\overline{\text{MHV}}$ three-point amplitudes are adjacent in a box topology the corresponding coefficient is zero. This can be illustrated by considering the following product of two on-shell MHV amplitude,

$$\begin{aligned} A^{2\times MHV} &= A_3^{(0)}(\ell_1^+, 2^-, \ell_2^-) A_3^{(0)}(\ell_2^+, 3^-, \ell_3^-) \\ &= \frac{\langle \ell_2 2\rangle^3}{\langle \ell_1 2\rangle \langle \ell_2 \ell_1\rangle} \frac{\langle \ell_3 3\rangle^3}{\langle \ell_2 3\rangle \langle \ell_3 \ell_2\rangle}. \end{aligned} \quad (3.6)$$

The complex solution of the on-shell constraints ensure that $[\ell_2 2] = 0$ from $(\ell_2 + p_2)^2 = 0$. However, the constraint at the second vertex implies that $(\ell_2 + p_3)^2 = 0$, for which the complex solution is that $[\ell_2 3] = 0$. This then implies that $[23] = 0$, or $|2] \propto |3]$. This solution is unphysical and as such we must throw it away.

Therefore we have established that the only box functions which can appear in the general one-loop ϕ-MHV amplitude are one and two-mass easy box functions. We will now classify the boxes and their solutions for general gluon multiplicities.

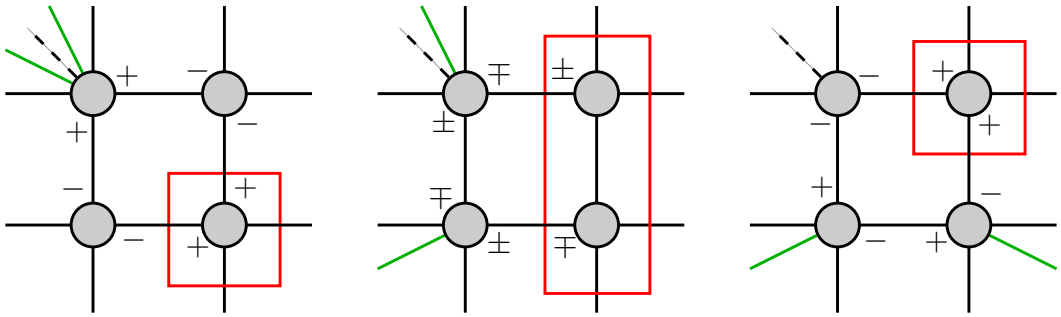

Figure 3.1: Configurations where the coefficient of the four-mass box vanishes, external particles are either; positive helicity gluons (solid black lines) of which there can be an arbitrary number at any vertex, negative helicity gluons (shown in green) of which there can be only two and one ϕ (dashed black line). In each configuration $(a)-(c)$ we find one zero tree-level amplitude, these are highlighted by the red boxes.

One-mass boxes

The one-mass box is simplest and we begin by classifying the two solutions for the loop momenta ℓ with the general kinematics shown in Fig.3.4. The on-shell conditions for the various loop momenta are as follows,

$$(\ell + m_1)^2 = 0 \tag{3.7}$$

$$\ell^2 = 0 \tag{3.8}$$

$$(\ell - m_2)^2 = 0 \tag{3.9}$$

$$(\ell - M_{23})^2 = 0 \tag{3.10}$$

where we have used the shorthand notation $M_{ij} = m_i + m_j$. We choose to expand ℓ in terms of two massless basis vectors m_1 and m_2 with four free parameters $\{\alpha, \beta, \rho, \delta\}$ which are fixed by the on-shell constraints.

$$\ell^\mu = \alpha m_1^\mu + \beta m_2^\mu + \frac{\rho}{2}\langle m_2|\gamma^\mu|m_1] + \frac{\delta}{2}\langle m_1|\gamma^\mu|m_2]. \tag{3.11}$$

The first and third on-shell constraint require that, $\alpha = \beta = 0$. Then setting ℓ on shell requires that either ρ or $\delta = 0$. We begin by choosing $\delta = 0$. Then the final

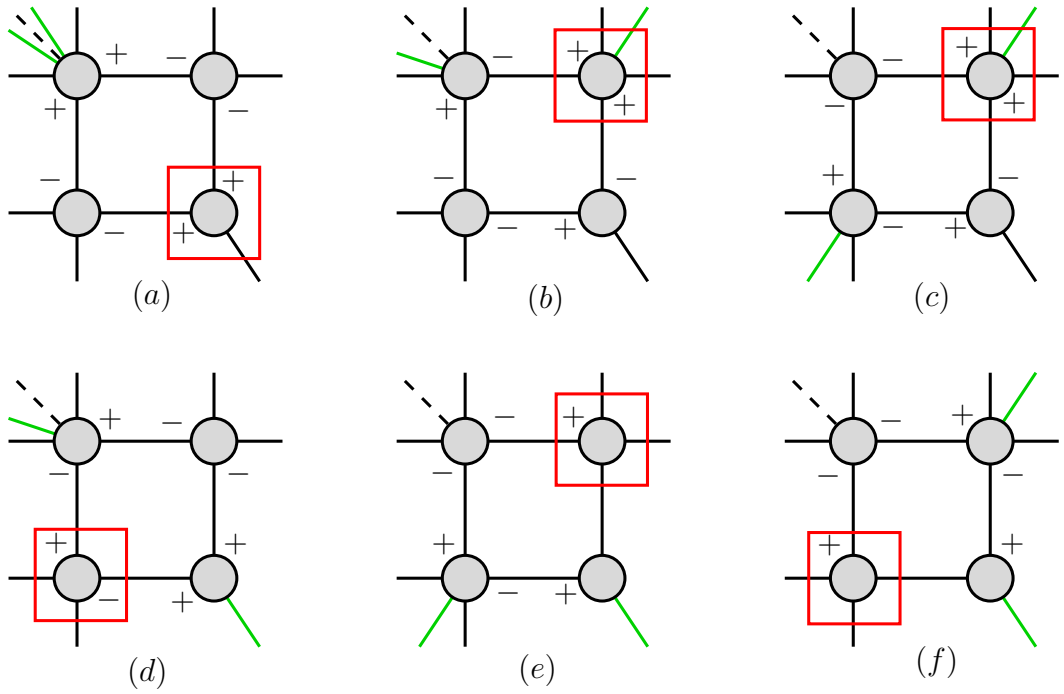

Figure 3.2: As in the four-mass case three-mass boxes do not contribute to ϕ-MHV amplitudes. External particles are either; positive helicity gluons (solid black lines) of which there can be an arbitrary number at any vertex, negative helicity gluons (shown in green) of which there can be only two and one ϕ (dashed black line). In each configuration $(a) - (f)$ we find that whichever way we distribute the helicities we have at least one zero tree-level amplitude (highlighted by the red boxes).

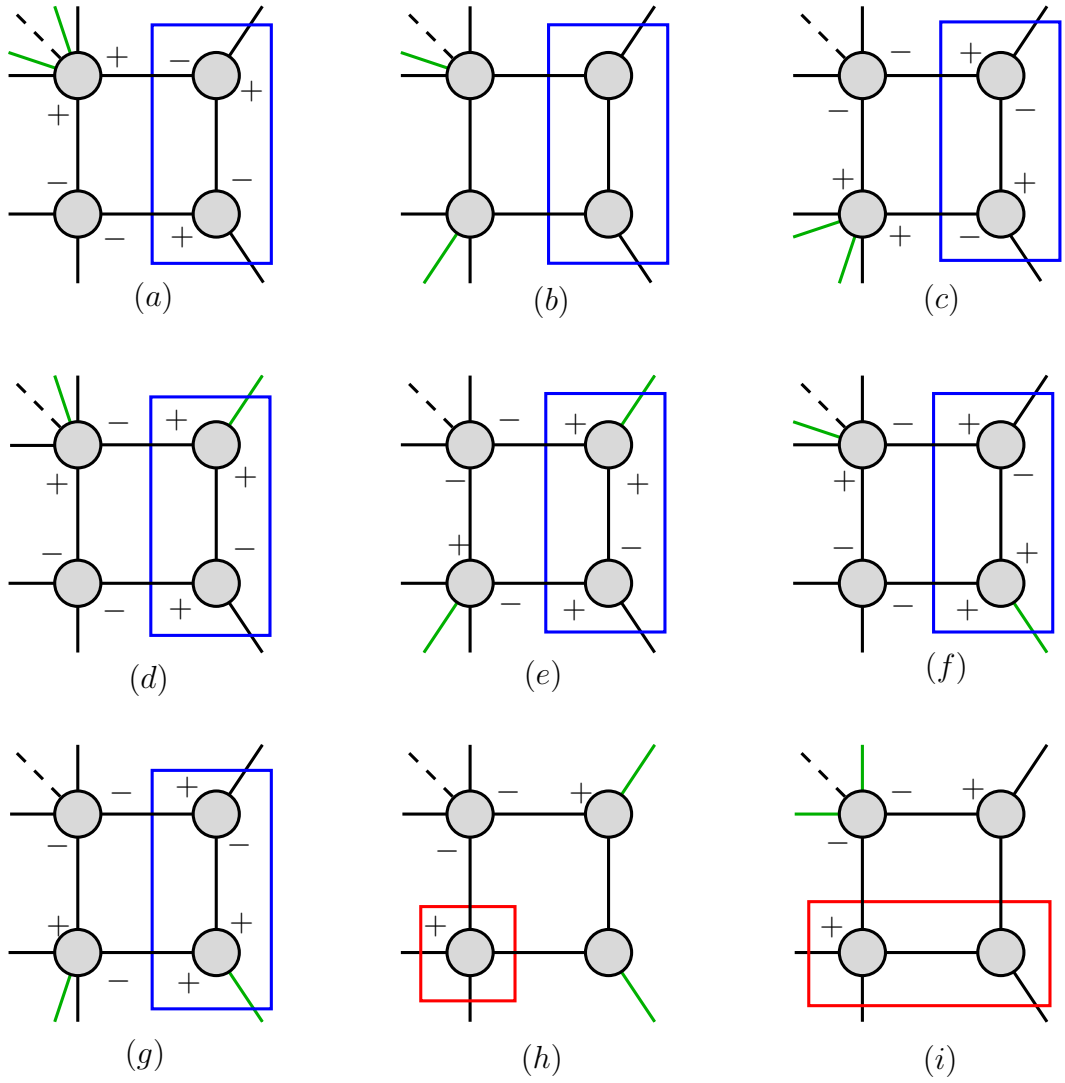

Figure 3.3: As in the four- and three-mass cases two-mass hard boxes do not contribute to ϕ-MHV amplitudes. Here for simplicity we suppress helicities which are unfixed (i.e. $\pm, \mp$). A new feature for the two-mass boxes which does not happen for three- and four-mass is the zeroing of diagrams with two adjacent MHV ($\overline{\text{MHV}}$) three point amplitudes. These are highlighted by the blue boxes.

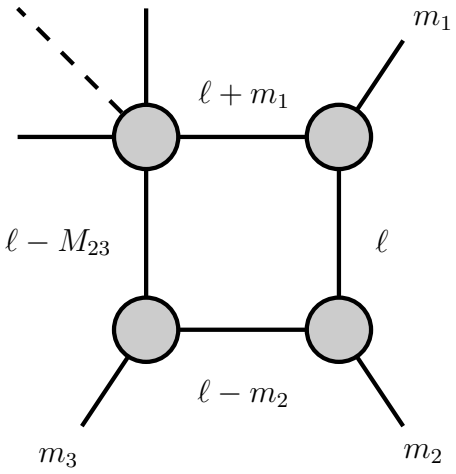

Figure 3.4: A one-mass box with arbitrary massless legs m_1, m_2 and m_3

on-shell constraint fixes ρ,

$$0 = s_{m_2 m_3} - \rho\langle m_2|m_3|m_1] \implies \rho = \frac{[m_2 m_3]}{[m_3 m_1]}. \tag{3.12}$$

If on the other hand we had taken $\rho = 0$ we would have found that

$$0 = s_{m_2 m_3} - \delta\langle m_1|m_3|m_2] \implies \delta = \frac{\langle m_2 m_3\rangle}{\langle m_1 m_3\rangle}, \tag{3.13}$$

so that the two solutions to the on-shell conditions are,

$$\ell^\mu_{(1)} = \frac{[m_2 m_3]}{2[m_3 m_1]}\langle m_2|\gamma^\mu|m_1] \quad \text{and} \quad \ell^\mu_{(2)} = \frac{\langle m_2 m_3\rangle}{2\langle m_1 m_3\rangle}\langle m_1|\gamma^\mu|m_2]. \tag{3.14}$$

We will average over the solutions, but in general one is always zero due to the helicities of m_1 and m_2. With the general solution in hand we now proceed to determine the types of one-mass box which can appear in the ϕ-MHV amplitude. Since there is only one-mass, ϕ must always be present at the massive vertex. We are then free to assign the two negative helicity gluons throughout the various vertices, for which the general topologies are shown in Fig. 3.5.

Diagrams 3.5(a), (b), (d) and (e) only allow gluons to propagate in the loop, and we consider these first, diagram 3.5(a) has the following integrand,

$$\begin{aligned}\mathcal{D}^{(a)} \;=\; & A^{(0)}_{n-1}(\phi, \ell_1^+, i^+, \ldots, 1^-, \ldots, m^-, \ldots, j^+, \ell_2^+) A^{(0)}_3(\ell_2^-, (j+1)^+, \ell_3^+) \\ & \times A^{(0)}_3(\ell_3^-, (j+2)^+, \ell_4^-) A^{(0)}_3(\ell_4^+, (i-1)^+, \ell_1^-)\end{aligned} \tag{3.15}$$

$$\begin{aligned}\mathcal{D}^{(a)} &= \frac{\langle 1m\rangle^4}{\prod_{\alpha=i}^{j-1}\langle\alpha(\alpha+1)\rangle\langle\ell_1 i\rangle\langle j\ell_2\rangle\langle\ell_2\ell_1\rangle}\frac{[(j+1)\ell_3]^3}{[\ell_2(j+1)][\ell_3\ell_2]} \\ &\quad\times\frac{\langle\ell_4\ell_3\rangle^3}{\langle\ell_3(j+2)\rangle\langle(j+2)\ell_4\rangle}\frac{[\ell_4(i-1)]^3}{[(i-1)\ell_1][\ell_1\ell_4]}\end{aligned} \tag{3.16}$$

$$D^{(a)} = A_n^{(0)}\left(\frac{[(j+1)|\ell_3\ell_4|(i-1)]^3\rho}{\langle j|\ell_2\ell_3|(j+2)\rangle\langle(j+2)|\ell_4\ell_1|i\rangle[(i-1)|\ell_1\ell_2|(j+1)]}\right) \tag{3.17}$$

Here, and in the rest of this chapter, we use $A_n^{(0)}$ to refer to the n-point ϕ-MHV tree amplitude given by eq. (3.1), $\rho = \langle j(j+1)\rangle\langle(j+1)(j+2)\rangle\langle(j+2)(i-1)\rangle\langle(i-1)i\rangle$. In terms of the general solution (eq. (3.14)) we have

$$\ell_3 = \ell \tag{3.18}$$

$$\ell_4 = \ell - p_{j+2} \tag{3.19}$$

$$\ell_1 = \ell_4 - p_{i-1} \tag{3.20}$$

$$\ell_2 = \ell + p_{j+1} \tag{3.21}$$

We can use these equations to write the integrand solely in terms of ℓ,

$$D^{(a)} = A_n^{(0)}\left(\frac{\langle(j+2)|\ell|(j+1)][(j+2)(i-1)]s_{i-1,j+2}\langle(j+1)(j+2)\rangle}{\langle(j+2)|\ell|(i-1)]}\right) \tag{3.22}$$

The two solutions for ℓ are as follows,

$$\begin{aligned}\ell_{(1)}^\mu &= \frac{[(j+2)(i-1)]}{2[(i-1)(j+1)]}\langle(j+2)|\gamma^\mu|(j+1)] \\ \ell_{(2)}^\mu &= \frac{\langle(j+2)(j+1)\rangle}{2\langle(j+1)(i-1)\rangle}\langle(j+1)|\gamma^\mu|(j+2)]\end{aligned} \tag{3.23}$$

$\mathcal{D}^{(a)}_{\ell\to\ell_{(1)}} = 0$ so that only the ℓ_2 solution contributes to the coefficient,

$$\mathcal{D}^{(a)} = \frac{A_n^{(0)}}{2}s_{i-1,j+2}s_{j+1,j+2}. \tag{3.24}$$

In a similar fashion, we find that the diagrams which only allow a gluon to propagate in the loop (Fig.3.5(b), (d) and (e)) have the same form of solution (with the relevant changes to i and j).

$$\mathcal{D}^{(\alpha)} = \frac{A_n^{(0)}}{2}s_{i-1,j+2}s_{j+1,j+2} \tag{3.25}$$

where $\alpha \in \{(b),(d),(e)\}$.

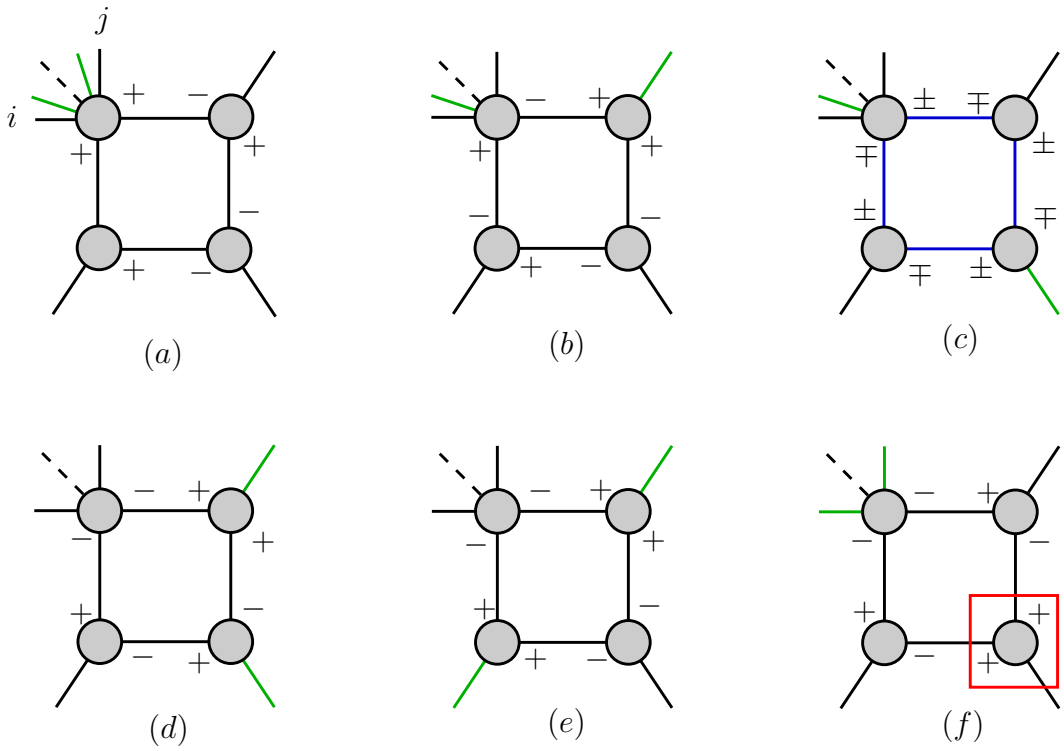

Figure 3.5: One-mass boxes for the ϕ-MHV amplitudes are defined by the position of the two negative helicity gluons, there can be an arbitrary number of positive helicity gluons at the massive vertex of which the end points are denoted i and j. Diagrams $(a) - (e)$ are non-zero whilst diagram (f) which is a special case for the 5-point amplitude, is zero. Diagram (c) is of interest since it allows fermions (and scalars) to propagate in the loop.

This leaves Fig.3.5(c), which has a far richer structure than those previously studied. Each loop helicity is unconstrained, which means that fermions as well as gluons can propagate around the loop. In addition, there are now two contributing topologies which we label $\mathcal{D}^{(c)}_{g,+}$ and $\mathcal{D}^{(c)}_{g,-}$ the subscript indicating the species and helicity of ℓ_1 in the ϕ containing amplitude.

$$\begin{aligned}\mathcal{D}^{(c)}_{g,+} &= A^{(0)}_{n-1}(\phi,\ell_1^+,(n-1)^+,\ldots,m^-,\ldots,3^+,\ell_2^-)A^{(0)}_3(\ell_2^+,2^+,\ell_3^-)\\ &\quad\times A^{(0)}_3(\ell_3^+,1^-,\ell_4^-)A^{(0)}_3(\ell_4^+,n^+,\ell_1^-),\end{aligned} \tag{3.26}$$

$$\begin{aligned}\mathcal{D}^{(c)}_{g,-} &= A^{(0)}_{n-1}(\phi,\ell_1^-,(n-1)^+,\ldots,m^-,\ldots,3^+,\ell_2^+)A^{(0)}_3(\ell_2^-,2^+,\ell_3^+)\\ &\quad\times A^{(0)}_3(\ell_3^-,1^-,\ell_4^+)A^{(0)}_3(\ell_4^-,n^+,\ell_1^+).\end{aligned} \tag{3.27}$$

There are two diagrams which have the same topology as (c), one with $p_1 \in P_{i,j}$ and one with $p_m \in P_{i,j}$ ($P_{i,j}$ represents the massive leg). For convenience we consider only the case where $p_m \in P_{i,j}$ explicitly, since it is trivial to obtain the remaining diagram from this one. The momentum constraints are as follows,

$$\ell_2 = \ell + p_2 \tag{3.28}$$

$$\ell_3 = \ell \tag{3.29}$$

$$\ell_4 = \ell - p_1 \tag{3.30}$$

$$\ell_1 = \ell_4 - p_n \tag{3.31}$$

and the two specific solutions for ℓ are

$$\ell^\mu_{(1)} = \frac{[1n]}{2[n2]}\langle 1|\gamma^\mu|2] \quad \text{and} \quad \ell^\mu_{(2)} = \frac{\langle 1n\rangle}{2\langle 2n\rangle}\langle 2|\gamma^\mu|1]. \tag{3.32}$$

Once again the solution associated with $\ell_{(1)}$ does not contribute and we are left with only $\ell \to \ell_{(2)}$. We combine the two helicity solutions (eqs. (3.26)-(3.27))

$$\mathcal{D}^{(c)}_g = \frac{\langle m|\ell_1|n]^4\langle 1|\ell_3|2]^4 + \langle m|\ell_2|2]^4\langle 1|\ell_4|n]^4}{\gamma\langle\ell_2\ell_1\rangle\langle\ell_1(n-1)\rangle\langle\ell_2 3\rangle\langle\ell_3\ell_4\rangle\langle\ell_3 1\rangle\langle\ell_4 1\rangle[\ell_3\ell_2][\ell_4\ell_1][n\ell_1][n\ell_4][2\ell_2][2\ell_3]}. \tag{3.33}$$

Here we have introduced $\gamma = \prod_{\alpha=n-1}^{4}\langle\alpha(\alpha-1)\rangle$ to simplify the formula. Next we use the momentum constraints to remove ℓ_1 and ℓ_2 from the numerator.

$$\mathcal{D}^{(c)}_g = \frac{\langle m|\ell_4|n]^4\langle 1|\ell_3|2]^4 + \langle m|\ell_3|2]^4\langle 1|\ell_4|n]^4}{\gamma\langle\ell_2\ell_1\rangle\langle\ell_1(n-1)\rangle\langle\ell_2 3\rangle\langle\ell_3\ell_4\rangle\langle\ell_3 1\rangle\langle\ell_4 1\rangle[\ell_3\ell_2][\ell_4\ell_1][n\ell_1][n\ell_4][2\ell_2][2\ell_3]}.$$

(3.34)

We can use the Schouten identity to rewrite the numerator

$$\begin{aligned}\langle m|\ell_4|n]^4\langle 1|\ell_3|2]^4 + \langle m|\ell_3|2]^4\langle 1|\ell_4|n]^4 = \langle 1m\rangle^4[2|\ell_3\ell_4|n]^4 \\ +4\langle 1m\rangle^2[2|\ell_3\ell_4|n]^2\langle m|\ell_4|n]\langle 1|\ell_3|2]\langle m|\ell_3|2]^4\langle 1|\ell_4|n] \\ +2\langle m|\ell_4|n]^2\langle 1|\ell_3|2]^2\langle m|\ell_3|2]^2\langle 1|\ell_4|n]^2. \end{aligned} \tag{3.35}$$

When we calculate the contributions which arise when a fermion propagates in the loop we find

$$\mathcal{D}_f^{(c)} = -\frac{\langle m|\ell_4|n]^3\langle 1|\ell_3|2]^3\langle m|\ell_3|2]\langle 1|\ell_4|n] + \langle m|\ell_3|2]^3\langle 1|\ell_4|n]^3\langle m|\ell_4|n]\langle 1|\ell_3|2]}{\mathcal{D}_g^{(c),denom}} \tag{3.36}$$

where $\mathcal{D}_g^{(c),denom}$ is the denominator of eq. (3.34). We expand the fermionic numerator into the following,

$$\begin{aligned}\langle m|\ell_4|n]^3\langle 1|\ell_3|2]^3\langle m|\ell_3|2]\langle 1|\ell_4|n] + \langle m|\ell_3|2]^3\langle 1|\ell_4|n]^3\langle m|\ell_4|n]\langle 1|\ell_3|2] = \\ \langle 1m\rangle^2[2|\ell_3\ell_4|n]^2\langle m|\ell_4|n]\langle 1|\ell_3|2]\langle m|\ell_3|2]^4\langle 1|\ell_4|n] \\ +2\langle m|\ell_4|n]^2\langle 1|\ell_3|2]^2\langle m|\ell_3|2]^2\langle 1|\ell_4|n]^2. \end{aligned} \tag{3.37}$$

The fermion and gluon loops are hence made of similar contributions. This will occur frequently in this chapter and we use the following notation to describe the relevant contributions,

$$\begin{aligned}\mathcal{D}^{(c)} &= \mathcal{D}_g^{(c)} + \frac{N_f}{N_c}\mathcal{D}_f^c \\ &= \mathcal{G}^{1m}(1) + 4\left(1 - \frac{N_f}{4N_c}\right)\mathcal{F}^{1m}(1) + 2\left(1 - \frac{N_f}{N_c}\right)\mathcal{S}^{1m}(1) \end{aligned} \tag{3.38}$$

Here the subscript indicates the cut integral we are referring to, and the brackets describe the kinematic dependence (here indicating that p_1 is the massless leg rather than p_m). These integrals have the following form,

$$\mathcal{G}^{1m}(1) = -A_n^{(0)}\frac{\langle(n-1)n\rangle\langle n1\rangle\langle 12\rangle\langle 23\rangle[2|\ell_3\ell_4|n]^3}{\langle\ell_1\ell_2\rangle\langle\ell_1(n-1)\rangle\langle\ell_2 3\rangle\langle\ell_3 1\rangle\langle\ell_4 1\rangle[\ell_3\ell_2][\ell_4\ell_1][n\ell_1][2\ell_2]} \tag{3.39}$$

$$\mathcal{F}^{1m}(1) = A_n^{(0)}\frac{\langle\ell_3\ell_4\rangle\langle\ell_3 m\rangle\langle\ell_4 m\rangle\langle(n-1)n\rangle\langle n1\rangle\langle 12\rangle\langle 23\rangle[n\ell_4]^3[2\ell_3]^3}{\langle\ell_1\ell_2\rangle\langle\ell_1(n-1)\rangle\langle\ell_2 3\rangle\langle 1m\rangle^2[\ell_3\ell_2][\ell_4\ell_1][n\ell_1][2\ell_2]} \tag{3.40}$$

$$\mathcal{S}^{1m}(1) = A_n^{(0)} \frac{\langle \ell_3 m\rangle^2 \langle \ell_4 m\rangle^2 \langle \ell_3 1\rangle \langle \ell_4 1\rangle \langle (n-1)n\rangle 3\langle n1\rangle \langle 12\rangle \langle 23\rangle [n\ell_4]^3 [2\ell_3]^3}{\langle \ell_1 \ell_2\rangle \langle \ell_1 (n-1)\rangle \langle \ell_2 3\rangle \langle 1m\rangle^4 \langle \ell_3 \ell_4\rangle [\ell_3 \ell_2][\ell_4 \ell_1][n\ell_1][2\ell_2]} \tag{3.41}$$

The procedure to calculate these quantities is straightforward, remove ℓ_1, ℓ_2 and ℓ_4 in terms of ℓ_3 and substitute in the solution $\ell_{(2)}$. This yields the following

$$\mathcal{G}^{1m}(1) = \frac{A_n^{(0)}}{2} s_{12} s_{1n}, \tag{3.42}$$

$$\mathcal{F}^{1m}(1) = \left(\frac{A_n^{(0)}}{2} s_{12} s_{1n}\right) \frac{\langle mn\rangle \langle 2m\rangle \langle 1n\rangle \langle 12\rangle}{\langle 1m\rangle^2 \langle 2n\rangle^2}, \tag{3.43}$$

$$\mathcal{S}^{1m}(1) = -\left(\frac{A_n^{(0)}}{2} s_{12} s_{1n}\right) \left(\frac{\langle mn\rangle \langle 2m\rangle \langle 1n\rangle \langle 12\rangle}{\langle 1m\rangle^2 \langle 2n\rangle^2}\right)^2. \tag{3.44}$$

This completes the analysis for one-mass boxes, we will observe in the next section that the calculation of the two-mass box coefficients proceeds in an identical fashion.

Two-mass boxes

When calculating the coefficients of one-mass boxes which appear in ϕ-MHV amplitudes we noted that there were two sorts of contributions. Diagrams in which the loop particle was constrained to be a gluon had a coefficient of the following form, $A_n^{(0)} s_1 s_2$ where s_1 and s_2 are the invariants associated with pairs of (adjacent) massless legs. The diagrams which allowed fermions to propagate in the loop have a more complicated structure, they also contain a piece of the form $A_n^{(0)} s_1 s_2$ but in addition contain pieces proportional to N_f, the number of light flavours.

We find an identical situation with the two-mass boxes which are depicted in Fig. 3.6. Diagrams (a), (b), (d) and (e) which contain a gluon loop alone have coefficients of the form $A_n^{(0)}(s_1 s_2 - P^2 Q^2)$ where P and Q are the momenta of the massive legs. An example of this type of term was given in the previous chapter. We also find that the diagrams which allow a fermion to propagate in the loop have the same breakdown as the one-mass boxes,

$$\mathcal{D}^{(c)} = \mathcal{G}^{2m}(a,i,j) + 4\left(1 - \frac{N_f}{4N_c}\right)\mathcal{F}^{2m}(a,i,j) + 2\left(1 - \frac{N_f}{N_c}\right)\mathcal{S}^{2m}(a,i,j). \tag{3.45}$$

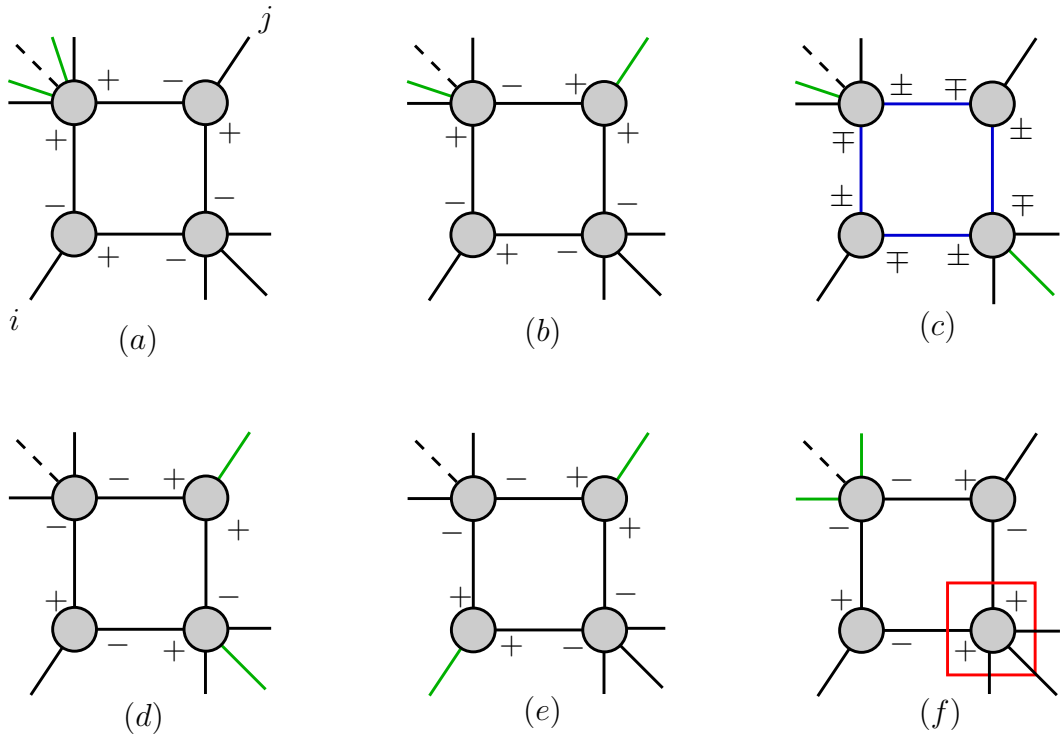

Figure 3.6: Two-mass easy boxes for the ϕ-MHV amplitudes are defined by the position of the two negative helicity gluons, there can be an arbitrary number of positive helicity gluons at the massive vertices. The two massless legs are denoted i and j. Diagrams $(a) - (e)$ are non-zero whilst diagram (f) which is a special case for the 5-point amplitude, is zero. Diagram (c) is of interest since it allows fermions (and scalars) to propagate in the loop.

Here $a \in \{1, m\}$ indicates which negative helicity gluon is not paired with ϕ at the massive vertex. The integration is almost identical to the one-mass case the only difference being that i and j now play the roles of p_2 and n (or $(m \pm 1)$). The coefficients are constructed from the following function,

$$b_{1m}^{ij} = \frac{\langle mi\rangle\langle j1\rangle\langle mj\rangle\langle i1\rangle}{\langle 1m\rangle^2\langle ij\rangle^2} = \frac{\mathrm{tr}_-(m,i,j,1)\,\mathrm{tr}_-(m,j,i,1)}{s_{ij}^2 s_{1m}^2} \tag{3.46}$$

where we have introduced the notation $\mathrm{tr}_-(a,b,c,d) = \langle ab\rangle[bc]\langle cd\rangle[da]$. In terms of this quantity we have the general results

$$\mathcal{G}^{2m}(a,i,j) = \frac{A_n^{(0)}}{2}(s_{i,j-1}s_{j,i-1} - s_{i,j}s_{i+1,j-1}) \tag{3.47}$$

$$\mathcal{F}^{2m}(a,i,j) = b_{1m}^{ij}\frac{A_n^{(0)}}{2}(s_{i,j-1}s_{j,i-1} - s_{i,j}s_{i+1,j-1}) \tag{3.48}$$

$$\mathcal{S}^{2m}(a,i,j) = -(b_{1m}^{ij})^2\frac{A_n^{(0)}}{2}(s_{i,j-1}s_{j,i-1} - s_{i,j}s_{i+1,j-1}) \tag{3.49}$$

We stress a crucial notation subtlety in the above sets of formula when we refer to s_{ij} we mean $s_{ij} = \langle ij\rangle[ji]$ and is the invariant formed between the pair of partons p_i and p_j. When we refer to $s_{i,j}$ we refer to $s_{i,j} = (p_i + p_{i+1} + \cdots + p_{j-1} + p_j)^2$ which is a mass associated with the two-mass box.

We observe that we can obtain the one-mass box coefficients from the soft-limit of the two mass boxes. This means that to finalise the box coefficients we merely have to define the summation over the allowed boxes. In total we find that the box coefficients associated with the ϕ-MHV amplitude equal

$$C_{n;1}^{4-cut}(\phi, 1^-, 2^+, \ldots, m^-, \ldots, n^+) = A_n^{(0)}\Bigg(A_{n;1}^{\phi G,4-cut}(m,n) - 4\left(1 - \frac{N_f}{4N_c}\right)A_{n;1}^{\phi F,4-cut}(m,n) - 2\left(1 - \frac{N_f}{N_c}\right)A_{n;1}^{\phi S,4-cut}(m,n)\Bigg), \tag{3.50}$$

where we defined $A_{n;1}^{\phi\{G,F,S\},4-cut}$ to be the tree-factored combinations of box integrals multiplied by their relevant coefficient. Explicitly

$$A_{n;1}^{\phi G,4-cut}(m,n) = -\frac{1}{2}\sum_{i=1}^{n}\sum_{j=i+3}^{n+i-1}\mathrm{F}_4^{2\mathrm{me}}(s_{i+1,j}, s_{i,j-1}; s_{i,j}, s_{i+1,j-1}) - \frac{1}{2}\sum_{i=1}^{n}\mathrm{F}_4^{1\mathrm{m}}(s_{i,i+1}, s_{i+1,i+2}; s_{i,i+2}) \tag{3.51}$$

We note that $A_{n;1}^{\phi G,4-cut}(m,n)$ is independent of the position of the two negative helicity gluons.

$$A_{n;1}^{\phi F,4-cut}(m,n) = \sum_{i=2}^{m-1}\sum_{j=m+1}^{n} b_{1m}^{ij}\,\mathrm{F}_4^{\mathrm{2me}}(s_{i+1,j}, s_{i,j-1}; s_{i,j}, s_{i+1,j-1}) + \sum_{i=2}^{m-1}\sum_{j=m+1}^{n} b_{1m}^{ij}\,\mathrm{F}_4^{\mathrm{2me}}(s_{j+1,i}, s_{j,i-1}; s_{j,i}, s_{j+1,i-1}) \quad (3.52)$$

and

$$A_{n;1}^{\phi S,4-cut}(m,n) = -\sum_{i=2}^{m-1}\sum_{j=m+1}^{n} (b_{1m}^{ij})^2\,\mathrm{F}_4^{\mathrm{2me}}(s_{i+1,j}, s_{i,j-1}; s_{i,j}, s_{i+1,j-1}) - \sum_{i=m+1}^{n}\sum_{j=2}^{m-1} (b_{1m}^{ij})^2\,\mathrm{F}_4^{\mathrm{2me}}(s_{i+1,j}, s_{i,j-1}; s_{i,j}, s_{i+1,j-1}). \quad (3.53)$$

We leave the explicit definitions of the basis functions $\mathrm{F}_4^{\mathrm{2me}}$ and $\mathrm{F}_4^{\mathrm{1m}}$ to Appendix B, noting that the definitions we use are related to the basis integral $\mathcal{I}_4$ by a kinematic factor (which cancels those appearing in the coefficients given in this chapter). The summations in $A_{n;1}^{\phi F,4-cut}$ and $A_{n;1}^{\phi S,4-cut}$ do not explicitly refer to one-mass boxes, this is because these terms arise naturally from the two-mass boxes when one of the massive legs becomes soft.

3.2.2 Triangle Coefficients

In this section we determine the coefficients associated with the triangle basis integrals. For the general ϕ-MHV configuration we show that there can never be any non-zero three-mass triangle coefficients. Further, we show that the remaining coefficients attributed to the one- and two-mass triangles can be split into two pieces. The first of these pieces is helicity blind whilst the second contains pieces proportional to N_f, and depends on the position of the two negative helicity gluons. Since the three-mass triangles do not contribute, knowledge of the triangle coefficients can also be determined by infra-red safety conditions.

The vanishing of three-mass triangle coefficients

The three-mass triangle integral is listed with the other basis integrals in Appendix B and is finite (i.e. it has no poles in the dimensional parameter ϵ) and as such the coefficient of the three-mass triangle cannot be fixed by infra-red safety conditions. However, for any ϕ-MHV helicity configuration there can be no non-zero three-mass triangle coefficients. The general topologies are shown in Fig. 3.7 for each one there is always at least one vertex which vanishes.

One- and two-mass triangle coefficients

The remaining triangle coefficients which are associated with one- and two-mass triangles can be calculated from infra-red safety conditions. To ensure correct infra-red behaviour the ϵ^{-2} pieces of the amplitude must have the following form,

$$A_n^{(1)} = -\frac{c_\Gamma}{\epsilon^2} A_n^{(0)} \sum_{i=1}^{n} \left(\frac{\mu^2}{-s_{i,i+1}} \right)^{\epsilon} + \mathcal{O}(\epsilon^0). \tag{3.54}$$

In general we expect the coefficients of the various triangles to possess a similar structure to the box coefficients, i.e. we expect to find the following sorts of terms in our amplitude,

$$C_{n;1}^{3-cut}(\phi, 1^-, 2^+, \ldots, m^-, \ldots, n^+) = A_n^{(0)} \Bigg(A_{n;1}^{\phi G,3-cut}(m,n) \\ -4\left(1 - \frac{N_f}{4N_c}\right) A_{n;1}^{\phi F,3-cut}(m,n) - 2\left(1 - \frac{N_f}{N_c}\right) A_{n;1}^{\phi S,3-cut}(m,n) \Bigg). \tag{3.55}$$

In this decomposition it is clear that only $A_{n;1}^{\phi G,3-cut}(m,n)$ can contribute to eq. (3.54), further we can infer that since no infra-red poles are proportional to N_f (since there exists no $(n+1)$ ϕ plus gluon tree amplitude which has an N_f dependence) we know that the triangles which occur in these pieces must cancel the poles which arise from the box contributions. The case where $m = 2$ has been calculated [108] and the following contributions were found,

$$A_{n;1}^{\phi G,3-cut}(2,n) = \sum_{i=1}^{n} (\mathrm{F}_3^{1\mathrm{m}}(s_{i,n+i-2}) - \mathrm{F}_3^{1\mathrm{m}}(s_{i,n+i-1})) \tag{3.56}$$

$$A_{n;1}^{\phi F,3-cut}(2,n) = A_{n;1}^{\phi S,3-cut}(2,n) = 0 \tag{3.57}$$

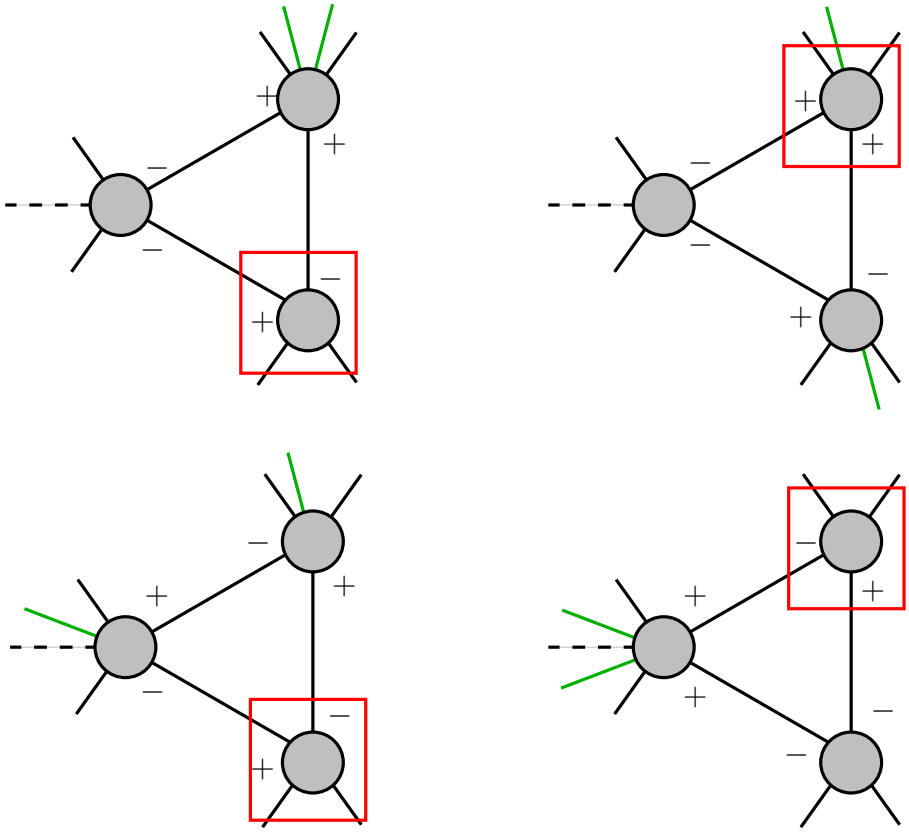

Figure 3.7: For each three mass triangle there is always at least one vertex corresponding to a zero tree-level amplitude. As in previous diagrams external negative heclicity gluons are represented as green lines and there can be an arbitrary number of positive helicity gluons at each vertex.

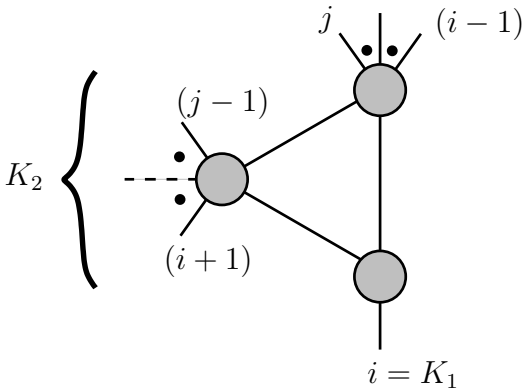

Figure 3.8: The kinematic structure of a generic two-mass triangle which appears in our calculations. The same kinematics can be used to represent the one-mass triangle with $(i-1) = j$ with no loss of generality.

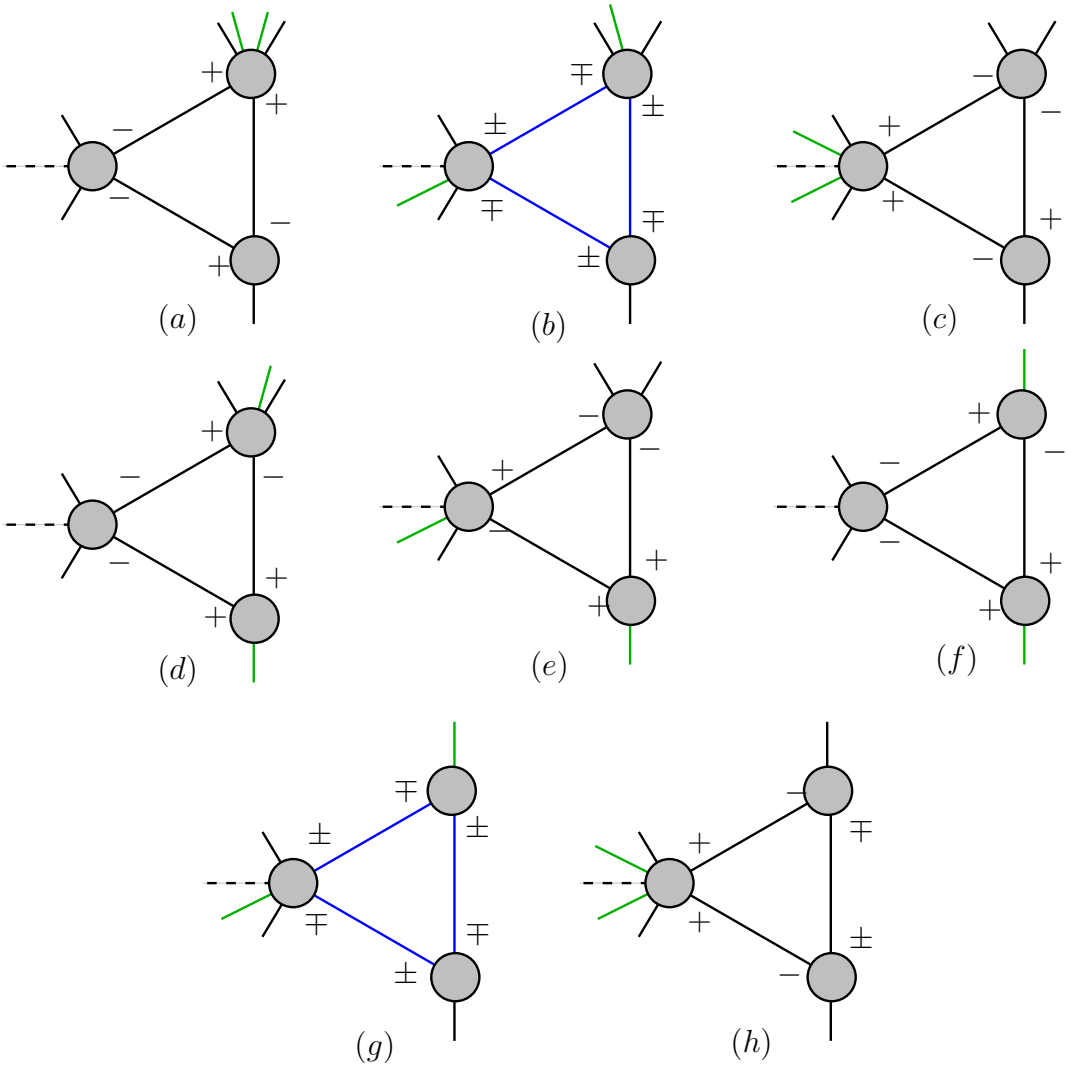

Figure 3.9: One- and two-mass topologies which appear in ϕ-MHV amplitudes. Of particular interest are topologies (b) and (g) which allow fermions and gluons to propagate in the loop and hence have a richer structure. The remaining diagrams factorise into a helicity blind integral and are the same as those which appear in [108].

We will presently show that $A^{\phi G,3-cut}$ is helicity blind and as such $A^{\phi G,3-cut}_{n;1}(2,n) = A^{\phi,G,3-cut}_{n;1}(m,n) = A^{\phi,G,3-cut}_{n;1}(n)$. It was also shown in [108] that the combination of $A^{\phi G,3-cut}$ and $A^{\phi G,4-cut}$ correctly generates the pole structure of eq. (3.54). The general structure of one- and two-mass triangles are shown in Fig. 3.9 of these (a) $(c)-(f)$ and (h) represent pieces which only contribute to $A^{\phi G}$. As an example we consider (a) in detail and show that the dependence on p_m factors into the tree-level prefactor. The product of tree amplitudes has the following form,

$$\begin{aligned}\mathcal{D}^{(a)} &= A^{(0}_3(\phi,\ell_1^-,\ell_2^-)A^{(0)}(\ell_2^+,i^+,\ell_3^-)A^{(0)}(\ell_3^-,(i+1)^+,1^-,\ldots,m^-,(i-1)^+,\ell_1^+)\\ &= -\langle\ell_1\ell_2\rangle^2\frac{[\ell_2 i]^3}{[i\ell_3][\ell_3\ell_2]}\frac{\langle 1m\rangle^4}{\langle\ell_3(i+1)\rangle\prod_{\alpha=i+1}^{i-2}\langle\alpha(\alpha+1)\rangle\langle(i-1)\ell_1\rangle\langle\ell_1\ell_3\rangle}\\ &= -A^{(0}_n\frac{\langle\ell_1\ell_2\rangle^2[\ell_2 i]^3\langle i(i+1)\rangle\langle(i-1)i\rangle}{[\ell_3\ell_2][i\ell_3]\langle\ell_3(i+1)\rangle\langle(i-1)\ell_1\rangle\langle\ell_1\ell_3\rangle}.\end{aligned} \tag{3.58}$$

It is trivial to show that diagrams $(c)-(f)$ and (h) factorise in the same manner. As such we know that these integrals will be identical to the adjacent minus ϕ-MHV case [108]. This leaves us with the task of determining the coefficients represented by Fig. 3.9(b) which allow both fermions and gluons to propagate in the loops. We follow the same procedure as we did for the box diagrams and decompose the diagram into constituent pieces,

$$\mathcal{D}^{(b)} = \mathcal{G}^{2,1m}(a,i,j) + 4\left(1-\frac{N_f}{4N_c}\right)\mathcal{F}^{2,1m}(a,i,j) + 2\left(1-\frac{N_f}{N_c}\right)\mathcal{S}^{2,1m}(a,i,j) \tag{3.59}$$

As before $a\in\{1,m\}$ indicates which of the negative helicity gluons is not paired with ϕ at a vertex. Here we do not distinguish explicitly between one- and two-mass triangles (i.e. we consider (b) knowing we can obtain (g) in the soft limit), in the approach we will use [122] we choose two momenta K_1 and K_2 (which are external momenta) and parameterise the loop momentum in terms of massless projections of these vectors. In these calculations we can always set $K_1^2=0$ $K_2^2\neq 0$ regardless of whether the triangle has one or two massive legs. A schematic representation of the kinematics we will use for the calculation is shown in Fig. 3.8. The massless projections of K_1 and K_2 which we will use to construct our basis in which the loop momentum is decomposed have the following form,

$$K_1^{\flat,\mu} = p_i^\mu, \tag{3.60}$$

$$K_2^{\flat,\mu} = P_{j;i}^{\mu} - \frac{P_{j;i}^2}{\langle i|P_{j;i}|i]} p_i^{\mu}. \tag{3.61}$$

The general solution for the loop momenta, as prescribed in [122] is,

$$\ell^{\mu} = \alpha_{02} K_1^{\flat,\mu} + \alpha_{01} K_2^{\flat,\mu} + \frac{t}{2}\langle K_1^{\flat}|\gamma^{\mu}|K_2^{\flat}] + \frac{\alpha_{01}\alpha_{02}}{2t}\langle K_2^{\flat}|\gamma^{\mu}|K_1^{\flat}]. \tag{3.62}$$

Specifically for the triangle topologies we are studying here, $\alpha_{01} = 0$, $\alpha_{02} = P_{j;i}^2/\langle i|P_{j;i}|i]$. Next we turn our attention to obtaining the $\mathcal{G}$, $\mathcal{F}$ and $\mathcal{S}$ integrands relevant for these coefficients. The product of trees is equal to,

$$\begin{aligned}\mathcal{D}_g^{(b),\pm} &= A^{(0)}(\phi, \ell^{\pm}, (i+1)^+, 1^-, (j-1)^+, \ell_2^{\mp}) \\ &\quad \times A^{(0)}(\ell_2^{\pm}, j^+, m^-, (i-1)^+, \ell_1^{\mp}) A^{(0)}(\ell_1^{\pm}, i^+, \ell^{\mp}).\end{aligned} \tag{3.63}$$

Combining the two diagrams we find

$$\mathcal{D}^{(b)} = \frac{\langle 1\ell_2\rangle^4\langle m\ell_1\rangle^4[\ell_1 i]^4 + \langle 1\ell\rangle^4\langle m\ell_2\rangle^4[\ell i]^4}{\langle \ell(i+1)\rangle \prod_{i+1}^{j-2}\langle (j-1)\ell_2\rangle\langle \ell_2\ell\rangle\langle \ell_2 j\rangle \prod_{j}^{i-2}\langle (i-1)\ell_1\rangle\langle \ell_1\ell_2\rangle[\ell_1 i][i\ell][\ell_1\ell]}. \tag{3.64}$$

Here we have introduced the short-hand notation $\prod_a^b = \prod_{\alpha=a}^b \langle \alpha(\alpha+1)\rangle$ to simplify the formula. Using the kinematics of the cut we can re-write the integrand as

$$\mathcal{D}^{(b)} = \frac{\langle 1\ell_2\rangle^4\langle m|\ell|i]^4 + \langle 1|\ell|i]^4\langle m\ell_2\rangle^4}{\langle \ell(i+1)\rangle \prod_{i+1}^{j-2}\langle (j-1)\ell_2\rangle\langle \ell_2\ell\rangle\langle \ell_2 j\rangle \prod_{j}^{i-2}\langle (i-1)\ell_1\rangle\langle \ell_1\ell_2\rangle[\ell_1 i][i\ell][\ell_1\ell]}. \tag{3.65}$$

From this we can extract $\mathcal{G}$, $\mathcal{F}$ and $\mathcal{S}$ in the same way as we did for the box terms,

$$\mathcal{D}^{(b)} = \mathcal{G}^{2,1m}(1,i,j) + 4\left(1 - \frac{N_f}{4N_c}\right)\mathcal{F}^{2,1m}(1,i,j) + 2\left(1 - \frac{N_f}{N_c}\right)\mathcal{S}^{2,1m}(1,i,j), \tag{3.66}$$

with

$$\mathcal{G}^{2,1m}(1,i,j) = A_n^{(0)} \frac{\langle \ell_2\ell\rangle^2[\ell i]\langle (j-1)j\rangle\langle i(i+1)\rangle}{\langle \ell(i+1)\rangle\langle (j-1)\ell_2\rangle\langle \ell_2 j\rangle}, \tag{3.67}$$

$$\mathcal{F}^{2,1m}(1,i,j) = A_n^{(0)} \frac{\langle 1\ell_2\rangle\langle m\ell\rangle\langle 1\ell\rangle\langle m\ell_2\rangle[\ell i]\langle (j-1)j\rangle\langle i(i+1)\rangle}{\langle 1m\rangle^2\langle \ell(i+1)\rangle\langle (j-1)\ell_2\rangle\langle \ell_2 j\rangle}, \tag{3.68}$$

$$\mathcal{S}^{2,1m}(1,i,j) = -A_n^{(0)} \frac{\langle 1\ell_2\rangle^2\langle m\ell\rangle^2\langle 1\ell\rangle^2\langle m\ell_2\rangle^2[\ell i]\langle (j-1)j\rangle\langle i(i+1)\rangle}{\langle 1m\rangle^4\langle \ell\ell_2\rangle^2\langle \ell(i+1)\rangle\langle (j-1)\ell_2\rangle\langle \ell_2 j\rangle}. \tag{3.69}$$

As expected we see that $\mathcal{G}$ factors onto the tree-level amplitude multiplying a helicity blind function. The denominators in the above equations have exactly the form we expect from our four-cut calculations. Spinor products of the form $\langle \ell j\rangle \propto (\ell - p_j)^2/[\ell j]$ are linked to Feynman propagators and can be associated with box diagrams. Indeed the residues of these propagators correspond to setting a further propagator on-shell and as such correspond to a four-cut. At first glance we observe three spinor products associated with inserting additional propagators $(\ell - p_j)^2$, $(\ell - p_{j+1})^2$ and $(\ell - p_{i+1})^2$. Of these the first two correspond to two-mass easy boxes and the third corresponds to a two-mass hard topology. We observed in the previous section that there are no such contributions to the ϕ-MHV amplitude, implying that somehow this residue must not contribute to a box-coefficient. Upon closer inspection we see that there is indeed no residue associated with this term since the non-vanishing three-point vertex in the triangle requires that $|\ell\rangle \propto |i\rangle$ and as such when the solution for the loop-momenta is inserted there is a cancellation between $\langle i(i+1)\rangle$ in the denominator and numerator.

To determine $\mathcal{F}$ and $\mathcal{S}$ one merely has to insert the parameterisation for the loop momentum in terms of eq. (3.62) and take the t^0 coefficient in a series expansion around $t = \infty$. We find,

$$\begin{aligned}\mathcal{F}^{2,1m}(1,i,j) &= A_n^{(0)}\frac{\langle j(j-1)\rangle}{\langle 1m\rangle^2}\Bigg(\frac{\langle im\rangle\langle i1\rangle^2\langle m|P_{j;i}|i]}{\langle ij\rangle\langle i(j-1)\rangle} + \frac{\langle im\rangle^2\langle i1\rangle\langle 1|P_{j;i}|i]}{\langle ij\rangle\langle i(j-1)\rangle} \\ &\quad - \frac{\langle im\rangle^2\langle i1\rangle^2\langle j|P_{j;i}|i]}{\langle ij\rangle^2\langle i(j-1)\rangle} - \frac{\langle im\rangle^2\langle i1\rangle^2\langle (j-1)|P_{j;i}|i]}{\langle ij\rangle\langle i(j-1)\rangle^2}\Bigg). \qquad (3.70)\end{aligned}$$

After using the Schouten identity to simplify the above formula we find

$$\mathcal{F}^{2,1m}(1,i,j) = A_n^{(0)}(-b_{1m}^{ij} + b_{1m}^{i(j-1)})\langle i|P_{j;i}|i], \qquad (3.71)$$

where b_{1m}^{ij} is defined as in eq. (3.46). The calculation for $\mathcal{S}$ is identical to that of $\mathcal{F}$ (although here the intermediate formulae are more complicated so we quote only the final result)

$$\mathcal{S}^{2,1m}(1,i,j) = A_n^{(0)}((b_{1m}^{ij})^2 - (b_{1m}^{i(j-1)})^2)\langle i|P_{j;i}|i]. \qquad (3.72)$$

With these solutions in hand we are now able to calculate the coefficient of any one- or two-mass triangle appearing in the ϕ-MHV amplitude. All that remains is

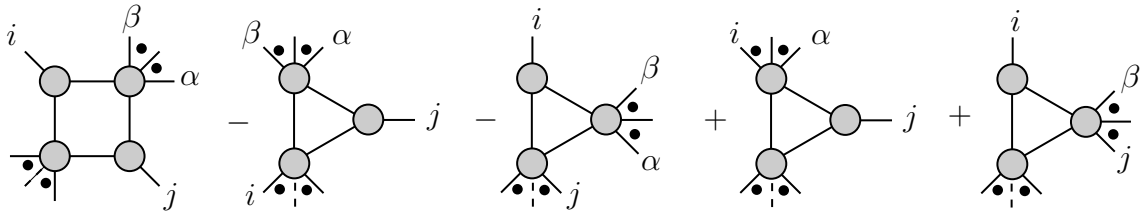

Figure 3.10: The above combination of four two-mass triangles with the two-mass easy box is IR finite. The above combinations uses the F definitions of Appendix B, these are related to the scalar basis integrals $\mathcal{I}$ by a kinematic factor. The definitions $\alpha = (j-1)$ and $\beta = (i+1)$ are used to simplify the Figure.

to correctly define the sum over allowed triangles and check the IR safety of the formula.

3.2.3 Cancellation of $N_f\epsilon^{-2}$ poles

We show how our results for the two-mass triangles result in the cancellation of the $N_f\epsilon^{-2}$ poles which arise from the two-mass boxes. We consider two-mass boxes which are proportional to $(1 - N_f/4N_c)$ (i.e $\mathcal{F}$ terms) for simplicity, however the proof for the $(1 - N_f/N_c)$ boxes proceeds identically.

A given two-mass box in $A^{\phi F,4-cut}_{n;1}$ has a coefficient b^{ij}_{1m}, we find four two-mass triangles which have a term proportional to b^{ij}_{1m}. The combination of all of the contributions with a piece proportional to b^{ij}_{1m} ($\mathcal{W}(b^{ij}_{1m})$) is given by,

$$\begin{aligned}
\mathcal{W}(b^{ij}_{1m}) &= -b^{ij}_{1m}\,\mathrm{F}^{\mathrm{2me}}_4(s_{i+1,j}, s_{i,j-1}; s_{i,j}, s_{i+1,j-1}) \\
&+ \Big((-b^{ij}_{1m} + b^{i(j+1)}_{1m})(\mathrm{F}^{\mathrm{1m}}_3(P^2_{i,j}) - \mathrm{F}^{\mathrm{1m}}_3(P^2_{i+1,j})) \\
&+ (-b^{ij}_{1m} + b^{(i-1)j)}_{1m})(\mathrm{F}^{\mathrm{1m}}_3(P^2_{i,j}) - \mathrm{F}^{\mathrm{1m}}_3(P^2_{i,j-1})) \\
&+ (-b^{i(j-1)}_{1m} + b^{ij}_{1m})(\mathrm{F}^{\mathrm{1m}}_3(P^2_{i,j-1}) - \mathrm{F}^{\mathrm{1m}}_3(P^2_{i+1,j-1})) \\
&+ (-b^{(i+1)j}_{1m} + b^{ij)}_{1m})(\mathrm{F}^{\mathrm{1m}}_3(P^2_{i+1,j}) - \mathrm{F}^{\mathrm{1m}}_3(P^2_{i+1,j-1}))\Big).
\end{aligned} \tag{3.73}$$

When we expand the above we find using the definitions in Appendix B

$$\mathcal{W}(b^{ij}_{1m}) = -b^{ij}_{1m}\,\mathrm{F}^{\mathrm{2me}}_{4\mathrm{F}}(s_{i,j}, s_{i+1,j-1}; s_{i+1,j}, s_{i,j-1}) + \ldots, \tag{3.74}$$

where ... indicates terms that are not proportional to b_{1m}^{ij} and as a result to do not contribute to this particular box. We observe that the triangles have exactly cancelled the pole pieces of the box function, leaving on the finite piece. The combination is shown in Fig 3.10, we note that the term $\langle i|P_{j;i}|i] = P_{j;i}^2 - P_{j;(i-1)}^2$ in eq. (3.71) explicitly cancels the kinematic factor appearing in the denominator of I_3^{2m} resulting in the $\mathrm{F}_3^{1\mathrm{m}}$ terms used in eq. (3.73).

By summing over all of the allowed triangle topologies we cancel all the poles associated with N_f boxes.

Combined quadruple and triple cuts

Putting the results from the previous two sections altogether we find for the combination of triple and quadruple cuts

$$\begin{aligned}
&C_{n;1}(\phi, 1^-, 2^+, \ldots, m^-, \ldots, n^+)|_{3,4cut} = \\
&A_n^{(0)}\Bigg(A_{n;1}^{\phi G}(m,n)|_{3,4cut} - 4\Bigg(1 - \frac{N_f}{4N_c}\Bigg)A_{n;1}^{\phi F}(m,n)|_{3,4cut} \\
&-2\Bigg(1 - \frac{N_f}{N_c}\Bigg)A_{n;1}^{\phi S}(m,n)|_{3,4cut}\Bigg),
\end{aligned} \tag{3.75}$$

where

$$\begin{aligned}
A_{n;1}^{\phi G}(m,n)|_{3,4cut} = &-\frac{1}{2}\sum_{i=1}^{n}\sum_{j=i+3}^{n+i-1}\mathrm{F}_4^{2\mathrm{me}}(s_{i+1,j}, s_{i,j-1}; s_{i,j}, s_{i+1,j-1}) \\
&-\frac{1}{2}\sum_{i=1}^{n}\mathrm{F}_4^{1\mathrm{m}}(s_{i,i+1}, s_{i+1,i+2}; s_{i,i+2}) + (\mathrm{F}_3^{1\mathrm{m}}(s_{i,n+i-2}) - \mathrm{F}_3^{1\mathrm{m}}(s_{i,n+i-1})),
\end{aligned} \tag{3.76}$$

$$\begin{aligned}
A_{n;1}^{\phi F}(m,n)|_{3,4cut} = &\sum_{i=2}^{m-1}\sum_{j=m+1}^{n} b_{1m}^{ij}\,\mathrm{F}_{4\mathrm{F}}^{2\mathrm{me}}(s_{i+1,j}, s_{i,j-1}; s_{i,j}, s_{i+1,j-1}) \\
&+\sum_{i=2}^{m-1}\sum_{j=m+1}^{n} b_{1m}^{ij}\,\mathrm{F}_{4\mathrm{F}}^{2\mathrm{me}}(s_{j+1,i}, s_{j,i-1}; s_{j,i}, s_{j+1,i-1}).
\end{aligned} \tag{3.77}$$

Finally

$$\begin{aligned}
A_{n;1}^{\phi S}(m,n)|_{3,4cut} = &-\sum_{i=2}^{m-1}\sum_{j=m+1}^{n} (b_{1m}^{ij})^2\,\mathrm{F}_{4\mathrm{F}}^{2\mathrm{me}}(s_{i+1,j}, s_{i,j-1}; s_{i,j}, s_{i+1,j-1}) \\
&-\sum_{i=m+1}^{n}\sum_{j=2}^{m-1} (b_{1m}^{ij})^2\,\mathrm{F}_{4\mathrm{F}}^{2\mathrm{me}}(s_{i+1,j}, s_{i,j-1}; s_{i,j}, s_{i+1,j-1})
\end{aligned} \tag{3.78}$$

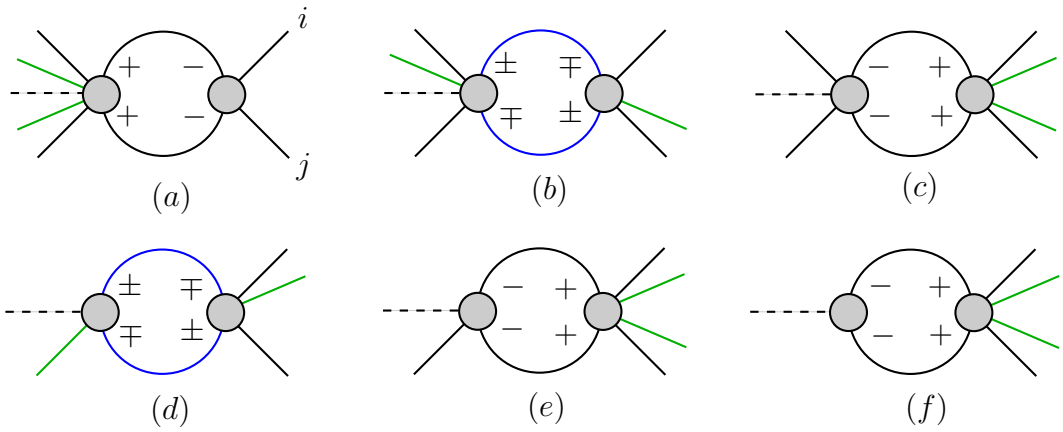

Figure 3.11: Double cut topologies which can appear in ϕ-MHV amplitudes. Diagrams which allow both fermions and gluons to propagate in the loop are coloured blue. The remaining diagrams only allow gluons to propagate in the loop.

In eq. (3.76)-(3.78) $\mathrm{F}^{\mathrm{2me}}_{\mathrm{4F}}$ represents the finite part of a two-mass box and is defined in Appendix B. The coefficients b^{ij}_{1m} are defined by eq. (3.46).

3.2.4 ϕ-MHV Double cuts

With the calculation of the box and triangle coefficients now complete we turn our attention to determining the coefficients of the various two point functions that appear in ϕ-MHV amplitudes. The general double cut topologies are depicted in Fig. 3.11, and, as was found with the four and three cut topologies, the position of the two negative helicity gluons determines what species of particle can propagate in the loop.

We begin by considering diagram 3.11(a), this diagram only allows gluonic contributions,

$$\begin{aligned}
\mathcal{D}^{(a)} &= A^{(0)}_{n+2-(j-i)}(\phi,\ell_1^+,(j+1)^+,\ldots,1^-,\ldots,m^-,\ldots,(i-1)^+,\ell_2^+) \\
&\quad \times A^{(0)}_{(j-i)+2}(\ell_2^-,i^+,\ldots,j^+,\ell_1^-) \\
&= -\frac{\langle 1m\rangle^4\langle \ell_2\ell_1\rangle^2}{\langle \ell_1(j+1)\rangle\prod_{\alpha=(j+1)}^{i-2}\langle\alpha(\alpha+1)\rangle\langle(i-1)\ell_2\rangle\langle\ell_2 i\rangle\prod_{\beta=i}^{j-1}\langle\beta(\beta+1)\rangle\langle\ell_1 j\rangle} \\
&= -A^{(0}_n\frac{\langle \ell_1\ell_2\rangle^2\langle(i-1)i\rangle\langle j(j+1)\rangle}{\langle \ell_1(j+1)\rangle\langle(i-1)\ell_2\rangle\langle\ell_2 i\rangle\langle\ell_1 j\rangle}.
\end{aligned} \tag{3.79}$$

It is trivial to see that diagrams 3.11(c), 3.11(e) and 3.11(f) have exactly the same integrand (with the relevant values of i and j). Therefore to consider the pure-glue diagrams we merely need perform the double cut integration of the following function,

$$\mathcal{I}^{ij} = \frac{\langle \ell_1 \ell_2 \rangle^2 \langle (i-1) i \rangle \langle j (j+1) \rangle}{\langle \ell_1 (j+1) \rangle \langle (i-1) \ell_2 \rangle \langle \ell_2 i \rangle \langle \ell_1 j \rangle}. \tag{3.80}$$

The Schouten identity can be used to relate I^{ij} to simpler functions G^{ij},

$$I^{ij} = -G^{ij} + G^{(i-1)j} + G^{i(j+1)} - G^{(i-1)(j+1)} \tag{3.81}$$

with

$$G^{ij} = \frac{\langle i \ell_1 \rangle \langle j \ell_2 \rangle}{\langle i \ell_2 \rangle \langle j \ell_1 \rangle}. \tag{3.82}$$

We will now proceed to integrate G^{ij} using the method of [132]. First remove ℓ_1 in favour of $\ell_2 = \ell_1 + P$ and replace $\ell_2 = t\lambda$, t is then fixed by the δ function, leaving the following integrand,

$$\int G^{ij} = \int d\lambda \frac{s_{P_{i,j}} \langle j \lambda \rangle \langle i | P | \lambda]}{\langle i \lambda \rangle \langle j | P | \lambda] \langle \lambda | P | \lambda]^2}. \tag{3.83}$$

Next we replace $|\lambda\rangle$ with $|p\rangle + z|\eta\rangle$ and integrate in z removing the pieces proportional to logarithms. It is interesting to note that if we had started with I^{ij} and integrated we would have found no pieces which are not proportional to logarithms and hence would have concluded that $I^{ij} \propto$ boxes and triangles. However, when we work with G^{ij} we find a non-zero piece which has a non-zero residue at $\overline{z} = 0$. In the previous chapter we described how these pieces arise from the integrand of a cut-bubble. This implies that G^{ij} contains bubbles whilst I^{ij} does not. For both these statements to be correct implies that G^{ij} does not depend on i or j, indeed we find that

$$\int G^{ij}|_{2-point} = 1, \tag{3.84}$$

which ensures that $I^{ij}|_{2-point} = 0$ as expected. In conclusion there are no pieces of diagrams 3.11(a), 3.11(c), 3.11(e) and 3.11(f), which are not proportional to boxes and triangles (and hence already known).

This leaves diagrams 3.11(b) and 3.11(d) which are related to each other ((d) can be obtained from (b)), here the integrands are more complicated since there are

two helicity solutions and two species can contribute. In previous sections we found that these types of terms had the following breakdown,

$$\mathcal{D} \propto \mathcal{G} + \left(1 - \frac{N_f}{4N_c}\right)\mathcal{F} + \left(1 - \frac{N_f}{N_c}\right)\mathcal{S} \tag{3.85}$$

with $\mathcal{G}$, $\mathcal{F}$ and $\mathcal{S}$ becoming increasingly more complicated. With this in mind we inspect the integrand of diagram (b),

$$\begin{aligned}
\mathcal{D}^{(b)}_{g,+} &= A^{(0)}_{n+2-(j-i)}(\phi, \ell_1^+, (j+1)^+, \ldots, 1^-, \ldots, (i-1)^+, \ell_2^-) \\
&\quad \times A^{(0)}_{(j-i)+2}(\ell_2^+, i^+, \ldots, m^-, \ldots, j^+, \ell_1^-) \\
&= -A^{(0)}_n \frac{\langle 1\ell_2\rangle^4 \langle m\ell_1\rangle^4 \langle (i-1)i\rangle \langle j(j+1)\rangle}{\langle \ell_1(j+1)\rangle \langle (i-1)\ell_2\rangle \langle \ell_2\ell_1\rangle^2 \langle \ell_2 i\rangle \langle j\ell_1\rangle \langle 1m\rangle^4},
\end{aligned} \tag{3.86}$$

$$\begin{aligned}
\mathcal{D}^{(b)}_{g,-} &= A^{(0)}_{n+2-(j-i)}(\phi, \ell_1^-, (j+1)^+, \ldots, 1^-, \ldots, (i-1)^+, \ell_2^+) \\
&\quad \times A^{(0)}_{(j-i)+2}(\ell_2^-, i^+, \ldots, m^-, \ldots, j^+, \ell_1^+) \\
&= -A^{(0)}_n \frac{\langle m\ell_2\rangle^4 \langle 1\ell_1\rangle^4 \langle (i-1)i\rangle \langle j(j+1)\rangle}{\langle \ell_1(j+1)\rangle \langle (i-1)\ell_2\rangle \langle \ell_2\ell_1\rangle^2 \langle \ell_2 i\rangle \langle j\ell_1\rangle \langle 1m\rangle^4}.
\end{aligned} \tag{3.87}$$

When we combine the two contributions we find the following,

$$\mathcal{D}^{(b)}_g = -A^{(0)}_n \frac{(\langle 1\ell_2\rangle^4 \langle m\ell_1\rangle^4 + \langle m\ell_2\rangle^4 \langle 1\ell_1\rangle^4) \langle (i-1)i\rangle \langle j(j+1)\rangle}{\langle \ell_1(j+1)\rangle \langle (i-1)\ell_2\rangle \langle \ell_2\ell_1\rangle^2 \langle \ell_2 i\rangle \langle j\ell_1\rangle \langle 1m\rangle^4} \tag{3.88}$$

The Schouten identity now can be applied in the same manner as previous cases and produces the following integrands,

$$\begin{aligned}
D^{(b)} = -A^{(0)}_n \Bigg(&\mathcal{G}^{2-cut}(a,i,j) + 4\left(1 - \frac{N_f}{4N_c}\right)\mathcal{F}^{2-cut}(a,i,j) \\
&+ 2\left(1 - \frac{N_f}{N_c}\right)\mathcal{S}^{2-cut}(a,i,j)\Bigg)
\end{aligned} \tag{3.89}$$

with,

$$\mathcal{G}^{2-cut}(a,i,j) = \frac{\langle (i-1)i\rangle \langle j(j+1)\rangle \langle \ell_1\ell_2\rangle^2}{\langle \ell_1(j+1)\rangle \langle (i-1)\ell_2\rangle \langle \ell_2 i\rangle \langle j\ell_1\rangle}, \tag{3.90}$$

$$\mathcal{F}^{2-cut}(a,i,j) = \frac{\langle 1\ell_2\rangle \langle m\ell_1\rangle \langle m\ell_2\rangle \langle 1\ell_1\rangle \langle (i-1)i\rangle \langle j(j+1)\rangle}{\langle \ell_1(j+1)\rangle \langle (i-1)\ell_2\rangle \langle \ell_2 i\rangle \langle j\ell_1\rangle \langle 1m\rangle^2}, \tag{3.91}$$

$$\mathcal{S}^{2-cut}(a,i,j) = \frac{\langle 1\ell_2\rangle^2 \langle m\ell_1\rangle^2 \langle m\ell_2\rangle^2 \langle 1\ell_1\rangle^2 \langle (i-1)i\rangle \langle j(j+1)\rangle}{\langle \ell_1(j+1)\rangle \langle (i-1)\ell_2\rangle \langle \ell_2 i\rangle \langle j\ell_1\rangle \langle 1m\rangle^4 \langle \ell_1\ell_2\rangle^2}. \tag{3.92}$$

In these equations $a \in \{1, m\}$ refers to the negative helicity leg which is not paired with ϕ. We note that $\mathcal{G}^{2-cut} = I^{ij}$ and as such has no 2-point coefficient associated with it. This leaves us with $\mathcal{F}$ and $\mathcal{S}$ which we will proceed to integrate.

We can compare $\mathcal{F}$ to $\mathcal{G}$ by using the same technique that was applied to I^{ij} to split the integrand into four simpler pieces,

$$\mathcal{F}^{2-cut}(a,i,j) = -f^{i,j} + f^{i,j+1} + f^{i-1,j} - f^{i-1,j+1}, \tag{3.93}$$

with

$$f^{ij} = \frac{\langle i\ell_1\rangle\langle j\ell_2\rangle\langle \ell_1 1\rangle\langle \ell_2 m\rangle\langle \ell_2 1\rangle\langle m\ell_1\rangle}{\langle i\ell_2\rangle\langle j\ell_1\rangle\langle \ell_1\ell_2\rangle^2\langle 1m\rangle^2} \tag{3.94}$$

We note that $f^{ij} \propto G^{ij}\langle \ell_1 1\rangle\langle \ell_2 m\rangle\langle \ell_2 1\rangle\langle m\ell_1\rangle$ and that G^{ij} contained only a pure bubble function which cancelled when the four G functions were combined. Here we see that there are products of spinors in the numerator, which will contribute to higher-rank tensor integrals some of which will reduce to 2-point functions. Therefore, from f we expect to find a less trivial 2-point coefficient than from G^{ij}.

$\mathcal{F}$ is actually simple enough to apply the method of [132] directly. We first remove ℓ_1 in favour of $\ell_2 = t\lambda$ and after integrating t with the second delta funtion we obtain the following integrand

$$\mathcal{F}^{2-cut}(1,i,j) = \int d\lambda \frac{s_{P_{i,j}}\langle 1m\rangle^2\langle 1\lambda\rangle\langle 4\lambda\rangle\langle 1|P_{i;j}|\lambda]\langle 4|P_{i,j}|\lambda]}{\langle (i-1)\lambda\rangle\langle i\lambda\rangle\langle j|P_{i,j}|\lambda]\langle (j+1)|P_{i,j}|\lambda]\langle \lambda|P_{i,j}|\lambda]^2}. \tag{3.95}$$

Next we define $|\lambda\rangle = |p\rangle + z|\eta\rangle$ and integrate in z discarding the logarithmic pieces (which as described earlier contribute only to box and triangle coefficients). In the remaining rational integral we define $|\lambda] = |p] + \overline{z}|\eta]$ which leaves us with the following term

$$\mathcal{F}^{2-point}(1,i,j) = -\oint d\overline{z} \frac{\langle 1m\rangle^2\beta(1)^2\beta(m)^2}{\overline{z}(1-z\overline{z})\beta(i-1)\beta(i)\beta(j)\beta(j+1)} \tag{3.96}$$

where $\beta(x) = (\overline{z}\langle px\rangle - \langle \eta x\rangle)$. To obtain the 2-point coefficient we are interested in, we use Cauchy's residue theorem to perform the integral. After some simplification using the Schouten identity we find,

$$\begin{aligned}\mathcal{F}^{2-point}(1,i,j) = {} & \frac{\langle 1(i-1)\rangle\langle 1m\rangle^2\langle (i-1)m\rangle^2\langle j(j+1)\rangle\langle 1|P_{i,j}|(i-1)]}{\langle (i-1)j\rangle\langle (i-1)(j+1)\rangle\langle (i-1)|P_{i,j}|(i-1)]} \\ -\frac{\langle 1i\rangle\langle 1m\rangle^2\langle im\rangle^2\langle j(j+1)\rangle\langle 1|P_{i,j}|i]}{\langle ij\rangle\langle i(j+1)\rangle\langle i|P_{i,j}|i]} & + \frac{\langle 1j\rangle\langle 1m\rangle^2\langle jm\rangle^2\langle (i-1)i\rangle\langle 1|P_{i,j}|j]}{\langle (i-1)j\rangle\langle (i-1)j\rangle\langle j|P_{i,j}|j]} \\ & -\frac{\langle 1(j+1)\rangle\langle 1m\rangle^2\langle (j+1)m\rangle^2\langle i(i-1)\rangle\langle 1|P_{i,j}|(j+1)]}{\langle (i-1)(j+1)\rangle\langle (i-1)(j+1)\rangle\langle (j+1)|P_{i,j}|(j+1)]}.\end{aligned} \tag{3.97}$$

Each of the terms in the above equation has an inverse power of the form $\langle i|P_{i,j}|i] = s_{i,j} - s_{i+1,j}$ and will match up with a term from a cut with a different i and j to form the coefficient of the L_i functions defined in Chapter 2. Schematically,

$$\begin{aligned} & \mathcal{F}^{2-point}(1,i,j)\log(s_{i,j}) + \mathcal{F}^{2-point}(1,i+1,j)\log(s_{i+1,j}) \\ \Longrightarrow & \left(\frac{c}{\langle i|P_{i,j}|i]} + \ldots\right)\log(s_{i,j}) + \left(-\frac{c}{\langle i|P_{i,j}|i]} + \ldots\right)\log(s_{i+1,j}) \\ & = cL_1(s_{i,j}, s_{i+1,j}) + \ldots \end{aligned} \tag{3.98}$$

Here the dots represent the other pieces which are not paired up from this particular cut combination. We find that when all cuts are considered every single log pairs to form an L_1. Since the bubble integral has the following ϵ expansion

$$\mathcal{I}_2(s) \propto \frac{1}{\epsilon} + 2 - \log(s) + \mathcal{O}(\epsilon), \tag{3.99}$$

the pairing of all the logarithms is equivalent to the disappearance of all ϵ^{-1} poles in the amplitude.

The technique for obtaining $\mathcal{S}$ is identical to that described above, however here the intermediate integrands are more complicated. We use the following form of the Schouten identity [123] to simplify the intermediate integrands, before we do the z integration,

$$\frac{\langle a\lambda\rangle}{\langle b\lambda\rangle\langle c\lambda\rangle} = \frac{1}{\langle bc\rangle}\left(\frac{\langle ab\rangle}{\langle b\lambda\rangle} - \frac{\langle ac\rangle}{\langle c\lambda\rangle}\right) \tag{3.100}$$

and this has the effect of separating poles and simplifying the resulting residues. To avoid repetition we delay explicitly writing out $\mathcal{S}$ until we combine all the cuts together in the following section.

3.2.5 Combined cuts: The cut-constructible pieces of the ϕ-MHV amplitude

We are finally ready to piece together the combination of four-, three- and two-cuts to obtain the full cut-constructible piece of the ϕ-MHV amplitude, $C_n(\phi, 1^-, \ldots, m^-, \ldots, n^+)$. In general we found that we could write C_n in the following way

$C_n(\phi, 1^-, 2^+, \ldots, m^-, \ldots, n^+)$

$$= A_n^{(0)}\left(A_{n;1}^{\phi G}(m,n) - 4\left(1-\frac{N_f}{4N_c}\right)A_{n;1}^{\phi F}(m,n) - 2\left(1-\frac{N_f}{N_c}\right)A_{n;1}^{\phi S}(m,n)\right), \tag{3.101}$$

with

$$A_{n;1}^{\phi G}(m,n) = -\frac{1}{2}\sum_{i=1}^{n}\sum_{j=i+3}^{n+i-1} \mathrm{F}_4^{\mathrm{2me}}(s_{i+1,j}, s_{i,j-1}; s_{i,j}, s_{i+1,j-1})$$
$$-\frac{1}{2}\sum_{i=1}^{n} \mathrm{F}_4^{\mathrm{1m}}(s_{i,i+1}, s_{i+1,i+2}; s_{i,i+2}) + (\mathrm{F}_3^{\mathrm{1m}}(s_{i,n+i-2}) - \mathrm{F}_3^{\mathrm{1m}}(s_{i,n+i-1})), \tag{3.102}$$

$$\begin{aligned}
A_{n;1}^{\phi F}(m,n) = & \sum_{i=2}^{m-1}\sum_{j=m+1}^{n} b_{1m}^{ij}\, \mathrm{F}_{4\mathrm{F}}^{\mathrm{2me}}(s_{i+1,j}, s_{i,j-1}; s_{i,j}, s_{i+1,j-1}) \\
& + \sum_{i=2}^{m-1}\sum_{j=m+1}^{n} b_{1m}^{ij}\, \mathrm{F}_{4\mathrm{F}}^{\mathrm{2me}}(s_{j+1,i}, s_{j,i-1}; s_{j,i}, s_{j+1,i-1}) \\
& - \sum_{i=2}^{m-1}\sum_{j=m}^{n} \frac{\mathrm{tr}_-(m, P_{(i,j)}, i, 1)}{s_{1m}^2} \mathcal{A}_{m1}^{ij} L_1(P_{(i+1,j)}, P_{(i,j)}) \\
& + \sum_{i=2}^{m-1}\sum_{j=m+1}^{1} \frac{\mathrm{tr}_-(1, P_{(j,i)}, i, m)}{s_{1m}^2} \mathcal{A}_{1m}^{i(j-1)} L_1(P_{(j,i-1)}, P_{(j,i)}) \\
& + \sum_{i=2}^{m}\sum_{j=m+1}^{n} \frac{\mathrm{tr}_-(m, P_{(i,j)}, j, 1)}{s_{1m}^2} \mathcal{A}_{m1}^{j(i-1)} L_1(P_{(i,j-1)}, P_{(i,j)}) \\
& - \sum_{i=1}^{m-1}\sum_{j=m+1}^{n} \frac{\mathrm{tr}_-(1, P_{(j,i)}, j, m)}{s_{1m}^2} \mathcal{A}_{1m}^{ji} L_1(P_{(j+1,i)}, P_{(j,i)}).
\end{aligned} \tag{3.103}$$

Here we have introduced the following function, which will make the collinear behaviour of eq. (3.103) more apparent,

$$\mathcal{A}_{1m}^{ij} = \left(\frac{\mathrm{tr}_-(1,i,j,m)}{s_{ij}} - (j \to j+1)\right). \tag{3.104}$$

The final piece of eq. (3.101) is the most complicated and has the following structure,

$$\begin{aligned}
A_{n;1}^{\phi S}(m,n) = & -\sum_{i=2}^{m-1}\sum_{j=m+1}^{n} (b_{1m}^{ij})^2\, \mathrm{F}_{4\mathrm{F}}^{\mathrm{2me}}(s_{i+1,j}, s_{i,j-1}; s_{i,j}, s_{i+1,j-1}) \\
& - \sum_{i=m+1}^{n}\sum_{j=2}^{m-1} (b_{1m}^{ij})^2\, \mathrm{F}_{4\mathrm{F}}^{\mathrm{2me}}(s_{i+1,j}, s_{i,j-1}; s_{i,j}, s_{i+1,j-1}) \\
& + \sum_{i=2}^{m-1}\sum_{j=m}^{n} \Bigg[-\frac{\mathrm{tr}_-(m, P_{(i,j)}, i, 1)^3}{3 s_{1m}^4} \mathcal{A}_{m1}^{ij} L_3(P_{(i+1,j)}, P_{(i,j)})
\end{aligned}$$

$$
\begin{aligned}
&\qquad -\frac{\mathrm{tr}_-(m,P_{(i,j)},i,1)^2}{2s_{1m}^4}\mathcal{K}_{m1}^{ij}L_2(P_{(i+1,j)},P_{(i,j)}) \\
&\qquad +\frac{\mathrm{tr}_-(m,P_{(i,j)},i,1)}{s_{1m}^4}\mathcal{I}_{m1}^{ij}L_1(P_{(i+1,j)},P_{(i,j)})\Bigg] \\
&+\sum_{i=1}^{m-1}\sum_{j=m+1}^{n}\Bigg[-\frac{\mathrm{tr}_-(1,P_{(j,i)},j,m)^3}{3s_{1m}^4}\mathcal{A}_{1m}^{ji}L_3(P_{(j+1,i)},P_{(j,i)}) \\
&\qquad -\frac{\mathrm{tr}_-(1,P_{(j,i)},j,m)^2}{2s_{1m}^4}\mathcal{K}_{1m}^{ji}L_2(P_{(j+1,i)},P_{(j,i)}) \\
&\qquad +\frac{\mathrm{tr}_-(1,P_{(j,i)},j,m)}{s_{1m}^4}\mathcal{I}_{1m}^{ji}L_1(P_{(j+1,i)},P_{(j,i)})\Bigg] \\
&+\sum_{i=2}^{m}\sum_{j=m+1}^{n}\Bigg[\frac{\mathrm{tr}_-(m,P_{(i,j)},j,1)^3}{3s_{1m}^4}\mathcal{A}_{m1}^{j(i-1)}L_3(P_{(i,j-1)},P_{(i,j)}) \\
&\qquad +\frac{\mathrm{tr}_-(m,P_{(i,j)},j,1)^2}{2s_{1m}^4}\mathcal{K}_{m1}^{j(i-1)}L_2(P_{(i,j-1)},P_{(i,j)}) \\
&\qquad -\frac{\mathrm{tr}_-(m,P_{(i,j)},j,1)}{s_{1m}^4}\mathcal{I}_{m1}^{j(i-1)}L_1(P_{(i,j-1)},P_{(i,j)})\Bigg] \\
&+\sum_{i=2}^{m-1}\sum_{j=m+1}^{1}\Bigg[\frac{\mathrm{tr}_-(1,P_{(j,i)},i,m)^3}{3s_{1m}^4}\mathcal{A}_{1m}^{i(j-1)}L_3(P_{(j,i-1)},P_{(j,i)}) \\
&\qquad +\frac{\mathrm{tr}_-(1,P_{(j,i)},i,m)^2}{2s_{1m}^4}\mathcal{K}_{1m}^{i(j-1)}L_2(P_{(j,i-1)},P_{(j,i)}) \\
&\qquad -\frac{\mathrm{tr}_-(1,P_{(j,i)},i,m)}{s_{1m}^4}\mathcal{I}_{1m}^{i(j-1)}L_1(P_{(j,i-1)},P_{(j,i)})\Bigg].
\end{aligned}
\tag{3.105}
$$

The new functions appearing in $A^{\phi,S}$ have the following form,

$$
\mathcal{K}_{1m}^{ij} = \left(\frac{\mathrm{tr}_-(1,i,j,m)^2}{s_{ij}^2} - (j \to j+1)\right), \tag{3.106}
$$

$$
\mathcal{I}_{1m}^{ij} = \left(\frac{\mathrm{tr}_-(1,i,j,m)^2\,\mathrm{tr}_-(1,j,i,m)}{s_{ij}^3} - (j \to j+1)\right). \tag{3.107}
$$

3.3 The rational pieces

In this section we will derive the various rational pieces associated with the ϕ-MHV amplitude. Since we are ultimately interested in the ϕ plus four parton amplitude, $A_4^{(1)}(\phi,1^-,2^+,3^-,4^+)$, we will not present the overlap or recursive terms for all

parton multiplicities. It is simple, however, to generalise the methods described in the following sections to include increasing numbers of partons. When calculating the rational terms it is simplest to include the cut-completion terms with C_n, we defined the following rational terms

$$\widehat{R}_n = R_n^D + O_n - \text{Inf}\, A_n, \tag{3.108}$$

merging the remaining rational terms with the cut-constructible pieces

$$\widehat{C}_n = C_n + CR_n. \tag{3.109}$$

In the above equations Inf A_n, represents the pieces of the amplitude which do not vanish as $z \to \infty$ (where z is the BCFW shift parameter). In our calculation we will find that CR_n contributes an infinite piece of this sort. In the following sections we will analyse each of these rational contributions before putting the whole rational piece together.

3.3.1 The cut-completion terms

The basis-set of logarithmic functions in which eq. (3.103) and eq. (3.105) are written contains unphysical singularities, which we remove by adding in rational pieces, the so-called cut completion terms. The new basis is given by the transformation,

$$\begin{aligned} L_1(s,t) &= \hat{L}_1(s,t), \\ L_2(s,t) &= \hat{L}_2(s,t) + \frac{1}{2(s-t)}\left(\frac{1}{t}+\frac{1}{s}\right), \\ L_3(s,t) &= \hat{L}_3(s,t) + \frac{1}{2(s-t)^2}\left(\frac{1}{t}+\frac{1}{s}\right). \end{aligned} \tag{3.110}$$

From the breakdown of our amplitude it is clear that only $A_n^{\phi S}$ needs to be completed. When considering the overlap terms in the next section it proves most convenient to write the cut-completion terms in the following form,

$$CR_n(\phi, 1^-, \ldots, m^-, \ldots, n^+) = \Gamma_n \Bigg[\\ \sum_{i=2}^{m}\sum_{j=m+1}^{n} \rho_{m1}^{j,i-1}(P_{(i,j-1)})\left(\frac{1}{s_{i,j-1}}+\frac{1}{s_{i,j}}\right) - \sum_{i=2}^{m-1}\sum_{j=m}^{n} \rho_{m1}^{i,j}(P_{(i+1,j)})\left(\frac{1}{s_{i+1,j}}+\frac{1}{s_{i,j}}\right)$$

$$+ \quad \sum_{i=2}^{m-1}\sum_{j=m+1}^{n+1}\rho_{1m}^{i,j-1}(P_{(j,i-1)})\left(\frac{1}{s_{j,i-1}}+\frac{1}{s_{j,i}}\right)-\sum_{i=1}^{m-1}\sum_{j=m+1}^{n}\rho_{1m}^{j,i}(P_{(j+1,i)})\left(\frac{1}{s_{j+1,i}}+\frac{1}{s_{j,i}}\right)\Bigg]. \tag{3.111}$$

The factor Γ_n is given by,

$$\Gamma_n = \frac{N_P}{2\Pi_{\alpha=1}^{n}\langle\alpha\,\alpha+1\rangle}, \tag{3.112}$$

and

$$\rho_{m1}^{a,b}(P_{(i,j)}) = \frac{\langle m|\,P_{(i,j)}\,a|\,1\rangle^3}{3\left\langle a\,|P_{(i,j)}|\,a\right]^2}A_{m1}^{ab}+\frac{\langle m\,|P_{(i,j)}\,a|\,1\rangle^2}{2\left\langle a\,|P_{(i,j)}|\,a\right]}K_{m1}^{ab}, \tag{3.113}$$

with

$$A_{m1}^{ab} = \frac{\langle m\,a\rangle\,\langle b\,1\rangle}{\langle a\,b\rangle}-(b\to b+1), \tag{3.114}$$

$$K_{m1}^{ab} = \frac{\langle m\,a\rangle^2\,\langle b\,1\rangle^2}{\langle a\,b\rangle^2}-(b\to b+1). \tag{3.115}$$

We have also introduced the short-hand notation,

$$N_P = 2\left(1-\frac{N_f}{N_c}\right). \tag{3.116}$$

Ultimately we will require the cut-completion terms for the four parton amplitude $A_4^{(1)}(\phi,1^-,2^+,3^-,4^+)$,

$$\begin{aligned} CR_4(\phi,1^-,2^+,3^-,4^+) &= \frac{N_P}{2}\frac{1}{\langle 1\,2\rangle\,\langle 2\,3\rangle\,\langle 3\,4\rangle\,\langle 4\,1\rangle} \\ \times\quad &\left[\left(-\frac{\langle 3|\,2\,4\,|1\rangle^3}{3(s_{234}-s_{23})^2}\frac{\langle 3\,4\rangle\,\langle 2\,1\rangle}{\langle 4\,2\rangle}-\frac{\langle 3|\,2\,4\,|1\rangle^2}{2(s_{234}-s_{23})}\frac{\langle 3\,4\rangle^2\,\langle 2\,1\rangle^2}{\langle 4\,2\rangle^2}\right)\left(\frac{1}{s_{23}}+\frac{1}{s_{234}}\right)\right] \\ &+(2\leftrightarrow 4)+(1\leftrightarrow 3)+(1\leftrightarrow 3,2\leftrightarrow 4). \end{aligned} \tag{3.117}$$

3.3.2 The recursive terms

We make a complex shift [106, 140, 141, 161–163] of the two negative gluons such that

$$|\hat{1}\rangle = |1\rangle + z|3\rangle, \qquad |\hat{3}] = |3] - z|1], \tag{3.118}$$

ensuring that overall momentum is conserved since

$$p_1^\mu(z) = p_1^\mu + \frac{z}{2}\langle 3\,|\gamma^\mu|\,1]\,, \qquad p_3^\mu(z) = p_3^\mu - \frac{z}{2}\langle 3\,|\gamma^\mu|\,1]\,. \tag{3.119}$$

The direct recursive terms are obtained using the following formula

$$R_n^D = \sum_i \frac{A_L^{(0)}(z)R_R(z) + R_L(z)A_R^{(0)}(z)}{P_i^2}. \tag{3.120}$$

For our chosen shift (3.118), the allowed diagrams are shown in Fig. 3.12. Due to our choice of shifts the tree amplitudes

$$A^{(0)}(j^+, \hat{1}^-, -P^-_{(1,j)}), \qquad A^{(0)}(j^+, \hat{m}^-, -P^+_{(m,j)})$$

are both zero, (here $j \in \{2, 4\}$). Other terms that vanish are $R_2(\phi, -+)$ which is required to be zero by angular momentum conservation, and $R_3(j^+, \hat{m}^-, \hat{P}^\pm)$ since the corresponding splitting function has no rational pieces.

To complete our calculation we require the one-loop gluon amplitude with one negative helicity gluon. These are finite one-loop amplitudes and are entirely rational. The finite $\phi - + \ldots +$ amplitudes were computed for arbitrary numbers of positive helicity gluons in ref. [106]. As a concrete example, the three-gluon amplitude is given by,

$$R_3(\phi; 1^-, 2^+, 3^+) = \frac{N_P}{6}\frac{\langle 12\rangle\langle 31\rangle[23]}{\langle 23\rangle^2} - 2A_3^{(0)}(\phi^\dagger; 1^-, 2^+, 3^+). \tag{3.121}$$

Similarly, the pure QCD $-+\ldots+$ amplitudes are given to all orders in ref. [161,203]. In the four gluon case, the result is,

$$R_4(1^-, 2^+, 3^+, 4^+) = \frac{N_P}{6}\frac{\langle 2\,4\rangle\,[2\,4]^3}{[1\,2]\,\langle 2\,3\rangle\,\langle 3\,4\rangle\,[4\,1]} \tag{3.122}$$

Finally, there the "homogenous" terms in the recursion which depend on the ϕ-MHV amplitude with one gluon fewer. The first few ϕ-MHV amplitudes are known,

$$R_2(\phi; 1^-, 2^-) = 2A^{(0)}(\phi, 1^-, 2^-), \tag{3.123}$$

$$R_3(\phi; 1^-, 2^-, 3^+) = 2A^{(0)}(\phi, 1^-, 2^-, 3^+), \tag{3.124}$$

$$R_3(\phi; 1^-, 2^+, 3^-) = 2A^{(0)}(\phi, 1^-, 2^+, 3^-). \tag{3.125}$$

The direct rational contribution is generated by the recursion relation (3.120) and is given by,

$$R_4(\phi, 1^-, 2^+, 3^-, 4^+) = A^{(0)}(\phi, \hat{1}^-, \hat{P}^-_{234})\frac{1}{s_{234}}R(-\hat{P}^+_{234}, 2^+, \hat{3}^-, 4^+)$$

$$
\begin{aligned}
&+R(4^+,\hat{1}^-,2^+,-\hat{P}^+_{412})\frac{1}{s_{412}}A^{(0)}(\phi,\hat{P}^-_{412},\hat{3}^-)\\
&+R(\phi,\hat{1}^-,2^+,-\hat{P}^+_{34},)\frac{1}{s_{34}}A^{(0)}(\hat{P}^-_{34},\hat{3}^-,4^+)\\
&+R(\phi,\hat{1}^-,4^+,-\hat{P}^+_{23})\frac{1}{s_{23}}A^{(0)}(\hat{P}^-_{23},2^+,\hat{3}^-)\\
&+A^{(0)}(\hat{1}^-,\hat{P}^+_{41},4^+)\frac{1}{s_{41}}R(\phi,-\hat{P}^-_{41},2^+,\hat{3}^-)\\
&+A^{(0)}(\hat{1}^-,\hat{P}^+_{12},2^+)\frac{1}{s_{12}}R(\phi,-\hat{P}^-_{12},\hat{3}^-,4^+), \qquad (3.126)
\end{aligned}
$$

where we recycle the known lower point amplitudes. For the four-point amplitude, we require the rational parts of the ϕ amplitude with one minus and two positive helicity gluons (3.121), the two and three-point ϕ-MHV amplitudes given in eqs. (3.123), (3.124) and (3.125), as well as the pure four-gluon QCD amplitude with a single negative helicity of eq. (3.122).

We find that

$$
R_4^{234} = \frac{N_P}{6}\frac{m_H^4}{s_{234}}\frac{\langle 2\,4\rangle\,[2\,4]\,\langle 3\,|P_{234}|\,1]^2}{\langle 4\,|P_{234}|\,1]^2\,\langle 2\,|P_{234}|\,1]^2}. \qquad (3.127)
$$

Similarly,

$$
R_4^{23} = -2A^{(0)}(\phi^\dagger,4^+,2^+,3^-,1^-) - \frac{N_P}{6}s_{123}\frac{[2\,4]\,[2\,1]}{[3\,1]\,[2\,3]}\frac{\langle 4\,|P_{123}|\,2]}{\langle 4\,|P_{123}|\,1]^2}, \qquad (3.128)
$$

$$
R_4^{34} = R_4^{23} \quad (2\leftrightarrow 4). \qquad (3.129)
$$

In the other channels,

$$
\begin{aligned}
R_4^{41} &= -2A^{(0)}(\phi,1^-,3^-,2^+,4^+) && (3.130)\\
R_4^{12} &= R_4^{41} \quad (4\leftrightarrow 2), && (3.131)
\end{aligned}
$$

and finally,

$$
R_4^{412} = \frac{N_P}{6}\frac{[2\,4]^3}{s_{412}}\frac{\langle 3\,|P_{412}|\,1]^2}{\langle 2\,4\rangle\,[1\,2]^2\,[4\,1]^2}. \qquad (3.132)
$$

3.3.3 The overlap terms

The overlap terms are defined as [108, 124],

$$
O_n = \sum_i \mathrm{Res}_{z=z_i}\frac{CR_n(z)}{z}. \qquad (3.133)
$$

They can be obtained by evaluating the residue of the cut completion term CR_n given in eq. (3.111) in each of the physical channels. Each of the rational pieces in the previous section contributes an overlap piece,

$$O_4(\phi, 1^-, 2^+, 3^-, 4^+) = O_4^{234} + O_4^{23} + O_4^{34} + O_4^{41} + O_4^{12} + O_4^{412}. \tag{3.134}$$

Evaluating each term explicitly,

$$\begin{aligned} O_4^{234} = \quad & \frac{N_P}{2s_{234}}\left(\frac{1}{3}\frac{\langle 3|\, P_{234}\, P_{1234}|\, 2\rangle^2\, [4\,2]}{\langle 2\,4\rangle\, \langle 2\,|P_{234}|\, 1]^2} \right. \\ & \left. + \frac{1}{2}\frac{\langle 3\,2\rangle\, \langle 3\,|P_{234}\, P_{1234}|\, 2\rangle\, \langle 3\,|P_{234}\, P_{1234}|\, 4\rangle\, [4\,2]}{\langle 2\,4\rangle^2\, \langle 2\,|P_{234}|\, 1]\, \langle 3\,|P_{234}|\, 1]} + (2 \leftrightarrow 4)\right). \end{aligned} \tag{3.135}$$

The overlap pieces in the s_{23} and s_{34} channels are given by,

$$\begin{aligned} O_4^{23} = \quad & -\frac{N_P}{2s_{23}}\left(-\frac{\langle 3\,2\rangle^2\, \langle 4\,|P_{123}|\, 2]^2\, [2\,4]}{3\, \langle 4\,|P_{123}|\, 1]^2\, \langle 4\,2\rangle} \right. \\ & \left. + \frac{\langle 3\,2\rangle\, \langle 3\,4\rangle\, [2\,4]\, \langle 2\,|P_{123}|\, 2]\, \langle 4\,|P_{123}|\, 2]}{2\, [1\,2]\, \langle 4\,2\rangle^2\, \langle 4\,|P_{123}|\, 1]}\right), \end{aligned} \tag{3.136}$$

$$O_4^{34} = \quad O_4^{23} \quad (4 \leftrightarrow 2). \tag{3.137}$$

O^{41} and O^{12} both vanish, whilst

$$O_4^{412} = -\frac{N_P}{2s_{412}}\left(\frac{1}{2}\frac{\langle 2\,3\rangle\, \langle 4\,3\rangle\, \langle 3\,|P_{412}|\, 4]\, [4\,2]^2}{\langle 2\,4\rangle\, \langle 3\,|P_{412}|\, 1]\, [4\,1]} - \frac{1}{3}\frac{\langle 2\,3\rangle^2\, [4\,2]^3}{\langle 2\,4\rangle\, [4\,1]^2} + (2 \leftrightarrow 4)\right). \tag{3.138}$$

3.3.4 The large z behaviour of the completion terms

In order for the direct recursive contribution to correctly generate the rational terms, the shifted amplitude $A_n^{(1)}(z)$ must vanish as $z \to \infty$. However, the cut-completion term $CR_n(z)$ introduced in eq. (3.111) to ensure that the cut constructible part does not have any spurious poles, does not vanish as $z \to \infty$. We therefore have to explicitly remove the contribution at infinity from the rational part, which now becomes [124, 165],

$$\hat{R}_n = R_n^D + O_n - \mathrm{Inf}\, CR_n, \tag{3.139}$$

where

$$\mathrm{Inf}\, CR_n = \lim_{z\to\infty} CR_n(z). \tag{3.140}$$

The calculation of $\mathrm{Inf}\, CR_n$ is straightforward. For the special case of adjacent negative helicities, corresponding to $m = 2$, the cut-completion terms behaves as $1/z$ as $z \to \infty$ so that,

$$\mathrm{Inf}\, CR_n(\phi, 1^-, 2^-, \ldots, n^+) = 0. \tag{3.141}$$

For the general, non-adjacent, case, there is a contribution as $z \to \infty$ and we find the contribution to be subtracted is,

$$\begin{aligned}
\mathrm{Inf}\, CR_n(\phi, 1^-, \ldots, m^-, \ldots, n^+) = \frac{N_P}{2\langle m\,2\rangle\langle n\,m\rangle\prod_{\alpha=2}^{n-1}\langle\alpha\,\alpha+1\rangle}\Bigg[& \\
\sum_{i=3}^{m}\sum_{j=m+1}^{n}\omega^{j,i-1}(P_{(i,j)})\left(\frac{1}{\langle m\,|P_{(i,j-1)}|\,1]}+\frac{1}{\langle m\,|P_{(i,j)}|\,1]}\right) & \\
-\sum_{i=2}^{m-1}\sum_{j=m+1}^{n}\omega^{i,j}(P_{(i,j)})\left(\frac{1}{\langle m\,|P_{(i+1,j)}|\,1]}+\frac{1}{\langle m\,|P_{(i,j)}|\,1]}\right) & \\
-\sum_{i=2}^{m-1}\sum_{j=m+1}^{n}\omega^{j,i}(P_{(i,j)})\left(\frac{1}{\langle m\,|P_{(i,j-1)}|\,1]}+\frac{1}{\langle m\,|P_{(i,j)}|\,1]}\right) & \\
+\sum_{i=2}^{m-1}\sum_{j=m}^{n-1}\omega^{i,j+1}(P_{(i,j)})\left(\frac{1}{\langle m\,|P_{(i+1,j)}|\,1]}+\frac{1}{\langle m\,|P_{(i,j)}|\,1]}\right) & \\
+\sum_{i=2}^{m-1}\sum_{j=m+2}^{n+1}\omega^{i,j-1}(\widetilde{P_{(j,i)}})\left(\frac{1}{\langle m\,|P_{(j,i-1)}|\,1]}+\frac{1}{\langle m\,|P_{(j,i)}|\,1]}\right) & \\
-\sum_{i=2}^{m-1}\sum_{j=m+1}^{n}\omega^{j,i}(\widetilde{P_{(j,i)}})\left(\frac{1}{\langle m\,|P_{(j+1,i)}|\,1]}+\frac{1}{\langle m\,|P_{(j,i)}|\,1]}\right) & \\
-\sum_{i=2}^{m-1}\sum_{j=m+1}^{n}\omega^{i,j}(\widetilde{P_{(j,i)}})\left(\frac{1}{\langle m\,|P_{(j,i-1)}|\,1]}+\frac{1}{\langle m\,|P_{(j,i)}|\,1]}\right) & \\
+\sum_{i=1}^{m-2}\sum_{j=m+1}^{n}\omega^{j,i+1}(\widetilde{P_{(j,i)}})\left(\frac{1}{\langle m\,|P_{(j+1,i)}|\,1]}+\frac{1}{\langle m\,|P_{(j,i)}|\,1]}\right)\Bigg], &
\end{aligned} \tag{3.142}$$

with

$$\omega^{a,b}(P_{(i,j)}) = \frac{\langle m\,|P_{(i,j)}\,a|\,m\rangle^2\langle a\,m\rangle\langle b\,m\rangle^2}{2\,[1\,a]\langle a\,b\rangle^2}, \tag{3.143}$$

and $\widetilde{P_{(j,i)}} = P_{(j,i)} - p_1$. Specifically when $n = 4$ and $m = 3$,

$$\mathrm{Inf}\, CR_4(\phi, 1^-, 2^+, 3^-, 4^+) = -\frac{N_P}{2}\frac{\langle 2\,3\rangle\langle 3\,4\rangle[2\,4]^2}{\langle 2\,4\rangle^2[1\,2][4\,1]}. \tag{3.144}$$

3.3.5 Combined rational pieces

Combining contributions, the full four-point amplitude is given by,

$$\begin{aligned} A_4^{(1)}(\phi,1^-,2^+,3^-,4^+) &= C_4(\phi,1^-,2^+,3^-,4^+) + CR_4(\phi,1^-,2^+,3^-,4^+) \\ &+ \hat{R}_4(\phi,1^-,2^+,3^-,4^+), \end{aligned} \tag{3.145}$$

with

$$\begin{aligned} \hat{R}(\phi,1^-,2^+,3^-,4^+) &= O_4(\phi,1^-,2^+,3^-,4^+) + R_4(\phi,1^-,2^+,3^-,4^+) \\ &- \mathrm{Inf}CR_4(\phi,1^-,2^+,3^-,4^+). \end{aligned} \tag{3.146}$$

After some algebra, the combination of overlapping and recursive terms can be written in the following form, free of spurious singularities [1],

$$\begin{aligned} &\hat{R}_4(\phi,1^-,2^+,3^-,4^+) = -2A^{(0)}(A,1^-,2^+,3^-,4^+) \\ &+ \frac{N_P}{6}\frac{[2\,4]^4}{[1\,2]\,[2\,3]\,[3\,4]\,[4\,1]}\left(-\frac{s_{23}s_{34}}{s_{24}s_{412}} + 3\frac{s_{23}s_{34}}{s_{24}^2} - \frac{s_{12}s_{41}}{s_{24}s_{234}} + 3\frac{s_{12}s_{41}}{s_{24}^2}\right), \end{aligned} \tag{3.147}$$

where $A^{(0)}(A,1^-,2^+,3^-,4^+)$ is the difference of ϕ and $\phi^\dagger$ amplitudes. We have checked this amplitude against a Feynman diagram calculation and found agreement. Finally the full Higgs amplitude is given by the sum of ϕ and $\phi^\dagger$ amplitudes

$$A_4^{(1)}(H,1^-,2^+,3^-,4^+) = A_4^{(1)}(\phi,1^-,2^+,3^-,4^+) + A_4^{(1)}(\phi^\dagger,1^-,2^+,3^-,4^+), \tag{3.148}$$

with,

$$A_4^{(1)}(\phi^\dagger,1^-,2^+,3^-,4^+) = A_4^{(1)}(\phi,2^-,3^+,4^-,1^+)_{\langle i\,j\rangle\leftrightarrow[i\,j]}. \tag{3.149}$$

We note that the rational terms not proportional to N_P in eq. (3.147) cancel when forming the Higgs amplitude, just as for the $A_4^{(1)}(H,1^-,2^-,3^+,4^+)$ amplitude of ref. [108].

[1] Which we have checked with the aid of the package S@M [204]

3.4 Cross Checks and Limits

3.4.1 Collinear limits

The general behaviour of a one-loop amplitude when gluons i and $(i+1)$ become collinear, such that $p_i \to zK$ and $p_{i+1} \to (1-z)K$, is well known,

$$\begin{aligned} & A_n^{(1)}(\ldots, i^{\lambda_i}, i+1^{\lambda_{i+1}}, \ldots) \overset{i\|i+1}{\longrightarrow} \\ \sum_{h=\pm} \Big[\; & A_{n-1}^{(1)}(\ldots, i-1^{\lambda_{i-1}}, K^h, i+2^{\lambda_{i+2}}, \ldots)\mathrm{Split}^{(0)}(-K^{-h}; i^{\lambda_i}, i+1^{\lambda_{i+1}}) \\ & + A_{n-1}^{(0)}(\ldots, i-1^{\lambda_{i-1}}, K^h, i+2^{\lambda_{i+2}}, \ldots)\mathrm{Split}^{(1)}(-K^{-h}; i^{\lambda_i}, i+1^{\lambda_{i+1}})\Big]. \end{aligned} \tag{3.150}$$

The universal splitting functions are given by [110, 111, 166],

$$\mathrm{Split}^{(0)}(-K^+; 1^-, 2^+) = \frac{z^2}{\sqrt{z(1-z)}\,\langle 1\,2\rangle}, \tag{3.151}$$

$$\mathrm{Split}^{(0)}(-K^+; 1^+, 2^-) = \frac{(1-z)^2}{\sqrt{z(1-z)}\,\langle 1\,2\rangle}, \tag{3.152}$$

$$\mathrm{Split}^{(0)}(-K^-; 1^+, 2^+) = \frac{1}{\sqrt{z(1-z)}\,\langle 1\,2\rangle}, \tag{3.153}$$

$$\mathrm{Split}^{(0)}(-K^-; 1^-, 2^-) = 0. \tag{3.154}$$

The one-loop splitting function can be written in terms of cut-constructible and rational components,

$$\mathrm{Split}^{(1)}(-K^{-h}, 1^{\lambda_1}, 2^{\lambda_2}) = \mathrm{Split}^{(1),C}(-K^{-h}, 1^{\lambda_1}, 2^{\lambda_2}) + \mathrm{Split}^{(1),R}(-K^{-h}, 1^{\lambda_1}, 2^{\lambda_2}) \tag{3.155}$$

where

$$\begin{aligned} & \mathrm{Split}^{(1),C}(-K^{\pm}, 1^-, 2^+) = \mathrm{Split}^{(0)}(-K^{\pm}, 1^-, 2^+)\frac{c_\Gamma}{\epsilon^2} \times \\ & \left(\frac{\mu^2}{-s_{12}}\right)^{\epsilon}\left(1 - {}_2F_1\left(1, -\epsilon; 1-\epsilon; \frac{z}{z-1}\right)\right) - {}_2F_1\left(1, -\epsilon; 1-\epsilon; \frac{z}{z-1}\right)\Big)\Big), \end{aligned} \tag{3.156}$$

$$\begin{aligned} & \mathrm{Split}^{(1),C}(-K^{+}, 1^-, 2^-) = \mathrm{Split}^{(0)}(-K^{+}, 1^-, 2^-)\frac{c_\Gamma}{\epsilon^2} \times \\ & \left(\frac{\mu^2}{-s_{12}}\right)^{\epsilon}\left(1 - {}_2F_1\left(1, -\epsilon; 1-\epsilon; \frac{z}{z-1}\right)\right) - {}_2F_1\left(1, -\epsilon; 1-\epsilon; \frac{z}{z-1}\right)\Big)\Big), \end{aligned}$$

(3.157)

$$\text{Split}^{(1),C}(-K^-,1^-,2^-)=0, \tag{3.158}$$

$$\text{Split}^{(1),R}(-K^\pm,1^-,2^+)=0, \tag{3.159}$$

$$\text{Split}^{(1),R}(-K^+,1^-,2^-)=\frac{N_P}{96\pi^2}\frac{\sqrt{z(1-z)}}{[1\,2]}, \tag{3.160}$$

$$\text{Split}^{(1),R}(-K^-,1^-,2^-)=\frac{N_P}{96\pi^2}\frac{\sqrt{z(1-z)}\,\langle 1\,2\rangle}{[1\,2]^2}. \tag{3.161}$$

Explicitly, the cut-constructible parts should satisfy,

$$\begin{aligned} C_n(\dots,i^{\lambda_i},i+1^{\lambda_{i+1}},\dots)&\overset{i\|i+1}{\longrightarrow}\sum_{h=\pm}\\ &C_{n-1}(\dots,i-1^{\lambda_{i-1}},K^h,i+2^{\lambda_{i+2}},\dots)\ \text{Split}^{(0)}(-K^{-h};i^{\lambda_i},i+1^{\lambda_{i+1}})\\ &+A^{(0)}_{n-1}(\dots,i-1^{\lambda_{i-1}},K^h,i+2^{\lambda_{i+2}},\dots)\ \text{Split}^{(1),C}(-K^{-h};i^{\lambda_i},i+1^{\lambda_{i+1}}), \end{aligned} \tag{3.162}$$

while the rational pieces obey,

$$\begin{aligned} R_n(\dots,i^{\lambda_i},i+1^{\lambda_{i+1}},\dots)&\overset{i\|i+1}{\longrightarrow}\sum_{h=\pm}\\ &R_{n-1}(\dots,i-1^{\lambda_{i-1}},K^h,i+2^{\lambda_{i+2}},\dots)\ \text{Split}^{(0)}(-K^{-h};i^{\lambda_i},i+1^{\lambda_{i+1}})\\ &+A^{(0)}_{n-1}(\dots,i-1^{\lambda_{i-1}},K^h,i+2^{\lambda_{i+2}},\dots)\ \text{Split}^{(1),R}(-K^{-h};i^{\lambda_i},i+1^{\lambda_{i+1}}). \end{aligned} \tag{3.163}$$

3.4.2 Collinear factorisation of the cut-constructible contributions

In Ref. [108], it was demonstrated that the helicity independent cut-constructible gluonic contribution obeys,

$$\begin{aligned} C_n^{\phi\{G\}}(\dots,i^{\lambda_i},i+1^{\lambda_{i+1}},\dots)&\overset{i\|i+1}{\longrightarrow}\sum_{h=\pm}\\ &C_{n-1}^{\phi\{G\}}(\dots,i-1^{\lambda_{i-1}},K^h,i+2^{\lambda_{i+2}},\dots)\ \text{Split}^{(0)}(-K^{-h};i^{\lambda_i},i+1^{\lambda_{i+1}})\\ &+A^{(0)}_{n-1}(\dots,i-1^{\lambda_{i-1}},K^h,i+2^{\lambda_{i+2}},\dots)\ \text{Split}^{(1),C}(-K^{-h};i^{\lambda_i},i+1^{\lambda_{i+1}}). \end{aligned} \tag{3.164}$$

Therefore to check the collinear behaviour of the general ϕ-MHV amplitude, we simply need to check that the fermionic and scalar contributions satisfy the following relation,

$$C_n^{\phi\{F,S\}}(\dots, i^{\lambda_i}, i+1^{\lambda_{i+1}}, \dots) \xrightarrow{i\|i+1} \sum_{h=\pm} C_{n-1}^{\phi\{F,S\}}(\dots, i-1^{\lambda_{i-1}}, K^h, i+2^{\lambda_{i+2}}, \dots)\ \mathrm{Split}^{(0)}(-K^{-h}; i^{\lambda_i}, i+1^{\lambda_{i+1}}). \tag{3.165}$$

In other words, the F and S contributions should factorise onto the tree-level splitting amplitude for the helicity of the gluons considered. According to the definition of C_n in eq. (3.75), there is an overall factor $A_n^{(0)}$, which in the collinear limit produces the correct tree-level splitting function. It therefore remains to show that,

$$A_{n;1}^{\phi F,\phi S} \to A_{n-1;1}^{\phi F,\phi S} \tag{3.166}$$

in the collinear limit with $A_{n;1}^{\phi F}(m,n)$ and $A_{n;1}^{\phi S}(m,n)$ given in eqs. (3.103) and (3.105) respectively.

Collinear behaviour of mixed helicity gluons

We first consider the limit where two adjacent gluons become collinear, one of which has negative helicity. For definiteness, we take the limit $(m-1) \parallel m$.

The coefficient of the box function b_{m1}^{ij} enters both $A^{\phi S}$ and $A^{\phi F}$. In this limit,

$$b_{m1}^{ij} \xrightarrow{m-1\|m} \frac{\mathrm{tr}_-(K,i,j,1)\,\mathrm{tr}_-(K,j,i,1)}{s_{ij}^2 s_{1K}^2} \equiv b_{K1}^{ij}. \tag{3.167}$$

For the special cases, $i = m-1$ and $j = m-1$, we have,

$$b_{m1}^{m-1,j} = b_{m1}^{i,m-1} = 0 \tag{3.168}$$

so that the box contribution correctly factorises onto the lower point amplitude.

The remaining terms in the sub-amplitudes are proportional to one of the auxiliary functions $\mathcal{F}_{m1}^{ij}$ with $\mathcal{F} = \mathcal{A}, \mathcal{K}$ and $\mathcal{I}$ and which are defined in eqs. (3.104), (3.106) and (3.107). We shall see that these too have the correct factorisation properties. Let us first consider the ranges $2 \le i \le m-1$ and $m \le j \le n$. When $i \le m-2$,

the momentum $P_{(i,j)}$ always contains both $m-1$ and m, while $P_{(j,i)}$ never includes either $m-1$ or m, and we find relations such as,

$$\begin{aligned}\frac{\mathrm{tr}_-(m,P_{(i,j)},i,1)}{s_{1m}^2}\mathcal{A}_{m1}^{ij} &\xrightarrow{m-1\|m} \frac{\mathrm{tr}_-(K,P_{(i,j)},i,1)}{s_{1K}^2}\mathcal{A}_{K1}^{ij},\\ \frac{\mathrm{tr}_-(1,P_{(j,i)},i,m)}{s_{1m}^2}\mathcal{A}_{1m}^{i(j-1)} &\xrightarrow{m-1\|m} \frac{\mathrm{tr}_-(1,P_{(j,i)},i,K)}{s_{1K}^2}\mathcal{A}_{1K}^{i(j-1)}.\end{aligned} \tag{3.169}$$

We note that for the special case $i=m-1$,

$$\begin{aligned}\mathcal{A}_{m1}^{m-1,j}=\frac{\mathrm{tr}_-(m,j,m-1,1)}{s_{m-1,j}}-\frac{\mathrm{tr}_-(m,j,m,1)}{s_{m,j}} &\xrightarrow{m-1\|m} 0,\\ \mathcal{A}_{1m}^{m-1,j} &\xrightarrow{m-1\|m} 0,\\ \mathcal{A}_{m1}^{i,m-1} &\xrightarrow{m-1\|m} 0.\end{aligned} \tag{3.170}$$

Similar relations hold for the terms involving $\mathcal{K}$ and $\mathcal{I}$. Therefore, all terms in the n-gluon version of $A_{n;1}^{\phi F}$ and $A_{n;1}^{\phi S}$ therefore either collapse onto similar terms, or vanish in such a way that the reduced summation precisely matches onto the corresponding $A_{n-1;1}^{\phi F}$ and $A_{n-1;1}^{\phi S}$.

Two positive collinear limit

Next we consider the limit when two positive helicity gluons become collinear. We focus on the specific example where $\ell-1 \parallel \ell$ with $3\leq\ell\leq m-1$. As in the previous subsection, let first consider the ranges $2\leq i\leq m-1$ and $m\leq j\leq n$. We note that,

$$\begin{aligned}b_{1m}^{\ell-1j} &\xrightarrow{\ell-1\|\ell} b_{1m}^{Kj},\\ b_{1m}^{\ell j} &\xrightarrow{\ell-1\|\ell} b_{1m}^{Kj}.\end{aligned} \tag{3.171}$$

The collinear factorisation of box functions has been well studied [110,111,166] and in this case, the relation,

$$\begin{aligned}\left(b_{1m}^{\ell-1j}\right)^n \mathrm{F}_{4\mathrm{F}}^{2\mathrm{me}}(s_{\ell-1,j},s_{\ell,j-1};s_{\ell,j},s_{\ell-1,j-1})+\left(b_{1m}^{\ell j}\right)^n \mathrm{F}_{4\mathrm{F}}^{2\mathrm{me}}(s_{\ell,j},s_{\ell+1,j-1};s_{\ell+1,j},s_{\ell,j-1})\\ \xrightarrow{\ell-1\|\ell}\left(b_{1m}^{Kj}\right)^n \mathrm{F}_{4\mathrm{F}}^{2\mathrm{me}}(s_{K,j},s_{\ell+1,j-1};s_{K,j},s_{\ell+1,j-1})\end{aligned} \tag{3.172}$$

ensures the box terms correctly factorise onto the lower point amplitude.

The next set of functions we consider are the triangle functions which have j as the second index, these functions possess the general form:

$$\sum_{i=\ell-1}^{\ell} \mathrm{tr}_-(m, P_{(i,j)}, j, 1)^n \mathcal{F}_{m1}^{j(i-1)} L_n(P_{(i,j-1)}, P_{(i,j)}). \tag{3.173}$$

There is no contribution when $i = \ell$, because $\mathcal{F}_{m1}^{j(\ell-1)} = \mathcal{F}_{1m}^{j(\ell-1)} = 0$, while the remaining $i = \ell - 1$ contribution collapses onto the correct term,

$$\mathrm{tr}_-(m, P_{(K,j)}, \ell-1, 1)^n \mathcal{F}_{m1}^{j(K-1)} L_n(P_{(K,j-1)}, P_{(K,j)}). \tag{3.174}$$

Similarly, when we consider

$$\sum_{i=\ell-1}^{\ell} \mathrm{tr}_-(m, P_{(j,i)}, j, 1)^n \mathcal{F}_{1m}^{ji} L_n(P_{(j+1,i)}, P_{(j,i)}), \tag{3.175}$$

there is no contribution when $i = \ell - 1$, while for $i = \ell$, we recover the correct contribution.

The remaining types of triangle function are of the form

$$\sum_{i=\ell-1}^{\ell} \mathrm{tr}_-(m, P_{(i,j)}, i, 1)^n \mathcal{F}_{m1}^{ij} L_n(P_{(i+1,j)}, P_{(i,j)}). \tag{3.176}$$

Since $\mathcal{F}_{m1}^{\ell j} = \mathcal{F}_{m1}^{(\ell-1)j}$ we have contributions from both terms, it is straightforward to show that,

$$\begin{aligned}\mathrm{tr}_-(m, P_{(\ell-1,j)}, \ell-1, 1)^n L_n(P_{(\ell,j)}, P_{(\ell-1,j)}) + \mathrm{tr}_-(m, P_{(\ell+1,j)}, \ell, 1)^n L_n(P_{(\ell+1,j)}, P_{(\ell,j)}) \\ \overset{\ell-1\|\ell}{\longrightarrow} \mathrm{tr}_-(m, P_{(\ell+1,j)}, K, 1)^n L_n(P_{(\ell+1,j)}, P_{(K,j)}).\end{aligned} \tag{3.177}$$

Similar considerations apply to

$$\sum_{i=\ell-1}^{\ell} \mathrm{tr}_-(1, P_{(j,i)}, i, m)^n \mathcal{F}_{1m}^{i(j-1)} L_n(P_{(j,i-1)}, P_{(j,i)}), \tag{3.178}$$

thus ensuring the correct collinear factorisation.

3.4.3 The cancellation of unphysical singularities

The cut constructible terms eq. (3.103) - (3.105) contain poles in $\langle i\, j\rangle$. For the most part, i and j are non-adjacent gluons and as such there should be no singularity

as these become collinear. In the following section we prove that this is indeed the case. To be explicit, we consider the collinear limit $i \parallel j$ with,

$$\begin{aligned} i &\to zK, \\ j &\to (1-z)K. \end{aligned} \tag{3.179}$$

Let us consider the cut-constructible pieces associated with the fermionic loop contribution, $A^{\phi F}_{n;1}(m,n)$ given in eq. (3.103). There are ten terms containing an explicit pole in s_{ij} which are given by,

$$\begin{aligned} & b^{ij}_{1m}\, \mathrm{F}^{\mathrm{2me}}_{\mathrm{4F}}(s_{i,j}, s_{i+1,j-1}; s_{i+1,j}, s_{i,j-1}) \\ & + b^{ij}_{1m}\, \mathrm{F}^{\mathrm{2me}}_{\mathrm{4F}}(s_{j,i}, s_{j+1,i-1}; s_{j+1,i}, s_{j,i-1}) \\ & - \frac{\mathrm{tr}_-(m, P_{(i+1,j)}, i, 1)}{s^2_{1m}} \frac{\mathrm{tr}_-(m,i,j,1)}{s_{ij}} L_1(P_{(i+1,j)}, P_{(i,j)}) \\ & + \frac{\mathrm{tr}_-(m, P_{(i+1,j-1)}, i, 1)}{s^2_{1m}} \frac{\mathrm{tr}_-(m,i,j,1)}{s_{ij}} L_1(P_{(i+1,j-1)}, P_{(i,j-1)}) \\ & - \frac{\mathrm{tr}_-(1, P_{(j,i-1)}, i, m)}{s^2_{1m}} \frac{\mathrm{tr}_-(1,i,j,m)}{s_{ij}} L_1(P_{(j,i-1)}, P_{(j,i)}) \\ & + \frac{\mathrm{tr}_-(1, P_{(j+1,i-1)}, i, m)}{s^2_{1m}} \frac{\mathrm{tr}_-(1,i,j,m)}{s_{ij}} L_1(P_{(j+1,i-1)}, P_{(j+1,i)}) \\ & - \frac{\mathrm{tr}_-(m, P_{(i,j-1)}, j, 1)}{s^2_{1m}} \frac{\mathrm{tr}_-(m,j,i,1)}{s_{ij}} L_1(P_{(i,j-1)}, P_{(i,j)}) \\ & + \frac{\mathrm{tr}_-(m, P_{(i+1,j-1)}, j, 1)}{s^2_{1m}} \frac{\mathrm{tr}_-(m,j,i,1)}{s_{ij}} L_1(P_{(i+1,j-1)}, P_{(i+1,j)}) \\ & - \frac{\mathrm{tr}_-(1, P_{(j+1,i)}, j, m)}{s^2_{1m}} \frac{\mathrm{tr}_-(1,j,i,m)}{s_{ij}} L_1(P_{(j+1,i)}, P_{(j,i)}) \\ & + \frac{\mathrm{tr}_-(1, P_{(j+1,i-1)}, j, m)}{s^2_{1m}} \frac{\mathrm{tr}_-(1,j,i,m)}{s_{ij}} L_1(P_{(j+1,i-1)}, P_{(j,i-1)}). \end{aligned} \tag{3.180}$$

Using $P_{(i+1,j)} = P_{(i+1,j-1)} + p_j$, $P_{(j,i-1)} = P_{(j+1,i-1)} + p_j$, $P_{(i,j-1)} = P_{(i+1,j-1)} + p_i$ and $P_{(j+1,i)} = P_{(j+1,i-1)} + p_i$, as well as $\mathrm{tr}_-(1,j,i,m) = -\mathrm{tr}_-(1,i,j,m) + \mathcal{O}(s_{ij})$ etc, we can rewrite these terms as

$$\begin{aligned} & b^{ij}_{1m} \left(\mathrm{F}^{\mathrm{2me}}_{\mathrm{4F}}(s_{i,j}, s_{i+1,j-1}; s_{i+1,j}, s_{i,j-1}) - s_{ij} L_1(P_{(i+1,j)}, P_{(i,j)}) - s_{ij} L_1(P_{(i,j-1)}, P_{(i,j)}) \right) \\ & + b^{ij}_{1m} \left(\mathrm{F}^{\mathrm{2me}}_{\mathrm{4F}}(s_{j,i}, s_{j+1,i-1}; s_{j+1,i}, s_{j,i-1}) - s_{ij} L_1(P_{(j,i-1)}, P_{(j,i)}) - s_{ij} L_1(P_{(j+1,i)}, P_{(j,i)}) \right) \\ & - \frac{\mathrm{tr}_-(m, P_{(i+1,j-1)}, i, 1)}{s^2_{1m}} \frac{\mathrm{tr}_-(m,i,j,1)}{s_{ij}} \left(L_1(P_{(i+1,j)}, P_{(i,j)}) - L_1(P_{(i+1,j-1)}, P_{(i,j-1)}) \right) \\ & + \frac{\mathrm{tr}_-(m, P_{(i+1,j-1)}, j, 1)}{s^2_{1m}} \frac{\mathrm{tr}_-(m,i,j,1)}{s_{ij}} \left(L_1(P_{(i,j-1)}, P_{(i,j)}) - L_1(P_{(i+1,j-1)}, P_{(i+1,j)}) \right) \end{aligned}$$

$$-\frac{\mathrm{tr}_-(1,P_{(j+1,i-1)},i,m)}{s_{1m}^2}\frac{\mathrm{tr}_-(1,i,j,m)}{s_{ij}}\left(L_1(P_{(j,i-1)},P_{(j,i)})-L_1(P_{(j+1,i-1)},P_{(j+1,i)})\right)$$
$$+\frac{\mathrm{tr}_-(1,P_{(j+1,i-1)},j,m)}{s_{1m}^2}\frac{\mathrm{tr}_-(1,i,j,m)}{s_{ij}}\left(L_1(P_{(j+1,i)},P_{(j,i)})-L_1(P_{(j+1,i-1)},P_{(j,i-1)})\right). \tag{3.181}$$

Finally, in the $i \parallel j$ collinear limit,

$$\begin{aligned}&\mathrm{tr}_-(m,P_{(i+1,j-1)},i,1)\left(L_1(P_{(i+1,j)},P_{(i,j)})-L_1(P_{(i+1,j-1)},P_{(i,j-1)})\right)\\ \to\ &\mathrm{tr}_-(m,P_{(i+1,j-1)},j,1)\left(L_1(P_{(i,j-1)},P_{(i,j)})-L_1(P_{(i+1,j-1)},P_{(i+1,j)})\right)\end{aligned} \tag{3.182}$$

and noting that the combination,

$$\mathrm{F}_{4\mathrm{F}}^{2\mathrm{me}}(s_{i,j},s_{i+1,j-1};s_{i+1,j},s_{i,j-1})-s_{ij}L_1(P_{(i+1,j)},P_{(i,j)})-s_{ij}L_1(P_{(i,j-1)},P_{(i,j)})\to\mathcal{O}(s_{ij}^2),$$

we see that all singularities cancel. The same arguments apply to the cut-constructible pieces associated with the scalar pieces.

3.4.4 Collinear factorisation of the rational pieces

This section is devoted to the collinear factorisation of the rational pieces of the four point amplitude. As a result of the symmetries of the amplitude there are two independent limits $1 \parallel 2$ and $2 \parallel 3$. We first consider the collinear limit $2 \parallel 3$. It is straightforward to see that the amplitude correctly factorises onto:

$$\begin{aligned}&\hat{R}_4(\phi,1^-,2^+,3^-,4^+)+CR_4(\phi,1^-,2^+,3^-,4^+)\overset{2\parallel 3}{\to}\\ &\qquad\sum_{i=\pm}R_3(\phi,1^-,K^i,4^+)\mathrm{Split}^{(0)}(-K^{-i},2^+,3^-)\end{aligned} \tag{3.183}$$

In a similar fashion the remaining non-trivial collinear limit takes the form,

$$\begin{aligned}&\hat{R}_4(\phi,1^-,2^+,3^-,4^+)+CR_4(\phi,1^-,2^+,3^-,4^+)\overset{1\parallel 2}{\to}\\ &\qquad\sum_{i=\pm}R_3(\phi,K^i,3^-,4^+)\mathrm{Split}^{(0)}(-K^{-i},1^-,2^+)\end{aligned} \tag{3.184}$$

3.4.5 Soft limit of $A_4^{(1)}(\phi, 1^-, 2^+, 3^-, 4^+)$

The final test is to take the limit as the ϕ momentum becomes soft, this limit occurs when $p_\phi \to 0$ such that $m_\phi^2 \to 0$. Our naive expectation is that in this limit, the ϕ field is essentially constant so that

$$C\phi \mathrm{tr} G_{SD\,\mu\nu} G_{SD}^{\mu,\nu} \to \mathrm{tr} G_{SD\,\mu\nu} G_{SD}^{\mu,\nu}. \tag{3.185}$$

In other words, the amplitude should collapse onto the gluon-only amplitude. In ref [106], it was postulated that the amplitude should factorise in following form,

$$A_n^{(1)}(\phi, n_- g^-, n_+ g^+) \overset{p_\phi \to 0}{\to} n_- \, A_n^{(1)}(n_- g^-, n_+ g^+), \tag{3.186}$$

while

$$A_n^{(1)}(\phi^\dagger, n_- g^-, n_+ g^+) \overset{p_\phi^\dagger \to 0}{\to} n_+ \, A_n^{(1)}(n_- g^-, n_+ g^+). \tag{3.187}$$

We first consider the cut constructible contributions. These factorise onto the four gluon amplitude in rather trivial manner since in our construction we separated gluon-only like diagrams and those which require a non-vanishing ϕ-momentum. In the soft limit, the one and two mass easy box and triangle functions have smooth limits so that,

$$\left(\frac{\mu^2}{-m_\phi^2}\right)^\epsilon \overset{p_\phi \to 0}{\to} 0, \tag{3.188}$$

$$\left(\frac{\mu^2}{-s_{\phi i}}\right)^\epsilon \overset{p_\phi \to 0}{\to} 0. \tag{3.189}$$

Furthermore, in the soft limit the L_k functions become the massless bubble functions,

$$L_k(s_{234}, s_{23}) = \frac{\mathrm{Bub}(s_{234}) - \mathrm{Bub}(s_{23})}{(s_{234} - s_{23})^k} \overset{p_\phi \to 0}{\to} \frac{(-1)^k}{s_{23}^k \epsilon(1-2\epsilon)} \left(\frac{\mu^2}{-s_{23}}\right)^\epsilon. \tag{3.190}$$

Altogether, we find that

$$C_4(\phi, 1^-, 2^+, 3^-, 4^+) \overset{p_\phi \to 0}{\to} 2C_4(1^-, 2^+, 3^-, 4^+), \tag{3.191}$$

where $C_4(1^-, 2^+, 3^-, 4^+)$ is the cut-constructible pieces of the four-gluon amplitude. This confirms that the cut-constructible terms of the amplitude do follow the naive factorisation of eq. (3.186)

The rational terms of eqs. (4.45) and (3.117), are each apparently singular in this limit. However, careful combination reveals the soft behaviour,

$$\hat{R}_4(\phi, 1^-, 2^+, 3^-, 4^+) + CR_4(\phi, 1^-, 2^+, 3^-, 4^+) \overset{p_\phi \to 0}{\to} \frac{N_P}{3} A^{(0)}(1^-, 2^+, 3^-, 4^+). \tag{3.192}$$

This is similar to the soft limit found in ref. [108,205] for the MHV amplitudes with adjacent negative helicities, but, as anticipated in ref. [106], is not consistent with the naive limit of eq. (3.186).

3.5 Summary

In this chapter we have investigated the ϕ-MHV amplitude with general helicities. Detailed descriptions of the unitarity method used to generate the cut-constructible pieces for all n have been given. The rational pieces have also been studied, however to limit the number and complexity of the equations we have focused on the four-gluon amplitude for the overlap and recursive pieces. We have performed several checks on our results, including soft Higgs and collinear checks. In the next chapter we will use the methods described in this chapter to generate the ϕ-NMHV amplitude.

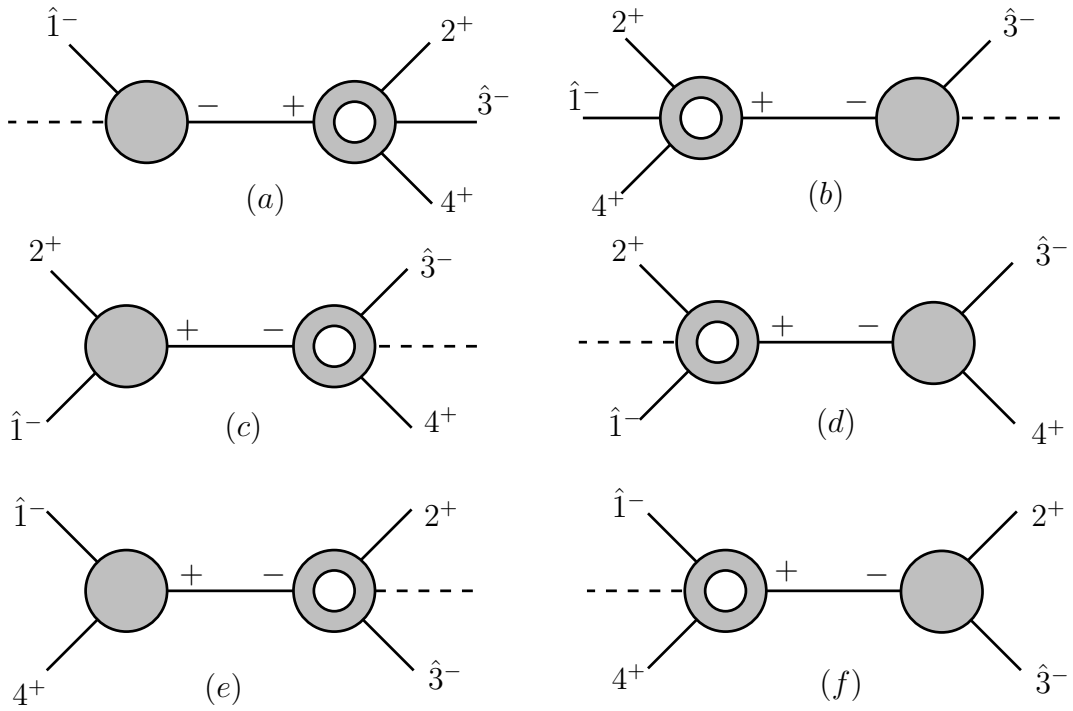

Figure 3.12: Allowed diagrams which contribute to the direct recursive rational pieces associated with the $[3,1\rangle$ spinor shift .

Chapter 4

One-loop Higgs plus four-gluon amplitudes: full analytic results

4.1 Introduction

In this chapter we will calculate the ϕ-NMHV amplitude $A_4^{(1)}(\phi, 1^+, 2^-, 3^-, 4^-)$. We will use the unitarity methods introduced in chapters 2 and 3 to calculate the various cut-constructible parts of the amplitude. For this amplitude we generate the rational parts proportional to N_f from Feynman diagrams. The other rational piece is generated from the recursion relations. We also write down the amplitude $A_4^{(1)}(\phi, 1^-, 2^+, 3^-, 4^+)$ using the results of chapter 3. We then summarise the Higgs plus four gluon amplitudes by giving explicit formulae for each of the helicity amplitudes $A_4^{(1)}(H, 1^{\lambda_1}, 2^{\lambda_2}, 3^{\lambda_3}, 4_4^{\lambda})$.

We choose to expand the one-loop primitive amplitude in the following form,

$$A_4^{(1)}(\phi, 1^+, 2^-, 3^-, 4^-) = c_\Gamma(C_4(\phi, 1^+, 2^-, 3^-, 4^-) + R_4(\phi, 1^+, 2^-, 3^-, 4^-)), \quad (4.1)$$

where

$$c_\Gamma = \frac{\Gamma^2(1-\epsilon)\Gamma(1+\epsilon)}{(4\pi)^{2-\epsilon}\Gamma(1-2\epsilon)}. \quad (4.2)$$

In (4.1), $C_4(\phi, 1^+, 2^-, 3^-, 4^-)$ denotes the cut-constructible parts of the amplitude, whilst $R_4(\phi, 1^+, 2^-, 3^-, 4^-)$ contains the remaining rational pieces. In section 4.2, we focus our attention on $C_4(\phi, 1^+, 2^-, 3^-, 4^-)$, while an analytic expression for

$R_4(\phi, 1^+, 2^-, 3^-, 4^-)$ is derived in section 4.3. Throughout this chapter we use the following expression for the ϕ-NMHV tree amplitude

$$A_n^{(0)}(\phi, 1^+, 2^-, 3^-, 4^-) = \\ -\frac{m_\phi^4 \langle 24\rangle^4}{s_{124}\langle 12\rangle\langle 14\rangle\langle 2|p_\phi|3]\langle 4|p_\phi|3]} + \frac{\langle 4|p_\phi|1]^3}{s_{123}\langle 4|p_\phi|3][12][23]} - \frac{\langle 2|p_\phi|1]^3}{s_{134}\langle 2|p_\phi|3][14][34]}. \quad (4.3)$$

This compact form can be derived using the BCFW recursion relations [140, 141] and agrees numerically with the previously known expression derived from MHV rules [95]. It clearly possesses the correct symmetry properties under the exchange $\{2 \leftrightarrow 4\}$, and factors onto the correct gluon tree amplitude (which is zero) in the limit of vanishing p_ϕ. Other tree amplitudes needed in this chapter can be found in Appendix A.

4.2 Cut-Constructible Contributions

As in chapter 3, we employ the generalised unitarity method [120, 122, 123, 127, 128, 132] to calculate the cut-constructible parts of the one-loop amplitude. We can further decompose C_4 in (4.1) into a sum over constituent basis integrals,

$$C_4(\phi, 1^+, 2^-, 3^-, 4^-) = \sum_i C_{4;i} I_{4;i} + \sum_i C_{3;i} I_{3;i} + \sum_i C_{2;i} I_{2;i}. \quad (4.4)$$

As usual $I_{j;i}$ represents a j-point scalar basis integral, with a coefficient $C_{j;i}$. The sum over i represents the sum over the partitions of the external momenta over the j legs of the basis integral.

As in previous chapters we use the methods of generalised unitarity to extract the various coefficients of the basis integrals, four-cuts for boxes [120], triple cuts for triangles [122] and double cuts for bubbles [132].

4.2.1 Box Integral Coefficients

We begin our calculation of the ϕ-NMHV amplitude by computing the coefficients of the scalar boxes using generalised unitarity with complex momenta [120]. In general

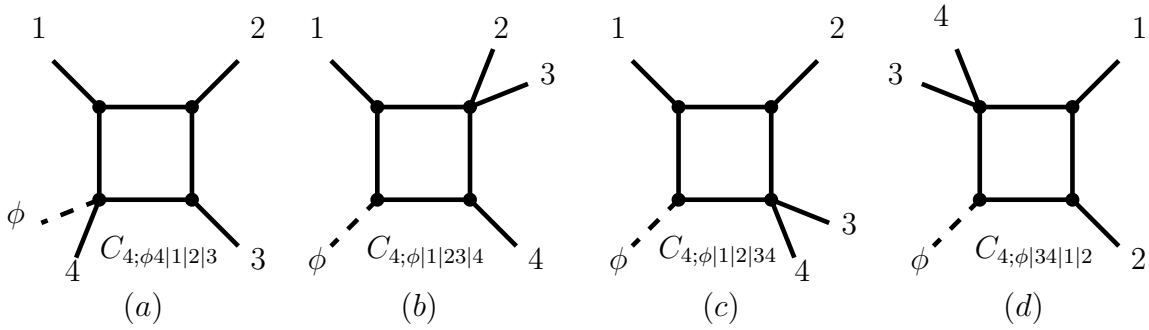

Figure 4.1: The various box integral topologies that appear for $A_4^{(1)}(\phi, 1, 2, 3, 4)$. From the four topologies we must also include cyclic permutations of the four gluons. Here (a) has one off-shell leg (one-mass) whilst (b)-(d) have two off-shell legs. In (b) the two off-shell legs are not adjacent and we refer to this configuration to as the two-mass easy box, while in (c) and (d) the two off-shell legs are adjacent and we label them as two-mass hard boxes.

there are sixteen box topologies, which can be obtained from cyclic permutations of those shown in Fig. 4.1. We find, after application of the solutions of the loop momenta, that the coefficients of all the two-mass easy box configurations are zero. Of the remaining 12 coefficients, a further 5 are related to each other by the $\{2 \leftrightarrow 4\}$ symmetry,

$$C_{4;\phi 4|1|2|3}(\phi, 1^+, 2^-, 3^-, 4^-) = C_{4;\phi 2|3|4|1}(\phi, 1^+, 4^-, 3^-, 2^-), \tag{4.5}$$

$$C_{4;\phi|23|4|1}(\phi, 1^+, 2^-, 3^-, 4^-) = C_{4;\phi|1|2|34}(\phi, 1^+, 4^-, 3^-, 2^-), \tag{4.6}$$

$$C_{4;\phi|34|1|2}(\phi, 1^+, 2^-, 3^-, 4^-) = C_{4;\phi|4|1|23}(\phi, 1^+, 4^-, 3^-, 2^-), \tag{4.7}$$

$$C_{4;\phi|12|3|4}(\phi, 1^+, 2^-, 3^-, 4^-) = C_{4;\phi|2|3|41}(\phi, 1^+, 4^-, 3^-, 2^-), \tag{4.8}$$

$$C_{4;\phi|3|4|12}(\phi, 1^+, 2^-, 3^-, 4^-) = C_{4;\phi|41|2|3}(\phi, 1^+, 4^-, 3^-, 2^-). \tag{4.9}$$

We find that two of the one-mass box coefficients (Fig 4.1(a)) are given by,

$$C_{4;\phi 1|2|3|4}(\phi, 1^+, 2^-, 3^-, 4^-) = \frac{s_{23} s_{34} s_{234}^3}{2\langle 1|p_\phi|2]\langle 1|p_\phi|4][23][34]}, \tag{4.10}$$

$$C_{4;\phi 2|3|4|1}(\phi, 1^+, 2^-, 3^-, 4^-) = \frac{s_{34} s_{41} \langle 2|p_\phi|1]^3}{2 s_{134}\langle 2|p_\phi|3][34][41]} + \frac{s_{34} s_{41}\langle 34\rangle^3 m_\phi^4}{2 s_{134}\langle 1|p_\phi|2]\langle 3|p_\phi|2]\langle 41\rangle}. \tag{4.11}$$

We also find that three of the two-mass hard boxes (Fig. 4.1(d)) have coefficients related to the coefficients of eqs. (4.5), (4.10) and (4.11),

$$C_{4;\phi|12|3|4}(\phi,1^+,2^-,3^-,4^-) = \frac{s_{123}s_{34}}{s_{23}s_{12}} C_{4;\phi4|1|2|3}(\phi,1^+,2^-,3^-,4^-), \tag{4.12}$$

$$C_{4;\phi|23|4|1}(\phi,1^+,2^-,3^-,4^-) = \frac{s_{234}s_{41}}{s_{23}s_{34}} C_{4;\phi1|2|3|4}(\phi,1^+,2^-,3^-,4^-), \tag{4.13}$$

$$C_{4;\phi|34|1|2}(\phi,1^+,2^-,3^-,4^-) = \frac{s_{134}s_{12}}{s_{41}s_{34}} C_{4;\phi2|3|4|1}(\phi,1^+,2^-,3^-,4^-). \tag{4.14}$$

The final two-mass hard box coefficient is,

$$\begin{aligned} C_{4;\phi|3|4|12}(\phi,1^+,2^-,3^-,4^-) \;=\; & \frac{s_{34}}{2}\Bigg(\frac{\langle 3|p_\phi|1]^4}{\langle 3|p_\phi|2]\langle 3|p_\phi|4][21][41]} \\ & + \frac{\langle 24\rangle^4 m_\phi^4}{\langle 12\rangle\langle 14\rangle\langle 2|p_\phi|3]\langle 4|p_\phi|3]}\Bigg) \end{aligned} \tag{4.15}$$

The remaining one-mass box configuration $C_{4;\phi3|4|1|2}$ is the only one which receives contributions from N_f fermionic loops,

$$\begin{aligned} C_{4;\phi3|4|1|2}(\phi,1^+,2^-,3^-,4^-) = s_{41}s_{12}\Bigg(& \frac{1}{s_{124}s_{34}} C_{4;\phi|3|4|12}(\phi,1^+,2^-,3^-,4^-) \\ & - \left(1-\frac{N_f}{4N_c}\right)\frac{2\langle 3|p_\phi|1]^2}{s_{124}[24]^2} - \left(1-\frac{N_f}{N_c}\right)\frac{[12][41]\langle 3|p_\phi|2]\langle 3|p_\phi|4]}{s_{124}[24]^4}\Bigg). \end{aligned} \tag{4.16}$$

Each of the coefficients (4.11), (4.10), (4.15) and (4.16) correctly tends to zero in the soft Higgs limit ($p_\phi \to 0$).

4.2.2 Triangle Integral Coefficients

Altogether, there are twenty-four triangle topologies, which can be obtained from cyclic permutations of those shown in Fig. 4.2. The different topologies can be characterised by the number of off-shell legs. Fig. 4.2(a) has one off-shell leg, Figs. 4.2(b)-(e) have two off-shell legs while for Fig. 4.2(f) all legs are off-shell. We refer to the triangle integrals with one- and two-off-shell legs as one-mass and two-mass respectively. They have the following form,

$$I_3^{1m}(s) \propto \frac{1}{\epsilon^2}\frac{1}{s}\left(\frac{\mu^2}{-s}\right)^\epsilon, \qquad I_3^{2m}(s,t) \propto \frac{1}{\epsilon^2}\frac{1}{(s-t)}\left(\left(\frac{\mu^2}{-s}\right)^\epsilon - \left(\frac{\mu^2}{-t}\right)^\epsilon\right) \tag{4.17}$$

and therefore only contribute pole pieces in ϵ to the overall amplitude (as was discussed in detail in chapter 3. In fact, the sole role of these functions is to ensure

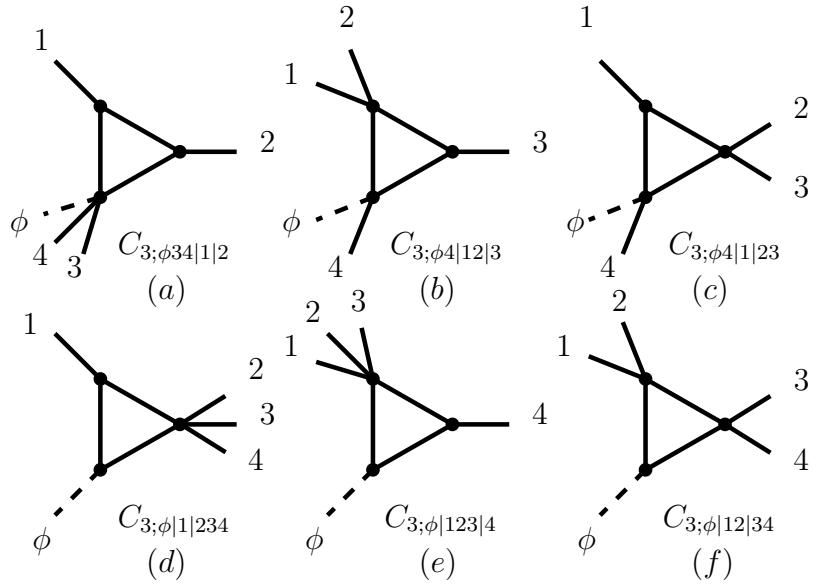

Figure 4.2: The various triangle integral topologies that appear for $A_4^{(1)}(\phi, 1, 2, 3, 4)$. From the six topologies we must also include cyclic permutations of the four gluons. (a) has one off-shell leg, (b)-(e) have two off-shell legs while in (f) all legs are off-shell.

the correct infrared behaviour by combining with the box pieces to generate the following pole structure,

$$A^{(1)}(\phi, 1^+, 2^-, 3^-, 4^-) = -A^{(0)}(\phi, 1^+, 2^-, 3^-, 4^-)\frac{c_\Gamma}{\epsilon^2}\sum_{i=1}^{4}\left(\frac{\mu^2}{-s_{ii+1}}\right)^{\epsilon} + \mathcal{O}(\epsilon^0). \quad (4.18)$$

This relation holds for arbitrary external helicities [107, 108, 206]. We computed the coefficients of all one- and two-mass triangles and explicitly verified eq. (4.18). The non-trivial relationship between the triangle and box coefficients provides a strong check of our calculation. However, since we now wish to obtain compact results for the four gluon amplitude, we find it more compact to present the final answer in a basis free of one- and two-mass triangles. That is, we choose to expand the box integral functions into divergent and finite pieces, combining the divergent pieces with the one- and two- mass triangles to form (4.18) and giving explicit results for the finite pieces of the box functions.

A new feature in the ϕ-NMHV amplitudes is the presence of three-mass triangles, shown in Fig. 4.2(f). In previous calculations [106–109, 206] the external gluon helicities prevented these contributions from occurring.

There are four three-mass triangles, which satisfy,

$$C_{3;\phi|34|12}(\phi,1^+,2^-,3^-,4^-) = C_{3;\phi|12|34}(\phi,1^+,2^-,3^-,4^-) \tag{4.19}$$

$$C_{3;\phi|41|23}(\phi,1^+,2^-,3^-,4^-) = C_{3;\phi|23|41}(\phi,1^+,2^-,3^-,4^-). \tag{4.20}$$

The symmetry under the exchange of gluons with momenta p_2 and p_4 relates the remaining two coefficients,

$$C_{3;\phi|23|41}(\phi,1^+,2^-,3^-,4^-) = C_{3;\phi|12|34}(\phi,1^+,4^-,3^-,2^-). \tag{4.21}$$

To compute $C_{3;\phi|23|41}$ we use both Forde's method [122] and the spinor integration technique [128]. For a given triangle coefficient $C_{3;K_1|K_2|K_3}(\phi,1^+,2^-,3^-,4^-)$ with off-shell momenta K_1, K_2 and K_3, we introduce the following massless projection vectors

$$\begin{aligned} K_1^{\flat\mu} &= \gamma\frac{\gamma K_1^\mu - K_1^2 K_2^\mu}{\gamma^2 - K_1^2 K_2^2}, \\ K_2^{\flat\mu} &= \gamma\frac{\gamma K_2^\mu - K_2^2 K_1^\mu}{\gamma^2 - K_1^2 K_2^2}, \\ \gamma_\pm(K_1,K_2) &= K_1\cdot K_2 \pm \sqrt{K_1\cdot K_2^2 - K_1^2 K_2^2}. \end{aligned} \tag{4.22}$$

In terms of these quantities we find,

$$C_{3;\phi|12|34}(\phi,1^+,2^-,3^-,4^-) = \sum_{\gamma=\gamma_\pm(p_\phi,p_1+p_2)} -\frac{m_\phi^4\langle K_1^\flat 2\rangle^3\langle 34\rangle^3}{2\gamma(\gamma+m_\phi^2)\langle K_1^\flat 1\rangle\langle K_1^\flat 3\rangle\langle K_1^\flat 4\rangle\langle 12\rangle}, \tag{4.23}$$

which, as expected, correctly vanishes in the soft Higgs limit ($p_\phi \to 0$).

4.2.3 Bubble Integral Coefficients

The non-vanishing bubble topologies for the ϕ-NMHV amplitude are shown in Fig. 4.3. We find that the double-cuts associated with Fig. 4.3(a) contain only contributions from boxes and triangles, and therefore the coefficient of $\log(s_{1234})$ is zero. In a similar fashion, the double cuts associated with diagram Fig. 4.3(c) with two external gluons with negative helicity emitted from the right hand vertex have only box and triangle contributions, so that the coefficients of $\log(s_{23})$ and $\log(s_{34})$ are also zero.

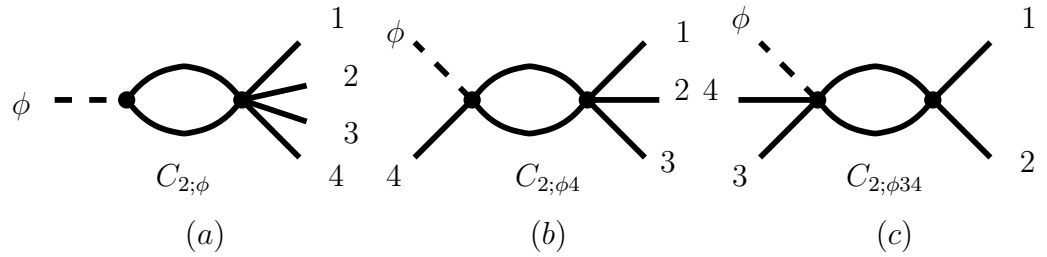

Figure 4.3: The three bubble integral topologies that appear for $A_4^{(1)}(\phi, 1, 2, 3, 4)$. We must also include cyclic permutations of the four gluons.

The leading singularity of the bubble integral is $\mathcal{O}(1/\epsilon)$,

$$I_2(s) \propto \frac{1}{(1-2\epsilon)\epsilon}\left(\frac{\mu^2}{-s}\right)^{\epsilon}. \tag{4.24}$$

However for the total amplitude there is no overall ϵ pole, and this implies a relation amongst the bubble coefficients such that,

$$\sum_{k=1}^{4}\left(C_{2;\phi k} + C_{2;\phi k k+1}\right) = 0. \tag{4.25}$$

It is therefore most natural to work with log's of ratios of kinematic scales (rather than $\log(s/\mu^2)$), since the coefficients of individual logarithms must cancel pairwise. To this end, as in the last chapter, we express our result in terms of the following functions,

$$L_k(s,t) = \frac{\log(s/t)}{(s-t)^k}. \tag{4.26}$$

Using the Stokes' theorem method [132], we generated compact analytic expressions for the coefficients of each bubble-function, which we also checked numerically with Forde's method [122]. The combination of all double-cuts is given by,

$$C_2(\phi, 1^+, 2^-, 3^-, 4^-) = \left(4 - \frac{N_f}{N}\right) C_2^{(1)} + \left(1 - \frac{N_f}{N_c}\right) C_2^{(2)} \tag{4.27}$$

with

$$C_2^{(1)} = -\left\{\frac{\langle 24\rangle\langle 3|p_\phi|1]^2}{s_{124}[42]} L_1\left(s_{124}, s_{12}\right) - \frac{\langle 23\rangle\langle 4|p_\phi|1]^2}{s_{123}[32]} L_1\left(s_{123}, s_{12}\right)\right\} - \Big\{(2 \leftrightarrow 4)\Big\} \tag{4.28}$$

and

$$
\begin{aligned}
C_2^{(2)} = -\Bigg\{ & \frac{2s_{124}\langle 24\rangle\langle 34\rangle^2[41]^2}{3[42]} L_3\left(s_{124}, s_{12}\right) \\
& + \frac{\langle 34\rangle[41]\left(3s_{124}\langle 34\rangle[41] + \langle 24\rangle\langle 3|p_\phi|1][42]\right)}{3[42]^2} L_2\left(s_{124}, s_{12}\right) \\
& + \left(\frac{2s_{124}\langle 34\rangle^2[41]^2}{\langle 24\rangle[42]^3} - \frac{\langle 24\rangle\langle 3|p_\phi|1]^2}{3s_{124}[42]} \right) L_1\left(s_{124}, s_{12}\right) \\
& + \frac{\langle 3|p_\phi|1]\left(4s_{124}\langle 34\rangle[41] + \langle 3|p_\phi|1](2s_{14} + s_{24})\right)}{s_{124}\langle 24\rangle[42]^3} L_0\left(s_{124}, s_{12}\right) \\
& - \frac{2s_{123}\langle 23\rangle\langle 34\rangle^2[31]^2}{3[32]} L_3\left(s_{123}, s_{12}\right) + \frac{\langle 23\rangle\langle 34\rangle[31]\langle 4|p_\phi|1]}{3[32]} L_2\left(s_{123}, s_{12}\right) \\
& + \frac{\langle 23\rangle\langle 4|p_\phi|1]^2}{3s_{123}[32]} L_1\left(s_{123}, s_{12}\right) \Bigg\} - \Big\{ (2 \leftrightarrow 4) \Big\}. \qquad (4.29)
\end{aligned}
$$

In the above formulae (and those following) we stress that the symmetrising action applies to the entire formula, and also acts on the kinematic invariants of the basis functions. We see that $C_2(\phi, 1^+, 2^-, 3^-, 4^-)$ vanishes in the soft Higgs limit $p_\phi \to 0$.

4.2.4 The Cut-Completion terms

The basis functions $L_3(s,t)$ and $L_2(s,t)$ are singular as $s \to t$. Since this is an unphysical limit one expects to find some cut-predictable rational pieces which ensure the correct behaviour of the amplitude as these quantities approach each other. These rational pieces are called the cut-completion terms and are obtained by making the following replacements in (4.29)

$$
\begin{aligned}
L_3(s,t) \to \hat{L}_3(s,t) &= L_3(s,t) - \frac{1}{2(s-t)^2}\left(\frac{1}{s} + \frac{1}{t}\right), \\
L_2(s,t) \to \hat{L}_2(s,t) &= L_2(s,t) - \frac{1}{2(s-t)}\left(\frac{1}{s} + \frac{1}{t}\right), \\
L_1(s,t) \to \hat{L}_1(s,t) &= L_1(s,t), \\
L_0(s,t) \to \hat{L}_0(s,t) &= L_0(s,t). \qquad (4.30)
\end{aligned}
$$

4.3 Rational Terms

We now turn our attention to the calculation of the remaining rational part of the amplitude. In general the cut-unpredictable rational part of ϕ plus gluon amplitudes

contains two types of pieces, a homogeneous piece, which is insensitive to the number of active flavours and a piece proportional to $(1 - N_f/N_c)$,

$$R_4(\phi, 1^+, 2^-, 3^-, 4^-) = R_4^h(\phi, 1^+, 2^-, 3^-, 4^-) + \left(1 - \frac{N_f}{N_c}\right) R_4^{N_P}(\phi, 1^+, 2^-, 3^-, 4^-). \tag{4.31}$$

The homogeneous term $R_4^h(\phi, 1^+, 2^-, 3^-, 4^-)$ can be simply calculated using the BCFW recursion relations [140, 141],

$$R_4^h(\phi, 1^+, 2^-, 3^-, 4^-) = 2A^{(0)}(\phi, 1^+, 2^-, 3^-, 4^-). \tag{4.32}$$

This contribution cancels against a similar homogeneous term for the $\phi^\dagger$ amplitude when combining the ϕ and $\phi^\dagger$ amplitudes to form the Higgs amplitude.

The N_P piece allows the propagation of quarks in the loop, and can be completely reconstructed by considering only the fermion loop contribution. Furthermore, one can extract the ϕ contribution to $R_4^{N_P}$ by considering the full Higgs amplitude and removing the fully rational $\phi^\dagger$ contribution calculated in [106]. Since there is no direct $Hq\overline{q}$ coupling in the effective theory, the most complicated structure is a second-rank tensor box configuration. Of the 739 diagrams contributing to the $Hgggg$ amplitude[1], only 136 contain fermion loops and are straightforward to evaluate.

After subtracting the cut-completion and homogeneous rational terms from the explicit Feynman diagram calculation the following rational pieces remain.

$$\begin{aligned} R_4^{N_P}(H, 1^+, 2^-, 3^-, 4^-) = \Bigg\{ \frac{1}{2} \Bigg(& \frac{\langle 23\rangle\langle 34\rangle\langle 4|p_H|1][31]}{3s_{123}\langle 12\rangle[21][32]} - \frac{\langle 3|p_H|1]^2}{s_{124}[42]^2} \\ & + \frac{\langle 24\rangle\langle 34\rangle\langle 3|p_H|1][41]}{3s_{124}s_{12}[42]} - \frac{[12]^2\langle 23\rangle^2}{s_{14}[42]^2} - \frac{\langle 24\rangle(s_{23}s_{24} + s_{23}s_{34} + s_{24}s_{34})}{3\langle 12\rangle\langle 14\rangle[23][34][42]} \\ & + \frac{\langle 2|p_H|1]\langle 4|p_H|1]}{3s_{234}[23][34]} - \frac{2[12]\langle 23\rangle[31]^2}{3[23]^2[41][34]} \Bigg) \Bigg\} + \Big\{ (2 \leftrightarrow 4) \Big\}. \end{aligned} \tag{4.33}$$

The last line in the above equation is the one-loop rational expression for the $\phi^\dagger$ contribution [106]. We can thus define the rational terms for the ϕ contribution.

$$R_4^{N_P}(\phi, 1^+, 2^-, 3^-, 4^-) = \left\{ \frac{1}{2} \left(\frac{\langle 23\rangle\langle 34\rangle\langle 4|p_H|1][31]}{3s_{123}\langle 12\rangle[21][32]} - \frac{\langle 3|p_H|1]^2}{s_{124}[42]^2} \right.\right.$$

[1] Feynman diagrams were generated with the aid of `QGRAF` [207].

$$+\frac{\langle 24\rangle\langle 34\rangle\langle 3|p_H|1][41]}{3s_{124}s_{12}[42]} - \frac{[12]^2\langle 23\rangle^2}{s_{14}[42]^2} - \frac{\langle 24\rangle(s_{23}s_{24}+s_{23}s_{34}+s_{24}s_{34})}{3\langle 12\rangle\langle 14\rangle[23][34][42]}\Bigg)\Bigg\}$$
$$+\Big\{(2\leftrightarrow 4)\Big\}. \quad (4.34)$$

4.4 Higgs plus four gluon amplitudes

In this section we present complete expressions for the one-loop amplitudes needed to calculate the process $0 \to Hgggg$ at NLO.

The one-loop amplitudes presented here are computed in the four-dimensional helicity scheme and are not renormalised. To perform an $\overline{MS}$ renormalisation, one should subtract an $\overline{MS}$ counterterm (in the t'Hooft-Veltman scheme) from $A_4^{(1)}$,

$$A_4^{(1)} \to A_4^{(1)} - c_\Gamma 2\frac{\beta_0}{\epsilon}A_4^{(0)}. \quad (4.35)$$

The Wilson coefficient eq. (1.53) produces an additional finite contribution,

$$A_4^{(1)} \to A_4^{(1)} + \frac{11}{(4\pi)^2}\,A_4^{(0)}. \quad (4.36)$$

We choose to split the un-renormalised amplitude into (completed) cut-constructible pieces and rational terms. We also separate the infra-red divergent and finite parts of the amplitude. The basis functions for the finite part of the cut-constructable pieces are one-mass and two-mass boxes, three-mass triangles, and completed functions $\hat{L}_i(s,t)$ of eq. (4.30). We define the finite pieces of the box and three-mass triangle integrals in Appendix B.

We express a generic helicity configuration in the following form

$$A_4^{(1)}(H,1^{\lambda_1},2^{\lambda_2},3^{\lambda_3},4^{\lambda_4}) = c_\Gamma(C_4(H,1^{\lambda_1},2^{\lambda_2},3^{\lambda_3},4^{\lambda_4}) + R_4(H,1^{\lambda_1},2^{\lambda_2},3^{\lambda_3},4^{\lambda_4})), \quad (4.37)$$

where C_4 represents the cut-constructible part of the amplitude and R_4 the rational pieces. We further separate $C_4(H,1^{\lambda_1},2^{\lambda_2},3^{\lambda_3},4^{\lambda_4})$ into divergent and finite pieces,

$$C_4(H,1^{\lambda_1},2^{\lambda_2},3^{\lambda_3},4^{\lambda_4}) = V_4(H,1^{\lambda_1},2^{\lambda_2},3^{\lambda_3},4^{\lambda_4}) + F_4(H,1^{\lambda_1},2^{\lambda_2},3^{\lambda_3},4^{\lambda_4}). \quad (4.38)$$

The divergent part V_4 contain the ϵ singularities generated by the box and triangle contributions, and which satisfy the helicity independent infrared singularity condition,

$$V_4(H,1^{\lambda_1},2^{\lambda_2},3^{\lambda_3},4^{\lambda_4}) = -A^{(0)}(H,1^{\lambda_1},2^{\lambda_2},3^{\lambda_3},4^{\lambda_4})\frac{1}{\epsilon^2}\left(\sum_{i=1}^{4}\left(\frac{\mu^2}{-s_{i(i+1)}}\right)^{\epsilon}\right). \quad (4.39)$$

The remaining cut-constructible and rational terms are finite, and depend non-trivially on the helicity configuration of the gluons.

4.4.1 The all-minus amplitude $A_4^{(1)}(H,1^-,2^-,3^-,4^-)$

The all-minus amplitude is symmetric under cyclic permutations of the four gluons. The finite part (of the cut-constructible piece) is [107],

$$\begin{aligned} F_4(H,1^-,2^-,3^-,4^-) = \Bigg\{ &- \frac{m_H^4}{2[12][23][34][41]}\Bigg(\frac{1}{2}\,\mathrm{F}_{4\mathrm{F}}^{2\mathrm{me}}(s_{123},s_{234};m_H^2,s_{23}) \\ &+\frac{1}{2}\,\mathrm{F}_{4\mathrm{F}}^{2\mathrm{me}}(s_{123},s_{124};m_H^2,s_{12}) + \mathrm{F}_{4\mathrm{F}}^{1\mathrm{m}}(s_{23},s_{34};s_{234})\Bigg)\Bigg\} \\ &+\Big\{(1\leftrightarrow 4),(2\leftrightarrow 3)\Big\} \\ &+\Big\{(1\leftrightarrow 2),(3\leftrightarrow 4)\Big\} + \Big\{(1\leftrightarrow 3),(2\leftrightarrow 4)\Big\} \end{aligned} \quad (4.40)$$

while the rational part is given by [106, 107]

$$\begin{aligned} R_4(H,1^-,2^-,3^-,4^-) = &\left\{\frac{1}{3}\left(1-\frac{N_f}{N_c}\right)\left(-\frac{s_{13}\langle 4|P_H|2]^2}{s_{123}[12]^2[23]^2} + \frac{\langle 34\rangle^2}{[12]^2}\right.\right. \\ &\left.\left. +2\frac{\langle 34\rangle\langle 41\rangle}{[12][23]} + \frac{s_{12}s_{34}+s_{123}s_{234}-s_{12}^2}{2[12][23][34][41]}\right)\right\} + \text{ cyclic permutations.} \end{aligned} \quad (4.41)$$

4.4.2 The MHV amplitude $A_4^{(1)}(H,1^-,2^-,3^+,4^+)$

For the MHV amplitude with adjacent negative helicity gluons there is an overall ($(1\leftrightarrow 2)$,$(3\to 4)$) symmetry. The finite cut-constructible part is [108],

$$\begin{aligned} F_4(H,1^-,2^-,3^+,4^+) = \Bigg\{\Bigg[&- \frac{\langle 12\rangle^3}{2\langle 23\rangle\langle 34\rangle\langle 41\rangle}\Bigg(\mathrm{F}_{4\mathrm{F}}^{2\mathrm{me}}(s_{123},s_{234};m_H^2,s_{23}) \\ &+\frac{1}{2}\,\mathrm{F}_{4\mathrm{F}}^{2\mathrm{me}}(s_{234},s_{134};m_H^2,s_{34}) + \frac{1}{2}\,\mathrm{F}_{4\mathrm{F}}^{2\mathrm{me}}(s_{124},s_{123};m_H^2,s_{12}) \\ &+\mathrm{F}_{4\mathrm{F}}^{1\mathrm{m}}(s_{23},s_{34};s_{234}) + \mathrm{F}_{4\mathrm{F}}^{1\mathrm{m}}(s_{14},s_{12};s_{124})\Bigg) \end{aligned}$$

$$
\begin{aligned}
&-4\left(1-\frac{N_f}{4N_c}\right)\frac{\langle 12\rangle^2[43]}{\langle 34\rangle}\hat{L}_1(s_{134},s_{14})\\
&-\left(1-\frac{N_f}{N_c}\right)\left(\frac{[43]\langle 13p_H2\rangle(\langle 13p_H2\rangle+\langle 1432\rangle)}{3\langle 34\rangle}\hat{L}_3(s_{134},s_{14})\right.\\
&\left.-\frac{\langle 12\rangle^2[43]}{3\langle 34\rangle}\hat{L}_1(s_{134},s_{14})\right)\Bigg]+\Big[(1\leftrightarrow 3),(2\leftrightarrow 4)\Big]_{\langle ij\rangle\leftrightarrow[ij]}\Bigg\}\\
&+\Big\{(1\leftrightarrow 2),(3\leftrightarrow 4)\Big\}. \qquad (4.42)
\end{aligned}
$$

The rational terms R_4 have the same symmetries [108],

$$
\begin{aligned}
R_4(H,1^-,2^-,3^+,4^+) &= \Bigg\{\Bigg[\left(1-\frac{N_f}{N_c}\right)\frac{[34]}{3\langle 34\rangle}\Bigg(-\frac{\langle 23\rangle\langle 1|p_H|3]^2}{\langle 34\rangle[43][32]s_{234}}\\
&-\frac{\langle 14\rangle\langle 3|P_{12}|3]}{\langle 34\rangle[12][32]}+\frac{\langle 12\rangle^2}{2\langle 34\rangle[43]}-\frac{\langle 12\rangle}{2[12]}-\frac{\langle 12\rangle\langle 2|P_{13}|4]}{2[41]s_{341}}+\frac{\langle 12\rangle^2}{2s_{41}}\Bigg)\Bigg]\\
&+\Big[(1\leftrightarrow 3),(2\leftrightarrow 4)\Big]_{\langle ij\rangle\leftrightarrow[ij]}\Bigg\}+\Big\{(1\leftrightarrow 2),(3\leftrightarrow 4)\Big\}. \qquad (4.43)
\end{aligned}
$$

4.4.3 The MHV amplitude $A_4^{(1)}(H,1^-,2^+,3^-,4^+)$

The alternating helicity MHV configuration has the larger set of symmetries, $(1\leftrightarrow 3)$, $(2\leftrightarrow 4)$ and $((1\leftrightarrow 3),(2\leftrightarrow 4))$. The finite cut-constructible contribution is [206] (chapter 3),

$$
\begin{aligned}
F_4(H,1^-,2^+,3^-,4^+) &= \Bigg\{\Bigg[-\frac{\langle 13\rangle^4}{2\langle 12\rangle\langle 23\rangle\langle 34\rangle\langle 41\rangle}\Bigg(\mathrm{F}^{\mathrm{2me}}_{\mathrm{4F}}(s_{123},s_{234};m_H^2,s_{23})\\
&+\frac{1}{2}\,\mathrm{F}^{\mathrm{1m}}_{\mathrm{4F}}(s_{23},s_{34};s_{234})+\frac{1}{2}\,\mathrm{F}^{\mathrm{1m}}_{\mathrm{4F}}(s_{34},s_{14};s_{134})\Bigg)\\
&+4\left(1-\frac{N_f}{4N_c}\right)\Bigg(-\frac{\langle 13\rangle^2}{\langle 24\rangle}\Bigg(\frac{1}{4\langle 24\rangle}\,\mathrm{F}^{\mathrm{1m}}_{\mathrm{4F}}(s_{23},s_{34};s_{234})\\
&-[42]\hat{L}_1(s_{234},s_{23})\Bigg)\Bigg)+2\left(1-\frac{N_f}{N_c}+\frac{N_s}{N_c}\right)\Bigg(-\frac{\langle 12\rangle\langle 41\rangle\langle 23\rangle\langle 34\rangle}{\langle 24\rangle^3}\\
&\times\left(\frac{1}{4\langle 24\rangle}\,\mathrm{F}^{\mathrm{1m}}_{\mathrm{4F}}(s_{23},s_{34};s_{234})-[42]\hat{L}_1(s_{234},s_{23})\right)\\
&-\frac{\langle 23\rangle\langle 41\rangle[42]^2}{\langle 24\rangle}\Bigg(\frac{\langle 14\rangle\langle 23\rangle[42]}{3}\hat{L}_3(s_{234},s_{23})\\
&-\frac{\langle 12\rangle\langle 34\rangle}{2\langle 24\rangle}\hat{L}_2(s_{234},s_{23})\Bigg)\Bigg)\Bigg]+\Big[(1\leftrightarrow 2),(3\leftrightarrow 4)\Big]_{\langle ij\rangle\leftrightarrow[ij]}\Bigg\}\\
&+\Big\{(1\leftrightarrow 3)\Big\}+\Big\{(2\leftrightarrow 4)\Big\}+\Big\{(1\leftrightarrow 3),(2\leftrightarrow 4)\Big\} \qquad (4.44)
\end{aligned}
$$

while the rational part is given by [206],

$$
\begin{aligned}
R_4(H,1^-,2^+,3^-,4^+) \;=\; & \left\{\left[-\left(1-\frac{N_f}{N_c}\right)\frac{[24]^4}{12[12][23][34][41]}\left(\frac{s_{23}s_{34}}{s_{24}s_{124}}-3\frac{s_{23}s_{34}}{s_{24}^2}\right)\right]\right. \\
& \left.+\Big[(1\leftrightarrow 2),(3\leftrightarrow 4)\Big]_{\langle ij\rangle\leftrightarrow[ij]}\right\} \\
& +\Big\{(1\leftrightarrow 3)\Big\}+\Big\{(2\leftrightarrow 4)\Big\}+\Big\{(1\leftrightarrow 3),(2\leftrightarrow 4)\Big\}. \qquad (4.45)
\end{aligned}
$$

4.4.4 The NMHV amplitude $A_4^{(1)}(H,1^+,2^-,3^-,4^-)$

By combining the results for the NMHV ϕ amplitudes given in sections 4.2 and 4.3 and the rational $\phi^\dagger$ amplitude of [106] according to eq. (A.2.21), we obtain the Higgs NMHV-amplitude, which is symmetric under the exchange $(2\leftrightarrow 4)$. The finite cut-constructible contribution is,

$$
\begin{aligned}
F_4(H,1^+,2^-,3^-,4^-) = \Big\{ & -\frac{s_{234}^3}{4\langle 1|p_H|2]\langle 1|p_H|4][23][34]}W^{(1)} \\
& -\left(\frac{\langle 2|p_H|1]^3}{2s_{134}\langle 2|p_H|3][34][41]}+\frac{\langle 34\rangle^3 m_H^4}{2s_{134}\langle 1|p_H|2]\langle 3|p_H|2]\langle 41\rangle}\right)W^{(2)} \\
& +\frac{1}{4s_{124}}\left(\frac{\langle 3|p_H|1]^4}{\langle 3|p_H|2]\langle 3|p_H|4][21][41]}+\frac{\langle 24\rangle^4 m_H^4}{\langle 12\rangle\langle 14\rangle\langle 2|p_H|3]\langle 4|p_H|3]}\right)W^{(3)} \\
& -\left(\sum_{\gamma=\gamma_\pm(p_H,p_1+p_2)}\frac{m_\phi^4\langle K_1^\flat 2\rangle^3\langle 34\rangle^3}{\gamma(\gamma+m_\phi^2)\langle K_1^\flat 1\rangle\langle K_1^\flat 3\rangle\langle K_1^\flat 4\rangle\langle 12\rangle}\right)\mathrm{F}_3^{\mathrm{3m}}(m_H^2,s_{12},s_{34}) \\
& +\left(1-\frac{N_f}{4N_c}\right)\left(\frac{\langle 3|p_H|1]^2}{s_{124}[24]^2}\,\mathrm{F}_{4\mathrm{F}}^{\mathrm{1m}}(s_{12},s_{14};s_{124})\right. \\
& \left.-\frac{4\langle 24\rangle\langle 3|p_H|1]^2}{s_{124}[42]}\hat{L}_1(s_{124},s_{12})+\frac{4\langle 23\rangle\langle 4|p_H|1]^2}{s_{123}[32]}\hat{L}_1(s_{123},s_{12})\right) \\
& -\left(1-\frac{N_f}{N_c}\right)\left(\frac{[12][41]\langle 3|p_H|2]\langle 3|p_H|4]}{2s_{124}[24]^4}\,\mathrm{F}_{4\mathrm{F}}^{\mathrm{1m}}(s_{12},s_{14};s_{124})\right. \\
& +\frac{2s_{124}\langle 24\rangle\langle 34\rangle^2[41]^2}{3[42]}\hat{L}_3(s_{124},s_{12}) \\
& +\frac{\langle 34\rangle[41]\left(3s_{124}\langle 34\rangle[41]+\langle 24\rangle\langle 3|p_H|1][42]\right)}{3[42]^2}\hat{L}_2(s_{124},s_{12}) \\
& \left.+\left(\frac{2s_{124}\langle 34\rangle^2[41]^2}{\langle 24\rangle[42]^3}-\frac{\langle 24\rangle\langle 3|p_H|1]^2}{3s_{124}[42]}\right)\hat{L}_1(s_{124},s_{12})\right) \\
& +\frac{\langle 3|p_H|1](4s_{124}\langle 34\rangle[41]+\langle 3|p_H|1](2s_{14}+s_{24}))}{s_{124}\langle 24\rangle[42]^3}\hat{L}_0(s_{124},s_{12}) \\
& -\frac{2s_{123}\langle 23\rangle\langle 34\rangle^2[31]^2}{3[32]}\hat{L}_3(s_{123},s_{12})+\frac{\langle 23\rangle\langle 34\rangle[31]\langle 4|p_H|1]}{3[32]}\hat{L}_2(s_{123},s_{12})
\end{aligned}
$$

$$+\frac{\langle 23\rangle\langle 4|p_H|1]^2}{3s_{123}[32]}\hat{L}_1\left(s_{123},s_{12}\right)\Bigg)\Bigg\}$$
$$+\Big\{(2\leftrightarrow 4)\Big\}. \quad (4.46)$$

For convenience we have introduced the following combinations of the finite pieces of one-mass ($\mathrm{F}^{\mathrm{1m}}_{\mathrm{4F}}$) and two-mass hard ($\mathrm{F}^{\mathrm{2mh}}_{\mathrm{4F}}$) box functions (see Appendix B),

$$\begin{aligned}
W^{(1)} &= \mathrm{F}^{\mathrm{1m}}_{\mathrm{4F}}(s_{23},s_{34};s_{234})+\mathrm{F}^{\mathrm{2mh}}_{\mathrm{4F}}(s_{41},s_{234};m_H^2,s_{23})+\mathrm{F}^{\mathrm{2mh}}_{\mathrm{4F}}(s_{12},s_{234};s_{34},m_H^2)\\
W^{(2)} &= \mathrm{F}^{\mathrm{1m}}_{\mathrm{4F}}(s_{14},s_{34};s_{134})+\mathrm{F}^{\mathrm{2mh}}_{\mathrm{4F}}(s_{12},s_{134};m_H^2,s_{34})+\mathrm{F}^{\mathrm{2mh}}_{\mathrm{4F}}(s_{23},s_{134};s_{14},m_H^2)\\
W^{(3)} &= \mathrm{F}^{\mathrm{1m}}_{\mathrm{4F}}(s_{12},s_{14};s_{124})+\mathrm{F}^{\mathrm{2mh}}_{\mathrm{4F}}(s_{23},s_{124};m_H^2,s_{14})+\mathrm{F}^{\mathrm{2mh}}_{\mathrm{4F}}(s_{34},s_{124};s_{12},m_H^2).
\end{aligned}$$

In addition, to simplify the coefficients of the three-mass triangle $\mathrm{F}^{\mathrm{3m}}_3(K_1^2,K_2^2,K_3^2)$ with three off-shell legs $K_1^2,\ K_2^2,\ K_3^2\neq 0$, we use the notation of eq. (4.22). The rational part of the Higgs NMHV amplitude is given by eq. (4.33) (which incorporates the rational $A_4^{(1)}(\phi^\dagger,1^+,2^-,3^-,4^-)$ amplitude derived in [106]),

$$\begin{aligned}
R_4(H,1^+,2^-,3^-,4^-) = \Bigg\{\Bigg(1-\frac{N_f}{N_c}\Bigg)\frac{1}{2}\Bigg(&\frac{\langle 23\rangle\langle 34\rangle\langle 4|p_H|1][31]}{3s_{123}\langle 12\rangle[21][32]}-\frac{\langle 3|p_H|1]^2}{s_{124}[42]^2}\\
&+\frac{\langle 24\rangle\langle 34\rangle\langle 3|p_H|1][41]}{3s_{124}s_{12}[42]}-\frac{[12]^2\langle 23\rangle^2}{s_{14}[42]^2}-\frac{\langle 24\rangle(s_{23}s_{24}+s_{23}s_{34}+s_{24}s_{34})}{3\langle 12\rangle\langle 14\rangle[23][34][42]}\\
&+\frac{\langle 2|p_H|1]\langle 4|p_H|1]}{3s_{234}[23][34]}-\frac{2[12]\langle 23\rangle[31]^2}{3[23]^2[41][34]}\Bigg)\Bigg\}+\Big\{(2\leftrightarrow 4)\Big\}. \quad (4.47)
\end{aligned}$$

4.5 Numerical Evaluation

In this section we provide numerical values for the helicity amplitudes given in the previous section at a particular phase space point. To this end, we redefine the finite part of the Higgs amplitude as:

$$\begin{aligned}
A_4^{(1)}(H,1^{\lambda_1},2^{\lambda_2},3^{\lambda_3},4^{\lambda_4}) = c_\Gamma A^{(0)}(H,1^{\lambda_1},2^{\lambda_2},3^{\lambda_3},4^{\lambda_4})\Bigg(&-\frac{1}{\epsilon^2}\sum_{i=1}^{4}\left(\frac{-\mu^2}{s_{i,i+1}}\right)^{\epsilon} \quad (4.48)\\
&+M_4^{\mathcal{F},g}(\lambda_1,\lambda_2,\lambda_3,\lambda_4)+\frac{N_f}{N_c}M_4^{\mathcal{F},f}(\lambda_1,\lambda_2,\lambda_3,\lambda_4)+\frac{N_s}{N_c}M_4^{\mathcal{F},s}(\lambda_1,\lambda_2,\lambda_3,\lambda_4)\Bigg).
\end{aligned}$$

We evaluate the amplitudes at the phase space point used by Ellis et al. [104],

$$\begin{aligned}
p_H^\mu &= (-1.00000000000,0.00000000000,0.00000000000,0.00000000000),\\
p_1^\mu &= (+0.30674037867,-0.17738694693,-0.01664472021,-0.24969277974),
\end{aligned}$$

$$
\begin{aligned}
p_2^\mu &= (+0.34445032281, +0.14635282800, -0.10707762397, +0.29285022975), \\
p_3^\mu &= (+0.22091667641, +0.08911915938, +0.19733901856, +0.04380941793), \\
p_4^\mu &= (+0.12789262211, -0.05808504045, -0.07361667438, -0.08696686795).
\end{aligned}
\tag{4.49}
$$

The results are presented in table 4.1 where we have chosen the renormalisation scale to be $\mu^2 = m_H^2$.[2]

Helicity	$A^{(0)}$	$M_4^{\mathcal{F},g}$	$M_4^{\mathcal{F},f}$	$M_4^{\mathcal{F},s}$
$----$	-116.526220-18.681775 i	-9.540396-0.001010 i	-0.176850+0.001010 i	0.176850-0.001010 i
$+---$	10.308088-0.824204 i	-10.809925+0.056646 i	-0.388288+0.198369 i	0.296783-0.155132 i
$--++$	20.511457-0.888525 i	-10.991033+0.320009 i	0.268501-0.068414 i	0.066595-0.015451 i
$-+-+$	4.683784+4.242678 i	-10.332320+0.149216 i	0.028668-0.066437 i	0.166800+0.038844 i

Table 4.1: Numerical values for the finite parts of the Higgs + 4 gluon helicity amplitudes at the phase space point given in eq. (6.2).

4.6 Summary

In this chapter we have calculated the last (analytically) unknown building block of the Higgs plus four gluon amplitude, the ϕ-NMHV amplitude $A_4^{(1)}(\phi, 1^+, 2^-, 3^-, 4^-)$. We chose to split the calculation into two parts, one being cut-constructible (to which we applied the techniques of four-dimensional unitarity) and a rational part, which is insensitive to four-dimensional cuts. We used the unitarity methods described in chapters 2 and 3 to calculate the cut-constructible pieces. We used Feynman diagrams to calculate the rational pieces proportional to N_f and BCFW recursion relations to calculate the remaining pieces. We checked our results for the ϕ-MHV and ϕ-NMHV amplitudes against the semi-numerical code of Ref. [104].

In the next chapter we will compute the remaining helicity amplitude, the $\phi q\overline{q}$-NMHV amplitude, completing the analytic calculation of ϕ + parton amplitudes. We shall observe that although similar to the calculation carried out in this chapter,

[2]We have been informed by John Campbell, that the entries for $M_4^{F,g}$ and $M_4^{F,q}$ in Table 4.1 are in agreement with results obtained using the seminumerical code described in Ref. [104].

the addition of quarks into the final state introduces new complexities, and as a result the formulae reflect this increase in complexity.

Chapter 5

The $\phi\bar{q}qgg$- NMHV amplitude

5.1 Introduction

In this chapter we calculate the most complicated of the ϕ plus four parton one-loop amplitudes, $A_4^{(1)}(\phi, 1_q^-, 2_{\overline{q}}^+, 3_g^-, 4_g^-)$, which we call the $\phi q\overline{q}$-NMHV amplitude [1]. This amplitude is more complicated than others for two reasons. Firstly, as in chapter 4 the NMHV helicity configuration increases the complexity of tree-level amplitudes appearing in the cuts, and as result the complexity of the basis integral coefficients. Secondly, the presence of quarks in the external state creates a larger number of independent primitive amplitudes that must be calculated (due to the more complicated colour structure). Indeed, the growth in complexity is twofold since not only are there more terms to calculate but the different colour structures of loop amplitudes actually prevents simplifications when different topologies are combined as in previous chapters. In this chapter we do not describe in detail the method of the calculation, since the methods of unitarity have been explained in detail in chapters 2 and 3 and the specifics of an NMHV calculation were covered in chapter 4. Therefore in this chapter we focus primarily on the additional complications of the

[1] In this chapter we explicitly label partons appearing in helicity amplitudes, e.g. in $A_4^{(1)}(\phi, 1_q^-, 2_{\overline{q}}^+, 3_g^-, 4_g^-)$ we denote gluons with a subscript g, in previous chapters this was an unnecessary complication.

increased number of primitive amplitudes and the expressions for the amplitudes.

5.1.1 Definition of colour ordered amplitudes

The colour decomposition of the $H\bar{q}qgg$ amplitudes is exactly the same as for the case $\bar{q}qgg$ which was written down in ref. [117]. For the tree-level case there are two colour stripped amplitudes,

$$\mathcal{A}_4^{(0)}(\phi, 1_{\bar{q}}, 2_q, 3_g, 4_g) = Cg^2 \sum_{\sigma\in S_2} (T^{a_{\sigma(3)}} T^{a_{\sigma(4)}})_{i_2}^{\bar{\imath}_1} \, A_4^{(0)}(\phi, 1_{\bar{q}}, 2_q, \sigma(3), \sigma(4)) \,. \tag{5.1}$$

At one-loop level the colour decomposition is,

$$\begin{aligned} \mathcal{A}_4^{(1)}(\phi, 1_{\bar{q}}, 2_q, 3_g, 4_g) &= Cg^4 \, c_\Gamma \Bigg[N_c \sum_{\sigma\in S_2} (T^{a_{\sigma(3)}} T^{a_{\sigma(4)}})_{i_2}^{\bar{\imath}_1} \, A_{4;1}(\phi, 1_{\bar{q}}, 2_q, \sigma(3), \sigma(4)) \\ &\qquad + \delta^{a_3 a_4} \, \delta_{i_2}^{\bar{\imath}_1} A_{4;3}(\phi, 1_{\bar{q}}, 2_q; 3_g, 4_g) \Bigg] \,. \end{aligned} \tag{5.2}$$

In these equations g is the strong coupling constant and c_Γ is the ubiquitous one-loop factor,

$$c_\Gamma \equiv \frac{1}{(4\pi)^{2-\epsilon}} \frac{\Gamma(1+\epsilon)\Gamma^2(1-\epsilon)}{\Gamma(1-2\epsilon)} \,. \tag{5.3}$$

The colour stripped amplitudes $A_{4;1}$ and $A_{4;3}$ can further be decomposed into primitive amplitudes,

$$\begin{aligned} A_{4;1}(\phi, 1_{\bar{q}}, 2_q, 3_g, 4_g) &= A_4^L(\phi, 1_{\bar{q}}, 2_q, 3_g, 4_g) - \frac{1}{N_c^2} A_4^R(\phi, 1_{\bar{q}}, 2_q, 3_g, 4_g) \\ &\qquad + \frac{N_f}{N_c} \, A_4^{\mathrm{f}}(\phi, 1_{\bar{q}}, 2_q, 3_g, 4_g) \,, \end{aligned} \tag{5.4}$$

and,

$$\begin{aligned} A_{4;3}(\phi, 1_{\bar{q}}, 2_q; 3_g, 4_g) &= A_4^L(\phi, 1_{\bar{q}}, 2_q, 3_g, 4_g) + A_4^R(\phi, 1_{\bar{q}}, 2_q, 3_g, 4_g) \\ &+ A_4^L(\phi, 1_{\bar{q}}, 3_g, 2_q, 4_g) + A_4^L(\phi, 1_{\bar{q}}, 2_q, 4_g, 3_g) \\ &+ A_4^R(\phi, 1_{\bar{q}}, 2_q, 4_g, 3_g) + A_4^L(\phi, 1_{\bar{q}}, 4_g, 2_q, 3_g) \,. \end{aligned} \tag{5.5}$$

All of these colour decomposition equations, namely eqs. (5.1, 5.2, 5.4, 5.5) are equally valid if ϕ is replaced by a $\phi^\dagger$ or a Higgs boson H. Sample diagrams contributing to each of the primitive amplitudes are shown in Figure 5.1.

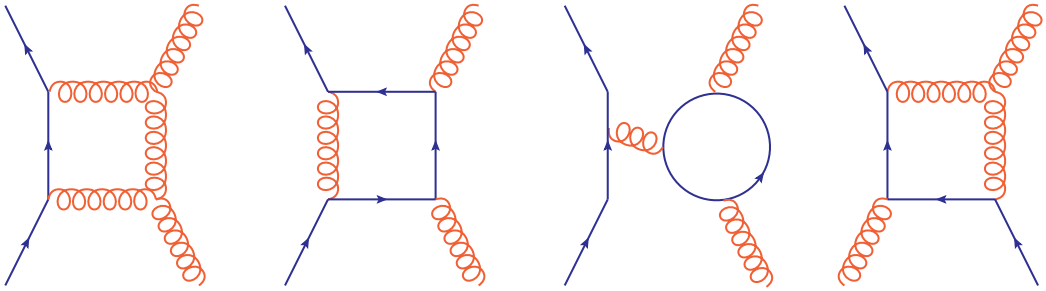

Figure 5.1: Sample diagrams contributing to the primitive amplitudes, from left to right we have; the left piece $A_4^L(\phi, 1_{\bar{q}}, 2_q, 3_g, 4_g)$, the subleading right piece $A_4^R(\phi, 1_{\bar{q}}, 2_q, 3_g, 4_g)$, terms which contain a closed fermion loop (the N_f piece), $A_4^{\rm f}(\phi, 1_{\bar{q}}, 2_q, 3_g, 4_g)$ and the subleading left piece $A_4^L(\phi, 1_{\bar{q}}, 2_g, 3_q, 4_g)$. The ϕ field can attach to any gluon line in the diagram.

5.1.2 Known analytic results for $Hq\bar{q}jj$ amplitudes

In this section we review results from the literature and collect formulae, for both tree and one-loop results, that will be useful in constructing the Higgs NMHV amplitude.

Tree level results

The results for the tree graphs that are primarily of interest here, i.e. $\phi\bar{q}qgg$ amplitudes with gluons of the same helicity, are:

$$\begin{aligned} -iA_4^{(0)}(\phi, 1_{\bar{q}}^-, 2_q^+, 3_g^-, 4_g^-) &= -\frac{\langle 3\,|p_\phi|\,2]^2\,\langle 4\,1\rangle}{[2\,4]\;s_{124}}\left[\frac{1}{s_{12}}+\frac{1}{s_{41}}\right] \\ &\quad -\frac{\langle 4\,|p_\phi|\,2]^2\,\langle 1\,3\rangle}{[2\,3]\;s_{12}\,s_{123}}+\frac{\langle 1\,|p_\phi|\,2]^2}{\langle 1\,2\rangle\,[2\,4]\,[2\,3]\,[3\,4]}\,, \qquad (5.6) \\ -iA_4^{(0)}(\phi, 1_{\bar{q}}^-, 2_q^+, 3_g^+, 4_g^+) &= 0\,, \qquad (5.7) \end{aligned}$$

and for the subleading colour piece,

$$\begin{aligned} -iA_4^{(0)}(\phi, 1_{\bar{q}}^-, 2_g^-, 3_q^+, 4_g^-) &= -\frac{\langle 4\,|p_\phi|\,3]^2}{[1\,2]\,[2\,3]\;s_{123}}-\frac{\langle 2\,|p_\phi|\,3]^2}{[3\,4]\,[4\,1]\;s_{341}}\,, \qquad (5.8) \\ -iA_4^{(0)}(\phi, 1_{\bar{q}}^-, 2_g^+, 3_q^+, 4_g^+) &= 0\,. \qquad (5.9) \end{aligned}$$

A summary of our spinor notation is given in Appendix A. Compact analytic expressions for all helicity amplitudes are presented in references [109, 208].

By using parity and charge conjugation [209], we can relate these $\phi\bar{q}qgg$ amplitudes to ones for $\phi^\dagger\bar{q}qgg$ with the same helicity assignments of quark and antiquark. This relation, valid at any order of perturbation theory, n, reads,

$$\mathcal{A}_4^{(n)}(\phi^\dagger, 1_{\bar{q}}^{-h_q}, 2_q^{h_q}, 3_g^{h_3}, 4_g^{h_4}) = -\Big[\mathcal{A}_4^{(n)}(\phi, 2_{\bar{q}}^{-h_q}, 1_q^{h_q}, 4_g^{-h_4}, 3_g^{-h_3})\Big]\Big|_{\langle i\,j\rangle\leftrightarrow[j\,i]} . \tag{5.10}$$

We thus see that the $\phi^\dagger$ amplitude in which we are interested is zero,

$$-iA_4^{(0)}(\phi^\dagger, 1_{\bar{q}}^-, 2_q^+, 3_g^-, 4_g^-) = 0 , \tag{5.11}$$

so that, at tree-level, the NMHV Higgs amplitude in which we will ultimately be interested is simply given by Eq. (5.6).

$H\bar{q}q\bar{q}q$ amplitudes

The full one-loop results for this process, both for pairs of identical and non-identical quarks, are already available in the literature. The matrix element squared has been computed in ref. [104], with results for the amplitude presented in ref. [109].

$H\bar{q}qgg$ amplitudes

In principle there are 8 combinations of amplitudes, since helicity is conserved on the quark line, but because of parity invariance only four Higgs amplitudes are independent. The references to the amplitudes already calculated in the literature are given in Table 5.1. From this table we see that the Higgs amplitude $\mathcal{A}(H, 1_{\bar{q}}^-, 2_q^+, 3_g^-, 4_g^-)$ requires, in addition to the calculation of a previously unknown ϕ amplitude, also the results for the corresponding $\phi^\dagger$ amplitude from ref. [109].

The $\phi^\dagger$ results that we shall need can be derived from the following amplitudes in the case of $A_{4;1}$,

$$\begin{aligned} -iA_4^L(\phi, 1_{\bar{q}}^-, 2_q^+, 3_g^+, 4_g^+) &= 2i\,A_4^{(0)}(\phi^\dagger, 1_{\bar{q}}^-, 2_q^+, 3_g^+, 4_g^+) \\ &\quad + \frac{1}{2}\left[-\frac{\langle 1\,|p_\phi|\,4]}{\langle 2\,3\rangle\,\langle 3\,4\rangle} + \frac{\langle 1\,2\rangle\,[2\,3]\,\langle 3\,1\rangle}{\langle 2\,3\rangle\,\langle 3\,4\rangle\,\langle 4\,1\rangle}\right] - \frac{1}{3}\frac{\langle 1\,3\rangle\,[3\,4]\,\langle 4\,1\rangle}{\langle 1\,2\rangle\,\langle 3\,4\rangle^2} , \end{aligned} \tag{5.12}$$

$$-iA_4^R(\phi, 1_{\bar{q}}^-, 2_q^+, 3_g^+, 4_g^+) = -\frac{1}{2}\left[-\frac{\langle 1\,|p_\phi|\,4]}{\langle 2\,3\rangle\,\langle 3\,4\rangle} + \frac{\langle 1\,2\rangle\,[2\,3]\,\langle 3\,1\rangle}{\langle 2\,3\rangle\,\langle 3\,4\rangle\,\langle 4\,1\rangle}\right] , \tag{5.13}$$

H amplitude	ϕ amplitude	$\phi^\dagger$ amplitude
$\mathcal{A}(H,1_{\bar{q}}^-,2_q^+,3_g^+,4_g^+)$	$\mathcal{A}(\phi,1_{\bar{q}}^-,2_q^+,3_g^+,4_g^+)$ [106,109]	$\mathcal{A}(\phi^\dagger,1_{\bar{q}}^-,2_q^+,3_g^+,4_g^+)$
$\mathcal{A}(H,1_{\bar{q}}^-,2_q^+,3_g^-,4_g^-)$	$\mathcal{A}(\phi,1_{\bar{q}}^-,2_q^+,3_g^-,4_g^-)$	$\mathcal{A}(\phi^\dagger,1_{\bar{q}}^-,2_q^+,3_g^-,4_g^-)$ [106,109]
$\mathcal{A}(H,1_{\bar{q}}^-,2_q^+,3_g^+,4_g^-)$	$\mathcal{A}(\phi,1_{\bar{q}}^-,2_q^+,3_g^+,4_g^-)$ [109]	$\mathcal{A}(\phi^\dagger,1_{\bar{q}}^-,2_q^+,3_g^+,4_g^-)$ [109]
$\mathcal{A}(H,1_{\bar{q}}^-,2_q^+,3_g^-,4_g^+)$	$\mathcal{A}(\phi,1_{\bar{q}}^-,2_q^+,3_g^-,4_g^+)$ [109]	$\mathcal{A}(\phi^\dagger,1_{\bar{q}}^-,2_q^+,3_g^-,4_g^+)$ [109]

Table 5.1: ϕ and $\phi^\dagger$ amplitudes needed to construct a given one-loop $H\bar{q}qgg$ amplitude, together with the references where they can be obtained. In all cases the $\phi^\dagger$ amplitudes are constructed from the ϕ amplitudes given in the reference, using the parity operation. The cases where the gluons have the same helicity, which have no associated references, are the subject of this chapter.

$$-iA_4^{\rm f}(\phi,1_{\bar{q}}^-,2_q^+,3_g^+,4_g^+) \;=\; \frac{1}{3}\frac{\langle 1\,3\rangle\,[3\,4]\,\langle 4\,1\rangle}{\langle 1\,2\rangle\,\langle 3\,4\rangle^2}\,, \tag{5.14}$$

whilst the subleading partial amplitude $A_{4;3}$ also requires the results,

$$-iA_4^L(\phi,1_{\bar{q}}^-,2_g^+,3_q^+,4_g^+) \;=\; \frac{\langle 1\,3\rangle^2\,[3\,4]}{2\,\langle 1\,2\rangle\,\langle 2\,3\rangle\,\langle 3\,4\rangle} - \frac{2\langle 1\,|p_\phi|\,4]^2}{\langle 1\,2\rangle\,\langle 2\,3\rangle\;s_{123}} - \frac{\langle 1\,3\rangle\,\langle 1\,|p_\phi|\,2]}{2\,\langle 2\,3\rangle\,\langle 3\,4\rangle\,\langle 4\,1\rangle}, \tag{5.15}$$

$$A_4^{\rm f}(\phi,1_{\bar{q}}^-,2^+,3_q^+,4_g^+) \;=\; 0. \tag{5.16}$$

To obtain the form that is most useful for the calculation of $\mathcal{A}(H,1_{\bar{q}}^-,2_q^+,3_g^-,4_g^-)$, we relate the $\phi^\dagger\bar{q}qgg$ amplitudes to the $\phi\bar{q}qgg$ ones by using the relation in Eq. (5.10). Thus we obtain the required results by performing the transformation $1\leftrightarrow 2, 3\leftrightarrow 4$, $\langle\rangle\leftrightarrow[]$ and reversing the sign. The amplitudes contributing to $A_{4;1}$ are,

$$\begin{aligned} -iA_4^L(\phi^\dagger,1_{\bar{q}}^-,2_q^+,3_g^-,4_g^-) \;=\;& 2i\,A_4^{(0)}(\phi,1_{\bar{q}}^-,2_q^+,3_g^-,4_g^-) \\ &+\frac{1}{2}\left[-\frac{\langle 3\,|p_\phi|\,2]}{[1\,4]\,[3\,4]}+\frac{[2\,1]\,\langle 1\,4\rangle\,[2\,4]}{[1\,4]\,[3\,4]\,[2\,3]}\right]-\frac{1}{3}\frac{[2\,4]\,\langle 3\,4\rangle\,[2\,3]}{[1\,2]\,[3\,4]^2}\,. \end{aligned} \tag{5.17}$$

$$-iA_4^R(\phi^\dagger,1_{\bar{q}}^-,2_q^+,3_g^-,4_g^-) \;=\; \frac{1}{2}\left[\frac{\langle 3\,|p_\phi|\,2]}{[1\,4]\,[3\,4]}-\frac{[2\,1]\,\langle 1\,4\rangle\,[2\,4]}{[1\,4]\,[3\,4]\,[2\,3]}\right], \tag{5.18}$$

$$-iA_4^{\rm f}(\phi^\dagger,1_{\bar{q}}^-,2_q^+,3_g^-,4_g^-) \;=\; \frac{1}{3}\frac{[2\,4]\,\langle 3\,4\rangle\,[2\,3]}{[1\,2]\,[3\,4]^2}\,, \tag{5.19}$$

while the additional subleading contributions become,

$$-iA_4^L(\phi^\dagger,1_{\bar{q}}^-,3_g^-,2_q^+,4_g^-) \;=\; 2\,\frac{\langle 3\,|p_\phi|\,2]^2}{[2\,4]\,[4\,1]\;s_{124}}+\frac{1}{2}\left[\frac{[2\,1]\,\langle 4\,|p_\phi|\,2]}{[4\,1]\,[1\,3]\,[3\,2]}-3\frac{[1\,2]^2\,\langle 1\,3\rangle}{[2\,4]\,[4\,1]\,[1\,3]}\right]$$

$$
\begin{aligned}
&= i\, A_4^{(0)}(\phi, 1_{\bar{q}}^-, 3_g^-, 2_q^+, 4_g^-) \\
&+ \text{terms antisymmetric in } \{3 \leftrightarrow 4\}\ . \qquad (5.20)
\end{aligned}
$$

We note that all of these amplitudes are finite because of the vanishing of the corresponding tree-level results (see section 5.1.2).

5.2 One-loop results

In this section we present analytic expressions for the full one-loop corrections to the process $\mathcal{A}_4^{(1)}(\phi, 1_{\bar{q}}^-, 2_q^+, 3_g^-, 4_g^-)$. All expressions are presented un-renormalised in the four-dimensional helicity (FDH) scheme (setting $\delta_R = 0$) or 't Hooft-Veltman scheme (setting $\delta_R = 1$).

We employ the generalised unitarity method described in chapters 2 and 3 [120, 122, 123, 127, 128] to calculate the cut-constructible parts of the left-moving, right-moving and N_f one-loop amplitudes. This relies on the familiar expansion of a one-loop amplitude in terms of scalar basis integrals,

$$
A_4^{\text{cut}-\text{cons.}}(\phi, 1_{\overline{q}}^-, 2_q^+, 3_g^-, 4_g^-) = \sum_i C_{4;i} I_{4;i} + \sum_i C_{3;i} I_{3;i} + \sum_i C_{2;i} I_{2;i}. \qquad (5.21)
$$

In this sum each j-point scalar basis integral ($\mathcal{I}_{j;i}$) appears with a coefficient $C_{j;i}$. The sum over i represents the sum over the partitions of the external momenta over the j legs of the basis integral. We use the methods described in previous chapters [120, 122, 132] to obtain the coefficients. Results were obtained using the QGRAF [207], FORM [210] and S@M [204] packages in order to control the extensive algebra.

5.2.1 Results for $A_{4;1}(\phi, 1_{\bar{q}}, 2_q, 3_g^-, 4_g^-)$

The partial amplitude $A_{4;1}(\phi, 1_{\bar{q}}, 2_q, 3_g^-, 4_g^-)$ is calculated from three primitive amplitudes according to Eq. (5.4). We shall deal with each of these ingredients in turn.

$A_4^L(\phi, 1_{\bar{q}}^-, 2_q^+, 3_g^-, 4_g^-)$

The full result for this primitive amplitude is given by,

$$
\begin{aligned}
&- iA_4^L(\phi, 1_{\bar{q}}^-, 2_q^+, 3_g^-, 4_g^-) \;=\; -iA_4^{(0)}(\phi, 1_{\bar{q}}^-, 2_q^+, 3_g^-, 4_g^-) \times V_1^L \\
&- \frac{s_{134}^2}{2\,[1\,4]\,[3\,4]\,\langle 2\,|p_\phi|\,3]} \Big[\mathrm{F}_{4\mathrm{F}}^{1\mathrm{m}}(s_{14}, s_{34}; s_{134}) + \mathrm{F}_{4\mathrm{F}}^{2\mathrm{mh}}(s_{12}, s_{134}; s_{34}, m_\phi^2) \Big] \\
&+ \frac{\langle 1\,|p_\phi|\,2]^2}{2\langle 1\,|p_\phi|\,4]\,[2\,3]\,[3\,4]} \Big[\mathrm{F}_{4\mathrm{F}}^{1\mathrm{m}}(s_{34}, s_{23}; s_{234}) + \mathrm{F}_{4\mathrm{F}}^{2\mathrm{mh}}(s_{12}, s_{234}; s_{34}, m_\phi^2) \Big] \\
&+ \frac{1}{2}\Big[\frac{m_\phi^4 \langle 1\,4\rangle^2\,\langle 2\,4\rangle}{\langle 1\,2\rangle\,\langle 2\,|p_\phi|\,3]\,\langle 4\,|p_\phi|\,3]\,s_{124}} - \frac{\langle 3\,|p_\phi|\,2]^3}{[1\,2]\,[2\,4]\,\langle 3\,|p_\phi|\,4]\,s_{124}} \Big] \mathrm{F}_{4\mathrm{F}}^{1\mathrm{m}}(s_{12}, s_{14}; s_{124}) \\
&+ \frac{1}{2}\Big[\frac{[2\,3]^2 \langle 4\,|p_\phi|\,1]^3}{[1\,2]\,[1\,3]^3\,\langle 4\,|p_\phi|\,3]\,s_{123}} - \frac{m_\phi^4 \langle 1\,3\rangle^3}{\langle 1\,2\rangle\,\langle 1\,|p_\phi|\,4]\,\langle 3\,|p_\phi|\,4]\,s_{123}} \Big] \mathrm{F}_{4\mathrm{F}}^{1\mathrm{m}}(s_{12}, s_{23}; s_{123}) \\
&+ \frac{1}{2}\Big[\frac{\langle 4\,|p_\phi|\,2]^3}{[1\,2]\,[2\,3]\,\langle 4\,|p_\phi|\,3]\,s_{123}} - \frac{m_\phi^4 \langle 1\,3\rangle^3}{\langle 1\,2\rangle\,\langle 1\,|p_\phi|\,4]\,\langle 3\,|p_\phi|\,4]\,s_{123}} \Big] \\
&\times \Big[\mathrm{F}_{4\mathrm{F}}^{2\mathrm{mh}}(s_{34}, s_{123}; s_{12}, m_\phi^2) + \mathrm{F}_{4\mathrm{F}}^{2\mathrm{mh}}(s_{14}, s_{123}; s_{23}, m_\phi^2) \Big] \\
&+ \frac{1}{2}\Big[\frac{m_\phi^4 \langle 1\,4\rangle^2\,\langle 2\,4\rangle}{\langle 1\,2\rangle\,\langle 2\,|p_\phi|\,3]\,\langle 4\,|p_\phi|\,3]\,s_{124}} - \frac{\langle 3\,|p_\phi|\,2]^2\,\langle 3\,|p_\phi|\,1]}{[1\,2]\,[1\,4]\,\langle 3\,|p_\phi|\,4]\,s_{124}} \Big] \\
&\times \Big[\mathrm{F}_{4\mathrm{F}}^{2\mathrm{mh}}(s_{34}, s_{124}; s_{12}, m_\phi^2) + \mathrm{F}_{4\mathrm{F}}^{2\mathrm{mh}}(s_{23}, s_{124}; s_{14}, m_\phi^2) \Big] \\
&- C_{3;\phi|12|34}(\phi, 1_{\bar{q}}^-, 2_q^+, 3_g^-, 4_g^-)\, \mathrm{F}_3^{3\mathrm{m}}(s_{12}, s_{34}, m_\phi^2) \\
&- C_{3;\phi|41|23}(\phi, 1_{\bar{q}}^-, 2_q^+, 3_g^-, 4_g^-)\, \mathrm{F}_3^{3\mathrm{m}}(s_{23}, s_{14}, m_\phi^2) \\
&+ \frac{2\langle 1\,3\rangle^2\,\langle 3\,4\rangle\,\langle 4\,|p_\phi|\,3]\,[1\,2]}{3} \hat{L}_3(s_{123}, s_{12}) \\
&- \frac{\langle 3\,4\rangle\,\langle 3\,1\rangle\,(\langle 4\,|p_\phi|\,2]\,[1\,3] - 3\,\langle 4\,|p_\phi|\,1]\,[2\,3])}{6\,[3\,1]} \hat{L}_2(s_{123}, s_{12}) \\
&+ \frac{\langle 1\,3\rangle \left(16\langle 4\,|p_\phi|\,2]^2 [1\,3]^2 - 3\,\langle 4\,|p_\phi|\,2]\,\langle 4\,|p_\phi|\,3]\,[2\,1]\,[3\,1] + 6\langle 4\,|p_\phi|\,1]^2 [2\,3]^2 \right)}{6 s_{123} [3\,1]^2\,[3\,2]} \\
&\quad \times \hat{L}_1(s_{123}, s_{12}) \\
&- \frac{2 s_{124} \langle 3\,4\rangle^2\,\langle 1\,4\rangle\,[4\,2]}{3} \hat{L}_3(s_{124}, s_{12}) \\
&+ \langle 3\,4\rangle\,\langle 1\,4\rangle\,\frac{2\,\langle 3\,|p_\phi|\,2]\,[1\,4] - 3\,\langle 3\,|p_\phi|\,4]\,[1\,2]}{6\,[4\,1]} \hat{L}_2(s_{124}, s_{12}) \\
&+ \frac{\langle 3\,|p_\phi|\,2]\,(9\; s_{124}\,\langle 3\,4\rangle\,[2\,1] + 22\;\langle 3\,|p_\phi|\,2]\,\langle 4\,2\rangle\,[1\,2])}{6\; s_{124}\,[4\,1]\,[2\,1]} \hat{L}_1(s_{124}, s_{12}) \\
&- \frac{\langle 1\,4\rangle\,\langle 1\,3\rangle\,\langle 4\,|p_\phi|\,1]\,[1\,2]}{2\,[3\,1]} \hat{L}_2(s_{123}, s_{23})
\end{aligned}
$$

$$
\begin{aligned}
&- \langle 1\,3\rangle \langle 4\,|p_\phi|\,1]\,\frac{3\ \langle 4\,|p_\phi|\,2]\,[1\,3] + 2\ \langle 4\,|p_\phi|\,1]\,[2\,3]}{2s_{123}[1\,3]^2}\hat{L}_1(s_{123},s_{23}) \\
&+ \frac{s_{234}\,\langle 1\,4\rangle\,\langle 3\,4\rangle\,[4\,2]}{2\,[4\,3]}\hat{L}_2(s_{234},s_{23}) - 3\frac{\langle 3\,4\rangle\,\langle 1\,|p_\phi|\,2]}{2\,[4\,3]}\hat{L}_1(s_{234},s_{23}) \\
&+R^L(\phi,1_{\bar{q}}^-,2_q^+,3_g^-,4_g^-)\,,
\end{aligned}
\tag{5.22}
$$

with,

$$
V_1^L \;=\; -\frac{1}{\epsilon^2}\left[\left(\frac{\mu^2}{-s_{23}}\right)^\epsilon + \left(\frac{\mu^2}{-s_{34}}\right)^\epsilon + \left(\frac{\mu^2}{-s_{41}}\right)^\epsilon\right] + \frac{13}{6\epsilon}\left(\frac{\mu^2}{-s_{12}}\right)^\epsilon + \frac{119}{18} - \frac{\delta_R}{6}\,,
\tag{5.23}
$$

and the remaining rational terms given by,

$$
\begin{aligned}
&R^L(\phi,1_{\bar{q}}^-,2_q^+,3_g^-,4_g^-) = -\frac{\langle 3\,4\rangle\,\langle 3\,|p_\phi|\,2]\left(2\,\langle 2\,4\rangle\,[4\,2] - \langle 1\,2\rangle\,[2\,1]\right)}{12s_{124}\,\langle 1\,2\rangle\,[2\,1]\,[4\,1]} \\
&+\frac{\langle 2\,3\rangle\,\langle 4\,|p_\phi|\,2]^2\left(3\,\langle 1\,2\rangle\,[2\,1] - 2\,\langle 2\,3\rangle\,[3\,2]\right) + 2\,\langle 1\,3\rangle^2\,\langle 2\,4\rangle\,\langle 4\,|p_\phi|\,1]\,[2\,1]\,[3\,2]}{12s_{123}\,\langle 1\,2\rangle\,\langle 2\,3\rangle\,[2\,1]\,[3\,1]\,[3\,2]} \\
&+\frac{5\,\langle 3\,4\rangle^2}{12\,\langle 2\,3\rangle\,[3\,1]} - \frac{5\,\langle 3\,4\rangle\,\langle 4\,|p_\phi|\,2]}{6\,\langle 2\,3\rangle\,[3\,1]\,[3\,2]} + \frac{\langle 4\,|p_\phi|\,2]^2}{6\,\langle 1\,2\rangle\,[2\,1]\,[3\,1]\,[3\,2]} \\
&-\frac{\langle 1\,3\rangle\,\langle 1\,4\rangle\,\langle 2\,4\rangle\,[2\,1]}{3\,\langle 1\,2\rangle\,\langle 2\,3\rangle\,[3\,1]\,[3\,2]} - \frac{\langle 1\,3\rangle\,\langle 3\,4\rangle}{12\,\langle 1\,2\rangle\,[4\,1]} - \frac{\langle 3\,4\rangle^2\,[4\,2]}{6\,\langle 1\,2\rangle\,[2\,1]\,[4\,1]} + \frac{\langle 1\,3\rangle\,\langle 2\,4\rangle\,\langle 4\,|P_{13}|\,4]}{4\,\langle 1\,2\rangle\,\langle 2\,3\rangle\,[3\,1]\,[4\,3]} \\
&-\frac{\langle 1\,3\rangle\,\langle 4\,|P_{13}|\,4]}{3\,\langle 1\,2\rangle\,[4\,1]\,[4\,3]} - \frac{5\,\langle 1\,4\rangle^2\,[4\,1]}{12\,\langle 1\,2\rangle\,[3\,1]\,[4\,3]} + \frac{\langle 1\,4\rangle^2\,[4\,2]}{6\,\langle 1\,2\rangle\,[3\,2]\,[4\,3]}\,.
\end{aligned}
\tag{5.24}
$$

The coefficients of the three mass triangles were calculated using the method of ref. [122],

$$
C_{3;\phi|12|34}(\phi,1_{\bar{q}}^-,2_q^+,3_g^-,4_g^-) = \sum_{\gamma=\gamma_\pm}\frac{m_\phi^4\langle 3\,4\rangle^3\langle 1\,K_1^\flat\rangle^2}{\gamma(\gamma-m_\phi^2)\langle 1\,2\rangle\langle 3\,K_1^\flat\rangle\langle 4\,K_1^\flat\rangle}\,,
\tag{5.25}
$$

with $K_1 = -p_1-p_2-p_3-p_4, K_2 = -p_1-p_2$ and the massless vector $K_1^\flat$ given by,

$$
K_1^{\flat\,\mu} = \gamma\frac{\gamma K_1^\mu - K_1^2 K_2^\mu}{\gamma^2 - K_1^2K_2^2}\,,
\tag{5.26}
$$

and where γ is given by the two solutions,

$$
\gamma_\pm = K_1\cdot K_2 \pm \sqrt{(K_1\cdot K_2)^2 - K_1^2K_2^2}\,.
\tag{5.27}
$$

The other triangle coefficient is,

$$
C_{3;\phi|41|23}(\phi,1_{\bar{q}}^-,2_q^+,3_g^-,4_g^-) = -\sum_{\gamma=\gamma_\pm}\frac{m_\phi^4\langle 1\,4\rangle^2\langle 3\,K_1^\flat\rangle^2}{2\gamma(\gamma-m_\phi^2)\langle 1\,K_1^\flat\rangle\langle 2\,K_1^\flat\rangle}\,,
\tag{5.28}
$$

with $K_1 = -p_1 - p_2 - p_3 - p_4, K_2 = -p_1 - p_4$ and $K_1^\flat$ given in terms of these vectors by Eq. (5.26).

The definitions of the box integral functions $\mathrm{F}^{\mathrm{1m}}_{\mathrm{4F}}$ and $\mathrm{F}^{\mathrm{2mh}}_{\mathrm{4F}}$ can be found in Appendix B, together with expressions for $\hat{L}_1$, $\hat{L}_2$ and $\hat{L}_3$. In addition to logarithms and polynomial denominators, the latter functions also contain rational terms that protect them from unphysical singularities. Thus, for example,

$$\hat{L}_2(s,t) = \frac{\log(s/t)}{(s-t)^2} - \frac{1}{2(s-t)}\left(\frac{1}{s}+\frac{1}{t}\right) ,$$

which is finite in the limit that $s \to t$.

$A_4^R(\phi, 1_{\bar{q}}^-, 2_q^+, 3_g^-, 4_g^-)$

The result for the right-moving amplitude, $A_4^R(\phi, 1_{\bar{q}}^-, 2_q^+, 3_g^-, 4_g^-)$ is,

$$\begin{aligned}
& -iA_4^R(\phi, 1_{\bar{q}}^-, 2_q^+, 3_g^-, 4_g^-) \;=\; -iA_4^{(0)}(\phi, 1_{\bar{q}}^-, 2_q^+, 3_g^-, 4_g^-) \times V^R \\
+ \;& \frac{[1\,2]^2\langle 4\,|p_\phi|\,3]^2}{2[1\,3]^3[2\,3]s_{123}}\;\mathrm{F}^{\mathrm{1m}}_{\mathrm{4F}}(s_{12},s_{23};s_{123}) + \frac{\langle 3\,|p_\phi|\,2]^2}{2\,[1\,4]\,[2\,4]\,s_{124}}\;\mathrm{F}^{\mathrm{1m}}_{\mathrm{4F}}(s_{14},s_{12};s_{124}) \\
+ \;& \frac{\langle 1\,|p_\phi|\,2]^2}{2[2\,3][3\,4]\langle 1\,|p_\phi|\,4]}\;\mathrm{F}^{\mathrm{2mh}}_{\mathrm{4F}}(s_{14},s_{234};s_{23},m_\phi^2) \\
- \;& \frac{s_{134}^2}{2[1\,4][3\,4]\langle 2\,|p_\phi|\,3]}\;\mathrm{F}^{\mathrm{2mh}}_{\mathrm{4F}}(s_{23},s_{134};s_{14},m_\phi^2) \\
- \;& C_{3;\phi|41|23}(\phi, 1_{\bar{q}}^-, 2_q^+, 3_g^-, 4_g^-)\,\mathrm{F}_3^{\mathrm{3m}}(s_{23},s_{14},m_\phi^2) \\
- \;& \frac{1}{2}\frac{\langle 1\,4\rangle^2[1\,2]^2\langle 3\,|p_\phi|\,4]^2}{[1\,4]\,[2\,4]\,s_{124}}\;\hat{L}_2(s_{124},s_{12}) \\
- \;& 2\frac{\langle 3\,4\rangle\,\langle 3\,|p_\phi|\,2]}{[1\,4]}\;\hat{L}_1(s_{124},s_{12}) + \frac{1}{2}\frac{\langle 3\,|p_\phi|\,2]^2}{[1\,4]\,[2\,4]\,s_{124}}\;\hat{L}_0(s_{124},s_{12}) \\
+ \;& \frac{1}{2}\frac{\langle 1\,4\rangle^2[2\,4]^2 s_{234}^2}{[2\,3]\,[3\,4]\,\langle 1\,|p_\phi|\,4]}\;\hat{L}_2(s_{234},s_{23}) + 2\frac{\langle 3\,4\rangle\,\langle 1\,|p_\phi|\,2]}{[3\,4]}\;\hat{L}_1(s_{234},s_{23}) \\
- \;& \frac{1}{2}\frac{\langle 1\,|p_\phi|\,2]^2}{[2\,3]\,[3\,4]\,\langle 1\,|p_\phi|\,4]}\;\hat{L}_0(s_{234},s_{23}) \\
- \;& \frac{1}{2}\frac{\Big(\langle 1\,2\rangle\,[1\,2]\,\langle 4\,|p_\phi|\,1]\Big)^2\,[2\,3]}{[1\,3]^3 s_{123}}\;\hat{L}_2(s_{123},s_{23}) \\
+ \;& 2\frac{\langle 1\,3\rangle\,[1\,2]\,\langle 4\,|p_\phi|\,3]\,\langle 4\,|p_\phi|\,1]}{\langle 2\,3\rangle\,[1\,3]^2\,[2\,3]}\;\hat{L}_1(s_{123},s_{23}) \\
+ \;& \Big[-2\frac{\langle 1\,3\rangle\,[1\,2]\,\langle 4\,|p_\phi|\,3]\,\langle 4\,|p_\phi|\,1]}{s_{123}[1\,3]^2\,\langle 2\,3\rangle\,[2\,3]} + \frac{1}{2}\frac{\langle 4\,|p_\phi|\,1]^2\,[2\,3]}{[1\,3]^3 s_{123}}\Big]\;\hat{L}_0(s_{123},s_{23})
\end{aligned}$$

$$
\begin{aligned}
&- \frac{1}{2}\frac{\Big(\langle 1\,3\rangle\,[1\,2]\,\langle 4\,|p_\phi|\,3]\Big)^2}{[1\,3]\,[2\,3]\,s_{123}}\;\hat{L}_2(s_{123},s_{12})\\
&- \langle 3\,4\rangle\,[1\,2]\,\langle 4\,|p_\phi|\,3]\,\frac{(-2\,\langle 1\,3\rangle\,[1\,3]-\langle 2\,3\rangle\,[2\,3])}{\langle 2\,3\rangle\,[1\,3]^2\,[2\,3]}\;\hat{L}_1(s_{123},s_{12})\\
&+ [1\,2]\,\langle 4\,|p_\phi|\,3]\,\frac{\langle 2\,3\rangle\,\langle 4\,|p_\phi|\,2]+2\,\langle 1\,3\rangle\,\langle 4\,|p_\phi|\,1]}{[1\,3]^2\,\langle 2\,3\rangle\,[2\,3]\,s_{123}}\;\hat{L}_0(s_{123},s_{12})\\
&+ R^R(\phi,1_{\overline{q}}^-,2_q^+,3_g^-,4_g^-)\,,
\end{aligned}
\tag{5.29}
$$

with

$$
V^R \;=\; -\frac{1}{\epsilon^2}\left(\frac{\mu^2}{-s_{12}}\right)^\epsilon - \frac{3}{2\epsilon}\left(\frac{\mu^2}{-s_{12}}\right)^\epsilon - \frac{7}{2} - \frac{\delta_R}{2}\,. \tag{5.30}
$$

The remaining rational pieces in Eq. (have the following form:

$$
\begin{aligned}
R^R(\phi,1_{\overline{q}}^-,2_q^+,3_g^-,4_g^-) = &-\frac{\langle 2\,4\rangle^2\,[2\,1]^2}{2\,\langle 2\,3\rangle\,[3\,1]^3} + \frac{\langle 4\,|p_\phi|\,3]^2\,[2\,1]^2}{2s_{123}\,[3\,1]^3\,[3\,2]} - \frac{\langle 1\,4\rangle^2\,[2\,1]}{2\,\langle 1\,2\rangle\,[3\,1]\,[3\,2]}\\
&+\frac{[2\,1]\left(\langle 1\,3\rangle^2\,\langle 2\,3\rangle\,\langle 4\,|p_\phi|\,3]^2\,[3\,1]^2+\langle 1\,2\rangle^3\,\langle 4\,|p_\phi|\,1]^2\,[2\,1]\,[3\,2]\right)}{4s_{123}^2\,\langle 1\,2\rangle\,\langle 2\,3\rangle\,[3\,1]^3\,[3\,2]}\\
&+\frac{\langle 3\,|p_\phi|\,2]^2}{2s_{124}\,[4\,1]\,[4\,2]} - \frac{\langle 1\,3\rangle^2\,[2\,1]}{2\,\langle 1\,2\rangle\,[4\,1]\,[4\,2]} + \frac{\langle 1\,4\rangle^2\,\langle 3\,|p_\phi|\,4]^2\,[2\,1]}{4s_{124}^2\,\langle 1\,2\rangle\,[4\,1]\,[4\,2]}\\
&+\frac{\langle 1\,3\rangle\,\langle 1\,4\rangle\,[4\,2]}{2\,\langle 1\,|p_\phi|\,4]\,[4\,3]} + \frac{s_{234}\,\langle 1\,4\rangle^2\,[4\,2]^2}{4\,\langle 2\,3\rangle\,\langle 1\,|p_\phi|\,4]\,[3\,2]^2\,[4\,3]} + \frac{\langle 1\,4\rangle^2\,[4\,2]^2}{2\,\langle 1\,|p_\phi|\,4]\,[3\,2]\,[4\,3]}\,.
\end{aligned}
\tag{5.31}
$$

$A_4^{\rm f}(\phi,1_{\overline{q}}^-,2_q^+,3_g^-,4_g^-)$

The fermion loop contribution is,

$$
\begin{aligned}
-iA_4^{\rm f}(\phi,1_{\overline{q}}^-,2_q^+,3_g^-,4_g^-) \;=\; &-iA_4^{(0)}(\phi,1_{\overline{q}}^-,2_q^+,3_g^-,4_g^-)\times\left[-\frac{2}{3\epsilon}\left(\frac{\mu^2}{-s_{12}}\right)^\epsilon-\frac{10}{9}\right]\\
&-\frac{2}{3}\langle 1\,3\rangle^2\,\langle 3\,4\rangle\,[1\,2]\,\langle 4\,|p_\phi|\,3]\;\hat{L}_3(s_{123},s_{12}) - \frac{2}{3}\langle 1\,4\rangle^2\,\langle 3\,4\rangle\,[1\,2]\,\langle 3\,|p_\phi|\,4]\;\hat{L}_3(s_{124},s_{12})\\
&-\frac{1}{3}\,\langle 1\,3\rangle\,\langle 3\,4\rangle\,\langle 4\,|p_\phi|\,2]\;\hat{L}_2(s_{123},s_{12}) - \frac{1}{3}\,\langle 1\,4\rangle\,\langle 3\,4\rangle\,\langle 3\,|p_\phi|\,2]\;\hat{L}_2(s_{124},s_{12})\\
&-\frac{2}{3}\frac{\langle 1\,3\rangle\,\langle 4\,|p_\phi|\,2]^2}{\langle 1\,2\rangle\,[2\,3]\,[1\,2]}\;\hat{L}_1(s_{123},s_{12}) + \frac{2}{3}\frac{\langle 1\,4\rangle\,\langle 3\,|p_\phi|\,2]^2}{\langle 1\,2\rangle\,[2\,4]\,[1\,2]}\;\hat{L}_1(s_{124},s_{12})\\
&+\frac{2}{3}\frac{\langle 1\,3\rangle\,\langle 4\,|p_\phi|\,2]^2}{\langle 1\,2\rangle\,[1\,2]\,[2\,3]\,s_{123}}\;\hat{L}_0(s_{123},s_{12}) + \frac{2}{3}\frac{(s_{12}+s_{14})\langle 3\,|p_\phi|\,2]^2}{\langle 1\,2\rangle\,[1\,4]\,[2\,4]\,[1\,2]\,s_{124}}\;\hat{L}_0(s_{124},s_{12})\\
&+\frac{\langle 1\,3\rangle\,\langle 3\,4\rangle\,\langle 4\,|p_\phi|\,2]}{6\,\langle 1\,2\rangle\,[1\,2]\,s_{123}} + \frac{\langle 1\,4\rangle\,\langle 3\,4\rangle\,\langle 3\,|p_\phi|\,2]}{6\,\langle 1\,2\rangle\,[1\,2]\,s_{124}} - \frac{1}{3}\frac{\langle 1\,3\rangle\,\langle 1\,4\rangle}{\langle 1\,2\rangle\,[3\,4]}\,.
\end{aligned}
\tag{5.32}
$$

Relation for rational terms

We note that the rational terms in the three leading colour primitive amplitudes obey,

$$\mathcal{R}\Big\{ A_4^L(\phi, 1_{\bar{q}}, 2_q, 3_g, 4_g) + A_4^R(\phi, 1_{\bar{q}}, 2_q, 3_g, 4_g) + A_4^{\rm f}(\phi, 1_{\bar{q}}, 2_q, 3_g, 4_g) \Big\} + 2A_4^{(0)}(\phi^\dagger, 1_{\bar{q}}, 2_q, 3_g, 4_g) = 0 \,, \tag{5.33}$$

a formula analogous to that found in super-symmetric decompositions of QCD amplitudes [117]. This property is helicity independent and has also been checked for the previously known MHV amplitudes [109]. For the NMHV helicity assignment at hand, namely $(1_{\bar{q}}^-, 2_q^+, 3_g^-, 4_g^-)$, we note that the tree graph result that appears in Eq. (5.33) is zero (c.f. Eq. (5.11)). We stress that the $\mathcal{R}$ operation extracts the full rational term, including completion terms from the functions $\hat{L}_3$ and $\hat{L}_2$. Thus it corresponds to dropping all logarithms, box functions and V-functions.

We conclude this section by noting that the three primitive amplitudes for the helicity assignment $(1_{\bar{q}}^-, 2_q^+, 3_g^+, 4_g^+)$ also satisfy Eq. (5.33). For these amplitudes, which are purely rational, the $\mathcal{R}$ operation leaves the amplitude unchanged.

5.2.2 Results for $A_{4;3}(\phi, 1_{\bar{q}}, 2_q, 3_g^-, 4_g^-)$

We can calculate the result for $A_{4;3}$ using Eq. (5.5). Given the results for A_L^4 and A_R^4 in the previous section the only missing ingredient is $A_4^L(\phi, 1_{\bar{q}}^-, 2_g^-, 3_q^+, 4_g^-)$.

Box-related terms for $A_4^L(\phi, 1_{\bar{q}}^-, 2_g^-, 3_q^+, 4_g^-)$

The calculation of the box-related terms in $\phi\bar{q}gqg$ $(--+-)$ is easily performed using the methods given in ref. [120]. The result is,

$$\begin{aligned} -iA_4^{L,\rm box}(\phi, 1_{\bar{q}}^-, 2_g^-, 3_q^+, 4_g^-) \;&=\; -iA_4^{(0)}(\phi, 1_{\bar{q}}^-, 2_g^-, 3_q^+, 4_g^-) \times V_4^L \\ + \frac{1}{2}\Bigg(& \frac{\langle 1\,2\rangle^2 m_\phi^4}{\langle 1\,|p_\phi|\,4]\,\langle 3\,|p_\phi|\,4]\,s_{123}}\,{\rm F}_{\rm 4F}^{\rm 1m}(s_{12}, s_{23}; s_{123}) - \frac{\langle 2\,|p_\phi|\,3]^2}{[1\,4]\,[3\,4]\,s_{134}}\,{\rm F}_{\rm 4F}^{\rm 1m}(s_{14}, s_{34}; s_{134}) \\ - & \frac{[3\,4]^2\,\langle 1\,|p_\phi|\,2]^2}{[3\,2]\,[2\,4]^3\,\langle 1\,|p_\phi|\,4]}\,{\rm F}_{\rm 4F}^{\rm 1m}(s_{23}, s_{34}; s_{234}) - \frac{s_{124}^2}{[1\,2]\,[2\,4]\,\langle 3\,|p_\phi|\,4]}\,{\rm F}_{\rm 4F}^{\rm 1m}(s_{12}, s_{14}; s_{124}) \end{aligned}$$

$$
\begin{aligned}
&- \frac{\langle 3\,|p_\phi|\,1]\, s_{124}^2}{[1\,2]\,[1\,4]\,\langle 3\,|p_\phi|\,4]\,\langle 3\,|p_\phi|\,2]}\,\mathrm{F}_{4\mathrm{F}}^{2\mathrm{mh}}(s_{23}, s_{124}; s_{14}, m_\phi^2) \\
&+ \frac{\langle 1\,|p_\phi|\,3]^3}{[2\,3]\,[3\,4]\,\langle 1\,|p_\phi|\,4]\,\langle 1\,|p_\phi|\,2]}\,\mathrm{F}_{4\mathrm{F}}^{2\mathrm{mh}}(s_{12}, s_{234}; s_{34}, m_\phi^2) \\
&+ \frac{1}{s_{123}}\left[\frac{m_\phi^4 \langle 1\,2\rangle^2}{\langle 3\,|p_\phi|\,4]\,\langle 1\,|p_\phi|\,4]} + \frac{\langle 4\,|p_\phi|\,3]^2}{[1\,2]\,[2\,3]}\right] \\
&\times \left[\mathrm{F}_{4\mathrm{F}}^{2\mathrm{mh}}(s_{34}, s_{123}; s_{12}, m_\phi^2) + \mathrm{F}_{4\mathrm{F}}^{2\mathrm{mh}}(s_{14}, s_{123}; s_{23}, m_\phi^2)\right]\Bigg)\,, \qquad (5.34)
\end{aligned}
$$

with

$$
V_4^L \;=\; -\frac{1}{\epsilon^2}\left[\left(\frac{\mu^2}{-s_{34}}\right)^\epsilon + \left(\frac{\mu^2}{-s_{41}}\right)^\epsilon\right] + \frac{1}{3\epsilon}\left(\frac{\mu^2}{-s_{123}}\right)^\epsilon + \frac{7}{4} - \frac{\delta_R}{3}\,. \qquad (5.35)
$$

As we shall see in the next section, no further information is required for the calculation of the $A_{4;3}$ which is completely determined by box diagrams alone.

Full result for $A_{4;3}$

The full result for the partial amplitude $A_{4;3}$ is,

$$
\begin{aligned}
-\;& iA_{4;3}(\phi, 1_{\bar{q}}^-, 2_q^+, 3_g^-, 4_g^-) = -iA_4^{(0)}(\phi, 1_{\bar{q}}^-, 2_q^+, 3_g^-, 4_g^-) \times V_5(s_{12}, s_{34}, s_{13}, s_{24}) \\
&+ \Bigg\{\frac{1}{2}\Bigg(\frac{1}{s_{123}}\left[\frac{\langle 4\,|p_\phi|\,3]^2\,[1\,2]^2}{[1\,3]^3\,[2\,3]} + \frac{[2\,3]^2\,\langle 4\,|p_\phi|\,1]^3}{[1\,3]^3\,[1\,2]\,\langle 4\,|p_\phi|\,3]} - \frac{m_\phi^4\,\langle 1\,3\rangle^3}{\langle 1\,2\rangle\,\langle 1\,|p_\phi|\,4]\,\langle 3\,|p_\phi|\,4]}\right] \\
&\quad\times \mathrm{F}_{4\mathrm{F}}^{1\mathrm{m}}(s_{12}, s_{23}; s_{123}) \\
&+ \frac{1}{s_{124}}\left[\frac{m_\phi^4\,\langle 1\,4\rangle^2\,\langle 2\,4\rangle}{\langle 1\,2\rangle\,\langle 2\,|p_\phi|\,3]\,\langle 4\,|p_\phi|\,3]} - \frac{\langle 3\,|p_\phi|\,2]^2\,\langle 3\,|p_\phi|\,1]}{[1\,4]\,\langle 3\,|p_\phi|\,4]\,[1\,2]}\right]\mathrm{F}_{4\mathrm{F}}^{1\mathrm{m}}(s_{12}, s_{14}; s_{124}) \\
&+ \frac{1}{s_{123}}\left[\frac{m_\phi^4\,\langle 1\,3\rangle^2}{\langle 1\,|p_\phi|\,4]\,\langle 2\,|p_\phi|\,4]} - \frac{\langle 4\,|p_\phi|\,2]^2}{[1\,3]\,[2\,3]}\right]\mathrm{F}_{4\mathrm{F}}^{1\mathrm{m}}(s_{13}, s_{23}; s_{123}) \\
&- \frac{s_{341}^2}{[1\,3]\,[3\,4]\,\langle 2\,|p_\phi|\,4]}\left[\mathrm{F}_{4\mathrm{F}}^{1\mathrm{m}}(s_{13}, s_{14}; s_{341}) + \mathrm{F}_{4\mathrm{F}}^{2\mathrm{mh}}(s_{23}, s_{341}, s_{14}, m_\phi^2)\right] \\
&- \frac{s_{341}^2}{[1\,4]\,[3\,4]\,\langle 2\,|p_\phi|\,3]}\left[\mathrm{F}_{4\mathrm{F}}^{1\mathrm{m}}(s_{14}, s_{34}; s_{341}) + \mathrm{F}_{4\mathrm{F}}^{2\mathrm{mh}}(s_{12}, s_{341}, s_{34}, m_\phi^2)\right] \\
&+ \frac{\langle 1\,|p_\phi|\,2]^2}{[2\,3]\,[3\,4]\,\langle 1\,|p_\phi|\,4]}\left[\mathrm{F}_{4\mathrm{F}}^{1\mathrm{m}}(s_{23}, s_{34}; s_{234}) + \mathrm{F}_{4\mathrm{F}}^{2\mathrm{mh}}(s_{12}, s_{234}, s_{34}, m_\phi^2)\right] \\
&- \frac{[2\,4]^2\,\langle 1\,|p_\phi|\,3]^2}{[2\,3]\,[3\,4]^3\,\langle 1\,|p_\phi|\,4]}\,\mathrm{F}_{4\mathrm{F}}^{1\mathrm{m}}(s_{23}, s_{24}; s_{234}) \\
&+ \frac{\langle 1\,|p_\phi|\,2]^2}{\langle 1\,|p_\phi|\,3]\,[2\,4]\,[3\,4]}\,\mathrm{F}_{4\mathrm{F}}^{2\mathrm{mh}}(s_{14}, s_{234}, s_{23}, m_\phi^2)
\end{aligned}
$$

$$
\begin{aligned}
&+\frac{1}{s_{123}}\left[-\frac{m_\phi^4\,\langle 1\,3\rangle^2\,\langle 2\,3\rangle}{\langle 1\,2\rangle\,\langle 2\,|p_\phi|\,4]\,\langle 3\,|p_\phi|\,4]}+\frac{\langle 4\,|p_\phi|\,2]^2}{\langle 4\,|p_\phi|\,3]}\frac{\langle 4\,|p_\phi|\,1]}{[1\,2]\,[1\,3]}\right]\\
&\qquad\times \mathrm{F}^{\mathrm{2mh}}_{\mathrm{4F}}(s_{14},s_{123},s_{23},m_\phi^2)\\
&+\frac{1}{s_{123}}\left[\frac{m_\phi^4\,\langle 1\,3\rangle^3}{\langle 1\,2\rangle\,\langle 3\,|p_\phi|\,4]\,\langle 1\,|p_\phi|\,4]}-\frac{\langle 4\,|p_\phi|\,2]^3}{\langle 4\,|p_\phi|\,3]\,[1\,2]\,[2\,3]}\right]\\
&\qquad\times \mathrm{F}^{\mathrm{2mh}}_{\mathrm{4F}}(s_{24},s_{123},s_{13},m_\phi^2)\\
&+\frac{1}{s_{123}}\left[-\frac{m_\phi^4\,\langle 1\,3\rangle^2}{\langle 2\,|p_\phi|\,4]\,\langle 1\,|p_\phi|\,4]}+\frac{\langle 4\,|p_\phi|\,2]^2}{[1\,3]\,[2\,3]}\right]\mathrm{F}^{\mathrm{2mh}}_{\mathrm{4F}}(s_{34},s_{123},s_{12},m_\phi^2)\Bigg)\Bigg\}\\
&+\Big\{3\leftrightarrow 4\Big\}\,,
\end{aligned}
\tag{5.36}
$$

where the function containing poles and associated logarithms is conveniently written as,

$$
V_5(s_{12},s_{34},s_{13},s_{24})=-\frac{1}{\epsilon^2}\left[\left(\frac{\mu^2}{-s_{12}}\right)^{\epsilon}+\left(\frac{\mu^2}{-s_{34}}\right)^{\epsilon}-\left(\frac{\mu^2}{-s_{13}}\right)^{\epsilon}-\left(\frac{\mu^2}{-s_{24}}\right)^{\epsilon}\right]. \tag{5.37}
$$

We note that the apparent double pole in ϵ in Eq. (5.37) is cancelled upon expanding about $\epsilon = 0$.

This result for the ϕ amplitude is particularly simple, containing neither bubble contributions nor rational terms. This is also true for the helicity amplitude $A_{4;3}(\phi,1_{\bar{q}},2_q,3_g^-,4_g^+)$ [2], which can easily be checked using the previously calculated results in ref. [109]. It is therefore more efficient to program the full result for $A_{4;3}$, rather than to program the individual primitive amplitudes using Eq. (5.5).

Furthermore, for the case of two negative gluon helicities calculated here one can check using Eq. (5.5) that the corresponding $\phi^\dagger$ amplitude is zero. Therefore we have,

$$
A_{4;3}(H,1_{\bar{q}}^-,2_q^+,3_g^-,4_g^-)=iA_{4;3}(A,1_{\bar{q}}^-,2_q^+,3_g^-,4_g^-)=A_{4;3}(\phi,1_{\bar{q}}^-,2_q^+,3_g^-,4_g^-)\,. \tag{5.38}
$$

[2] The amplitude $A_{4;3}(\phi,1_{\bar{q}},2_q,3_g^+,4_g^-)$ is not independent and is obtained by swapping labels 3 and 4.

5.3 Numerical results

Here we present evaluations of the new amplitudes at the same kinematic point as used in the previous chapter (eq. 4.49) and in the literature [104, 109]. We have used a scale $\mu = m_H$, set $\delta_R = 1$ (corresponding to the 't Hooft-Veltman scheme) and, in assembling the amplitude $A_{4;1}$, have used $N_f = 5$. The results for the final Higgs amplitudes presented in Table 5.2 agree with those from the semi-numerical calculation of ref. [104] to one part in 10^8. Note that these results depend on an overall phase that can be removed by dividing out by the corresponding Born calculation. Using the analytic expressions for all the $Hgggg$, $H\bar{q}qgg$ and $H\bar{q}q\bar{q}'q'$ amplitudes that are now available we can also confirm the numerical values for the matrix elements squared given in ref. [104].

5.4 Summary

In this chapter we have computed the last analytically unknown helicity amplitude contributing to the NLO corrections to Higgs plus two jet production at hadron colliders. Once again we used the unitarity method to calculate the cut-constructible pieces of the amplitude, and Feynman diagrams to calculate the entire rational part. We verified our results using the semi-numerical code of [104]. The analytic calculations needed for this thesis are hence complete and in the next chapter we turn our attention to using the results to perform some phenomenology.

	$(\phi, 1_{\bar{q}}^-, 2_q^+, 3_g^-, 4_g^-)$			$(\phi^\dagger, 1_{\bar{q}}^-, 2_q^+, 3_g^-, 4_g^-)$
	$1/\epsilon^2$	$1/\epsilon$	ϵ^0	ϵ^0
$A_4^{(0)}$	0	0	$+6.49907535901$ $-2.39308144816\,i$	0
A_4^L	-19.49722607702 $+7.17924434447\,i$	-64.62496304875 $-45.76112071571\,i$	-31.60558356648 $-137.56039301452\,i$	-17.35549203005 $+6.14361664194\,i$
A_4^R	-6.49907535901 $+2.39308144816\,i$	-23.12631834140 $-14.67020390044\,i$	-48.74190400225 $-39.06265552875\,i$	$+4.58546771410$ $-1.38718545292\,i$
A_4^f	0	-4.33271690600 $+1.59538763210\,i$	-14.98058321393 $-9.88874973495\,i$	-0.22812640212 $+0.02973170727\,i$
$A_{4;1}$	-18.77510659269 $+6.91334640579\,i$	-69.27656696526 $-41.47211867326\,i$	-51.15745514499 $-149.70134751402\,i$	-18.24519911293 $+6.34730120438\,i$
$A_{4;3}$	0	$+2.61083477136$ $-0.05119106396\,i$	$+17.75737443413$ $+4.93097014463\,i$	0

Table 5.2: Numerical values of $\phi\bar{q}qgg$ and $\phi^\dagger\bar{q}qgg$ primitive amplitudes (above) and the amplitudes multiplying the two different colour structures (below), at the kinematic point defined in eq. (4.49).

Chapter 6

Phenomenological Studies

6.1 Introduction

In this chapter we present phenomenological results for the production of a Higgs boson in association with two jets. From chapter 1 we recall that our calculation is performed at next-to-leading order (NLO) using an effective Lagrangian to express the coupling of gluons to the Higgs field [65],

$$\mathcal{L}_H^{\rm int} = \frac{C}{2} H \ {\rm tr}\, G_{\mu\nu}\, G^{\mu\nu}\,, \tag{6.1}$$

where the trace is over the color degrees of freedom. At the order required in this paper, the coefficient C is given in the $\overline{\rm MS}$ scheme by [64, 72],

$$C = \frac{\alpha_S}{6\pi v}\Big(1 + \frac{11}{4\pi}\alpha_S\Big) + \mathcal{O}(\alpha_S^3),\ . \tag{6.2}$$

where v is the vacuum expectation value of the Higgs field, $v = 246$ GeV.

This effective Lagrangian replaces the full one-loop coupling of the Higgs boson to the gluons via an intermediate top quark loop by an effective local operator. This approximation is valid in the limit $m_H < 2m_t$ and, in the presence of additional jets, when the transverse momenta of the jets is not much larger than the top mass m_t [66]. A commonly used improvement of the effective Lagrangian approximation is to multiply the resulting differential jet cross section by a ratio R given by,

$$R = \frac{\sigma_{\text{finite } \mathrm{m_t}}(gg \to H)}{\sigma_{m_t\to\infty}(gg \to H)}\,, \tag{6.3}$$

where $\sigma(gg \to H)$ is the total cross section. Setting $x = 4m_t^2/m_H^2$ the correction for the finite mass of the top quark in the region $x > 1$ is [72],

$$R = \left[\frac{3x}{2}\Big(1 - (x-1)\Big[\sin^{-1}\frac{1}{\sqrt{x}}\Big]^2\Big)\right]^2 . \tag{6.4}$$

This quantity when used to normalise an effective theory cross section provides a good approximation of the cross section from the full theory, see Ref. [66] and references therein. However for the case of Higgs + 1 jet it has been found that the effect of bottom quark loops and additional electroweak diagrams can also be important [92] and these effects should also be included. Our numerical results for the Higgs cross section will not include the rescaling of Eqs. (6.3,6.4).

6.2 Improvements from the semi-numeric code

The phenomenology of the production of a Higgs boson in association with two jets has been presented in Ref. [104, 105] for the case of the LHC operating at $\sqrt{s} =$ 14 TeV. The NLO analysis in that paper was based on real matrix elements for the Higgs+5 parton processes given in Ref. [209], supplemented by the results of Ref. [95, 146] in the cases where these latter results lead to more efficient code. In Ref. [105] the virtual matrix element corrections for the Higgs + 4 parton process were taken from Ref. [104]. For the $Hgggg$ and $Hq\bar{q}gg$ sub-processes the virtual corrections were based on a semi-numerical technique [211], whilst the matrix elements squared for the one-loop processes $Hq\bar{q}q'\bar{q}'$ and $Hq\bar{q}q\bar{q}$ were given analytically in Ref. [104].

In the three years since Ref. [105] was published a great deal of effort has been devoted to the *analytic* calculation of one-loop corrections to Higgs + n-parton amplitudes, with particular emphasis on the $n = 4$ amplitudes which are relevant for this study. The complete set of one-loop amplitudes for all Higgs + 4 parton processes is now available and analytic expressions can be found in the following references:

- $Hgggg$: (Chapter 3, Chapter 4) Refs. [106–108, 206, 208];
- $H\bar{q}qgg$: (Chapter 5) Refs. [109, 212];

- $H\bar{q}q\bar{Q}Q$: Ref. [109].

These new analytic results have now been included in the MCFM package, version 5.7 (which may be downloaded from `mcfm.fnal.gov`), leading to a considerable improvement in the speed of the code. For the processes involving two quark-antiquark pairs, the matrix elements squared given in Ref. [104] are implemented in MCFM, rather than the amplitudes of Ref. [109], because they lead to faster code. The values of the amplitudes calculated by the new analytic code and the previous semi-numerical code [105] are in full numerical agreement for all amplitudes.

The improvement in the performance of our numerical code means that it is appropriate to revisit the phenomenology of Higgs + 2 jet production and to extend it in a number of ways. The improvement in the speed of the code means that it is possible to include the decays of the Higgs boson, specifically for the processes:

$$h_1 + h_2 \to H + j_1 + j_2 \to \tau^+ + \tau^- + j_1 + j_2 \tag{6.5}$$

$$h_1 + h_2 \to H + j_1 + j_2 \to b + \bar{b} + j_1 + j_2 \tag{6.6}$$

$$\begin{aligned} h_1 + h_2 \to H + j_1 + j_2 \;\; &\to \;\; W^- + W^+ + j_1 + j_2 \\ &\qquad\quad \big| \qquad \big\lfloor \to \nu + e^+ \\ &\qquad\quad \big\lfloor \to e^- + \bar{\nu} \end{aligned} \tag{6.7}$$

$$\begin{aligned} h_1 + h_2 \to H + j_1 + j_2 \;\; &\to \;\; Z + Z + j_1 + j_2 \\ &\qquad\quad \big| \qquad \big\lfloor \to e^- + e^+ \\ &\qquad\quad \big\lfloor \to \mu^- + \mu^+ \end{aligned} \tag{6.8}$$

where h_1, h_2 represent partons inside the incident hadron beams. All four of these processes are included in MCFM v5.7.

6.3 Parameters

Throughout this paper we make use of the MSTW2008 parton distribution functions [22], using the LO fit ($\alpha_s(M_Z) = 0.13939$ and 1-loop running) for the lowest order calculation and the NLO fit ($\alpha_s(M_Z) = 0.12018$ and 2-loop running) at NLO.

The W mass and width are chosen to be,

$$m_W = 80.398 \text{ GeV}, \qquad \Gamma_W = 2.1054 \text{ GeV} . \tag{6.9}$$

The mass is taken from Ref. [56]. The total width given in Eq. (6.9) is derived from the measured branching ratio for $W \to \ell\bar{\nu}$, $10.80 \pm 0.09\%$ [56] by using a lowest order calculation of the partial width,

$$\Gamma(W \to \ell\bar{\nu}) = \frac{G_F}{\sqrt{2}} \frac{m_W^2}{6\pi} . \tag{6.10}$$

This ensures that our calculation incorporates the best possible value for the W branching ratio which is determined to about 1%. The values of the total Higgs width are taken from the program `hdecay` [213], version 3.51.

To define the jets we perform clustering according to the k_T algorithm [32], with jet definitions detailed further below.

6.4 Tevatron results

We use a very simple set of inclusive cuts, with no requirements on the Higgs boson decay products,

$$p_t(\text{jet}) > 15 \text{ GeV}, \qquad |\eta_{\text{jet}}| < 2.5, \qquad R_{\text{jet,jet}} > 0.4 . \tag{6.11}$$

At the Tevatron the search for the Higgs boson has been divided into jet bins. To set the stage for this we show in Table 6.1 the expected cross section in each bin due to the gluon fusion mechanism. The parameter μ is the renormalization and factorization scale, which we set equal to m_H here. We note that next-to-next-to-leading order (NNLO) results for the Higgs + 0 jet cross section are given in [214], based on the earlier calculations in Refs. [78, 79, 81]. From table 6.1 columns 3 and 5, we see that the Higgs + ≥ 2 jets bin constitutes about 13% of the cross section for $|\eta_{\text{jet}}| < 2.5$ and 11% with $|\eta_{\text{jet}}| < 2$.

It is interesting to compare the number for the fraction of Higgs + ≥ 2 jet events ($|\eta_{\text{jet}}| < 2$) with the percentage extracted from Table 2 of [214], which is quoted

	$\lvert\eta_{\rm jet}\rvert < 2.5$		$\lvert\eta_{\rm jet}\rvert < 2$	
Process	σ_{LO} [fb]	σ_{NLO} [fb]	σ_{LO} [fb]	σ_{NLO} [fb]
Higgs + 0 jets	1.25	1.98	1.25	2.05
Higgs + 1 jets	0.84	1.16	0.74	1.07
Higgs + $\geq$ 2 jets	0.35	0.48	0.28	0.39

Table 6.1: Cross section for Higgs + jet production and decay into $W^-(\to \mu^-\bar{\nu})W^+(\to \nu e^+)$ at $\sqrt{s} = 1.96$ TeV for $M_H = \mu = 160$ GeV. In the second and third columns, only the cuts of Eq. (6.11) are applied. For the results in the final two columns the more stringent cut, $|\eta_{\rm jet}| < 2$ is applied, in order to allow a comparison with Ref. [214].

as 4.9%. Our number is deficient in that it does not include NNLO corrections to the Higgs + 0 jet rate. Our calculation treats all jet bins consistently at NLO. The inclusion of the NNLO correction to the Higgs + 0 jet bin will reduce our number. On the other hand, the calculation of Ref. [214] is deficient because it does not treat all bins consistently at NNLO, i.e. it does not include NNLO corrections for the Higgs +1 jet rate or NLO+NNLO effects for the Higgs + $\geq$ 2 jet rate. We roughly estimate that including the NNLO effects in the Higgs +0 jet bin would move our central value from 11% to 10%. Overall, because the corrections are quite substantial, the theoretical estimate of the fraction of events in the Higgs + $\geq$ 2 jet bin is quite uncertain.

Despite the fact that the fraction of events in the Higgs + $\geq$ 2 jet bin is small, it is important because the associated uncertainty is large. We investigate this issue in Table 6.2, where we give the cross section for the process of Eq. (6.7) using a selection of values for the Higgs mass of current interest for the Tevatron. In the table we give the results for the leading order and next-to-leading order cross sections, calculated using LO and NLO MSTW2008 PDFs respectively. For the range of Higgs masses considered, the QCD corrections increase the cross section by approximately 40% (for the central value, $\mu = m_H$). The theoretical error is estimated by varying the common renormalization and factorization scale in the

m_H [GeV]	150	160	165	170	180
Γ_H [GeV]	0.0174	0.0826	0.243	0.376	0.629
σ_{LO} [fb]	$0.329^{+92\%}_{-45\%}$	$0.345^{+92\%}_{-44\%}$	$0.331^{+92\%}_{-44\%}$	$0.305^{+92\%}_{-44\%}$	$0.245^{+91\%}_{-44\%}$
σ_{NLO} [fb]	$0.447^{+37\%}_{-30\%}$	$0.476^{+35\%}_{-31\%}$	$0.458^{+36\%}_{-31\%}$	$0.422^{+41\%}_{-30\%}$	$0.345^{+37\%}_{-31\%}$
R	1.098 ± 0.003	1.113 ± 0.003	1.122 ± 0.004	1.130 ± 0.005	1.149 ± 0.005

Table 6.2: Cross section for Higgs + 2 jet production and decay into $W^-(\to \mu^-\bar{\nu})W^+(\to \nu e^+)$ at $\sqrt{s} = 1.96$ TeV. Only the cuts of Eq. (6.11) are applied. The correction factor for each Higgs mass, given by Eq. (6.4), is also shown.

range, $m_H/2 < \mu < 2m_H$. As can be seen from the table, even though including the next-to-leading order corrections leads to a considerable improvement in the theoretical error, the remaining error is still quite sizeable. We do not include a factor to correct for the finite top mass, but in order to facilitate comparison with other calculations we also tabulate this factor R (computed using Eq. (6.4)) using a value for the top quark mass of $m_t = 172.5 \pm 2.5$ GeV.

In the spirit of Ref. [214], we can now estimate the theoretical uncertainty on the number of Higgs signal events originating from gluon fusion. By using the fractions of the Higgs cross section in the different multiplicity bins taken from Ref. [215], we can update Eq. (4.3) of Ref. [214] (for a Higgs boson of mass 160 GeV) with,

$$\frac{\Delta N_{\text{signal}}(\text{scale})}{N_{\text{signal}}} = 60\% \cdot \binom{+5\%}{-9\%} + 29\% \cdot \binom{+24\%}{-23\%} + 11\% \cdot \binom{+35\%}{-31\%} = \binom{+13.8\%}{-15.5\%} \qquad (6.12)$$

This equation represents the scale variation associated with the Higgs plus 0-, 1- and $\geq$ 2-jet cross sections using NNLO (0-jet) and NLO (1- and 2-jet) PDFs. Each term is weighted by the % of events with the relevant jet multiplicities reported by the CDF collaboration. Only the uncertainty on the Higgs + $\geq$ 2 jet bin has been modified, using the results from Table 6.2. The corresponding determination using the LO uncertainty in the Higgs + $\geq$ 2 jet bin is $(+20,0\%,-16.9\%)$ [214], so this represents a modest improvement in the overall theoretical error.

The correspondence of our results with those of Anastasiou et al. is somewhat obscured by the fact that the total Higgs width used in Ref. [214] is about 7% smaller at $m_H = 160$ GeV than the value given in our Table 6.2. Taking this fact

into account and including the finite top mass correction tabulated in Table 6.2 we find that our NLO Higgs + 1 jet and LO Higgs + 2 jet cross sections in Table 6.1 are in agreement with the corresponding numbers (1.280 and 0.336 fb) from Table 2 of Ref. [214].

6.4.1 Effect of additional search cuts

We also investigate the behaviour of the LO and NLO predictions in the kinematic region relevant for the latest Tevatron Higgs exclusion limits. Therefore, in addition to the jet cuts above, we also consider cuts on the decay products of the $W/W^\star$ that are produced by the Higgs boson. These cuts correspond very closely to a recent CDF analysis [216], although the treatment of lepton acceptance is simplified.

- One of the leptons from the W decays (the "trigger" lepton, ℓ_1) is required to be relatively hard and central, $p_t^{\ell_1} > 20$ GeV, $|\eta^{\ell_1}| < 0.8$ whilst the other (ℓ_2) may be either softer or produced at slightly higher pseudorapidity, $p_t^{\ell_2} > 10$ GeV, $|\eta^{\ell_2}| < 1.1$.

- The invariant mass of the lepton pair is bounded from below (to eliminate virtual photon contributions), $m_{\ell_1\ell_2} > 16$ GeV.

- Each lepton must be isolated. Any jet found by the algorithm that lies within a $\eta - \phi$ distance of 0.4 from a lepton should have a transverse momentum less than 10% of that of the lepton itself.

- The missing transverse momentum – in our parton level study, the sum of the two neutrino momenta – is constrained using the $\not{E}_t^{\rm spec}$ variable defined by [216],

$$\not{E}_t^{\rm spec} = \not{E}_t \sin\left[\min\left(\Delta\phi, \frac{\pi}{2}\right)\right] \ . \tag{6.13}$$

  $\Delta\phi$ is the distance between the $\not{E}_t$ vector and the nearest lepton or jet. We require that $\not{E}_t^{\rm spec} > 25$ GeV.

In Figure 6.1 we see the scale dependence of the LO and NLO cross sections for $m_H = 160$ GeV. The upper two curves show the case of the minimal set of cuts in

Eq. (6.11) and the lower curves show the results when including the Higgs search cuts above. Applying the additional cuts on the Higgs decay products does not change the scale dependence, indicating that the isolation and missing transverse momentum cuts (that are sensitive to additional radiation) do not play an important role. Applying the additional search cuts does not alter the behaviour of the NLO prediction in the Higgs + ≥ 2 jet bin, so that the results presented in the previous section (with no cuts on the Higgs decay products) are sufficient to estimate the percentage theoretical uncertainty.

6.5 LHC results

In order to study the impact of the NLO corrections at the LHC, we adopt a different set of cuts to define the jets. The rapidity range of the detectors is expected to be much broader, allowing for a larger jet separation too, and we choose a somewhat higher minimum transverse momentum,

$$p_t(\text{jet}) > 40 \text{ GeV}, \qquad |\eta_{\text{jet}}| < 4.5, \qquad R_{\text{jet,jet}} > 0.8 \, . \tag{6.14}$$

In this section we do not consider the decay of the Higgs boson for the sake of simplicity.

Since results for this scenario have already been discussed at some length [105], we restrict ourselves to a short survey of the essential elements of the phenomenology at the lower centre-of-mass energy, $\sqrt{s} = 10$ TeV. We present the scale dependence of the LHC cross section for Higgs + 2 jets ($m_H = 160$ GeV) in Figure 6.2. We have also checked the agreement of our calculation with previous results [105] at $\sqrt{s} = 14$ TeV, taking into account the different choice of parton distribution functions used in that reference. As noted in the earlier paper [105], the corrections are quite modest using our central scale choice, $\mu_0 = \mu_H$, increasing the cross section by approximately 15%. Once again, although the scale dependence is much reduced it is still substantial.

For the sake of illustration we have chosen $m_H = 160$ GeV in the study above. To illustrate the effect of the QCD corrections more broadly, in Table 6.3 we give the cross sections for Higgs masses in the range 120 GeV $< m_H <$ 200 GeV. It is

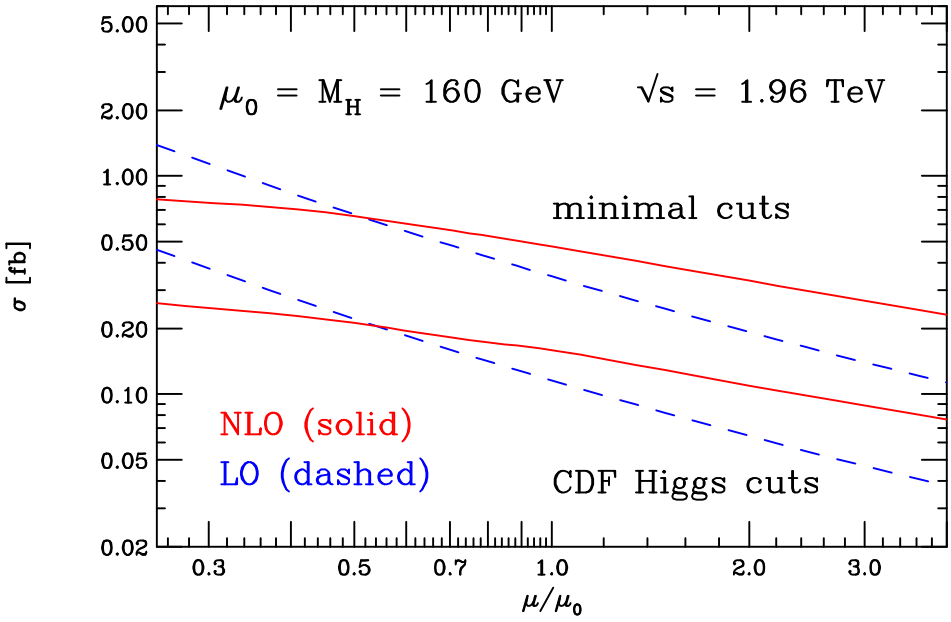

Figure 6.1: Scale dependence for the Higgs + 2 jet cross section, with the Higgs decay into $W^-(\to \mu^-\bar{\nu})W^+(\to \nu e^+)$, at the Tevatron and using the a central scale $\mu_0 = M_H$.Results are shown for the minimal set of cuts in Eq. (6.11) (upper curves) and for cuts that mimic the latest CDF $H \to WW^*$ analysis (lower curves).

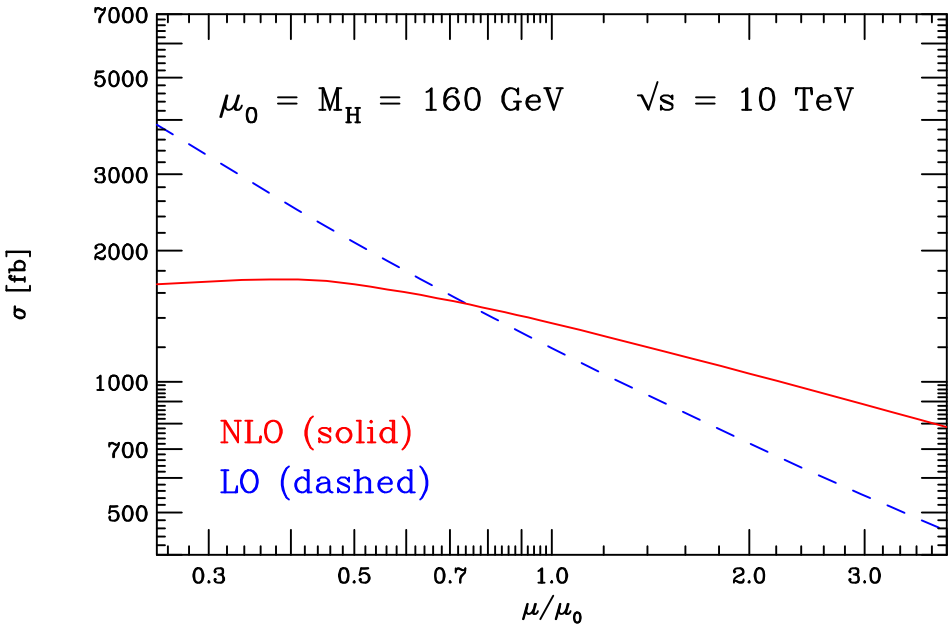

Figure 6.2: Scale dependence for the Higgs boson + 2 jet cross section, using the basic set of cuts in Eq. (6.14) and a central scale choice $\mu_0 = m_H$.

m_H [GeV]	120	140	160	180	200
Γ_H [GeV]	0.0036	0.0083	0.0826	0.629	1.426
σ_{LO} [pb]	$1.88^{+78\%}_{-40\%}$	$1.48^{+76\%}_{-40\%}$	$1.20^{+75\%}_{-40\%}$	$0.98^{+74\%}_{-39\%}$	$0.81^{+73\%}_{-39\%}$
σ_{NLO} [pb]	$1.98^{+20\%}_{-23\%}$	$1.63^{+22\%}_{-23\%}$	$1.36^{+23\%}_{-23\%}$	$1.15^{+24\%}_{-23\%}$	$0.98^{+25\%}_{-24\%}$
R	1.060 ± 0.002	1.084 ± 0.003	1.113 ± 0.004	1.149 ± 0.005	1.191 ± 0.007

Table 6.3: Cross section and uncertainties for Higgs + 2 jet production at $\sqrt{s} = 10$ TeV with the cuts of Eq. (6.14). The correction factor for each Higgs mass, given by Eq. (6.4), is also shown.

$p_t^{\min}$(jet) [GeV]	20	25	30	40	50
σ_{LO} [pb]	3.66	2.62	1.96	1.20	0.79
σ_{NLO} [pb]	4.17	3.02	2.26	1.36	0.88

Table 6.4: Cross section for Higgs + 2 jet production at $\sqrt{s} = 10$ TeV, with $m_H = 160$ GeV and the minimum jet p_t allowed to vary from that specified in Eq. (6.14).

within this range that the Higgs + 2 jet process considered here is of most interest, due to its interplay with the electroweak weak boson fusion channel. We observe that the effect of the QCD corrections increases from about 5% for $m_H = 120$ GeV to 21% for $m_H = 200$ GeV. Estimating the theoretical error in the same way as before, we see that the uncertainty is slightly less at the LHC than at the Tevatron.

It is also interesting to consider the dependence of the cross section on the minimum transverse momentum required for the observed jets. Results for several other values of this threshold, either side of our default value of 40 GeV, are shown in Table 6.4. As can be seen from the table, the percentage effect of the NLO corrections on the total rate is practically independent of the value of $p_t^{\min}$(jet) in the range studied.

6.5.1 Weak boson fusion

As noted above, the process studied in this thesis produces the same final state as expected from Higgs production via weak boson fusion (WBF). Although the elec-

troweak process is expected to dominate once appropriate search cuts are employed, the remaining fraction of events originating from gluon fusion must be taken into account when considering potential measurements of the Higgs coupling to W and Z bosons.

To address this issue, in this section we present a brief study of the rate of events expected using typical weak boson fusion search cuts. In addition to the cuts already imposed (Eq. (6.14)), these correspond to,

$$|\eta_{j_1} - \eta_{j_2}| > 4.2 \,, \qquad \eta_{j_1} \cdot \eta_{j_2} < 0 \,, \tag{6.15}$$

where j_1 and j_2 are the two jets with the highest transverse momenta. These cuts pick out the distinctive signature of two hard jets in opposite hemispheres separated by a large distance in pseudorapidity. This is illustrated in Fig6.3, where we compare the distributions of the jet pseudorapidity difference (without these cuts) in both gluon fusion and weak boson fusion. We note in passing that the shape of this distribution for the weak boson fusion process is slightly altered at NLO, whilst the shape of the prediction for the gluon fusion process is essentially unchanged.

In Fig 6.4 we show the dependence of the cross section on the c.o.m. energy, from $\sqrt{s} = 7$ TeV (corresponding to the initial running in 2010-11) to $\sqrt{s} = 14$ TeV (design expectations). We show the cross section both before and after application of the additional weak boson fusion search cuts given in Eq. (6.15), together with the corresponding results for the WBF process (also calculated using MCFM [99]). The QCD corrections to both processes decrease slightly as $\sqrt{s}$ is increased, whilst the ratio of the gluon fusion to WBF cross sections after the search cuts are applied increases from 20% at 7 TeV to 35% at 14 TeV. This indicates that, viewed as a background to the weak boson fusion process, the hadronic Higgs + 2 jet process is less troublesome at energies below the nominal design value.

6.5.2 Dynamic versus fixed scale choices

We wish to study the effects of different scale choices on our results. It has been noted [179–181] in $W + 3j$ calculations that certain fixed scale choices do a rather poor job

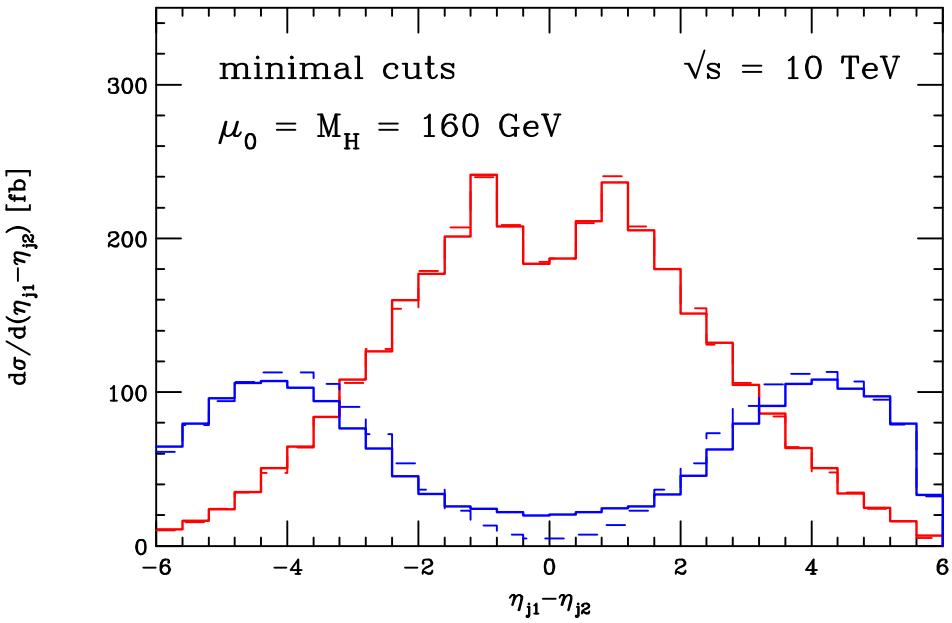

Figure 6.3: The jet pseudorapidity difference in gluon fusion (red) and weak boson fusion (blue). The NLO predictions are shown as solid histograms, while the dashed lines indicate the LO predictions normalized to the corresponding NLO cross sections.

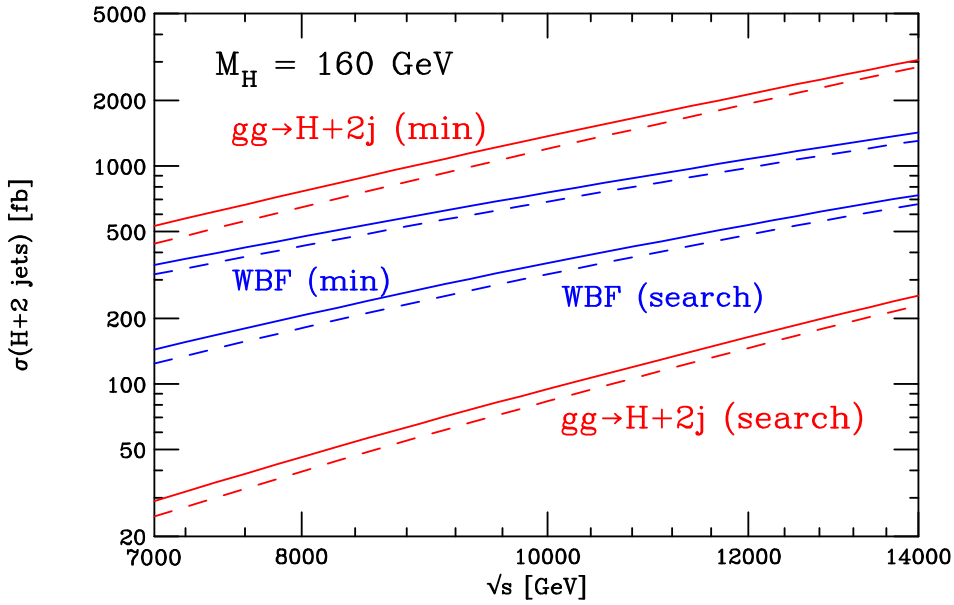

Figure 6.4: The $\sqrt{s}$ dependence of the cross section for $m_H = 160$ GeV at LO (dashed) and NLO (solid). Results are shown for the minimal set of cuts in Eq. (6.14) (two upper red curves) and after application of the additional WBF Higgs search cuts given in Eq. (6.15) (two lower red curves). The cross section for the weak boson fusion process is also shown for comparison (four central blue curves).

of describing Tevatron data. As a result, the dynamic scale H_T was suggested as a safer choice. H_T, or the hotness, is defined as the sum over the transverse energy of the final state particles,

$$H_T = \sum_j E_T^j + E_T^H. \tag{6.16}$$

The motivation for this being a superior scale choice is shown schematically in Fig 6.5. A fixed scale such as m_H may do a good job of describing the physics when the Higgs boson is radiated with a large p_T and the jets are softer in comparison to the Higgs. However when one produces two hard jets and a relatively soft Higgs m_H may not do such a good job of explaining the physics. Dynamic scales, which adjust on an event by event basis, on the other hand, should be able to cope with both sorts of kinematics in a reasonable manner. At the LHC high-p_T jets will be common, and hence the choice of scale could become an even more theoretically important issue than it is today.

To investigate the role of dynamic scales we calculated distributions for p_T and η for the two hardest jets, H_T, at the LHC ($\sqrt{s} = 7$ TeV) using the basic jet cuts of eq. (6.14). The results are shown in Figs. 6.6, 6.7 and 6.8. For the p_T and H_T distributions the dynamic scale choice $\mu = H_T$ preserves the shape of the LO calculation much better than $\mu = m_H$. As expected the deviations in shape (for the p_T distribution) are largest for the high-p_T region. As is also expected, the shape of the pseudorapidity distribution is stable under both scale choices.

We consider bands of scale uncertainty, which can be obtained by calculating cross sections at two different scale choices $\Delta(\mu_1, \mu_2) = [\sigma(\mu_1), \sigma(\mu_2)]$[1]. As is expected, performing a NLO calculation reduces Δ for both scale choices relative to the LO case. It is interesting to note that, when using a dynamic scale, one has to choose lower values μ_1 to obtain $\Delta^{NLO}(\mu_1, \mu_2) \in \Delta^{LO}(\mu_1, \mu_2)$. It is desirable for $\Delta^{NLO}(\mu_1, \mu_2) \in \Delta^{LO}(\mu_1, \mu_2)$ since this indicates that the perturbation series is converging, and further that the scale variation is indicative of the theoretical uncertainty. Typically when using fixed scales a choice of $\mu_1 \sim (0.75 - 0.5)m_i$ will

[1]Here we define $[x_1, x_2]$ to be the continuous region between x_1 and x_2 including endpoints.

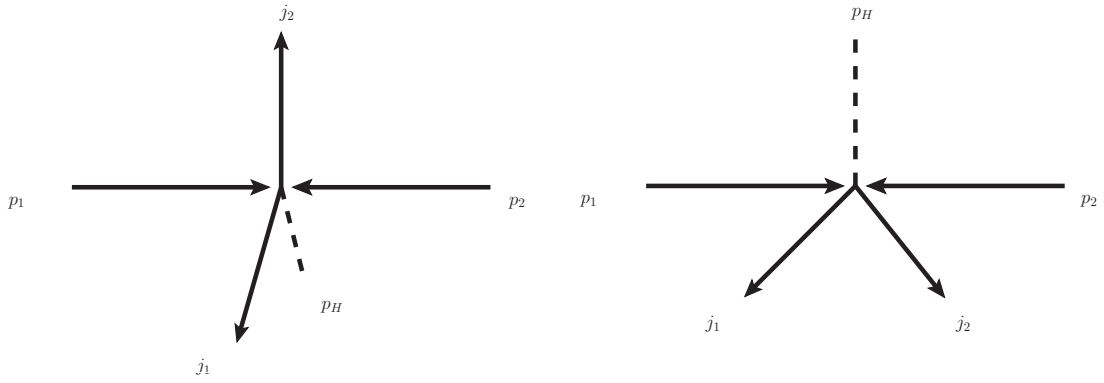

Figure 6.5: Possible momentum configurations in a Higgs plus two jet events. On the left hand diagram two jets are produced with large p_T and the Higgs is a relatively soft in comparison. On the right hand side the Higgs has a high p_T. Whilst $\mu = m_H$ might adequately describe the physics of the second diagram one might not expect it to be a good choice on the left hand side.

ensure that $\Delta^{NLO}(\mu_1, \mu_2) \in \Delta^{LO}(\mu_1, \mu_2)$, whereas to ensure this condition for H_T one finds, $\mu_1 \sim (0.3 - 0.4)H_T$. The results are summarised in Fig. 6.9 and we note that the total variation over the range $\mu_0/4 \leq \mu \leq 4\mu_0$ is roughly equal for both scale choices. What should be noted is that when attempting to estimate the total scale uncertainty for dynamic scales one should use a lower limit of around $H_T/4$ rather than $H_T/2$ (which is often the choice used for fixed scales).

6.5.3 Considerations from the effective theory

We observed in the previous section that the dynamic scale H_T preserved the shapes of the LO distributions for p_T and H_T, whereas the fixed scale m_H failed to do so. We note, however, that typical values of H_T are ~ 350 GeV $\approx 2m_t$. This is precisely the scale at which our effective theory breaks down, therefore one could argue that this scale choice is inappropriate for our calculation. In addition we note that top quark mass effects become important when $p_T > m_t$.

To clarify the situation we investigated the effects of the top mass on the p_T distribution for Higgs plus jet events at the LHC, (for which the full theory result

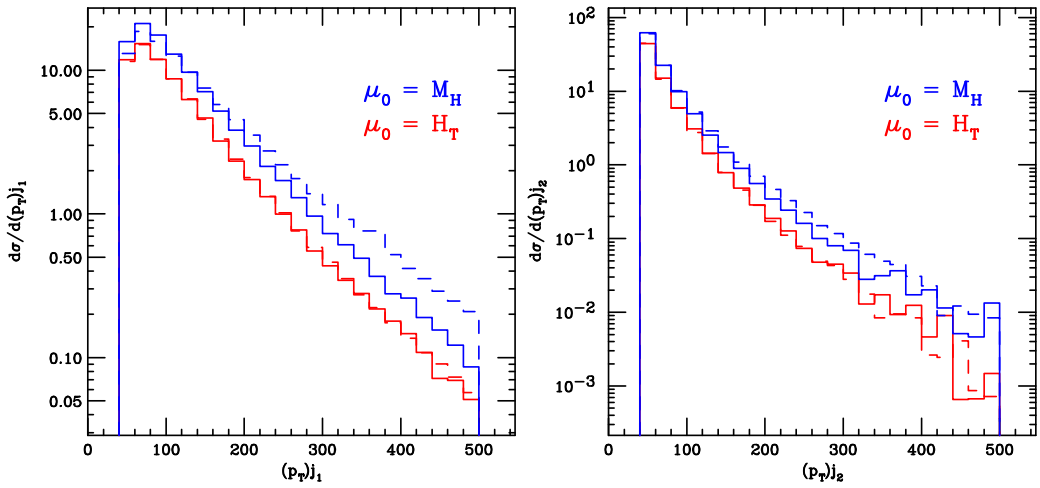

Figure 6.6: p_T distributions for the hardest (left) and second hardest (right) jets. The distribution with a dynamic scale choice $\mu = H_T$ is shown in red, whilst the blue curves represent the fixed scale choice $\mu = m_H$. In both cases the NLO results are represented by a solid line. The dashed line represents the LO distribution, normalised to the NLO cross section.

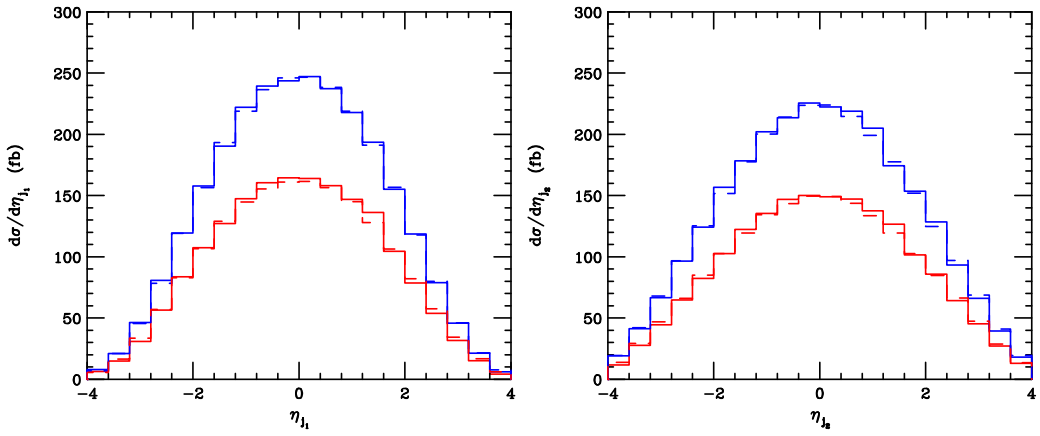

Figure 6.7: Pseudorapidity plots for the two hardest jets using different scale choices. The distribution with a dynamic scale choice $\mu = H_T$ is shown in red, whilst the blue curves represent the fixed scale choice $\mu = m_H$. In both cases the NLO results are represented by a solid line. The dashed line represents the LO distribution, normalised to the NLO cross section.

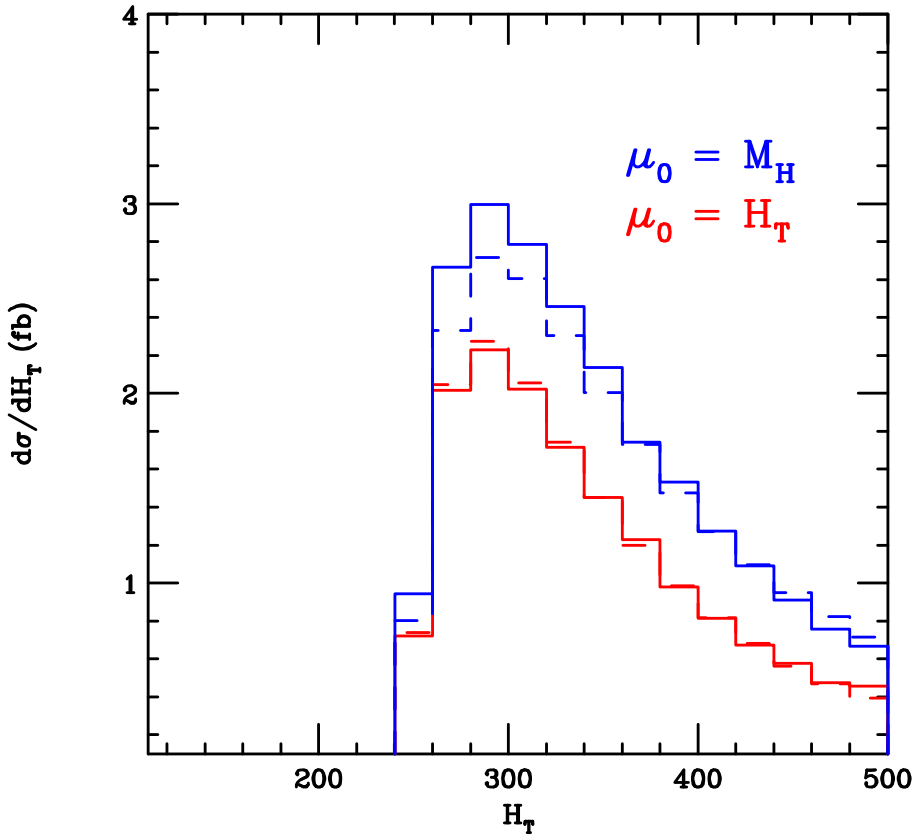

Figure 6.8: The H_T distribution for two different scale choices at the LHC. The distribution with a dynamic scale choice $\mu = H_T$ is shown in red, whilst the blue curves represent the fixed scale choice $\mu = m_H$. In both cases the NLO results are represented by a solid line. The dashed line represents the LO distribution, normalised to the NLO cross section.

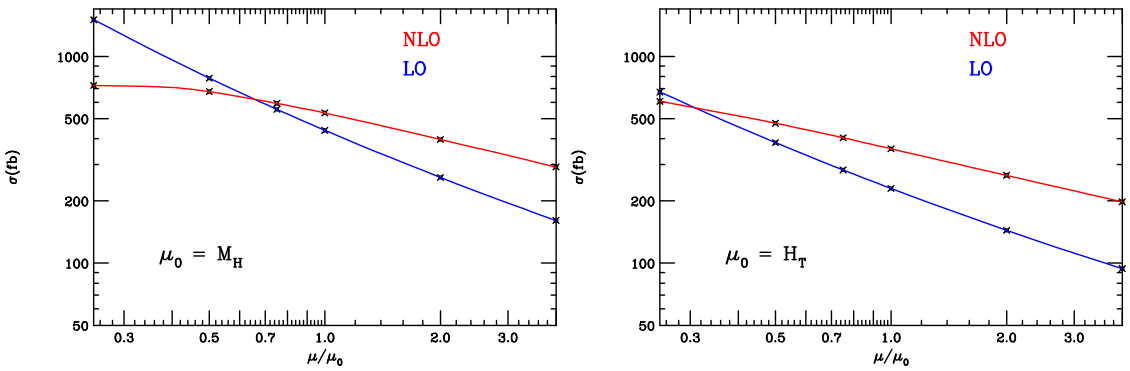

Figure 6.9: Scale variation plots for fixed (left) and dynamic (right) scales, in both cases we vary μ by a factor of 4 in both directions.

at LO and the effective theory result at NLO are both in MCFM). The results are plotted in Fig. 6.10, we have chosen the same jet cuts and $\sqrt{s}$ as the previous section. We have calculated the distributions for $\mu = H_T$ and $\mu = m_H$ at NLO in the effective theory ($m_t \to \infty$) and the LO result for the full (m_t dependent) theory. It is clear that the shape of the top-mass dependent LO result is more closely matched by the fixed order prediction. This is because both the top-mass effects and the fixed scale choice tend to reduce the number of high-p_T jets, whilst the dynamic scale increases them. Therefore, although there may be good physics reasons to motivate using a dynamic scale in general calculations, for calculations involving the Higgs effective theory the major differences between fixed scales and dynamic ones occur in the high-p_T regions. These regions are exactly those in which we expect the LO result to incorrectly predict the shape of distributions. Using a dynamic scale maintains this shape, whereas using a fixed scale has the effect of more closely matching top-mass effects by producing a softer spectrum.

6.6 Summary

In this chapter we have presented phenomenological predictions for the production of a Higgs boson and two jets through gluon fusion. These predictions have been made possible through the implementation of compact analytic results for the relevant 1-loop amplitudes (the most complicated being calculated in Chapters 3,4 and 5) [106–109, 206, 208, 212]. The speed with which these amplitudes can be evaluated has enabled us to improve upon an existing semi-numerical implementation of the same process [105], with various decays of the Higgs boson now included.

We have investigated the behaviour of the NLO cross section at the Tevatron, where contributions from this channel form part of the event sample for the latest Higgs searches [217]. We find that corrections to the event rate in the Higgs + $\geq$ 2 jet bin are modest and that the estimate of the theoretical error is reduced by approximately a factor of two compared to a LO calculation. The resulting error is still rather large, corresponding to approximately +40% and −30% across the region

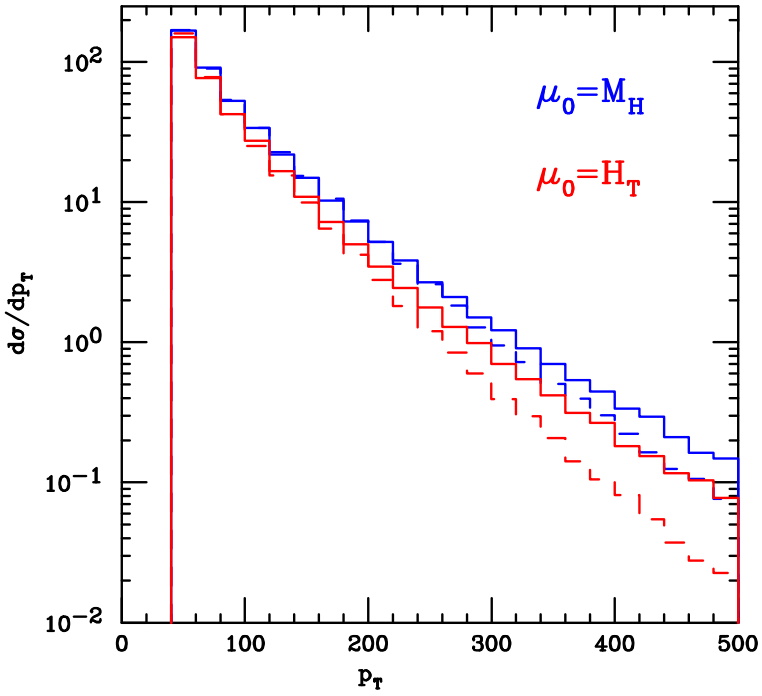

Figure 6.10: p_T distributions for Higgs plus jet events at the LHC $\sqrt{s}$=7 TeV. Shown are the NLO predictions in the effective theory for dynamic and fixed scale choices (solid lines). The dashed lines represent the LO full theory (m_t dependent) which have been normalised to the NLO effective theory cross section, illustrating differences in shape.

of Higgs masses, 150 GeV $< m_H <$ 180 GeV.

For the LHC we have provided a brief study of the behaviour of our predictions for collisions at $\sqrt{s} = 10$ TeV. We have also performed an analysis of this channel in the context of detecting a Higgs boson via weak boson fusion, where the improved theoretical prediction presented in this paper is essential in the long-term for making a measurement of the Higgs boson couplings to W and Z bosons.

We have also investigated the effects of using the dynamic scale H_T in our calculations. We found similar results to [179–181], distributions which are sensitive to high-p_T effects maintained their LO shape if a dynamic scale was used, whereas a fixed scale tended to alter these shapes at NLO. We investigated the potential role of top quark mass effects, and found that in the regions where a dynamic scale had the largest effect were exactly the regions where top mass effects are most important. This suggested that if one wanted to use the effective theory in the high-p_T region a fixed scale choice such as m_H may actually describe the results more accurately.

Chapter 7

Conclusions

In this thesis we have studied the hadronic production of a Higgs boson in association with two jets. At hadron colliders the Higgs is produced copiously through gluon fusion, therefore amplitudes containing a Higgs and additional QCD radiation are important backgrounds to Higgs search channels such as vector boson fusion. Hence knowledge of these amplitudes at Next-to-Leading Order (NLO) in a perturbative expansion in the strong coupling constant is an essential requirement for the LHC and Tevatron. The NLO calculation of Higgs plus two jets has previously been performed semi-numerically [104], however to improve the speed of the code analytic calculations of the amplitudes were desired.

In obtaining compact analytic expressions for the various Higgs plus parton helicity amplitudes we used various ideas from the recent advances in on-shell techniques. These techniques use on-shell tree-level amplitudes to construct one-loop amplitudes. Since tree-level amplitudes are sums of Feynman diagrams, gauge cancellations occur at the beginning of a calculation rather than at the end. Also the factorial growth of the number of Feynman diagrams is severely curtailed leading to a polynomial growth in complexity with increasing multiplicities.

The fundamental concept in generalised unitarity methods is that of multiple cuts together with the use of complex momenta. Multiple cuts allow the isolation of specific coefficients which enter the one-loop basis expansion, resulting in simplifications from the older double-cut analyses. Complex momenta are necessary so that

one can define a non-vanishing three parton amplitude. For real momenta $p_i \cdot p_j = 0$ requires that $\langle ij \rangle = [ij] = 0$. For complex momenta however, the conjugate spinors are independent variables such that **either** $\langle ij \rangle = 0$ or $[ij] = 0$.

This idea was first applied to four-cuts in Ref. [120] which allowed entire amplitudes in $\mathcal{N} = 4$ SYM to be calculated. In four-dimenions a quadruple cut freezes the loop momenta, such that extracting the coefficient of a box integral becomes an algebraic operation. These methods have since been extended to include the extraction of triangle coefficients from triple cuts [122]. Here one cannot completely freeze the loop momentum since there are now only three constraints. As such the loop momenta becomes dependent on a single parameter, cut box diagrams contribute extra propagators in this parameter and therefore enter the Laurent expansion as residues. The remaining pieces have a polynomial dependence in the parameter and, with suitable definitions, the extraction of the triangle coefficient is algorithmic.

Although complex momenta are not strictly necessary for double cuts (since a three vertex which vanishes for real momenta will correspond to the cut of a massless bubble) ideas from multiple cuts filtered down to the two cut level. The Laurent expansion method [122] again works in an algorithmic way to extract bubble coefficients. However, the formulae from this method often are more complicated than those obtained from spinor integration [123, 132]. This method reduces the extraction of bubble coefficients to taking residues.

When four-dimensional cuts are applied a vital piece of the amplitude is missed. These cut-unconstructible pieces are called rational pieces, since they possess no discontinuities in physical invariants. On-shell methods have been developed to obtain these pieces, such as the unitarity bootstrap [124, 161–165] , which uses the BCFW recursion relations [140, 141]. We used the unitarity bootstrap to obtain a formula for the rational pieces for the ϕ-MHV amplitude in chapter 3. However, for the calculation of ϕ-NMHV amplitudes (chapters 4 and 5), we found it easiest to work directly with Feynman diagrams.

Upon completing the analytic calculation of Higgs plus four parton amplitudes these were implemented into MCFM (chapter 6). This program, which is pub-

licly available, performs the NLO calculation of cross-sections. The user can define cuts for the external particles as required. Using this program we performed some phenomenology relevant for the Tevatron and the LHC. We observed that when experimentalists choose exclusive final states with specific numbers of jets, such as CDF have done in their recent $gg \to H \to WW^*$ studies . [215], one naturally encounters $H + 2$ jets. Higgs production through gluon fusion has been calculated through to NNLO [78, 79, 81], but when one explicitly selects two jets in the event it is inappropriate to use NNLO α_S running and PDF's. Rather, one should match these to the order in which the amplitude has been calculated in perturbation theory. In our case this is NLO therefore, we were able to improve the LO scale uncertainty [214]. We also studied some phenomenology at the LHC. We compared the gluon- and vector-boson fusion cross sections before and after VBF cuts finding that the ratio between the cross sections (after the cuts have been applied) shrinks as the centre of mass energy grows. We also studied the scale variation and minimum jet p_T dependence at the LHC. Finally we investigated the role of dynamic and fixed scales, finding that dynamic scales preserve the shape of leading order distributions. We observed, however, that this preservation in the high-p_T region may actually be undesirable since it is in this region that the effective theory LO distributions show deviations in shape due to top-mass effects.

It is hoped that the code will be of use to experimentalists as we enter an exciting period in the hunt for the Higgs.

Appendix A

Spinor Helicity Formalism and Tree-level Amplitudes

A.1 Spinor Helicity Formalism notation and conventions

A.1.1 Spinor notations

Throughout this thesis we define kinematic invariants associated with sums of gluon momenta as follows,

$$s_{ij} = (p_i + p_j)^2, \quad s_{ijk} = (p_i + p_j + p_k)^2, \quad s_{i,j} = (p_i + p_{i+1} + \cdots + p_j)^2 \text{ etc.} \tag{A.1.1}$$

Sums of external momenta are also written using the following shorthand notation,

$$p_i + p_j + p_k = P_{ijk} \tag{A.1.2}$$

We will express helicity amplitudes using the notation of the spinor-helicity formalism,

$$\langle ij \rangle = \overline{u}_-(k_i) u_+(k_j), \tag{A.1.3}$$

$$[ij] = \overline{u}_+(k_i) u_-(k_j), \tag{A.1.4}$$

where $u_\pm(k_i)$ represents a massless Dirac spinor associated with either positive or negative helicity (and a momentum k_i). Spinor products are related to kinematic

invariants through the following relation,

$$s_{ij} = \langle ij\rangle[ji]. \tag{A.1.5}$$

Chains of spinor products are written as

$$\langle i|j|k] = \langle ij\rangle[jk] \qquad \langle i|jk|l\rangle = \langle ij\rangle[jk]\langle kl\rangle, \qquad \text{etc.} \tag{A.1.6}$$

For example, using momentum conservation we have,

$$\langle i|p_\phi|k] = -\sum_{j=1}^{4}\langle ij\rangle[jk]. \tag{A.1.7}$$

For purely partonic amplitudes (i.e. with no Higgs, ϕ or $\phi^\dagger$ present) momentum conservation is represented by the following equation

$$0 = \sum_{i=1}^{n} p_i^\mu \quad \Longrightarrow \; 0 = \sum_{i=1}^{n}\langle ij\rangle[jk] \tag{A.1.8}$$

A good overview of the spinor helicity formalism and colour ordering (which is described in the following section) can be found in [218].

Intermittently in this thesis we have used the following notation to define a four-vector in terms of spinor indices [131]

$$p_{a\dot{a}} = \sigma^\mu_{a\dot{a}} p_\mu \tag{A.1.9}$$

we use $\sigma^\mu = (1, \overrightarrow{\sigma})$ and $\overrightarrow{\sigma}$ is a representation of the Pauli spin matrices. This means that we can expand $p_{a\dot{a}}$

$$p_{a\dot{a}} = p_0 + \overrightarrow{\sigma}\cdot\overrightarrow{p} \tag{A.1.10}$$

This last equation implies that

$$p^\mu p_\mu = \det(p_{a\dot{a}}) \tag{A.1.11}$$

Such that a vector is light-like if and only if the determinant of $p_{a\dot{a}}$ vanishes, a general 2×2 matrix has at most rank two so can be expanded in terms of spinors λ, μ as follows $p_{a\dot{a}} = \lambda_a\tilde{\lambda}_{\dot{a}} + \mu_a\tilde{\mu}_{\dot{a}}$. If the rank of a 2×2 matrix is less than two

then its determinant vanishes, in this case we may write a light-like vector in the following form,

$$p_{a\dot{a}} = \lambda_a \tilde{\lambda}_{\dot{a}}, \tag{A.1.12}$$

which is used occasionally in this thesis.

The following identities are useful and often used to simplify formulae in this thesis [218]: Gordon identity and Fierz rearrangement,

$$\langle i|\gamma^\mu|i] = 2k_i^\mu, \quad \langle i|\gamma^\mu|j]\langle k|\gamma^\mu|l] = 2\langle ik\rangle[lj] \tag{A.1.13}$$

The Schouten identity is also extremely useful,

$$\langle ij\rangle\langle kl\rangle = \langle ik\rangle\langle jl\rangle + \langle il\rangle\langle kj\rangle \tag{A.1.14}$$

Finally polarisation vectors associated with external gluons have the following representation,

$$\varepsilon_\mu^+(k,q) = +\frac{\langle q|\gamma_\mu|k]}{\sqrt{2}\langle qk\rangle} \quad \varepsilon_\mu^-(k,q) = -\frac{[q|\gamma_\mu|k\rangle}{\sqrt{2}[qk]} \tag{A.1.15}$$

where q is a reference momenta which reflects the freedom of on-shell gauge transformations.

A.1.2 Colour ordering of ϕ plus parton amplitudes at tree-level and one-loop

The tree level amplitudes linking a ϕ with n gluons can be decomposed into colour ordered amplitudes as [64, 209],

$$\mathcal{A}_n^{(0)}(\phi, \{k_i, \lambda_i, a_i\}) = iCg^{n-2} \sum_{\sigma \in S_n/Z_n} \mathrm{tr}(T^{a_{\sigma(1)}} \cdots T^{a_{\sigma(n)}})\, A_n^{(0)}(\phi, \sigma(1^{\lambda_1}, .., n^{\lambda_n})). \tag{A.1.16}$$

Here S_n/Z_n is the group of non-cyclic permutations on n symbols, and j^{λ_j} labels the momentum p_j and helicity λ_j of the j^{th} gluon, which carries the adjoint representation index a_i. The T^{a_i} are fundamental representation $\mathrm{SU}(N_c)$ colour matrices, normalised so that $\mathrm{Tr}(T^a T^b) = \delta^{ab}$. Tree-level amplitudes with a single quark-antiquark

pair can be decomposed into colour-ordered amplitudes as follows,

$$\mathcal{A}_n^{(0)}(\phi,\{p_i,\lambda_i,a_i\},\{p_j,\lambda_j,i_j\}) \tag{A.1.17}$$
$$= iCg^{n-2}\sum_{\sigma\in S_{n-2}}(T^{a_{\sigma(2)}}\cdots T^{a_{\sigma(n-1)}})_{i_1 i_n}\,A_n(\phi,1^\lambda,\sigma(2^{\lambda_2},\ldots,(n-1)^{\lambda_{n-1}}),n^{-\lambda})\,,$$

where S_{n-2} is the set of permutations of $(n-2)$ gluons. Quarks are characterised with fundamental colour label i_j and helicity λ_j for $j=1,n$. By current conservation, the quark and antiquark helicities are related such that $\lambda_1=-\lambda_n\equiv\lambda$ where $\lambda=\pm\frac{1}{2}$.

The one-loop amplitudes which are the main subject of this paper follow the same colour ordering as the pure QCD amplitudes [110] and can be decomposed as [106–108],

$$\mathcal{A}_n^{(1)}(\phi,\{k_i,\lambda_i,a_i\}) = iCg^n\sum_{c=1}^{[n/2]+1}\sum_{\sigma\in S_n/S_{n;c}}G_{n;c}(\sigma)A_n^{(1)}(\phi,\sigma(1^{\lambda_1},\ldots,n^{\lambda_n})) \tag{A.1.18}$$

where

$$G_{n;1}(1) = N_c\,\mathrm{tr}(T^{a_1}\cdots T^{a_n}) \tag{A.1.19}$$
$$G_{n;c}(1) = \mathrm{tr}(T^{a_1}\cdots T^{a_{c-1}})\,\mathrm{tr}(T^{a_c}\cdots T^{a_n})\ ,\ c>2. \tag{A.1.20}$$

The sub-leading terms can be computed by summing over various permutations of the leading colour amplitudes [110].

A.2 Tree-level amplitudes

In this section we list the tree level amplitudes which have been used as ingredients in the construction of Higgs plus four parton one-loop amplitudes. We also recall the following relations for constructing Higgs amplitudes,

$$A_n^{(l)}(H;\{p_k\}) = A_n^{(l)}(\phi,\{p_k\}) + A_n^{(l)}(\phi^\dagger,\{p_k\}). \tag{A.2.21}$$

We can also generate pseudo-scalar amplitudes from the difference of ϕ and $\phi^\dagger$ components,

$$A_n^{(l)}(A;\{p_k\}) = \frac{1}{i}\left(A_n^{(l)}(\phi,\{p_k\}) - A_n^{(l)}(\phi^\dagger,\{p_k\})\right). \tag{A.2.22}$$

Furthermore parity relates ϕ and $\phi^\dagger$ amplitudes,

$$A_n^{(m)}(\phi^\dagger, g_1^{\lambda_1}, \ldots, g_n^{\lambda_n}) = \left(A_n^{(m)}(\phi, g_1^{-\lambda_1}, \ldots, g_n^{-\lambda_n})\right)^*. \tag{A.2.23}$$

Hence we will only list ϕ-amplitudes, knowing that all others can be obtained using eqs. (A.2.21)–(A.2.23).

In this section we list the primitive amplitude which can be used to generate the full coloured amplitudes using the equations given in section A.1.2

A.3 Pure QCD amplitudes

The all multiplicity pure gluon MHV is given by

$$A_n^{(0)}(1^+, \ldots, i^-, \ldots, j^-, \ldots, n^+) = \frac{\langle ij\rangle^4}{\prod_{\alpha=1}^{n-1}\langle\alpha(\alpha+1)\rangle\langle n1\rangle} \tag{A.3.24}$$

The all multiplicity gluon plus quark pair MHV has the following form,

$$A_n^{(0)}(1_{\overline{q}}^-, 2^+, \ldots, j^-, \ldots, n_q^+) = \frac{\langle 1j\rangle^3\langle nj\rangle}{\prod_{\alpha=1}^{n-1}\langle\alpha(\alpha+1)\rangle\langle n1\rangle} \tag{A.3.25}$$

The following two quark pair amplitudes are also needed at various stages

$$A_n^{(0)}(1_q^+, \ldots, i_{\overline{Q}}^-, \ldots j_Q^+, \ldots, n_{\overline{q}}^-) = -\frac{\langle 1i\rangle\langle in\rangle^2\langle nj\rangle}{\prod_{\alpha=1}^{n-1}\langle\alpha(\alpha+1)\rangle\langle n1\rangle} \tag{A.3.26}$$

$$A_n^{(0)}(1_q^-, \ldots, i_{\overline{Q}}^-, \ldots j_Q^+, \ldots, n_{\overline{q}}^+) = \frac{\langle 1i\rangle^3\langle jn\rangle}{\prod_{\alpha=1}^{n-1}\langle\alpha(\alpha+1)\rangle\langle n1\rangle} \tag{A.3.27}$$

Although having no overall (non box or triangle) contribution to the double cuts of any Higgs plus gluon amplitude we need to use the 6-point NMHV amplitude when constructing the s_{1234} cut of the ϕ-NHMV amplitude.

$$A_6^{(0)}(1^-, 2^-, 3^-, 4^+, 5^+, 6^+) = \frac{1}{\langle 5|P_{34}|2]}\left(\frac{\langle 1|P_{23}|4]^3}{[23][34]\langle 56\rangle\langle 61\rangle s_{234}} + \frac{\langle 3|P_{45}|6]^3}{[61][12]\langle 34\rangle\langle 45\rangle s_{345}}\right) \tag{A.3.28}$$

We also note the vanishing of the following amplitudes,

$$A_n^{(0)}(1^\pm, 2^+, \ldots, n^+) = 0 \tag{A.3.29}$$

$$A_n^{(0)}(1_q^-, 2^+, \ldots, n_{\overline{q}}^\pm) = 0 \tag{A.3.30}$$

A.4 ϕ plus parton amplitudes

For the MHV configurations the ϕ plus parton amplitudes have the same structure as the pure QCD ones (although momentum is now no longer conserved amongst the partons only).

$$A_n^{(0)}(\phi,1^+,\ldots,i^-,\ldots,j^-,\ldots,n^+) = \frac{\langle ij\rangle^4}{\prod_{\alpha=1}^{n-1}\langle\alpha(\alpha+1)\rangle\langle n1\rangle} \quad (A.4.31)$$

$$A_n^{(0)}(\phi,1_{\overline{q}}^-,2^+,\ldots,j^-,\ldots,n_q^+) = \frac{\langle 1j\rangle^3\langle nj\rangle}{\prod_{\alpha=1}^{n-1}\langle\alpha(\alpha+1)\rangle\langle n1\rangle} \quad (A.4.32)$$

$$A_n^{(0)}(\phi,1_q^+,\ldots,i_{\overline{Q}}^-,\ldots j_Q^+,\ldots,n_{\overline{q}}^-) = -\frac{\langle 1i\rangle\langle in\rangle^2\langle nj\rangle}{\prod_{\alpha=1}^{n-1}\langle\alpha(\alpha+1)\rangle\langle n1\rangle} \quad (A.4.33)$$

$$A_n^{(0)}(\phi,1_q^-,\ldots,i_{\overline{Q}}^-,\ldots j_Q^+,\ldots,n_{\overline{q}}^+) = \frac{\langle 1i\rangle^3\langle jn\rangle}{\prod_{\alpha=1}^{n-1}\langle\alpha(\alpha+1)\rangle\langle n1\rangle} \quad (A.4.34)$$

The all plus and single minus ϕ amplitudes also vanish,

$$A_n^{(0)}(\phi,1^\pm,2^+,\ldots,n^+) = 0 \quad (A.4.35)$$

$$A_n^{(0)}(\phi,1_q^-,2^+,\ldots,n_{\overline{q}}^+) = 0 \quad (A.4.36)$$

The ϕ all-minus amplitude does not vanish however,

$$A_n^{(0)}(\phi,1^-,\ldots,n^-) = \frac{(-1)^n m_\phi^4}{\prod_{\alpha=1}^{n-1}[\alpha(\alpha+1)][n1]} \quad (A.4.37)$$

We will also need the following ϕ-NMHV amplitudes,

$$A_n^{(0)}(\phi,1^+,2^-,3^-,4^-) = -\frac{m_\phi^4\langle 24\rangle^4}{s_{124}\langle 12\rangle\langle 14\rangle\langle 2|p_\phi|3]\langle 4|p_\phi|3]} + \frac{\langle 4|p_\phi|1]^3}{s_{123}\langle 4|p_\phi|3][12][23]} - \frac{\langle 2|p_\phi|1]^3}{s_{134}\langle 2|p_\phi|3][14][34]}. \quad (A.4.38)$$

and the $\phi q\overline{q}$-NMHV amplitude,

$$A_n^{(0)}(\phi,1_q^+,2^-,3^-,4_{\bar{q}}^-) = \frac{\langle 24\rangle^3 m_\phi^4}{s_{124}\langle 14\rangle\langle 2|p_\phi|3]\langle 4|p_\phi|3]} - \frac{\langle 4|p_\phi|1]^2}{\langle 4|p_\phi|3][12][23]} + \frac{\langle 2|p_\phi|1]^2\langle 2|p_\phi|4]}{s_{134}\langle 2|p_\phi|3][14][34]}. \quad (A.4.39)$$

Finally for the subleading colour amplitudes we will need the following amplitude,

$$A_4^{(0)}(\phi,1_{\overline{q}}^-,2^-,3_q^+,4^-) = -\frac{\langle 4|p_\phi|3]^2}{[12][23]s_{123}} + \{2\leftrightarrow 4\} \quad (A.4.40)$$

Appendix B

One-loop Basis Integrals

In this appendix we present the basis integral functions used to construct the various contributions to the Higgs plus four parton helicity amplitudes.

B.1 Extraction of kinematic factors

In general a one-loop n point basis integral appearing in the basis expansion used throughout this thesis has the following structure,

$$\mathcal{I}_n[\{P_{ji}\}] = \int \frac{d^d\ell}{(2\pi)^d} \frac{1}{\prod_{\alpha=0}^{n-1}(\ell_\alpha^2)} \tag{B.1.1}$$

where $\ell_i = \ell - P_{ji}$ is a combination of a loop momenta and some subset of the external momenta. In general we find it convenient to work with the following basis integrals,

$$\begin{aligned}
\mathcal{I}_4^{1m}(s,t;P^2) &= \frac{1}{st}\,\mathrm{F}_4^{1\mathrm{m}}(s,t;P^2) && \text{(B.1.2)}\\
\mathcal{I}_4^{2me}(s,t;P^2Q^2) &= \frac{1}{(st-P^2Q^2)}\,\mathrm{F}_4^{2\mathrm{me}}(s,t;P^2,Q^2) && \text{(B.1.3)}\\
\mathcal{I}_4^{2mh}(s,t;P^2,Q^2) &= \frac{1}{st}\,\mathrm{F}_4^{2\mathrm{mh}}(s,t;P^2,Q^2) && \text{(B.1.4)}\\
\mathcal{I}_3^{2m}(s,t) &= \frac{1}{(s-t)}\Big(\,\mathrm{F}_3^{1\mathrm{m}}(s) - \mathrm{F}_3^{1\mathrm{m}}(t)\Big) && \text{(B.1.5)}\\
\mathcal{I}_3^{1m}(s) &= \frac{1}{s}\,\mathrm{F}_3^{1\mathrm{m}}(s) && \text{(B.1.6)}
\end{aligned}$$

and in this appendix we give explicit formulae for the F functions.

B.2 Box Integral Functions

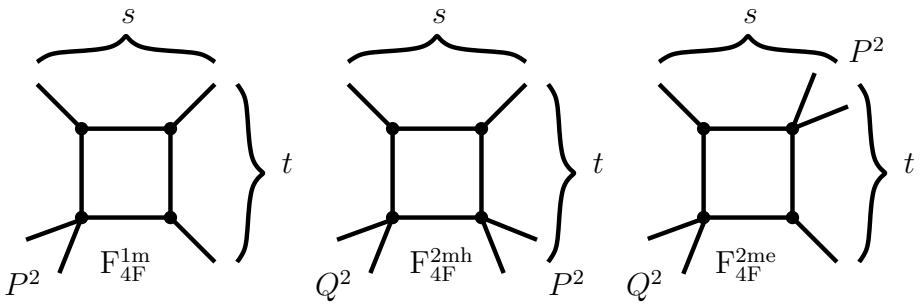

Figure B.1: Conventions for labelling the three scalar box integrals appearing in the one-loop H plus parton amplitudes.

Figure B.1 sets our labelling conventions. We express our results in terms of basis functions which are related to the scalar integral $\mathcal{I}$ by a kinematic factor, which cancels against the same factor in the coefficient. The zero-,one- and two-mass easy box have representations in terms of hypergeometric series to all orders in ϵ,

$$\begin{aligned} F_4^{0m}(s,t) = \frac{2}{\epsilon^2}\Bigg[& \left(\frac{\mu^2}{-s}\right)^{\epsilon} {}_2F_1\left(1,-\epsilon;1-\epsilon;-\frac{u}{t}\right) \\ & + \left(\frac{\mu^2}{-t}\right)^{\epsilon} {}_2F_1\left(1,-\epsilon;1-\epsilon;-\frac{u}{s}\right)\Bigg], \end{aligned} \tag{B.2.7}$$

$$\begin{aligned} F_4^{1m}(s,t;P^2) = \frac{2}{\epsilon^2}\Bigg[& \left(\frac{\mu^2}{-s}\right)^{\epsilon} {}_2F_1\left(1,-\epsilon;1-\epsilon;-\frac{u}{t}\right) \\ & + \left(\frac{\mu^2}{-t}\right)^{\epsilon} {}_2F_1\left(1,-\epsilon;1-\epsilon;-\frac{u}{s}\right) \\ & - \left(\frac{\mu^2}{-P^2}\right)^{\epsilon} {}_2F_1\left(1,-\epsilon;1-\epsilon;-\frac{uP^2}{st}\right)\Bigg], \end{aligned} \tag{B.2.8}$$

$$\begin{aligned} F_4^{2me}(s,t;P^2,Q^2) = \frac{2}{\epsilon^2}\Bigg[& \left(\frac{\mu^2}{-s}\right)^{\epsilon} {}_2F_1\left(1,-\epsilon;1-\epsilon;\frac{us}{P^2Q^2-st}\right) \\ & + \left(\frac{\mu^2}{-t}\right)^{\epsilon} {}_2F_1\left(1,-\epsilon;1-\epsilon;\frac{ut}{P^2Q^2-st}\right) \\ & - \left(\frac{\mu^2}{-P^2}\right)^{\epsilon} {}_2F_1\left(1,-\epsilon;1-\epsilon;\frac{uP^2}{P^2Q^2-st}\right) \\ & - \left(\frac{\mu^2}{-Q^2}\right)^{\epsilon} {}_2F_1\left(1,-\epsilon;1-\epsilon;\frac{uQ^2}{P^2Q^2-st}\right)\Bigg], \end{aligned} \tag{B.2.9}$$

when expanded in ϵ through to order ϵ^0 we find that the one- and two-mass easy

boxes relevant for this thesis have the following expansion,

$$\begin{aligned} \mathrm{F}_4^{\mathrm{1m}}(s,t,:P^2) &= \frac{2}{\epsilon^2}\left[\left(\frac{\mu^2}{-s}\right)^{\epsilon}+\left(\frac{\mu^2}{-t}\right)^{\epsilon}-\left(\frac{\mu^2}{-P^2}\right)^{\epsilon}\right] \\ &\quad +\mathrm{F}_{4\mathrm{F}}^{\mathrm{1m}}(s,t;P^2) \qquad \text{(B.2.10)} \\ \mathrm{F}_4^{\mathrm{2me}}(s,t,:P^2,Q^2) &= \frac{2}{\epsilon^2}\left[\left(\frac{\mu^2}{-s}\right)^{\epsilon}+\left(\frac{\mu^2}{-t}\right)^{\epsilon}-\left(\frac{\mu^2}{-P^2}\right)^{\epsilon}-\left(\frac{\mu^2}{-Q^2}\right)^{\epsilon}\right] \\ &\quad +\mathrm{F}_{4\mathrm{F}}^{\mathrm{2me}}(s,t;P^2,Q^2) \qquad \text{(B.2.11)} \end{aligned}$$

Whilst the two-mass hard box has the following ϵ expansion,

$$\begin{aligned} \mathrm{F}_4^{\mathrm{2mh}}(s,t;P^2,Q^2) &= \frac{2}{\epsilon^2}\left[\left(\frac{\mu^2}{-s}\right)^{\epsilon}+\left(\frac{\mu^2}{-t}\right)^{\epsilon}-\left(\frac{\mu^2}{-P^2}\right)^{\epsilon}-\left(\frac{\mu^2}{-Q^2}\right)^{\epsilon}\right] \\ &\quad +\mathrm{F}_{4\mathrm{F}}^{\mathrm{2mh}}(s,t;P^2,Q^2) \qquad \text{(B.2.12)} \end{aligned}$$

The finite parts of the one-mass and two-mass (easy and hard) have the following forms,

$$\mathrm{F}_{4\mathrm{F}}^{\mathrm{1m}}(s,t;P^2) = -2\left(\mathrm{Li}_2\left(1-\frac{P^2}{s}\right)+\mathrm{Li}_2\left(1-\frac{P^2}{t}\right)+\frac{1}{2}\ln^2\left(\frac{s}{t}\right)+\frac{\pi^2}{6}\right), \qquad \text{(B.2.13)}$$

$$\begin{aligned} \mathrm{F}_{4\mathrm{F}}^{\mathrm{2mh}}(s,t;P^2,Q^2) &= -2\left(\mathrm{Li}_2\left(1-\frac{P^2}{t}\right)+\mathrm{Li}_2\left(1-\frac{Q^2}{t}\right)+\frac{1}{2}\ln^2\left(\frac{s}{t}\right)\right. \\ &\quad \left.-\frac{1}{2}\ln\left(\frac{s}{P^2}\right)\ln\left(\frac{s}{Q^2}\right)\right), \qquad \text{(B.2.14)} \\ \mathrm{F}_{4\mathrm{F}}^{\mathrm{2me}}(s,t;P^2,Q^2) &= -2\left(\mathrm{Li}_2\left(1-\frac{P^2}{s}\right)+\mathrm{Li}_2\left(1-\frac{P^2}{t}\right)+\mathrm{Li}_2\left(1-\frac{Q^2}{s}\right)\right. \\ &\quad \left.+\mathrm{Li}_2\left(1-\frac{Q^2}{t}\right)-\mathrm{Li}_2\left(1-\frac{P^2Q^2}{st}\right)+\frac{1}{2}\ln^2\left(\frac{s}{t}\right)\right). \qquad \text{(B.2.15)} \end{aligned}$$

B.2.1 Triangle basis integrals

One- and two-mass triangles can be expressed in terms of the following function,

$$F_3^{1m}(s)=\frac{1}{\epsilon^2}\left(\frac{\mu^2}{-s}\right)^{\epsilon}, \qquad \text{(B.2.16)}$$

This function is used in chapter 3 explicitly, in latter chapters we expand the box functions and combine the ϵ^{-2} for the amplitude. Therefore, the above function is not seen in the formulae in chapters 4 and 5. The finite three-mass triangle is given by [121, 219],

$$\mathrm{F}_3^{\mathrm{3m}}(M_1^2,M_2^2,M_3^2) = \frac{i}{\sqrt{\Delta}}\sum_{k=1}^{3}\left(\mathrm{Li}_2\left(-\left(\frac{1+i\delta_k}{1-i\delta_k}\right)\right)-\mathrm{Li}_2\left(-\left(\frac{1-i\delta_k}{1+i\delta_k}\right)\right)\right),$$

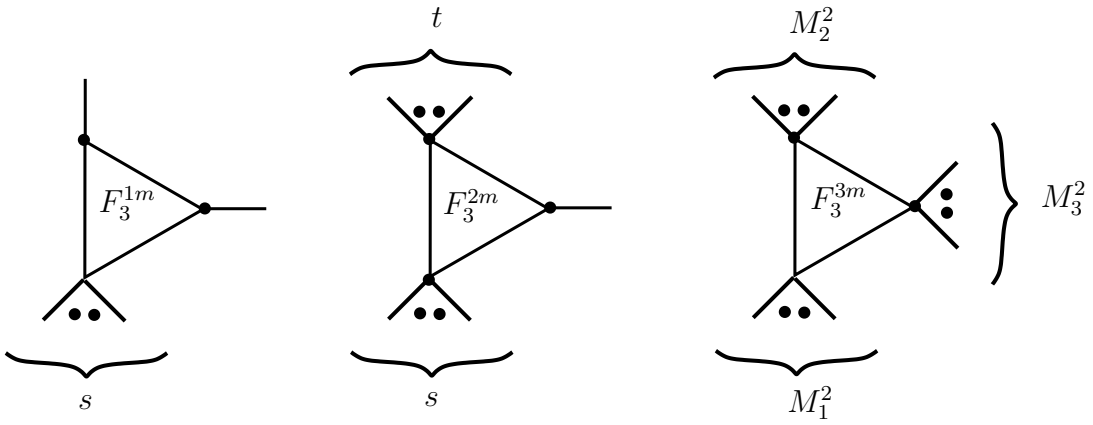

Figure B.2: Conventions for labelling the three scalar triangle integrals appearing in the one-loop H plus parton amplitudes.

(B.2.17)

where,

$$\Delta = \sum_{k=1}^{3} -M_k^4 + 2M_k^2 M_{k+1}^2 \tag{B.2.18}$$

$$\delta_k = \frac{M_k^2 - M_{k+1}^2 - M_{k+2}^2}{\sqrt{\Delta}}. \tag{B.2.19}$$

Alternative representations for these integrals can be found in references [186, 220, 221].

B.2.2 Bubble basis integrals

The two point bubble integral integrates to the following,

$$\mathcal{I}_2(s) = \frac{1}{\epsilon(1-2\epsilon)} \left(\frac{\mu^2}{-s}\right)^{\epsilon}. \tag{B.2.20}$$

in this thesis we combine bubble integrals to produce the following basis functions,

$$L_k(s,t) = \frac{\log(s/t)}{(s-t)^k}, \tag{B.2.21}$$

which we then complete to avoid the presence of spurious $(s \to t)$ singularities.

$$L_3(s,t) \to \hat{L}_3(s,t) = L_3(s,t) - \frac{1}{2(s-t)^2}\left(\frac{1}{s} + \frac{1}{t}\right),$$

$$
\begin{aligned}
L_2(s,t) \to \hat{L}_2(s,t) &= L_2(s,t) - \frac{1}{2(s-t)}\left(\frac{1}{s}+\frac{1}{t}\right), \\
L_1(s,t) \to \hat{L}_1(s,t) &= L_1(s,t), \\
L_0(s,t) \to \hat{L}_0(s,t) &= L_0(s,t).
\end{aligned} \tag{B.2.22}
$$

Bibliography

[1] R. K. Ellis and S. Veseli, *Strong radiative corrections to W b anti-b production in p anti-p collisions*, *Phys. Rev.* **D60** (1999) 011501 [hep-ph/9810489].

[2] J. M. Campbell and R. K. Ellis, *An update on vector boson pair production at hadron colliders*, *Phys. Rev.* **D60** (1999) 113006 [hep-ph/9905386].

[3] J. M. Campbell and R. K. Ellis, *Radiative corrections to Z b anti-b production*, *Phys. Rev.* **D62** (2000) 114012 [hep-ph/0006304].

[4] J. M. Campbell, R. K. Ellis and F. Tramontano, *Single top production and decay at next-to-leading order*, *Phys. Rev.* **D70** (2004) 094012 [hep-ph/0408158].

[5] J. M. Campbell, R. K. Ellis, F. Maltoni and S. Willenbrock, *Production of a Z boson and two jets with one heavy- quark tag*, *Phys. Rev.* **D73** (2006) 054007 [hep-ph/0510362].

[6] M. Peskin and D. Schroeder, *An Introduction to Quantum Field Theory*, *Westview Press* (1995).

[7] R. K. Ellis, W. J. Stirling and B. R. Webber, *QCD and Collider Physics*, *Cambridge University Press* (1996).

[8] R. Feynman, *Space-time approach to quantum electrodynamics*, *Phys. Rev* **76** (1949) 769.

[9] R. Feynman, *The theory of positrons*, *Phys. Rev* **76** (1949) 749.

[10] R. Feynman, *Mathematical formulation of the quantum theory of electromagnetic interaction*, *Phys. Rev* **80** (1950) 440.

[11] S. Tomonaga, *On a relativistically invariant formulation of the quantum theory of wave fields*, *Progress of Theoretical Physics* **1** (1946) 27.

[12] J. Schwinger, *On quantum-electrodynamics and the magnetic moment of the electron*, *Phys. Rev.* **73** (1948) 416.

[13] J. Schwinger, *Quantum-electrodynamics 1. a covariant formulation*, *Phys. Rev.* **74** (1948) 1439.

[14] C. Yang and R. Mills *Phys. Rev.* **96** (1954) 191.

[15] S. Bethke, *in Proc. QCD94 Conference, Montpellier, July 1984* , *Nucl. Phys.* **B** *(Proc. Suppl.)* **39BC** (1995) 198.

[16] G. Passarino and M. Veltman, , *Nucl. Phys. B* **B160** (1979) 151.

[17] G. 't Hooft and M. Veltman *Nucl. Phys.* **B44** (1972) 189.

[18] F. Bloch and A. Nordsieck, *Note on the radiation field of the electron*, *Phys. Rev* **52** (1937) 54–59.

[19] T. Kinoshita, *Mass singularities of Feynmann amplitudes*, *J. Math. Phys* **3** (1962) 650–677.

[20] T. D. Lee and M. Nauenberg, *Degenerate systems and mass singularities*, *Phys. Rev.* **133** (1964) B1549–B1562.

[21] R. K. Ellis, H. Georgi, M. Machacek, H. D. Politzer and G. G. Ross, *Perturbation Theory and the Parton Model in QCD*, *Nucl. Phys.* **B152** (1979) 285.

[22] A. D. Martin, W. J. Stirling, R. S. Thorne and G. Watt, *Parton distributions for the LHC*, *Eur. Phys. J.* **C63** (2009) 189–285 [0901.0002].

[23] P. M. Nadolsky *et. al.*, *Implications of CTEQ global analysis for collider observables*, *Phys. Rev.* **D78** (2008) 013004 [0802.0007].

[24] P. Jimenez-Delgado and E. Reya, *Dynamical NNLO parton distributions*, *Phys. Rev.* **D79** (2009) 074023 [0810.4274].

[25] R. D. Ball *et. al.*, *A first unbiased global NLO determination of parton distributions and their uncertainties*, *Nucl. Phys.* **B838** (2010) 136–206 [1002.4407].

[26] S. Alekhin, J. Blumlein, S. Klein and S. Moch, *The 3-, 4-, and 5-flavor NNLO Parton from Deep-Inelastic- Scattering Data and at Hadron Colliders*, *Phys. Rev.* **D81** (2010) 014032 [0908.2766].

[27] G. P. Salam and G. Soyez, *A practical Seedless Infrared-Safe Cone jet algorithm*, *JHEP* **05** (2007) 086 [0704.0292].

[28] M. Cacciari, G. P. Salam and G. Soyez, *The anti-k_t jet clustering algorithm*, *JHEP* **04** (2008) 063 [0802.1189].

[29] S. D. Ellis and D. E. Soper, *Successive combination jet algorithm for hadron collisions*, *Phys. Rev.* **D48** (1993) 3160–3166 [hep-ph/9305266].

[30] Y. L. Dokshitzer, G. D. Leder, S. Moretti and B. R. Webber, *Better Jet Clustering Algorithms*, *JHEP* **08** (1997) 001 [hep-ph/9707323].

[31] M. Wobisch and T. Wengler, *Hadronization corrections to jet cross sections in deep- inelastic scattering*, hep-ph/9907280.

[32] G. C. Blazey *et. al.*, *Run II jet physics*, hep-ex/0005012.

[33] S. Catani, F. Krauss, R. Kuhn and B. R. Webber, *QCD Matrix Elements + Parton Showers*, *JHEP* **11** (2001) 063 [hep-ph/0109231].

[34] G. Corcella *et. al.*, *HERWIG 6.5 release note*, hep-ph/0210213.

[35] S. Gieseke, A. Ribon, M. H. Seymour, P. Stephens and B. Webber, *Herwig++ 1.0: An event generator for e+ e- annihilation*, *JHEP* **02** (2004) 005 [hep-ph/0311208].

[36] M. Bahr *et. al.*, *Herwig++ Physics and Manual*, *Eur. Phys. J.* **C58** (2008) 639–707 [0803.0883].

[37] T. Gleisberg *et. al.*, *SHERPA 1.alpha, a proof-of-concept version*, *JHEP* **02** (2004) 056 [hep-ph/0311263].

[38] T. Gleisberg *et. al.*, *Event generation with SHERPA 1.1*, *JHEP* **02** (2009) 007 [0811.4622].

[39] T. Sjostrand, S. Mrenna and P. Z. Skands, *PYTHIA 6.4 Physics and Manual*, *JHEP* **05** (2006) 026 [hep-ph/0603175].

[40] T. Sjostrand, S. Mrenna and P. Z. Skands, *A Brief Introduction to PYTHIA 8.1*, *Comput. Phys. Commun.* **178** (2008) 852–867 [0710.3820].

[41] P. Higgs *Phys. Rev. Lett.* **12** (1964) 132.

[42] P. Higgs *Phys. Rev. Lett.* **13** (1964) 508.

[43] F. Englert and R. Brout *Phys. Rev. Lett.* **13** (1964) 321.

[44] G. Guralnik, C. Hagen and T. Kibble *Phys. Rev. Lett.* **13** (1964) 585.

[45] P. Higgs *Phys. Rev.* **145** (1966) 1156.

[46] J. Goldstone *Nuovo Cim* **19** (1961) 154.

[47] J. Goldstone and S. Weinberg *Phys. Rev.* **127** (1962) 965.

[48] **The LEP Collaborations** Collaboration, *A Combination of preliminary electroweak measurements and constraints on the standard model*, hep-ex/0212036.

[49] J. Ellis, M. Gaillard and D. Nanopoulos *Nucl. Phys.* **B106** (1976) 292.

[50] B. Lee, C. Quigg and H. Thacker *Phys. Rev.* **D16** ((1977)) 1519.

[51] **LEP Working Group for Higgs boson searches** Collaboration, R. Barate *et. al.*, *Search for the standard model Higgs boson at LEP*, *Phys. Lett.* **B565** (2003) 61–75 [hep-ex/0306033].

[52] **ALEPH** Collaboration, R. Barate *et. al. Phys. Lett.* **B526** (2002) 191.

[53] **DELPHI** Collaboration, J. Abdallah *et. al.*, *Final results from DELPHI on the searches for SM and MSSM neutral Higgs bosons*, *Eur. Phys. J.* **C32** (2004) 145–183 [hep-ex/0303013].

[54] **OPAL** Collaboration, G. Abbiendi *et. al.*, *Search for the standard model Higgs boson with the OPAL detector at LEP*, *Eur. Phys. J.* **C26** (2003) 479–503 [hep-ex/0209078].

[55] **L3** Collaboration, M. Acciarri *et. al. Phys. Lett.* **B517** (2001) 319.

[56] **Particle Data Group** Collaboration, C. Amsler *et. al.*, *Review of particle physics*, *Phys. Lett.* **B667** (2008) 1.

[57] M. S. Carena and H. E. Haber, *Higgs boson theory and phenomenology. ((V))*, *Prog. Part. Nucl. Phys.* **50** (2003) 63–152 [hep-ph/0208209].

[58] **CDF and D0** Collaboration, T. Aaltonen *et. al.*, *Combination of Tevatron searches for the standard model Higgs boson in the W+W- decay mode*, *Phys. Rev. Lett.* **104** (2010) 061802 [1001.4162].

[59] **The CDF** Collaboration, T. Aaltonen *et. al.*, *Inclusive Search for Standard Model Higgs Boson Production in the WW Decay Channel using the CDF II Detector*, *Phys. Rev. Lett.* **104** (2010) 061803 [1001.4468].

[60] **The D0** Collaboration, V. M. Abazov *et. al.*, *Search for Higgs boson production in dilepton and missing energy final states with 5.4* fb^{-1} *of* $p\bar{p}$ *collisions at* $\sqrt{s} = 1.96$ *TeV*, *Phys. Rev. Lett.* **104** (2010) 061804 [1001.4481].

[61] **The TEVNPH Working Group of the CDF and D0** Collaboration, *Combined CDF and D0 Upper Limits on Standard Model Higgs- Boson Production with up to 6.7* fb^{-1} *of Data*, 1007.4587.

[62] **The ATLAS** Collaboration, G. Aad *et. al.*, *Expected Performance of the ATLAS Experiment - Detector, Trigger and Physics*, 0901.0512.

[63] M. Shifman, A. Vainshtein and V. Zakharov, *Remarks on higgs-boson interactions with nucleons*, *Phys. Lett.* (1978) 443.

[64] S. Dawson and R. P. Kauffman, *Higgs boson plus multi - jet rates at the SSC*, *Phys. Rev. Lett.* **68** (1992) 2273–2276.

[65] F. Wilczek, *Decays of heavy vector mesons into Higgs particles*, *Phys. Rev. Lett.* **39** (1977) 1304.

[66] V. Del Duca, W. Kilgore, C. Oleari, C. Schmidt and D. Zeppenfeld, *Gluon-fusion contributions to H + 2 jet production*, *Nucl. Phys.* **B616** (2001) 367–399 [hep-ph/0108030].

[67] V. Del Duca, W. Kilgore, C. Oleari, C. Schmidt and D. Zeppenfeld, *H + 2 jets via gluon fusion*, *Phys. Rev. Lett.* **87** (2001) 122001 [hep-ph/0105129].

[68] V. Del Duca, W. Kilgore, C. Oleari, C. R. Schmidt and D. Zeppenfeld, *Kinematical limits on Higgs boson production via gluon fusion in association with jets*, *Phys. Rev.* **D67** (2003) 073003 [hep-ph/0301013].

[69] D. Neill, *Analytic Virtual Corrections for Higgs Transverse Momentum Spectrum at $O(\alpha_s^2/m_t^3)$ via Unitarity Methods*, 0911.2707.

[70] K. G. Chetyrkin, B. A. Kniehl and M. Steinhauser, *Decoupling relations to O(alpha(s)**3) and their connection to low-energy theorems*, *Nucl. Phys.* **B510** (1998) 61–87 [hep-ph/9708255].

[71] T. Inami, T. Kubota and Y. Okada, *Effective gauge theory and the effect of heavy quarks in Higgs boson decays*, *Z. Phys.* **C18** (1983) 69.

[72] A. Djouadi, M. Spira and P. M. Zerwas, *Production of Higgs bosons in proton colliders: QCD corrections*, *Phys. Lett.* **B264** (1991) 440–446.

[73] S. Dawson, *Radiative corrections to Higgs boson production*, *Nucl. Phys.* **B359** (1991) 283–300.

[74] M. Spira, A. Djouadi, D. Graudenz and P. M. Zerwas, *Higgs boson production at the LHC*, *Nucl. Phys.* **B453** (1995) 17–82 [hep-ph/9504378].

[75] C. Anastasiou and K. Melnikov, *Higgs boson production at hadron colliders in NNLO QCD*, *Nucl. Phys.* **B646** (2002) 220–256 [hep-ph/0207004].

[76] V. Ravindran, J. Smith and W. L. van Neerven, *NNLO corrections to the total cross section for Higgs boson production in hadron hadron collisions*, *Nucl. Phys.* **B665** (2003) 325–366 [hep-ph/0302135].

[77] C. Anastasiou, K. Melnikov and F. Petriello, *Higgs boson production at hadron colliders: Differential cross sections through next-to-next-to-leading order*, *Phys. Rev. Lett.* **93** (2004) 262002 [hep-ph/0409088].

[78] C. Anastasiou, K. Melnikov and F. Petriello, *Fully differential Higgs boson production and the di- photon signal through next-to-next-to-leading order*, *Nucl. Phys.* **B724** (2005) 197–246 [hep-ph/0501130].

[79] C. Anastasiou, G. Dissertori and F. Stockli, *NNLO QCD predictions for the $H \to WW \to l\, l\, \nu\nu$ signal at the LHC*, *JHEP* **09** (2007) 018 [0707.2373].

[80] S. Catani and M. Grazzini, *An NNLO subtraction formalism in hadron collisions and its application to Higgs boson production at the LHC*, *Phys. Rev. Lett.* **98** (2007) 222002 [hep-ph/0703012].

[81] M. Grazzini, *NNLO predictions for the Higgs boson signal in the $H \to WW \to l\nu\, l\nu$ and $H \to ZZ \to 4l$ decay channels*, *JHEP* **02** (2008) 043 [0801.3232].

[82] C. Anastasiou, S. Bucherer and Z. Kunszt, *HPro: A NLO Monte-Carlo for Higgs production via gluon fusion with finite heavy quark masses*, *JHEP* **10** (2009) 068 [0907.2362].

[83] S. Marzani, R. D. Ball, V. Del Duca, S. Forte and A. Vicini, *Higgs production via gluon-gluon fusion with finite top mass beyond next-to-leading order*, *Nucl. Phys.* **B800** (2008) 127–145 [0801.2544].

[84] A. Pak, M. Rogal and M. Steinhauser, *Finite top quark mass effects in NNLO Higgs boson production at LHC*, *JHEP* **02** (2010) 025 [0911.4662].

[85] R. V. Harlander and K. J. Ozeren, *Finite top mass effects for hadronic Higgs production at next-to-next-to-leading order*, *JHEP* **11** (2009) 088 [0909.3420].

[86] R. V. Harlander and K. J. Ozeren, *Top mass effects in Higgs production at next-to-next-to- leading order QCD: virtual corrections*, *Phys. Lett.* **B679** (2009) 467–472 [0907.2997].

[87] A. Pak, M. Rogal and M. Steinhauser, *Virtual three-loop corrections to Higgs boson production in gluon fusion for finite top quark mass*, *Phys. Lett.* **B679** (2009) 473–477 [0907.2998].

[88] R. V. Harlander, H. Mantler, S. Marzani and K. J. Ozeren, *Higgs production in gluon fusion at next-to-next-to- leading order QCD for finite top mass*, *Eur. Phys. J.* **C66** (2010) 359–372 [0912.2104].

[89] S. Catani, D. de Florian, M. Grazzini and P. Nason, *Soft-gluon resummation for Higgs boson production at hadron colliders*, *JHEP* **07** (2003) 028 [hep-ph/0306211].

[90] S. Moch and A. Vogt, *Higher-order soft corrections to lepton pair and Higgs boson production*, *Phys. Lett.* **B631** (2005) 48–57 [hep-ph/0508265].

[91] E. Laenen and L. Magnea, *Threshold resummation for electroweak annihilation from DIS data*, *Phys. Lett.* **B632** (2006) 270–276 [hep-ph/0508284].

[92] W.-Y. Keung and F. J. Petriello, *Electroweak and finite quark-mass effects on the Higgs boson transverse momentum distribution*, *Phys. Rev.* **D80** (2009) 013007 [0905.2775].

[93] R. K. Ellis, I. Hinchliffe, M. Soldate and J. J. van der Bij, *Higgs decay to $\tau^+\tau^-$: A possible signature of intermediate mass higgs bosons at the ssc*, *Nucl. Phys.* **B297** (1988) 221.

[94] U. Baur and E. W. N. Glover, *Higgs boson production at large transverse momentum in hadronic collisions*, *Nucl. Phys.* **B339** (1990) 38–66.

[95] L. J. Dixon, E. W. N. Glover and V. V. Khoze, *MHV rules for Higgs plus multi-gluon amplitudes*, *JHEP* **12** (2004) 015 [hep-th/0411092].

[96] A. Djouadi, *The Anatomy of electro-weak symmetry breaking. I: The Higgs boson in the standard model*, *Phys. Rept.* **457** (2008) 1–216 [hep-ph/0503172].

[97] T. Han, G. Valencia and S. Willenbrock, *Structure function approach to vector boson scattering in p p collisions*, *Phys. Rev. Lett.* **69** (1992) 3274–3277 [hep-ph/9206246].

[98] T. Figy, C. Oleari and D. Zeppenfeld, *Next-to-leading order jet distributions for Higgs boson production via weak-boson fusion*, *Phys. Rev.* **D68** (2003) 073005 [hep-ph/0306109].

[99] E. L. Berger and J. M. Campbell, *Higgs boson production in weak boson fusion at next-to- leading order*, *Phys. Rev.* **D70** (2004) 073011 [hep-ph/0403194].

[100] M. Ciccolini, A. Denner and S. Dittmaier, *Strong and electroweak corrections to the production of Higgs+2jets via weak interactions at the LHC*, *Phys. Rev. Lett.* **99** (2007) 161803 [0707.0381].

[101] M. Ciccolini, A. Denner and S. Dittmaier, *Electroweak and QCD corrections to Higgs production via vector-boson fusion at the LHC*, *Phys. Rev.* **D77** (2008) 013002 [0710.4749].

[102] J. R. Andersen, T. Binoth, G. Heinrich and J. M. Smillie, *Loop induced interference effects in Higgs Boson plus two jet production at the LHC*, *JHEP* **02** (2008) 057 [0709.3513].

[103] R. P. Kauffman, S. V. Desai and D. Risal, *Production of a Higgs boson plus two jets in hadronic collisions*, *Phys. Rev.* **D55** (1997) 4005–4015 [hep-ph/9610541].

[104] R. K. Ellis, W. T. Giele and G. Zanderighi, *Virtual QCD corrections to Higgs boson plus four parton processes*, *Phys. Rev.* **D72** (2005) 054018 [hep-ph/0506196].

[105] J. M. Campbell, R. K. Ellis and G. Zanderighi, *Next-to-leading order Higgs + 2 jet production via gluon fusion*, *JHEP* **10** (2006) 028 [hep-ph/0608194].

[106] C. F. Berger, V. Del Duca and L. J. Dixon, *Recursive construction of higgs+multiparton loop amplitudes: The last of the ϕ-nite loop amplitudes*, *Phys. Rev.* **D74** (2006) 094021 [hep-ph/0608180].

[107] S. D. Badger and E. W. N. Glover, *One-loop helicity amplitudes for $H \to$ gluons: the all- minus configuration*, *Nucl. Phys. Proc. Suppl.* **160** (2006) 71–75 [hep-ph/0607139].

[108] S. D. Badger, E. W. N. Glover and K. Risager, *One-loop phi-MHV amplitudes using the unitarity bootstrap*, *JHEP* **07** (2007) 066 [0704.3914].

[109] L. J. Dixon and Y. Sofianatos, *Analytic one-loop amplitudes for a Higgs boson plus four partons*, *JHEP* **08** (2009) 058 [0906.0008].

[110] Z. Bern, L. J. Dixon, D. C. Dunbar and D. A. Kosower, *One-Loop n-Point Gauge Theory Amplitudes, Unitarity and Collinear Limits*, *Nucl. Phys.* **B425** (1994) 217–260 [hep-ph/9403226].

[111] Z. Bern, L. J. Dixon, D. C. Dunbar and D. A. Kosower, *Fusing gauge theory tree amplitudes into loop amplitudes*, *Nucl. Phys.* **B435** (1995) 59–101 [hep-ph/9409265].

[112] Z. Bern, L. J. Dixon, D. C. Dunbar and D. A. Kosower, *One-loop self-dual and $N = 4$ superYang-Mills*, *Phys. Lett.* **B394** (1997) 105–115 [hep-th/9611127].

[113] Z. Bern, V. Del Duca, L. J. Dixon and D. A. Kosower, *All non-maximally-helicity-violating one-loop seven-gluon amplitudes in $N = 4$ super-Yang-Mills theory*, *Phys. Rev.* **D71** (2005) 045006 [hep-th/0410224].

[114] Z. Bern, L. J. Dixon and D. A. Kosower, *All next-to-maximally helicity-violating one-loop gluon amplitudes in N = 4 super-Yang-Mills theory*, *Phys. Rev.* **D72** (2005) 045014 [hep-th/0412210].

[115] A. Brandhuber, B. J. Spence and G. Travaglini, *One-loop gauge theory amplitudes in N = 4 super Yang-Mills from MHV vertices*, *Nucl. Phys.* **B706** (2005) 150–180 [hep-th/0407214].

[116] J. Bedford, A. Brandhuber, B. J. Spence and G. Travaglini, *A twistor approach to one-loop amplitudes in N = 1 supersymmetric Yang-Mills theory*, *Nucl. Phys.* **B706** (2005) 100–126 [hep-th/0410280].

[117] Z. Bern, L. J. Dixon and D. A. Kosower, *One loop corrections to two quark three gluon amplitudes*, *Nucl. Phys.* **B437** (1995) 259–304 [hep-ph/9409393].

[118] Z. Bern, L. J. Dixon, D. A. Kosower and S. Weinzierl, *One-loop amplitudes for $e^+e^- \to \overline{q}q\overline{Q}Q$ *, *Nucl. Phys.* **B489** (1997) 3–23 [hep-ph/9610370].

[119] Z. Bern, L. J. Dixon and D. A. Kosower, *One-loop amplitudes for e+ e- to four partons*, *Nucl. Phys.* **B513** (1998) 3–86 [hep-ph/9708239].

[120] R. Britto, F. Cachazo and B. Feng, *Generalized unitarity and one-loop amplitudes in N = 4 super-Yang-Mills*, *Nucl. Phys.* **B725** (2005) 275–305 [hep-th/0412103].

[121] Z. Bern, L. J. Dixon and D. A. Kosower, *Dimensionally regulated pentagon integrals*, *Nucl. Phys.* **B412** (1994) 751–816 [hep-ph/9306240].

[122] D. Forde, *Direct extraction of one-loop integral coefficients*, *Phys. Rev.* **D75** (2007) 125019 [0704.1835].

[123] R. Britto, E. Buchbinder, F. Cachazo and B. Feng, *One-loop amplitudes of gluons in SQCD*, *Phys. Rev.* **D72** (2005) 065012 [hep-ph/0503132].

[124] C. F. Berger, Z. Bern, L. J. Dixon, D. Forde and D. A. Kosower, *Bootstrapping one-loop QCD amplitudes with general helicities*, *Phys. Rev.* **D74** (2006) 036009 [hep-ph/0604195].

[125] G. Ossola, C. G. Papadopoulos and R. Pittau, *Reducing full one-loop amplitudes to scalar integrals at the integrand level*, *Nucl. Phys.* **B763** (2007) 147–169 [hep-ph/0609007].

[126] C. F. Berger *et. al.*, *An Automated Implementation of On-Shell Methods for One- Loop Amplitudes*, *Phys. Rev.* **D78** (2008) 036003 [0803.4180].

[127] R. Britto, B. Feng and P. Mastrolia, *The cut-constructible part of QCD amplitudes*, *Phys. Rev.* **D73** (2006) 105004 [hep-ph/0602178].

[128] P. Mastrolia, *On triple-cut of scattering amplitudes*, *Phys. Lett.* **B644** (2007) 272–283 [hep-th/0611091].

[129] T. Binoth, G. Heinrich, T. Gehrmann and P. Mastrolia, *Six-Photon Amplitudes*, *Phys. Lett.* **B649** (2007) 422–426 [hep-ph/0703311].

[130] F. Cachazo, P. Svrcek and E. Witten, *MHV vertices and tree amplitudes in gauge theory*, *JHEP* **09** (2004) 006 [hep-th/0403047].

[131] E. Witten, *Perturbative gauge theory as a string theory in twistor space*, *Commun. Math. Phys.* **252** (2004) 189–258 [hep-th/0312171].

[132] P. Mastrolia, *Double-Cut of Scattering Amplitudes and Stokes' Theorem*, *Phys. Lett.* **B678** (2009) 246–249 [0905.2909].

[133] C. Anastasiou, R. Britto, B. Feng, Z. Kunszt and P. Mastrolia, *D-dimensional unitarity cut method*, *Phys. Lett.* **B645** (2007) 213–216 [hep-ph/0609191].

[134] C. Anastasiou, R. Britto, B. Feng, Z. Kunszt and P. Mastrolia, *Unitarity cuts and reduction to master integrals in d dimensions for one-loop amplitudes*, *JHEP* **03** (2007) 111 [hep-ph/0612277].

[135] R. Britto and B. Feng, *Unitarity cuts with massive propagators and algebraic expressions for coefficients*, *Phys. Rev.* **D75** (2007) 105006 [hep-ph/0612089].

[136] R. Britto, B. Feng and P. Mastrolia, *Closed-Form Decomposition of One-Loop Massive Amplitudes*, *Phys. Rev.* **D78** (2008) 025031 [0803.1989].

[137] R. Britto, B. Feng and G. Yang, *Polynomial Structures in One-Loop Amplitudes*, *JHEP* **09** (2008) 089 [0803.3147].

[138] C. K. Fong, *http://mathstat.carleton.ca/∼ckfong/*, .

[139] F. Cachazo, P. Svrcek and E. Witten, *Gauge theory amplitudes in twistor space and holomorphic anomaly*, *JHEP* **10** (2004) 077 [hep-th/0409245].

[140] R. Britto, F. Cachazo and B. Feng, *New Recursion Relations for Tree Amplitudes of Gluons*, *Nucl. Phys.* **B715** (2005) 499–522 [hep-th/0412308].

[141] R. Britto, F. Cachazo, B. Feng and E. Witten, *Direct Proof Of Tree-Level Recursion Relation In Yang- Mills Theory*, *Phys. Rev. Lett.* **94** (2005) 181602 [hep-th/0501052].

[142] S. J. Parke and T. R. Taylor, *An Amplitude for n Gluon Scattering*, *Phys. Rev. Lett.* **56** (1986) 2459.

[143] P. Mansfield, *The Lagrangian origin of MHV rules*, *JHEP* **03** (2006) 037 [hep-th/0511264].

[144] J. H. Ettle and T. R. Morris, *Structure of the MHV-rules Lagrangian*, *JHEP* **08** (2006) 003 [hep-th/0605121].

[145] J. Bedford, A. Brandhuber, B. J. Spence and G. Travaglini, *Non-supersymmetric loop amplitudes and MHV vertices*, *Nucl. Phys.* **B712** (2005) 59–85 [hep-th/0412108].

[146] S. D. Badger, E. W. N. Glover and V. V. Khoze, *MHV rules for Higgs plus multi-parton amplitudes*, *JHEP* **03** (2005) 023 [hep-th/0412275].

[147] R. Boels and C. Schwinn, *CSW rules for a massive scalar*, *Phys. Lett.* **B662** (2008) 80–86 [0712.3409].

[148] R. Boels and C. Schwinn, *Deriving CSW rules for massive scalar legs and pure Yang- Mills loops*, *JHEP* **07** (2008) 007 [0805.1197].

[149] E. W. Nigel Glover and C. Williams, *One-Loop Gluonic Amplitudes from Single Unitarity Cuts*, *JHEP* **12** (2008) 067 [0810.2964].

[150] S. D. Badger, E. W. N. Glover, V. V. Khoze and P. Svrcek, *Recursion Relations for Gauge Theory Amplitudes with Massive Particles*, *JHEP* **07** (2005) 025 [hep-th/0504159].

[151] S. D. Badger, E. W. N. Glover and V. V. Khoze, *Recursion Relations for Gauge Theory Amplitudes with Massive Vector Bosons and Fermions*, *JHEP* **01** (2006) 066 [hep-th/0507161].

[152] D. Forde and D. A. Kosower, *All-multiplicity amplitudes with massive scalars*, *Phys. Rev.* **D73** (2006) 065007 [hep-th/0507292].

[153] K. J. Ozeren and W. J. Stirling, *Scattering amplitudes with massive fermions using BCFW recursion*, *Eur. Phys. J.* **C48** (2006) 159–168 [hep-ph/0603071].

[154] C. Duhr, S. Hoche and F. Maltoni, *Color-dressed recursive relations for multi-parton amplitudes*, *JHEP* **08** (2006) 062 [hep-ph/0607057].

[155] K. J. Ozeren and W. J. Stirling, *MHV techniques for QED processes*, *JHEP* **11** (2005) 016 [hep-th/0509063].

[156] S. Badger, N. E. J. Bjerrum-Bohr and P. Vanhove, *Simplicity in the Structure of QED and Gravity Amplitudes*, *JHEP* **02** (2009) 038 [0811.3405].

[157] N. E. J. Bjerrum-Bohr, D. C. Dunbar, H. Ita, W. B. Perkins and K. Risager, *MHV-vertices for gravity amplitudes*, *JHEP* **01** (2006) 009 [hep-th/0509016].

[158] A. Brandhuber, S. McNamara, B. Spence and G. Travaglini, *Recursion Relations for One-Loop Gravity Amplitudes*, *JHEP* **03** (2007) 029 [hep-th/0701187].

[159] P. Benincasa, C. Boucher-Veronneau and F. Cachazo, *Taming tree amplitudes in general relativity*, *JHEP* **11** (2007) 057 [hep-th/0702032].

[160] N. Arkani-Hamed and J. Kaplan, *On Tree Amplitudes in Gauge Theory and Gravity*, *JHEP* **04** (2008) 076 [0801.2385].

[161] Z. Bern, L. J. Dixon and D. A. Kosower, *On-shell recurrence relations for one-loop QCD amplitudes*, *Phys. Rev.* **D71** (2005) 105013 [hep-th/0501240].

[162] Z. Bern, L. J. Dixon and D. A. Kosower, *The last of the finite loop amplitudes in QCD*, *Phys. Rev.* **D72** (2005) 125003 [hep-ph/0505055].

[163] Z. Bern, L. J. Dixon and D. A. Kosower, *Bootstrapping multi-parton loop amplitudes in QCD*, *Phys. Rev.* **D73** (2006) 065013 [hep-ph/0507005].

[164] Z. Bern, N. E. J. Bjerrum-Bohr, D. C. Dunbar and H. Ita, *Recursive calculation of one-loop QCD integral coefficients*, *JHEP* **11** (2005) 027 [hep-ph/0507019].

[165] C. F. Berger, Z. Bern, L. J. Dixon, D. Forde and D. A. Kosower, *All One-loop Maximally Helicity Violating Gluonic Amplitudes in QCD*, *Phys. Rev.* **D75** (2007) 016006 [hep-ph/0607014].

[166] Z. Bern, V. Del Duca, W. B. Kilgore and C. R. Schmidt, *The infrared behavior of one-loop QCD amplitudes at next-to-next-to-leading order*, *Phys. Rev.* **D60** (1999) 116001 [hep-ph/9903516].

[167] Z. Bern, V. Del Duca and C. R. Schmidt, *The infrared behavior of one-loop gluon amplitudes at next-to-next-to-leading order*, *Phys. Lett.* **B445** (1998) 168–177 [hep-ph/9810409].

[168] D. A. Kosower and P. Uwer, *One-loop splitting amplitudes in gauge theory*, *Nucl. Phys.* **B563** (1999) 477–505 [hep-ph/9903515].

[169] D. A. Kosower, *All-order collinear behavior in gauge theories*, *Nucl. Phys.* **B552** (1999) 319–336 [hep-ph/9901201].

[170] Z. Bern and A. G. Morgan, *Massive Loop Amplitudes from Unitarity*, *Nucl. Phys.* **B467** (1996) 479–509 [hep-ph/9511336].

[171] A. Brandhuber, S. McNamara, B. J. Spence and G. Travaglini, *Loop amplitudes in pure Yang-Mills from generalised unitarity*, *JHEP* **10** (2005) 011 [hep-th/0506068].

[172] S. D. Badger, *Direct Extraction Of One Loop Rational Terms*, *JHEP* **01** (2009) 049 [0806.4600].

[173] B. Feng and G. Yang, *Unitarity Method with Spurious Pole*, *Nucl. Phys.* **B811** (2009) 305–352 [0806.4016].

[174] A. Bredenstein, A. Denner, S. Dittmaier and S. Pozzorini, *NLO QCD corrections to top anti-top bottom anti-bottom production at the LHC: 1. quark-antiquark annihilation*, *JHEP* **08** (2008) 108 [0807.1248].

[175] A. Bredenstein, A. Denner, S. Dittmaier and S. Pozzorini, *NLO QCD corrections to $pp \to t$ anti-t b anti-b + X at the LHC*, *Phys. Rev. Lett.* **103** (2009) 012002 [0905.0110].

[176] A. Bredenstein, A. Denner, S. Dittmaier and S. Pozzorini, *NLO QCD corrections to top anti-top bottom anti-bottom production at the LHC: 2. full hadronic results*, *JHEP* **03** (2010) 021 [1001.4006].

[177] T. Binoth *et. al.*, *Next-to-leading order QCD corrections to $pp \to b\bar{b}b\bar{b} + X$ at the LHC: the quark induced case*, *Phys. Lett.* **B685** (2010) 293–296 [0910.4379].

[178] C. F. Berger *et. al.*, *One-Loop Multi-Parton Amplitudes with a Vector Boson for the LHC*, 0808.0941.

[179] C. F. Berger *et. al.*, *Precise Predictions for W + 3 Jet Production at Hadron Colliders*, *Phys. Rev. Lett.* **102** (2009) 222001 [0902.2760].

[180] C. F. Berger *et. al.*, *Next-to-Leading Order QCD Predictions for W+3-Jet Distributions at Hadron Colliders*, *Phys. Rev.* **D80** (2009) 074036 [0907.1984].

[181] C. F. Berger *et. al.*, *Next-to-Leading Order QCD Predictions for Z,γ^*+3-Jet Distributions at the Tevatron*, 1004.1659.

[182] W. T. Giele and G. Zanderighi, *On the Numerical Evaluation of One-Loop Amplitudes: The Gluonic Case*, *JHEP* **06** (2008) 038 [0805.2152].

[183] R. K. Ellis, W. T. Giele and Z. Kunszt, *A Numerical Unitarity Formalism for Evaluating One-Loop Amplitudes*, *JHEP* **03** (2008) 003 [0708.2398].

[184] W. T. Giele, Z. Kunszt and K. Melnikov, *Full one-loop amplitudes from tree amplitudes*, *JHEP* **04** (2008) 049 [0801.2237].

[185] R. K. Ellis, W. T. Giele and Z. Kunszt, *A Numerical Unitarity Formalism for One-Loop Amplitudes*, *PoS* **RADCOR2007** (2007) 020 [0802.4227].

[186] R. K. Ellis and G. Zanderighi, *Scalar one-loop integrals for QCD*, *JHEP* **02** (2008) 002 [0712.1851].

[187] R. K. Ellis, K. Melnikov and G. Zanderighi, *Generalized unitarity at work: first NLO QCD results for hadronic W+ 3jet production*, *JHEP* **04** (2009) 077 [0901.4101].

[188] R. Keith Ellis, K. Melnikov and G. Zanderighi, *W+3 jet production at the Tevatron*, *Phys. Rev.* **D80** (2009) 094002 [0906.1445].

[189] T. Melia, K. Melnikov, R. Rontsch and G. Zanderighi, *Next-to-leading order QCD predictions for W+W+jj production at the LHC*, 1007.5313.

[190] G. Bevilacqua, M. Czakon, C. G. Papadopoulos, R. Pittau and M. Worek, *Assault on the NLO Wishlist: pp $\to$ tt bb*, *JHEP* **09** (2009) 109 [0907.4723].

[191] G. Bevilacqua, M. Czakon, C. G. Papadopoulos and M. Worek, *Dominant QCD Backgrounds in Higgs Boson Analyses at the LHC: A Study of pp $\to$ t*

anti-t + 2 jets at Next-To-Leading Order, *Phys. Rev. Lett.* **104** (2010) 162002 [1002.4009].

[192] A. van Hameren, C. G. Papadopoulos and R. Pittau, *Automated one-loop calculations: a proof of concept*, *JHEP* **09** (2009) 106 [0903.4665].

[193] F. del Aguila and R. Pittau, *Recursive numerical calculus of one-loop tensor integrals*, *JHEP* **07** (2004) 017 [hep-ph/0404120].

[194] G. Ossola, C. G. Papadopoulos and R. Pittau, *CutTools: a program implementing the OPP reduction method to compute one-loop amplitudes*, *JHEP* **03** (2008) 042 [0711.3596].

[195] G. Ossola, C. G. Papadopoulos and R. Pittau, *On the Rational Terms of the one-loop amplitudes*, *JHEP* **05** (2008) 004 [0802.1876].

[196] T. Binoth, G. Ossola, C. G. Papadopoulos and R. Pittau, *NLO QCD corrections to tri-boson production*, *JHEP* **06** (2008) 082 [0804.0350].

[197] P. Mastrolia, G. Ossola, C. G. Papadopoulos and R. Pittau, *Optimizing the Reduction of One-Loop Amplitudes*, *JHEP* **06** (2008) 030 [0803.3964].

[198] T. Binoth *et. al.*, *Precise predictions for LHC using a GOLEM*, 0807.0605.

[199] T. Binoth, J. P. Guillet, G. Heinrich, E. Pilon and T. Reiter, *Golem95: a numerical program to calculate one-loop tensor integrals with up to six external legs*, *Comput. Phys. Commun.* **180** (2009) 2317–2330 [0810.0992].

[200] T. Binoth, J. P. Guillet and G. Heinrich, *Algebraic evaluation of rational polynomials in one-loop amplitudes*, *JHEP* **02** (2007) 013 [hep-ph/0609054].

[201] T. Binoth, J. P. Guillet, G. Heinrich, E. Pilon and C. Schubert, *An algebraic / numerical formalism for one-loop multi-leg amplitudes*, *JHEP* **10** (2005) 015 [hep-ph/0504267].

[202] T. Binoth, J. P. Guillet and G. Heinrich, *Reduction formalism for dimensionally regulated one-loop N-point integrals*, *Nucl. Phys.* **B572** (2000) 361–386 [hep-ph/9911342].

[203] G. Mahlon, *Multi - gluon helicity amplitudes involving a quark loop*, *Phys. Rev.* **D49** (1994) 4438–4453 [hep-ph/9312276].

[204] D. Maitre and P. Mastrolia, *S@M, a Mathematica Implementation of the Spinor-Helicity Formalism*, *Comput. Phys. Commun.* **179** (2008) 501–574 [0710.5559].

[205] K. Risager, *Unitarity and On-Shell Recursion Methods for Scattering Amplitudes*, 0804.3310.

[206] E. W. N. Glover, P. Mastrolia and C. Williams, *One-loop phi-MHV amplitudes using the unitarity bootstrap: the general helicity case*, *JHEP* **08** (2008) 017 [0804.4149].

[207] P. Nogueira, *Automatic Feynman graph generation*, *J. Comput. Phys.* **105** (1993) 279–289.

[208] S. Badger, E. W. Nigel Glover, P. Mastrolia and C. Williams, *One-loop Higgs plus four gluon amplitudes: Full analytic results*, *JHEP* **01** (2010) 036 [0909.4475].

[209] V. Del Duca, A. Frizzo and F. Maltoni, *Higgs boson production in association with three jets*, *JHEP* **05** (2004) 064 [hep-ph/0404013].

[210] J. A. M. Vermaseren, *The FORM project*, *Nucl. Phys. Proc. Suppl.* **183** (2008) 19–24 [0806.4080].

[211] R. K. Ellis, W. T. Giele and G. Zanderighi, *Semi-numerical evaluation of one-loop corrections*, *Phys. Rev.* **D73** (2006) 014027 [hep-ph/0508308].

[212] S. Badger, J. M. Campbell, R. K. Ellis and C. Williams, *Analytic results for the one-loop NMHV Hqqgg amplitude*, *JHEP* **12** (2009) 035 [0910.4481].

[213] A. Djouadi, J. Kalinowski and M. Spira, *HDECAY: A program for Higgs boson decays in the standard model and its supersymmetric extension*, *Comput. Phys. Commun.* **108** (1998) 56–74 [hep-ph/9704448].

[214] C. Anastasiou, G. Dissertori, M. Grazzini, F. Stockli and B. R. Webber, *Perturbative QCD effects and the search for a H→WW→l ν l ν signal at the Tevatron*, *JHEP* **08** (2009) 099 [0905.3529].

[215] **CDF** Collaboration, *Search for $H \to WW^*$ production at cdf using 3.0fb^{-1} of data*, *CDF note 9500*.

[216] **CDF** Collaboration, *Search for $H \to WW^*$ production at cdf using 4.8fb^{-1} of data*, *CDF note 9887*.

[217] The CDF and the D0 and Collaborations, the Tevatron New Physics and Higgs Working Group, *Combined CDF and D0 Upper Limits on Standard Model Higgs- Boson Production with 2.1 - 5.4 fb^{-1} of Data*, 0911.3930.

[218] L. J. Dixon, *Calculating scattering amplitudes efficiently*, hep-ph/9601359.

[219] H. J. Lu and C. A. Perez, *Massless one loop scalar three point integral and associated Clausen, Glaisher and L functions*, . SLAC-PUB-5809.

[220] T. Binoth, J. P. Guillet, G. Heinrich and C. Schubert, *Calculation of 1-loop hexagon amplitudes in the Yukawa model*, *Nucl. Phys.* **B615** (2001) 385–401 [hep-ph/0106243].

[221] A. van Hameren, J. Vollinga and S. Weinzierl, *Automated computation of one-loop integrals in massless theories*, *Eur. Phys. J.* **C41** (2005) 361–375 [hep-ph/0502165].